A DC CHOPPER CONTROLLER FOR A BATTERY ELECTRIC VEHICLE

BY

MICHAEL DAVID CLAASSEN

PRESENTED FOR THE DEGREE OF

MASTER OF SCIENCE

IN ELECTRICAL ENGINEERING

AT THE

UNIVERSITY OF CAPE TOWN

DECEMBER 1973

CONTENTS

ACKNOWLEDGEMENTS

Financial assistance from the Council for Scientific and Industrial Research for the years 1970 and 1971 is gratefully acknowledged.

The author also wishes to thank Professor N.C. de V. Enslin for his supervision and encouragement, J.N. Wright and D.J.B. Kenyon who undertook the constructional work, and all members of the Department of Electrical Engineering, U.C.T., who made valuable suggestions.

The many hours spent by Mrs. A.E. Claassen in the typing of this thesis is appreciated by the author.

ABSTRACT

The battery electric vehicle is presented as a pollution-free alternative to the internal combustion engined vehicle as a form of commuter transport in city centres. To conserve battery energy as much as possible, an efficient drive system, consisting of a chopper controller and a permanent magnet motor, is described and tested in four modes of operation --- two modes of motoring and two of regenerative braking.

From the experimental results, it was estimated that approximately 10% of the energy expended by the vehicle during motoring could be returned to the battery if regenerative braking is employed under stop-start driving conditions.

The operation of transistor and thyristor choppers is described, and their suitability for use in a vehicle drive system is discussed. A proposed vehicle control system, incorporating a thyristor array and associated logic for implementing the mode selection, is described and evaluated.

LIST OF PRINCIPAL SYMBOLS

E_M = Motor back-emf

V_B = Average battery voltage

V_M = Average voltage applied to the motor

I_M, I_B = average values of motor and battery currents

I_M', I_B' = RMS value of motor and battery currents

t_m = on time of chopper

t_s = off time of chopper

T_o = period of chopper = $t_m + t_s$

f = chopper frequency = $1/T_o$

v_M = instantaneous applied motor voltage

i_p = instantaneous maximum value of current

i_v = instantaneous minimum value of current

K = current bandwidth = $i_p - i_v$

R = total circuit resistance

R_a = armature resistance

L = inductance

$(f.f.)_M$, $(f.f.)_B$ = form factors of motor and battery currents

r = ripple factor

N = motor speed

P_{CU} = copper power loss

CHAPTER 1

INTRODUCTION

The project is an investigation of an improved electric drive suitable for use in a small, battery powered commuter-type vehicle. The requirements and components of the electric drive are considered and the system is compared with existing drives.

1.1 THE CASE FOR THE ELECTRIC CAR

There is a very real need for an alternative to the internal combustion - engined vehicle as a form of commuter transport. The pollution of our enviroment is gaining more attention each day. In particular, air pollution caused by exhaust fumes of internal combustion - engined vehicles has poisoned the air in large cities to such an extent that it has produced a health hazard. In Johannesburg, the level of carbon monoxide has recently been measured [43] as high as 90 p.p.m. during the morning rush hour. Exposure for long periods of time to levels of over 50 p.p.m. is considered undesirable.

A partial solution to this problem would be to prevent all non-essential vehicles from entering the city centre complex for the major portion of the day - this has recently been effected in Tokyo with some degree of success. However, the use of a battery-operated vehicle offers a more complete and effective remedy to the pollution problem.

It can be expected that the initial cost of an electrice vehicle will be significantly higher than the initial cost of a comparable petrol - engined vehicle. For an electric vehicle with full electronic control, this difference may be as high as 100% [15] .

However, this increase in cost is offset to some extent by the increase in the operating life of the vehicle, and the reduced running costs, which Hender [15] gives as being 30% less than for a petrol - engined vehicle.

A recent survey [15] showed that at present, about 80% of the cars which are used for commuting each day travel less than 35km. per day. Therefore, a car which is able to travel at normal traffic speeds of 60 km/h with a range of 50 km, would satisfy a large percentage of the population, if only as a second car.

1.2 THE IMPORTANCE OF AN EFFICIENT DRIVE SYSTEM

The greatest single problem associated with battery powered vehicles is the relatively low specific output (kWh/kg) of the storage batteries which is approximately 1000 times less than that obtainable from chemical fuels used in internal combustion - engined vehicles. The maximum range and speed capability of any battery powered vehicle is therefore greatly influenced by the efficiency of the drive system, including the speed controller, motor and transmission. The dc storage battery suggests the use of some form of dc motor, although a system using a three - phase induction motor as the power unit has been built and tested [18,50]. An analysis undertaken by Murphy [49] indicates that such an ac drive system is not an economic proposition below 15 kW output power. As the power required to drive a 600 kg vehicle at speeds of 60 km/h is less than 7kW [51] , a dc drive system was decided upon.

(i) The Advantages of Chopper Controllers

As the speed of a dc motor is a function of the applied armature voltage, some converter capable of producing an variable voltage

must be placed between the motor and battery. This converter must have a high part-load efficiency, as a vehicle designed to operate in urban traffic may be used for long periods at a fraction of its maximum speed. Resistive controllers should be avoided because of the large amounts of energy wasted in the resistors, especially under conditions of low speed and high torque. A switched battery system, as used on one commercially available vehicle [19] offers low losses, but fails to provide smooth control between speed notches. A chopper-type controller, incorporating a high - speed semiconductor switch that cylically connects the motor to the battery, is able to offer an efficiency of the order of 95%, infinitely variable speed control and freedom from maintainance.

(ii) The Suitability of the Permanent Magnet Motor

The use of a chopper controller influences the choice of the most suitable type of motor. The natural choice for a dc drive system would be a series motor, which is a robust machine with suitable characteristics for traction, and is widely used in electric vehicle drives [1-9, 28, 32, 45] . However, the pulsating flux caused by the on/off action of the chopper produces a transformer - emf in the commutated coil, increasing the armature copper loss [1] . This indicates an advantage in using a constant flux instead of a series machine.

Because the flux of a separately excited motor is at a maximum, the values of torque/amp and volts/rad/s are as high as possible, enabling the separately excited motor to operate more efficiently than a comparable series machine. Typical experimental results are shown in figure 1.1 for the two types of motors operating in the regenerative braking mode. The motor and chopper controller may be

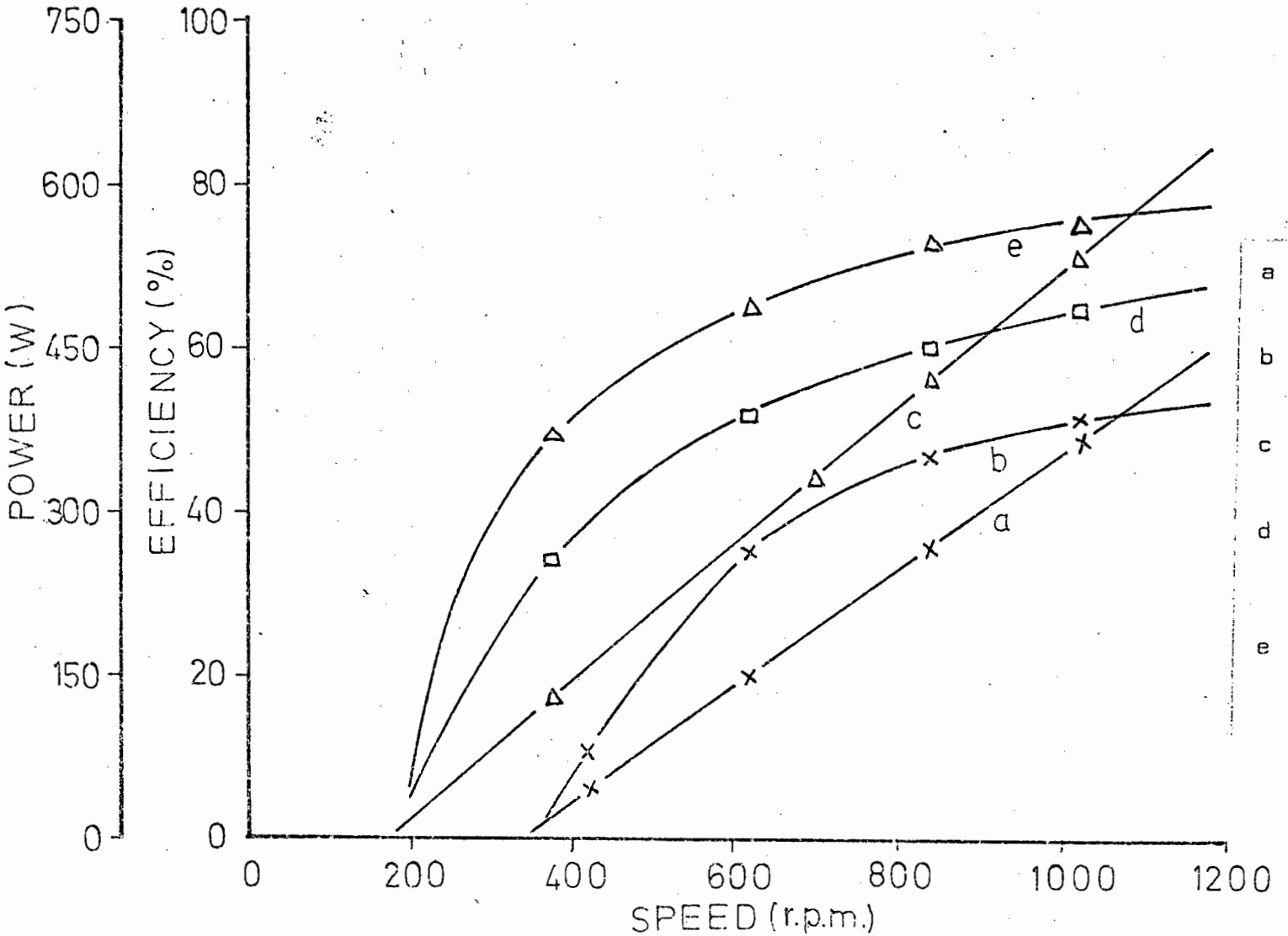

a : Power regenerated, series connection.

b : Efficiency of regeneration, series connection.

c : Power regenerated, shunt connection.

d : Efficiency of regeneration, shunt connection (with field losses)

e : Efficiency of regeneration, shunt connection (neglecting field losses)

FIGURE 1.1 : COMPARISON BETWEEN SERIES AND SHUNT CONNECTION UNDER REGENERATIVE BRAKING AT 0,75 T_{FL} (f=70Hz)

used in this mode for retarding the vehicle by returning energy to the battery. The results were obtained from a 1100 W series motor with modified field connections, enabling it to be operated either as a series or separately excited motor. For the separate excitation, a 0,2H inductor was connected in series with the armature, replacing the series field.

The results indicate that, for a particular speed and torque, the constant flux connection is approximately 15% more efficient, and this figure may be increased by a further 10% if the field loss is neglected, as would be the case if a permanent magnet motor were used. Another advantege of the constant flux connection is that regeneration is possible at lower speeds than if the series connection were used.

Therefore, this thesis will investigate the feasibility of using a permanent magnet motor in place of a series motor in a battery powered vehicle drive.

1.3 THE FOUR DESIRED MODES OF OPERATION OF THE MOTOR.

To implement an efficient drive system, using the permanent magnet motor and the chopper controller, the following four modes of operation are proposed. In each case, the motor back-emf is given by E_M and the battery voltage by V_B.

(i) Motoring over the range $0 \leq E_M \leq V_B$

This is the conventional mode of operation of all battery vehicle systems. The motor is accelerated from rest to base speed, which is when $E_M = V_B$.

(ii) Motoring over the range $E_M \geq V_B$

If $E_M = V_B$, and the vehicle travels down a slight decline, so

that the torque demand on the motor decreases, it would be desireable to further increase the maximum speed of the vehicle. This may be achieved by weakening the flux of the motor. However, to obtain maximum efficiency at all times, the flux of the machine is kept constant and the speed is increased by raising the terminal voltage above the battery voltage, using a voltage step-up technique.

(iii) Regenerative braking over the range, $E_M \geq V_B$

Consideration should also be given to the best method of braking the vehicle, because of the significant amount of stored energy involved at normal traffic speeds of 20 - 70 km/h. The range of vehicle can be improved if this stored energy is returned to the battery, instead of being wastefully dissipated as heat, as occurs when mechanical or dynamic braking is used. When the back-emf is greater than the battery voltage, energy may be returned directly to the battery, using the chopper to control the energy flow.

(iv) Regenerative braking over range $0 \leq E_M \leq V_B$

When $E_M < V_B$, energy can still be returned to the battery if the voltage step-up technique is again used. This braking would be effective down to speeds of about 8 km/h, where the mechanical brakes would take over. With existing systems, it has been found that, when regenerative braking is employed in stop-start driving conditions, 10% increase in range can be obtained [16], although this figure depends on the driving conditions.

The performance of the machine in these four modes is described in chapters 2 - 5.

1.4 OTHER ASPECTS OF THE VEHICLE CONTROL SYSTEM

Thyristor and transistor choppers, which may be used as motor controllers, are described and evaluated in chapters 6 and 7. A method of mode selection, using a hybrid transistor/thyristor chopper, is presented, enabling the machine to be operated either in the mode of motoring or braking when $E_M < V_B$.

The power and energy required by the electric vehicle to achieve a specified top speed and range are considered in chapter 8.

Finally, using the knowledge gained from previous chapters, a complete control system for an electric vehicle is proposed and evaluated in chapter 9.

CHAPTER 2

REALIZATION OF THE FOUR MODES

The advantages of providing efficient control of the motor during motoring and braking have been outlined. This chapter will examine in more detail the four modes of operation that are suggested to achieve this.

2.1 MOTORING OVER THE RANGE $0 \leq E_M \leq V_B$.

The speed of the motor may be controlled using a system such as that shown in figure 2.1(a). The semiconductor switch, represented by S, is operated cyclically, connecting the motor to the battery for a time t_m, and disconnecting the motor for a time t_s. The average voltage applied to the motor is given by:

$$V_M = V_B \, t_m \, / \, (t_m + t_s) \quad \ldots\ldots\ldots\ldots\ldots\ldots\ldots\ldots\ldots\ldots (2.1)$$

By altering the duty ratio, $t_m \, / \, (t_m + t_s)$, the average voltage may be varied over a wide range, as shown in figure (2.1(b).

When the switch is opened, the diode D provides an alternative path for the stored electrical energy associated with the inductance of the armature, so avoiding large voltage transients appearing across the switch. This diode is therefore refered to as the "free-wheel-diode". If the armature inductance is very low, the motor current will rapidly fall to zero during the period t_s, causing energy to be supplied to the motor in the form of discrete pulses. To achieve maximum torque at low speeds, very high current peaks would then be necessary to realise the required average value of motor current. This may be avoided if the motor current is maintained throughout the off period t_s, by increasing the value of the inductance associated with the motor. This may be accomplished

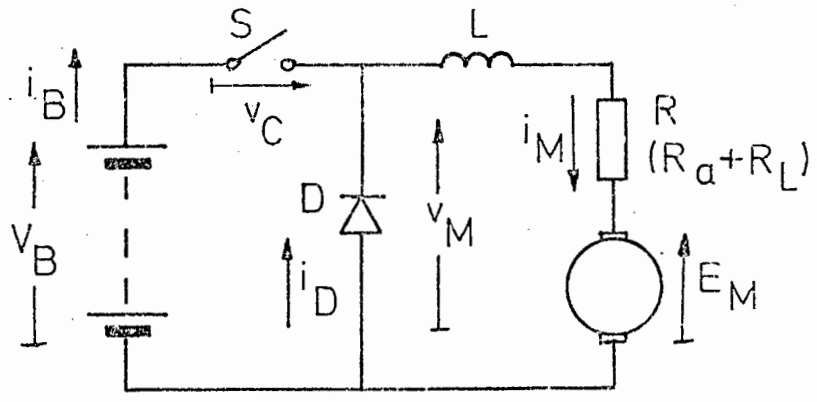

FIGURE 2.1 (a) BASIC D.C. CHOPPER

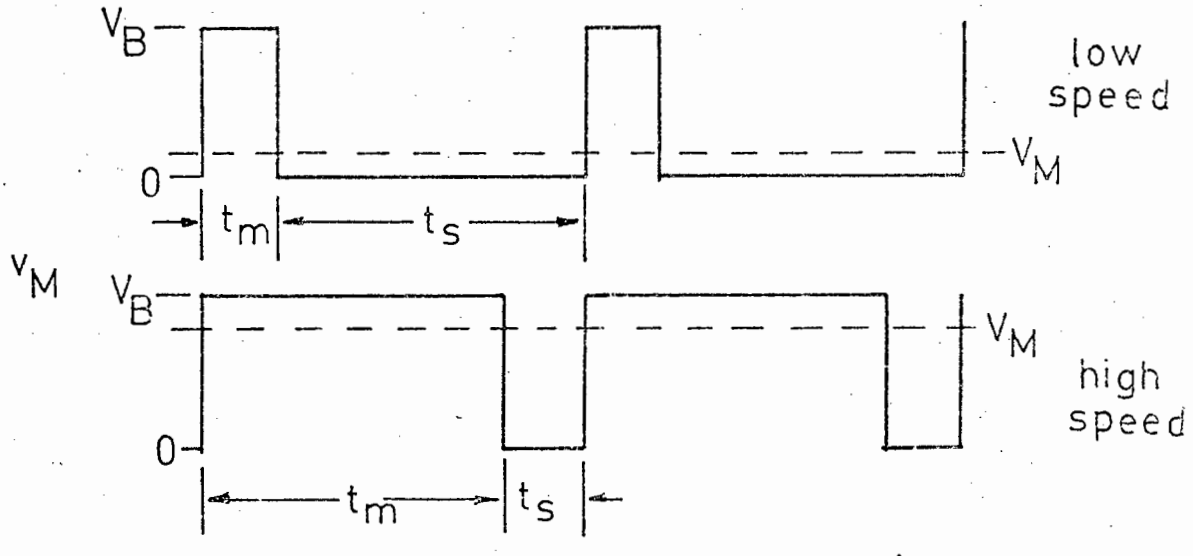

FIGURE 2.1(b) OUTPUT VOLTAGE OF CHOPPER

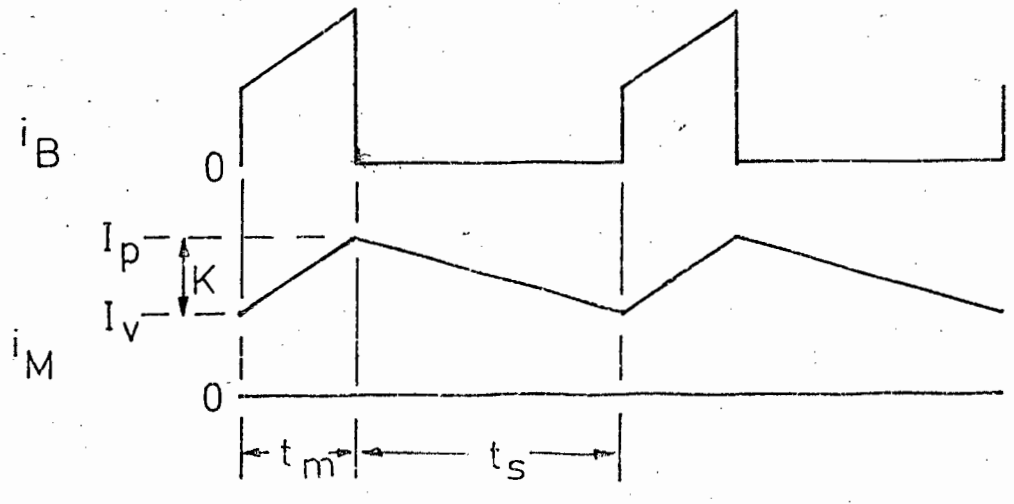

FIGURE 2.1(c) BATTERY AND MOTOR CURRENTS

by inserting additional inductance in series with the armature, as shown in figure 2.1(a). If the inductance does not saturate at the levels of current present in the armature, and if the inductance is sufficiently large to maintain the motor current during t_s, for a given chopper frequency, the chopper acts as a dc transformer. Assuming the chopper to be lossless, the average output power then equals the average input power, or

$$V_M I_M = V_B I_B \quad \ldots\ldots\ldots\ldots\ldots\ldots\ldots\ldots\ldots\ldots\ldots\ldots (2.2)$$

I_M and I_B are the average values of the motor and battery currents respectively.

From equation (2.1), it follows that

$$I_M / I_B = (t_m + t_s)/t_m \quad \ldots\ldots\ldots\ldots\ldots\ldots\ldots\ldots\ldots\ldots (2.3)$$

The ratio I_M/I_B is known as the "current multiplication ratio", and in a lossless system varies with the inverse of speed, from unity at maximum speed to infinity at stall, for a given torque. Under conditions of high torque and low speed, a high current is maintained, while the current drawn from the battery is in the form of short pulses of duration t_m, as shown in figure 2.1(c). Current multiplication reduces the average current drain on the battery and allows better utilisation of the available battery energy.

2.2 REGENERATIVE BRAKING OVER THE RANGE $0 \leq E_M \leq V_B$

Although the motor back-emf is lower than the battery voltage, energy may be returned to the battery by using a voltage step-up technique as shown in figure 2.2. The essential element of this converter is the inductor L, which is used as an energy storage device. When the switch S is closed, the motor current increases at a rate determined by the back-emf and the time constant of the

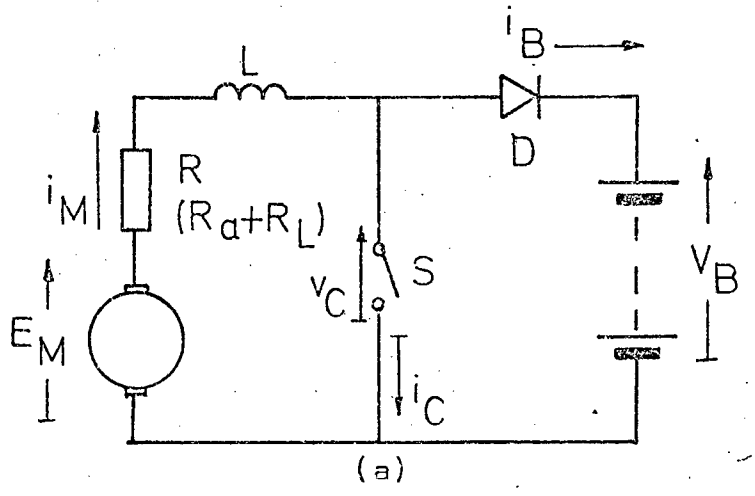

(a)

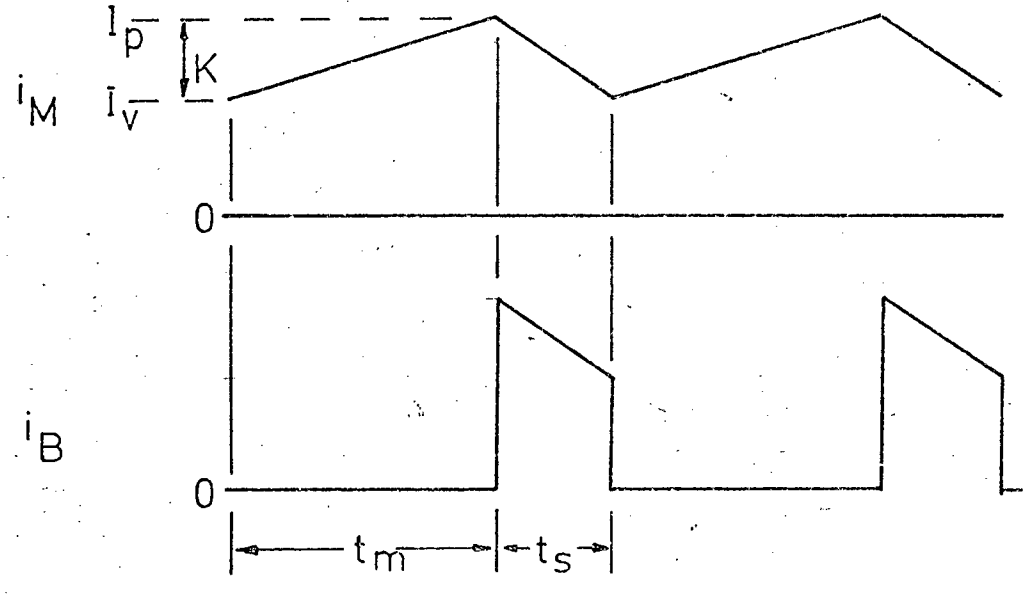

(b)

FIGURE 2.2 : REGENERATIVE BRAKING

circuit. When the switch is opened, the stored energy in the inductance causes the voltage across it to rise until the Diode D conducts, and energy is returned to the battery. If the stored energy is sufficiently large, current will be returned to the battery in the form of a pulse of duration t_s, as illustrated in figure 2.2. To achieve this, the inductance must be large enough for a given frequency to maintain the motor current throughout the period t_s. The motor current then rises and falls with a time constant L/R, as in the case of motoring when $E_M \leq V_B$.

In the ideal case of a lossless system, the chopper and inductance act as a perfect step-up converter so that the average power supplied by the motor equals the average power returned to the battery.

$$E_M I_M = V_B I_B \quad \ldots\ldots\ldots\ldots\ldots\ldots\ldots\ldots\ldots\ldots\ldots\ldots (2.4)$$

Therefore, for a given motor and vehicle speed, the power returned to the battery is proportional to the braking torque of the motor. From figure 2.2, it is seen that

$$I_B = I_M \, t_s \; / \; (t_m + t_s) \quad \ldots\ldots\ldots\ldots\ldots\ldots\ldots\ldots (2.5)$$

It is theoretically possible to achieve regeneration over the entire speed range, however, in practice, this is not possible at very low speeds because of the chopper voltage drop, and the armature resistance.

2.3 MOTORING OVER RANGE $E_M \geqq V_B$.

At higher speeds of motoring the motor back-emf increases above the battery voltage. To drive the motor in this region, a step-up converter similar to that described above in section 2.2 is used. Figure 2.3(a) shows the basic circuit. Energy, supplied by the battery when the switch S is closed, is stored in the Inductance L.

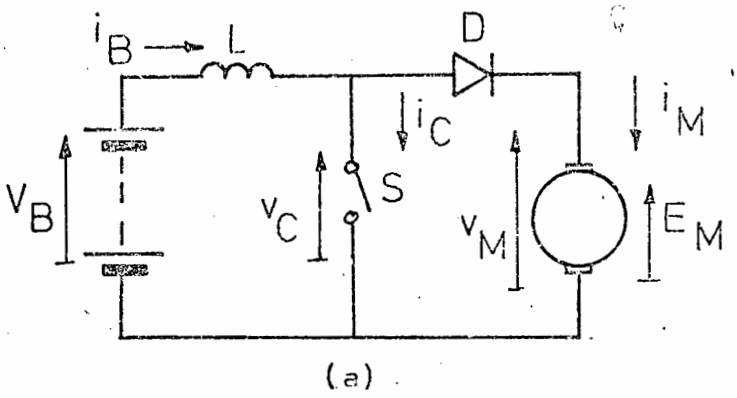

(a)

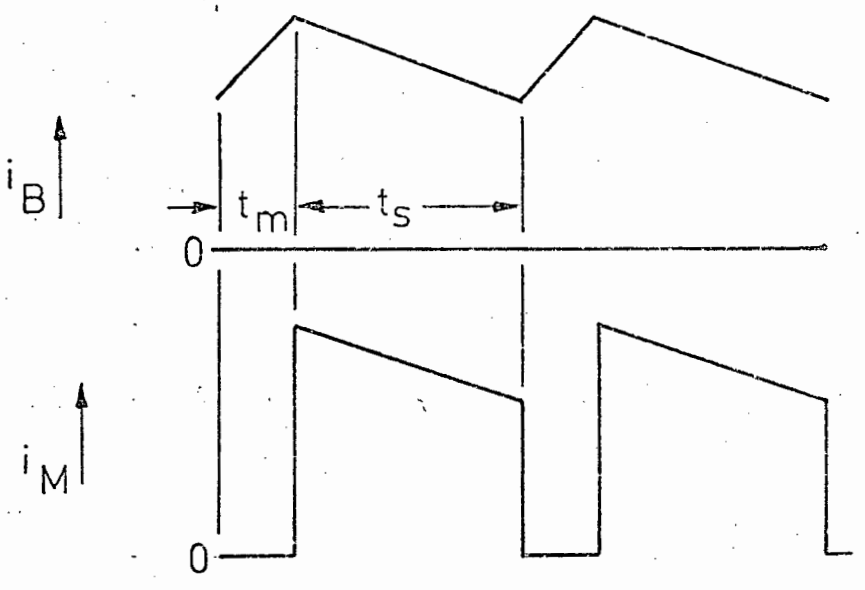

(b)

FIGURE 2.3: MOTORING OVER THE RANGE $E_M \geq V_B$

When the switch is again opened, the energy is transferred to the motor, causing its terminal voltage to rise. Diode D prevents energy flow in the reverse direction.

The motor current is therefore supplied in the form of pulses of duration t_s, while the battery current is continuous, provided the value of the inductance is large enough for a given frequency of operation. From figure 2.3(b) it can be seen that the average motor and battery currents are related by:

$$I_M = I_B \, t_s / (t_m + t_s) \quad \ldots\ldots\ldots\ldots\ldots\ldots\ldots\ldots (2.6)$$

If the chopper is considered as being lossless, the motor back-emf. for a fixed value of motor current is given by:

$$E_M = V_B \, (t_m + t_s) / t_s \quad \ldots\ldots\ldots\ldots\ldots\ldots\ldots\ldots (2.7)$$

This equation shows that a high speed and high torque of the motor (E_M and I_M large), a high battery current is demanded. A heavy drain would be imposed on the battery if the motor was operated under these conditions continuously. This mode is therefore intended to achieve a high speed at a low torque, for instance when the vehicle is proceeding down a slight decline, or to achieve a high speed at a high torque for short durations, when overtaking slower vehicles.

2.4 REGENERATIVE BRAKING OVER THE RANGE $E_M \geq V_B$.

This fourth mode of operation would be used to brake the vehicle from the high speed mode of motoring, described in the previous section. As the back-emf of the motor is greater than the battery voltage, regenerative braking may be achieved with the circuit shown in figure 2.4(a). This circuit is identical to that of figure 2.1(a), except that the motor and battery are interchanged.

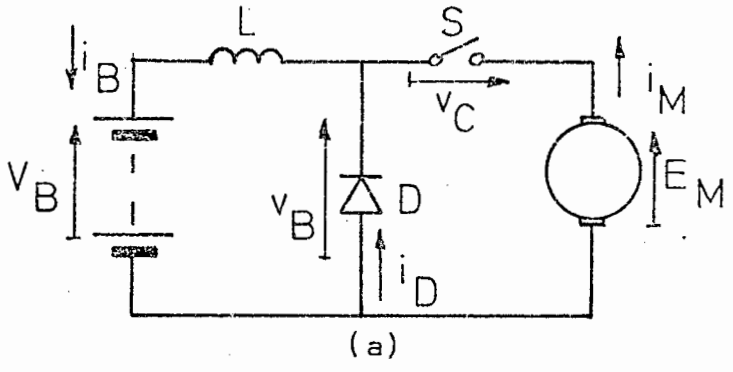

(a)

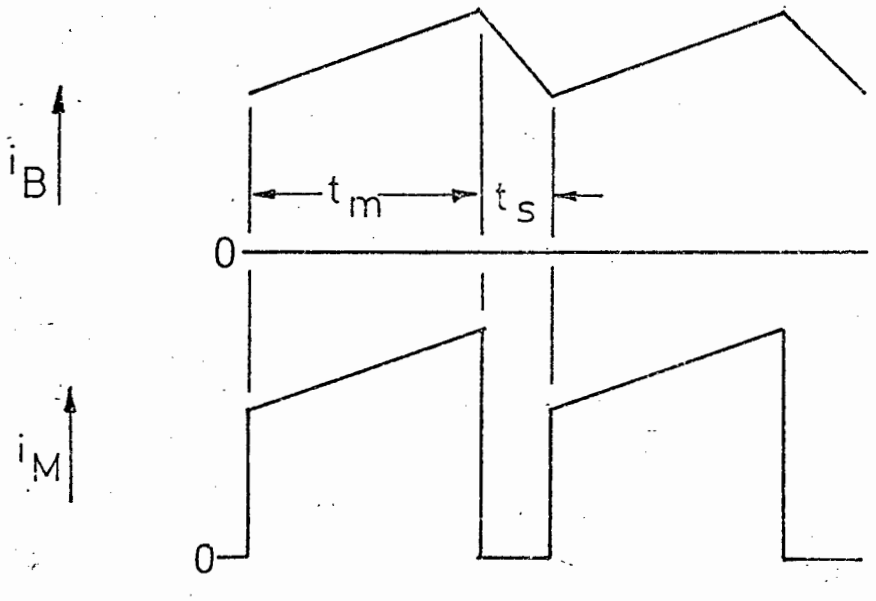

(b)

FIGURE: 2.4 REGENERATIVE BRAKING OVER THE RANGE $E_M \geq V_B$

When the switch S is closed for a time t_m, current is returned to the battery via the inductor L. When the switch is again opened for a time t_s, this current is maintained in the battery circuit by the free-wheel diode D. Providing the inductance does not saturate at the level of current used, and that the inductance is sufficiently large for a given frequency of operation, a continuous battery current is maintained throughout the period t_s, as shown in figure 2.4(b). The motor current is then in the form of pulses of duration t_m.

The average motor and battery currents are related by the equation:

$$I_M = I_B \, t_m / (t_m + t_s) \quad \ldots\ldots\ldots\ldots\ldots\ldots (2.8)$$

To allow the motor current to flow, and so brake the machine, the per unit mark, $t_m / (t_m + t_s)$, must satisfy the condition

$$E_M \, t_m / t_m + t_s) \geq V_B \quad \ldots\ldots\ldots\ldots\ldots\ldots (2.9)$$

This equation implies that the average value of the back-emf obtained via the chopper must exceed the battery voltage for braking to be effective.

2.5 THE EFFECT OF THE FORM FACTOR OF THE MOTOR CURRENT ON THE COPPER LOSSES AND COMMUTATION, IN ALL MODES OF OPERATION.

In all four modes described, the motor current is not constant, but varies periodically with the opening and closing of the switch S. This current can be resolved in terms of the average value, producing the average torque of the machine and the RMS value, which generates the copper loss in the armature. As the form factor is greater than unity, the copper loss is larger than for normal dc operation of the motor, when the average and RMS values of the current are identical. The armature copper loss, P_{cu}, for normal dc operation is given by:-

$$P_{cu} = I_M^2 R_a \quad \text{.....(2.10)}$$

where R_a = armature resistance

For chopper operation, the copper loss is expressed as:-

$$P_{cu} = (I_M')^2 R_a \quad \text{.....(2.11)}$$

where I_M' = RMS value of motor current.

The fractional increase in copper loss is:-

$$P_{cu}' = \frac{(I_M')^2 R_a - I_M^2 R_a}{I_M^2 R_a}$$

$$= (\text{form factor})^2 - 1 \quad \text{.....(2.12)}$$

As this expression is a function of the square of form factor, it is necessary to keep the current excursions as low as is practical. For instance if the form factor is 1.1, the copper losses will be 21% above the dc value, causing a corresponding reduction in efficiency of the motor. In addition, the high current peaks associated with a form factor much greater than unity lead to poor commutation and sparking [5, 13] , particularly in the region of half speed where the form factor of the current waveform is greatest.

2.6 CURRENT RIPPLE AND FORM FACTOR FOR THE VARIOUS MODES IN TERMS OF THE CHOPPER FREQUENCY AND INDUCTANCE.

In the previous section, the effects of a high form factor of the motor current waveform were described. To reduce the form factor, it is necessary to know the factors that influence the current ripple (or the form factor), and their relationship to the current ripple. The equations expressing the ripple factor in terms of the chopper frequency and inductance will now be derived for each of the four modes.

To simplify the analyses in this and the next section, the following conditions are necessary:

(a) The inductance must not saturate at the levels of current present;

(b) The inductance must be sufficiently large for a given chopper frequency to ensure that the current is maintained in the inductive circuit throughout the chopper "off" time;

(c) The period of operation of the chopper, $t_m + t_s$, must be much less than the time constant of the circuit, i.e.

$$T_o \ll L/R$$

(i) Motoring over the range $0 \leq E_M \leq V_B$

The ripple factor, r, is defined as:

$$r\ (\%) = \frac{I_p - I_v}{I_p + I_v} \times 100 \quad \text{.....(2.13)}$$

I_p and I_v are instantaneous maximum and minimum currents reached under steady-state conditions.

The form factor (f.f.) may be expressed in terms of the ripple factor i.e.

$$\text{f.f.} = \sqrt{1+1/3r^2} \quad \text{..... (2.14)}$$

[Appendix]

When steady-state is reached, the peak-to-peak ripple, $I_p - I_v$, is given by:

$$I_p - I_v = \frac{(V_B - E_M)\ (t_m)^2 + E_M\ (t_s)^2}{LT_o} \quad \text{.....(2.15)}$$

[Appendix]

$I_p - I_v$ is referred to as the current bandwidth, K, and has a maximum value when $t_m = t_s = \frac{1}{2} T_o$

From equation (2.15),

$$K_{max} = \frac{V_B T_o}{4\ L} \quad \text{.....(2.16)}$$

Substituting this equation (2.13),

$$r_{max} = \frac{V_B}{8 I_M f L} \quad \text{.....(2.17)}$$

where $I_M = \frac{1}{2} (I_p + I_v)$

the ripple factor for mark/space other than 1/1 is given by:

$$r = 4\, r_{max}\, (t_m/T_o)\, (1 - t_m/T_o) \quad \text{.....(2.18)}$$

The dependence of form factor, the ripple factor and the copper losses on the ratio I_v/I_p is shown graphically in figure 2.5.

A number of important points are illustrated by equations (2.17) and (2.18). For a given motor current, the ripple factor is controlled mainly by the chopper frequency and inductance; the maximum ripple occurs at mark/space ratio of I/I, which corresponds approximately to half speed of the motor; and the ripple factor is inversely proportional to the average current.

(ii) Regenerative braking over the range $0 \leq E_M \leq V_B$

When steady-state conditions exist,

$$I_p - I_v = \frac{E_M (t_m)^2 + V_B - E_M)\, (t_s)^2}{L\, T_o} \quad \text{.....(2.19)}$$

[Appendix]

This leads to an identical expression for the ripple factor as in the case of motoring (equation 2.18). Therefore, the value of inductance, selected for use in the motoring mode, will produce exactly the same amount of current ripple when used in the braking mode, provided the same conditions of torque and chopper frequency exist.

(iii) Motoring and Braking over the range $E_M \geq V_B$

As the circuit configurations of these two modes are similar

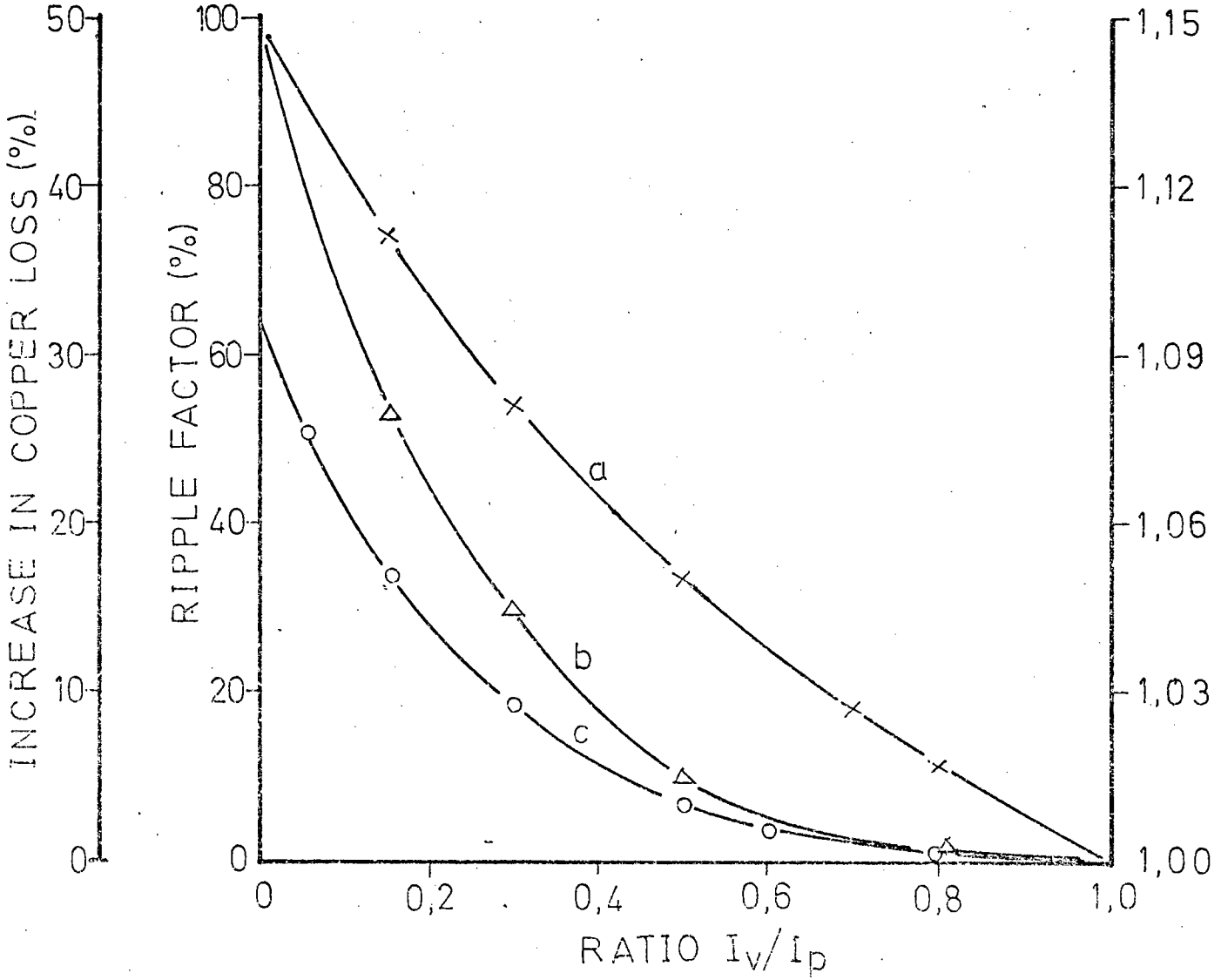

FIGURE 2.5 :

RIPPLE AND FORM FACTOR AS FUNCTIONS OF THE RATIO I_v/I_p

a : Ripple factor (%)

b : Form factor

c : Percentage increase in armature copper loss

to those of the previous two modes, as seen in figures 2.1 - 2.4, the derivation of the equations may be simplified. The two groups of connections ($E_M < V_B$ and $E_M > V_B$) are identical except for the battery and motor being interchanged. In each case, the ripple factor of the battery current may be found from the relavent equation, and from this the corresponding form factor for the motor current deduced. The form factor is used instead here, as the ripple factor is meaningless for a non-continuous current waveform.

The form factors of the motor and battery currents $(f.f.)_M$ and $(f.f.)_B$, are related by the equation:

$$(f.f.)_M = T_o/t_s \ (f.f.)_B \quad \text{.....(2.20)}$$

[Appendix]

for motoring, and

$$(f.f.)_M = T_o/t_m \ (f.f.)_B \quad \text{.....(2.21)}$$

[Appendix]

for braking

(iv) Factors affecting the selection of a particular form factor.

Achieving the rated torque of the motor when the current form factor is greater than unity, means exceeding the RMS current rating of the machine, and reducing its efficiency. The amount of overload that is permissible depends on the design of the motor being used. A 100 kW traction motor tested by Sie and Moser [5] was run at full load with a form factor of 1,025, which caused an additional armature temperature rise of 10 degrees C, corresponding to an increase of 10 - 15%. The efficiency of the motor was reduced by 0,5%, compared to the efficiency when it was operated on pure dc.

As the form factor at a given torque varies with the mark/space ratio, the fraction of the duty cycle that will be spent in the region of half-speed, where the losses in the machine are greatest, must be determined.

The improvement in efficiency of the motor must be considered in relation to the increases in chopper frequency and size and cost of the inductance that will be necessary to achieve the desired form factor. However, by using the maximum practicable frequency, the size and cost of the choke may be kept to a minimum. This upper limit of the frequency is determined by the switching losses of the semiconductor used in the chopper, and the hysteresis and eddy current losses in the choke.

Although the battery voltage has no direct influence on the motor efficiency, the significance of the chopper voltage drop may be reduced by increasing the battery voltage. However, as a battery system of a given capacity is more economically realised by having a small number of cells of high amp-hour capacity, instead of a large number of cells of lower amp-hour capacity, some compromise is necessary.

2.7 AVERAGE MOTOR CURRENT IN THE FOUR MODES.

As the output torque of the permanent magnet motor is proportional to the average motor current, it is important to investigate the relationship between the average current and other parameters of the chopper system.

Under steady-state conditions, the average motor current for each of the modes is given by:

Motoring when $0 \leq E_M \leq V_B$

$$I_M = 1/R\ (V_B t_m/T_o - E_M) \quad \text{.....(2.22)}$$

[Appendix]

where R = total circuit resistance.

Regenerative braking when $0 \leq E_M \leq V_B$

$$I_M = 1/R\ (E_M - V_B\ t_s/T_o) \quad \text{.....(2.23)}$$

[Appendix]

Motoring when $E_M \geq V_B$

$$I_M = 1/R\ (V_B t_s/T_o - E_M t_s^2/T_o^2 \quad \text{.....(2.24)}$$

[Appendix]

Regenerative braking when $E_M \geq V_B$

$$I_M = 1/R\ (E_M t_m^2/T_o^2 - V_B t_m/T_o) \quad \text{.....(2.25)}$$

[Appendix]

The above equations show that, provided the conditions stated in the previous section are adhered to, the average motor current is independant of the chopper frequency and value of inductance, but is determined by the motor back-emf and the per unit mark. In addition, the equations indicate that for a given value of E_M, a certain per unit mark, t_m/T_o, must be achieved before any motor current will flow. The validity of this will be verified by experimental results, which will be discussed in later chapters.

CHAPTER 3

THE PERFORMANCE OF THE MACHINE WHEN MOTORING OVER THE RANGE $0 \leq E_M \leq V_B$

3.1 INTRODUCTION

The operation of the chopper in the four modes has been outlined, and basic equations for each mode have been presented. This chapter will deal with the experimental results obtained in the mode of motoring over the range $0 \leq E_M \leq V_B$. The correlation between the predicted and the measured values of the average current and the current ripple will be investigated, and the performance of the mode will be evaluated from the load tests that were conducted.

3.2 EXPERIMENTAL DETAILS

(i) The Permanent Magnet motor used

The motor used in the following tests is a dc permanent magnet machine with a rating of 5kW at 150V and 3000 r.p.m. The combined effect of lower mass and high speed capability, both due to the novel construction of the motor, gave the machine a high specific output of 167W/kg, instead of the value of 110W/kg for conventional machines. The inductance of the disc-type armature was very low, being approximately 0,1mH.

Further specifications of the motor and details of the performance of the machine under normal dc conditions may be found in the appendix of chapter 10.

(ii) Measurement Techniques

To evaluate the performance of the chopper and motor, it was necessary to measure average voltage, average current, RMS current, power and energy. To ensure sufficient accuracy at the high chopper frequency used (400 Hz), high quality electrodynamic instruments

were used wherever possible. Details of the instruments used, and the procedures adopted for checking their accuracies are described in the appendix:

(iii) Selection of a battery voltage and value of inductance

The rated value of 150V for the motor voltage was considered to be too high for the type of semiconductor choppers used, and also an unrealistic voltage for use in a small battery vehicle, because of the large number of cells that would have to be provided. The voltage chosen was 84V, which then also limited the maximum speed to approximately 1800 r.p.m.

The value of the inductance may be kept to a minimum by using as high a chopper frequency as possible. However, a compromise is necessary, as a high frequency causes additional losses in the circuit, such as switching losses in the semiconductors of the chopper, and iron losses in the choke. A value of 400 Hz was chosen as being the highest practicable frequency.

Traction motors can tolerate a ripple factor of 30% in their current waveform, as shown by Sie and Moser [5]. But, the manufacturers of the permanent magnet motor warned that the RMS rating of the machine should not be exceeded, and as the motor could be run for long periods in the laboratory at half speed, when the current ripple is at its greatest, the designed ripple factor was kept low. A maximum value of 15% at full load torque was chosen, as this increases the copper losses by only 2% above the pure dc value. The value of inductance required to achieve this is calculated by:

$$L = \frac{V_B}{8\, I_M\, r_{max}\, f}$$

$$= \frac{84}{8 \times 37 \times 0{,}15 \times 400}$$

giving L = 4,7mH.

Two chokes, each of 2 mH and 40A rating, were used in series.

3.3 THE CORRELATION BETWEEN THE THEORETICAL AND MEASURED VALUES OF THE AVERAGE MOTOR CURRENT.

In the previous chapter, it was shown that the average value of the motor current was independent of the chopper frequency and value of inductance, but was determined by:

(i) The back-emf of the motor

(ii) The per unit mark (t_m/T_o)

(iii) The circuit resistance

The average motor current was then given by:

$$I_M = 1/R\ (V_B\ t_m/T_o - E_M)$$

The above equation also indicates that for a fixed value of E_M, there is a value of t_m/T_o for which $I_M = 0$.

The correlation between the predicted and experimental values of I_M is shown graphically in figure 3.1. The curves agree to within 5%, except at low values of current, where the inductance is insufficient to maintain a continuous current in the motor. By increasing the inductance from 4 mH to 12 mH, a better correlation is obtained, however only for very large values of inductance will the curves agree better at low currents.

3.4 THE CORRELATION BETWEEN THE THEORETICAL AND MEASURED VALUES OF THE CURRENT RIPPLE.

The ripple content of the motor current is determined by the chopper frequency and value of inductance used. In the previous chapter, it was shown that the ripple factor was given by the equation:

$$r_{MAX} = \frac{V_B}{8 I_M f L}$$

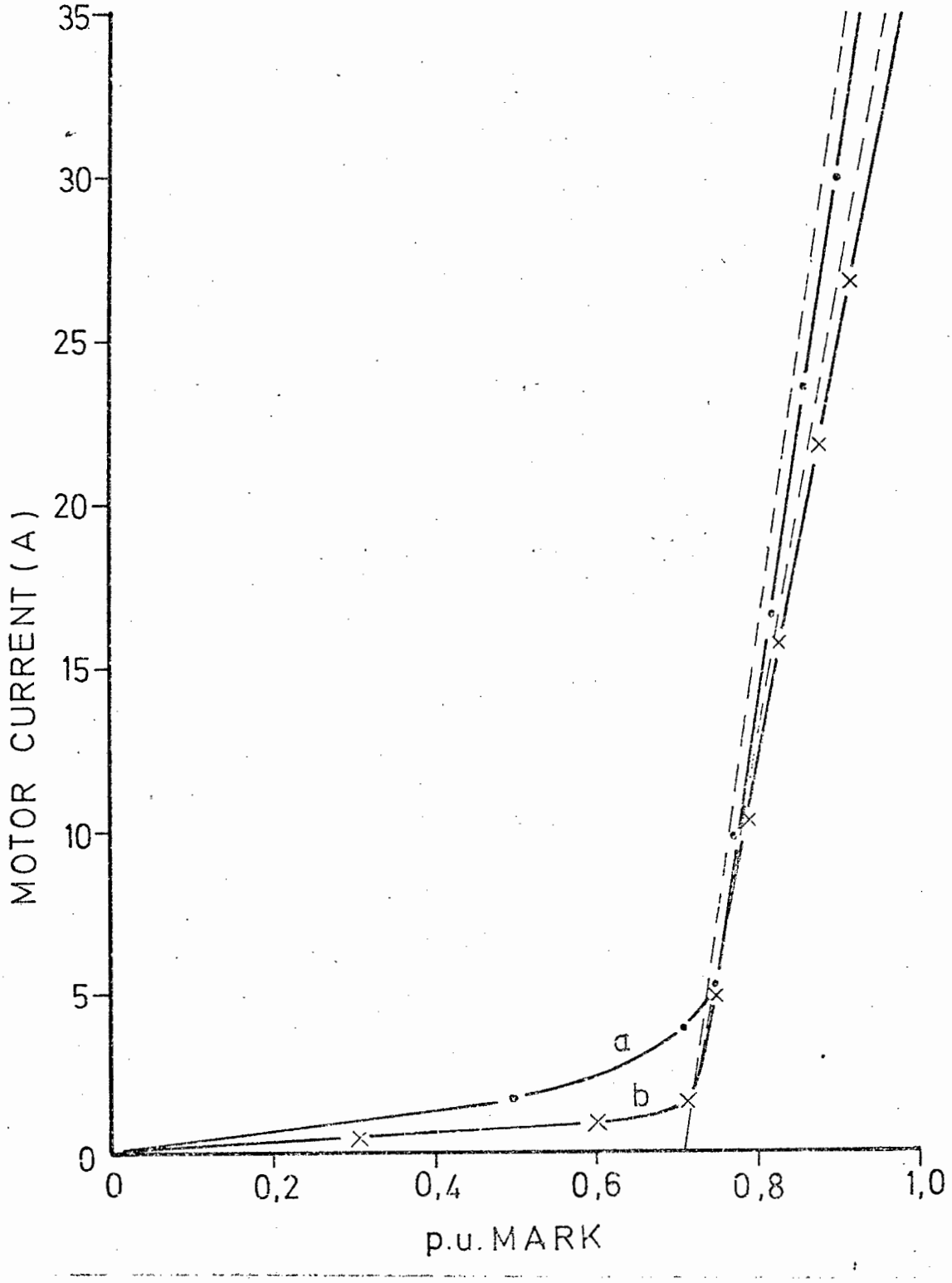

FIGURE 3.1 : DETERMINATION OF MOTOR CURRENT UNDER MOTORING CONDITIONS AT CONSTANT SPEED OF 1330 r.p.m.

--------- Theoretical curve

_____ Experimental curve

a : 4 mH in series with motor

b : 12 mH in series with motor

It was on the basis of this equation that the value of the inductance to be used was calculated. The correlation between the predicted and experimental values of ripple factor are shown graphically in figure 3.2. The curves agree to within 3% for I_M = 37A, and to within 7% for I_M = 20A. However, the agreement between the curves I_M = 10A is not good, as the approximations used in deriving the above equation are not sufficiently correct for large ratios of I_p/I_v.

3.5 EVALUATION OF THE PERFORMANCE OF THE CHOPPER AND MOTOR

To evaluate the performance of both the chopper and the motor, load tests were conducted and the results are shown in figures 3.3 - 3.8. These load tests served a dual purpose:

(a) They allowed the investigation of factors such as efficiency of operation, form factor and current multiplication.

(b) They enabled the total losses occurring in the motor and chopper to be separated into their constituent parts.

(i) Efficiency

The performance of the chopper and motor when operating at constant torque is shown in figures 3.3 and 3.4. Although the results indicate that the chopper and choke reduce the output efficiency at maximum speed by approximately 8%, this figure would be reduced to 5% if the motor was operated at its rated voltage of 150V.

(ii) Form Factor of the Motor Current

The variation of the form factor of the motor current with the per unit (p.u.) mark at the loadings of the motor (I_M = 37A, 20A) is shown in figure 3.5.

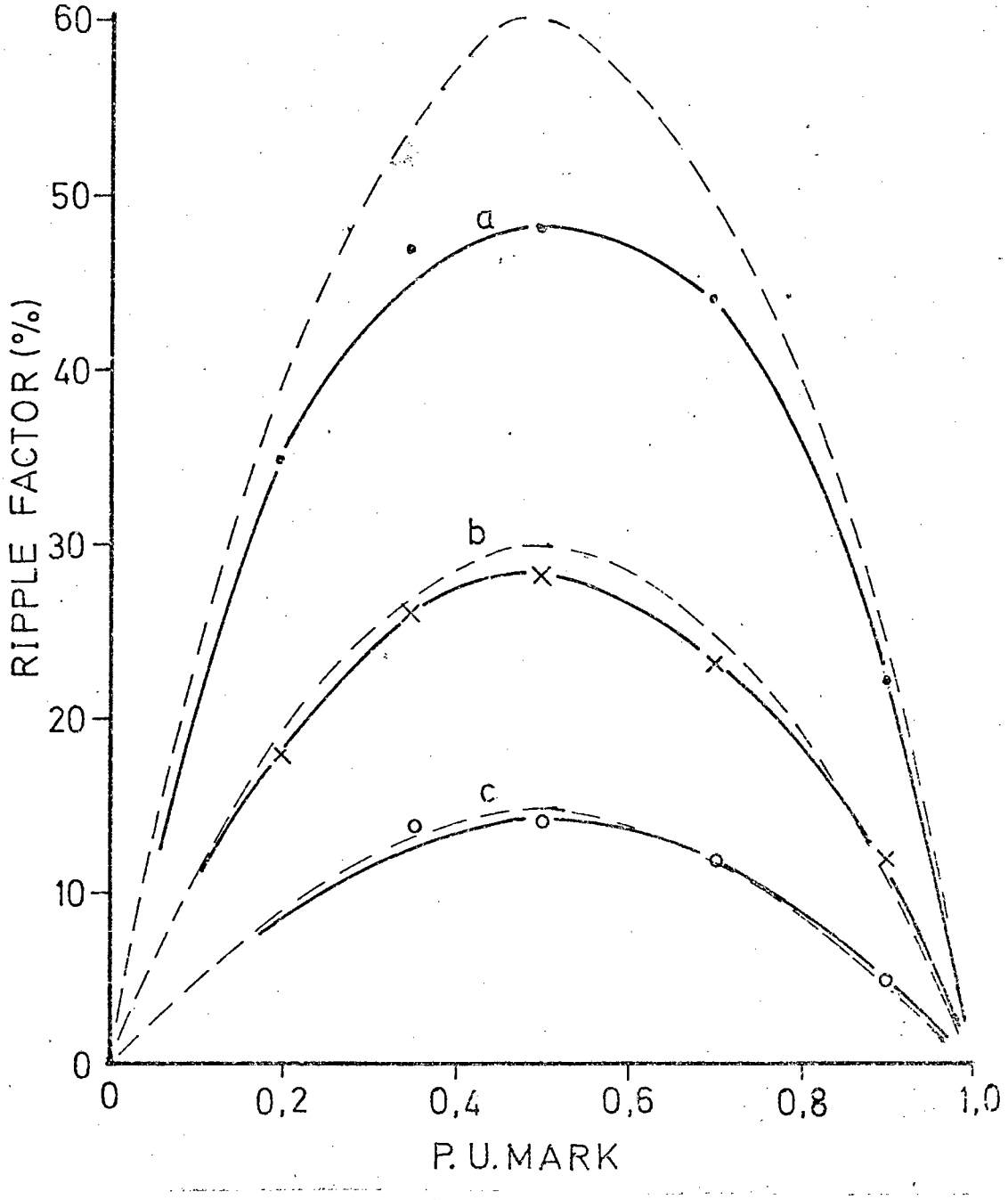

FIGURE 3.2 : RIPPLE FACTOR OF MOTOR CURRENT IN MOTORING

--------- Theoretical

_____ Experimental

a: I_M = 10A

b: I_M = 20A

c: I_M = 37A

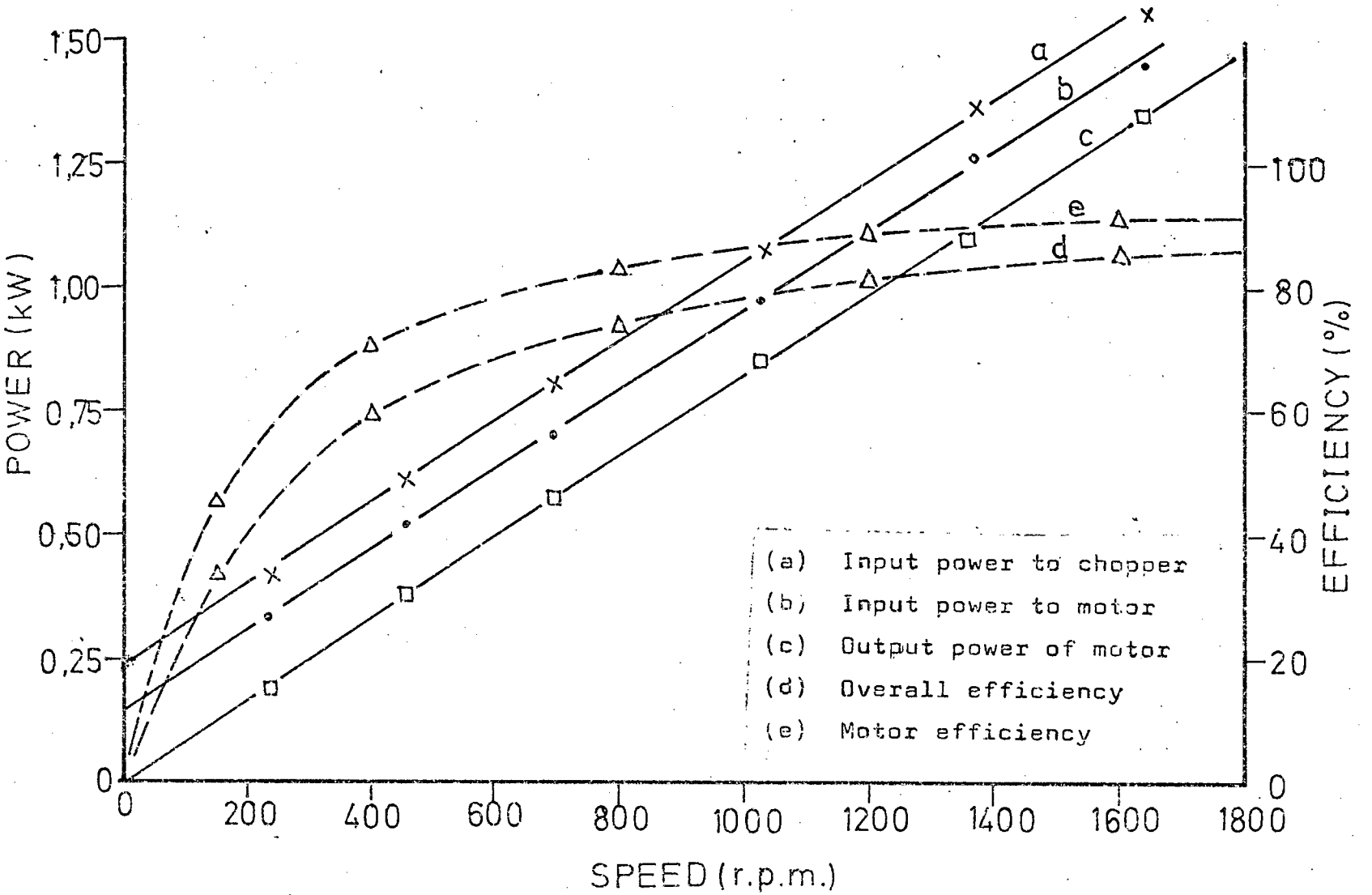

FIGURE 3.3 : PERFORMANCE OF MACHINE WHEN MOTORING AT CONSTANT ARMATURE CURRENT OF 20A SUPPLIED FROM CHOPPER.

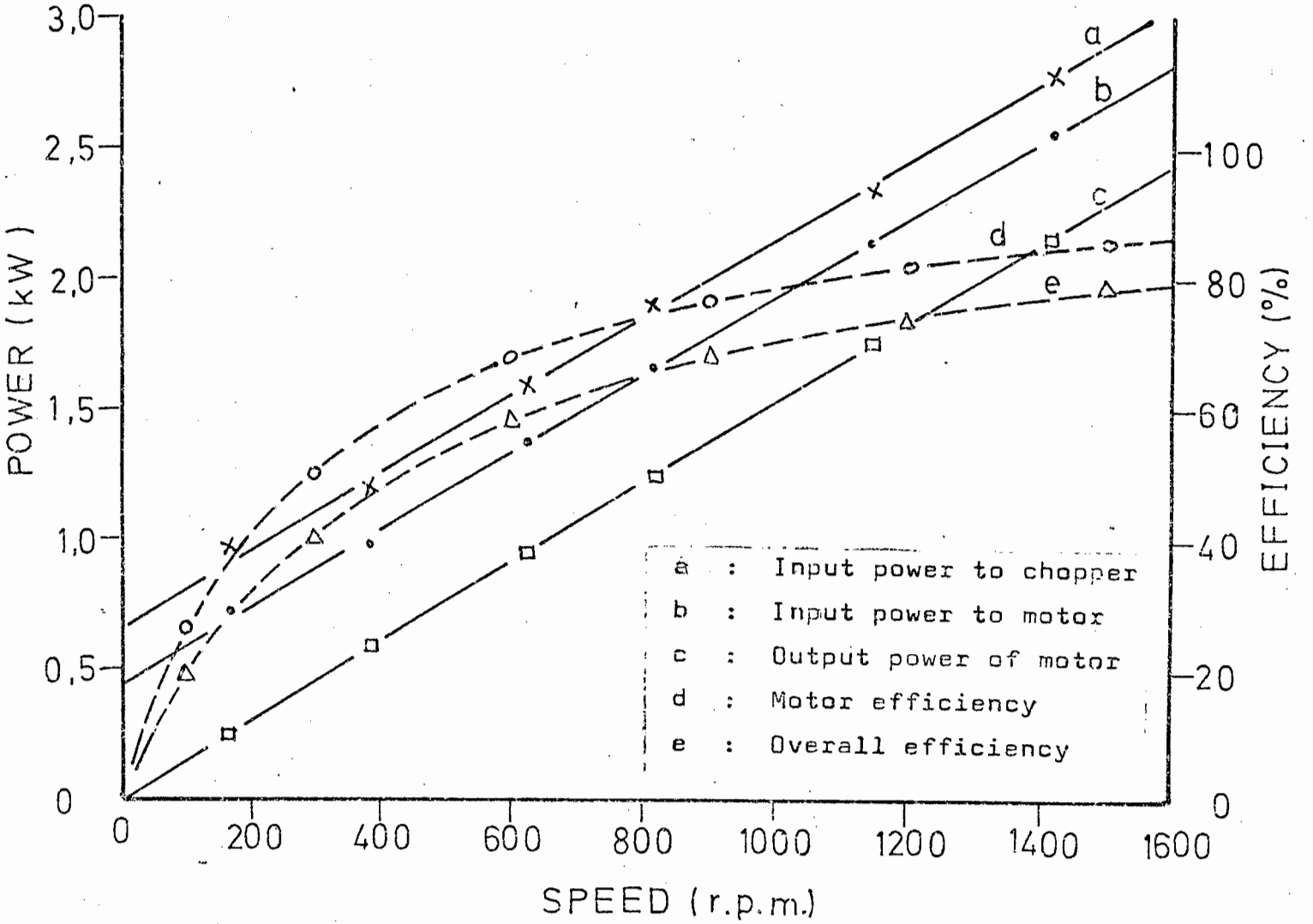

FIGURE 3.4: PERFORMANCE OF MACHINE MOTORING AT CONSTANT ARMATURE CURRENT OF 37A SUPPLIED FROM CHOPPER

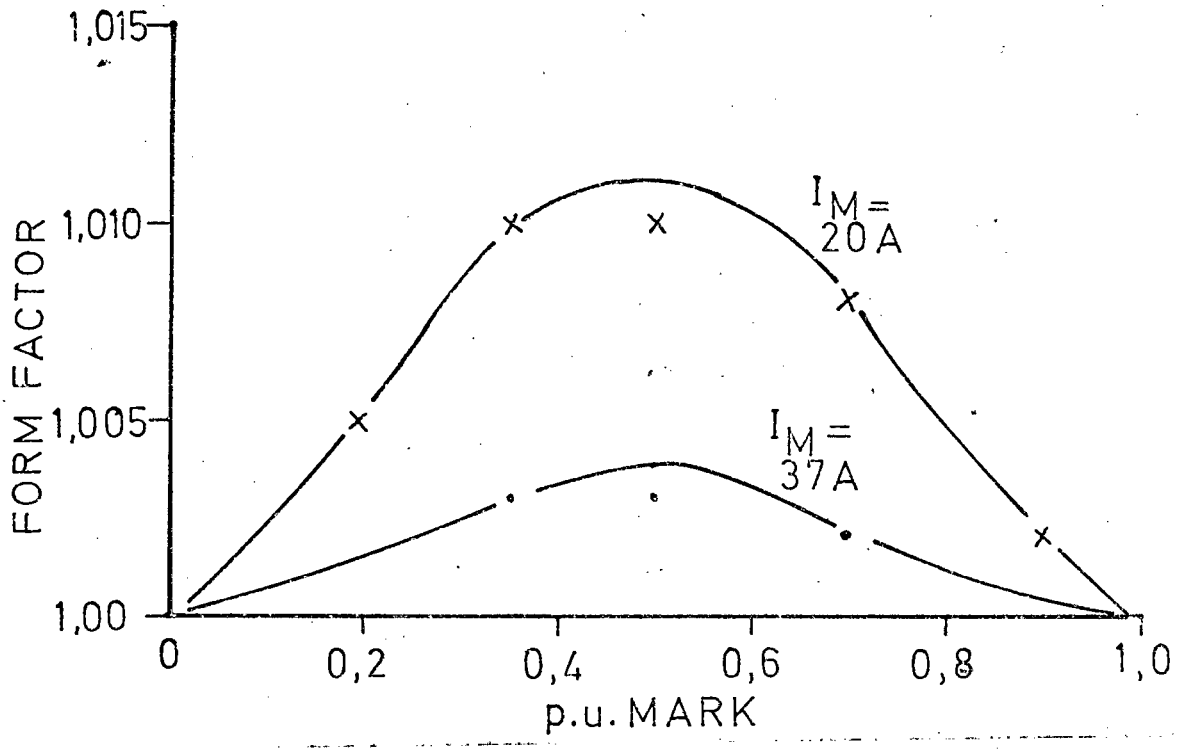

FIGURE 3.5 : FORM FACTOR OF MOTOR CURRENT AS A FUNCTION OF THE p.u. MARK.

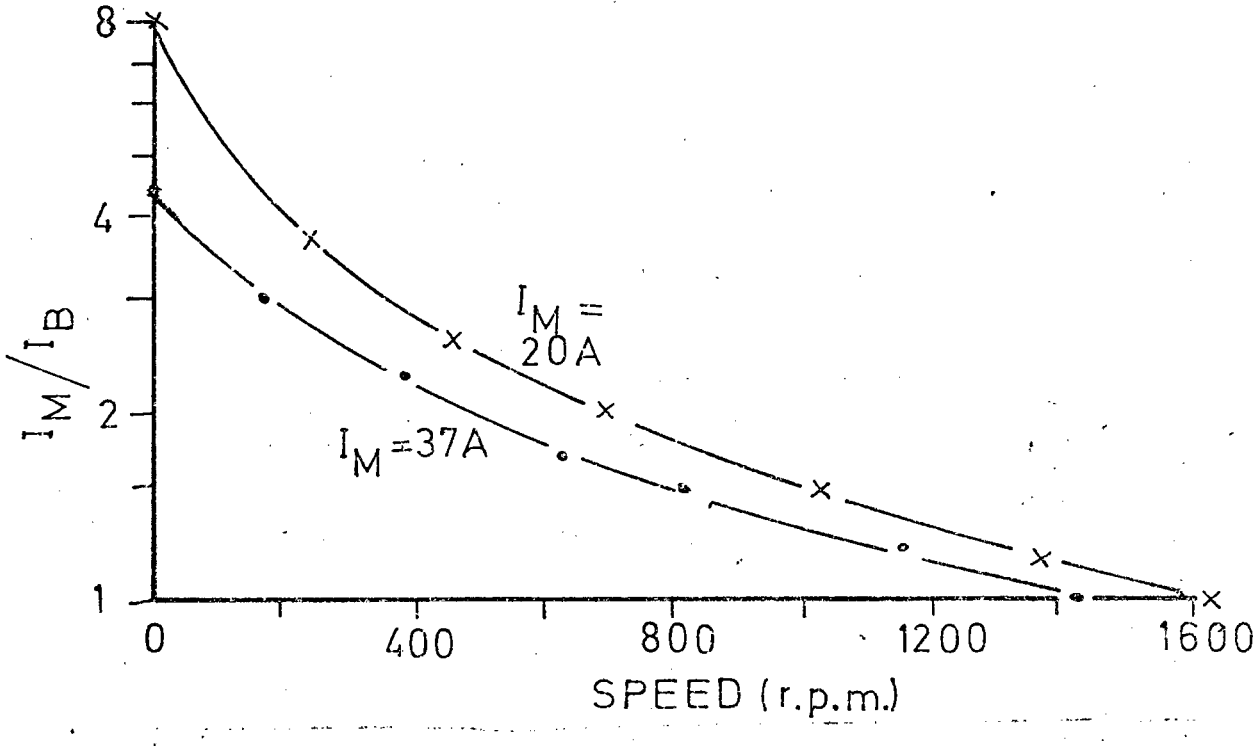

FIGURE 3.6 : CURRENT MULTIPLICATION RATIO FOR MOTOR AT CONSTANT TORQUE.

From these results it can be deduced that the maximum temperature rise in the armature will occur when the motor is operated continuously at full load torque in the region of half speed, i.e. for values of p.u. mark from 0,3 to 0,7. However, a vehicle operating in urban traffic may spend only a minor portion of its duty cycle in this speed region. Therefore, if the same battery/motor combination were used in a vehicle drive, the value of inductance could be reduced by as much as 50%, without causing the mean armature temperature to rise above the maximum value that would be recorded in a test such as that of figure 3.5.

(iii) Current Multiplication Ratio

The ratio I_M/I_B is shown as a function of speed in figure 3.6. The low values at stall (4.3 for 37A and 8.1 for 20A) can be ascribed to the motor being supplied from 84V instead of 150V. At a higher voltage, smaller values of t_m/T_o could be used to attain the same speed and torque, thereby increasing I_M/I_B by at least 50%. However, the results presented here do demonstrate the high ratio of motor to battery current that is possible at low speeds.

(iv) Power loss in Choke

In evaluating the efficiency of the motor and chopper, it is essential that the amount of power lost in the choke is known. These losses are shown as a function of the RMS current in figure 3.7. To create the maximum possible ripple in the current waveform at any given load, the chopper was set at 0,5 p.u. mark.

The power loss of 80W at 37A corresponds to 5% of the input power to the motor and half speed. At full speed, this percentage will be approximately halved. As the choke tested was designed for 50 Hz operation, the power loss could be reduced by 5 - 10% by using thinner laminations in the core.

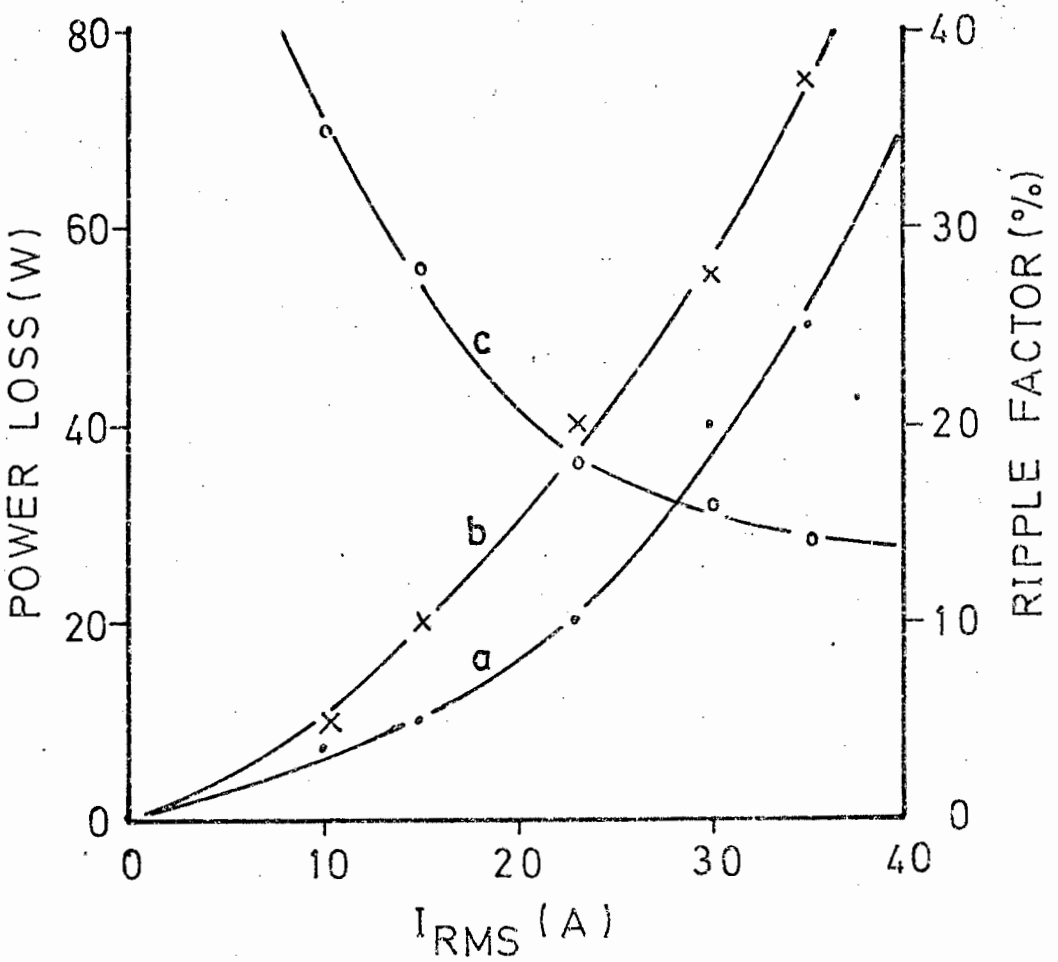

FIGURE 3.7 : POWER LOSS AND RIPPLE FACTOR OF A 4 mH CHOKE

a : Copper loss

b : Iron and Copper loss 400 Hz

c : Ripple Factor

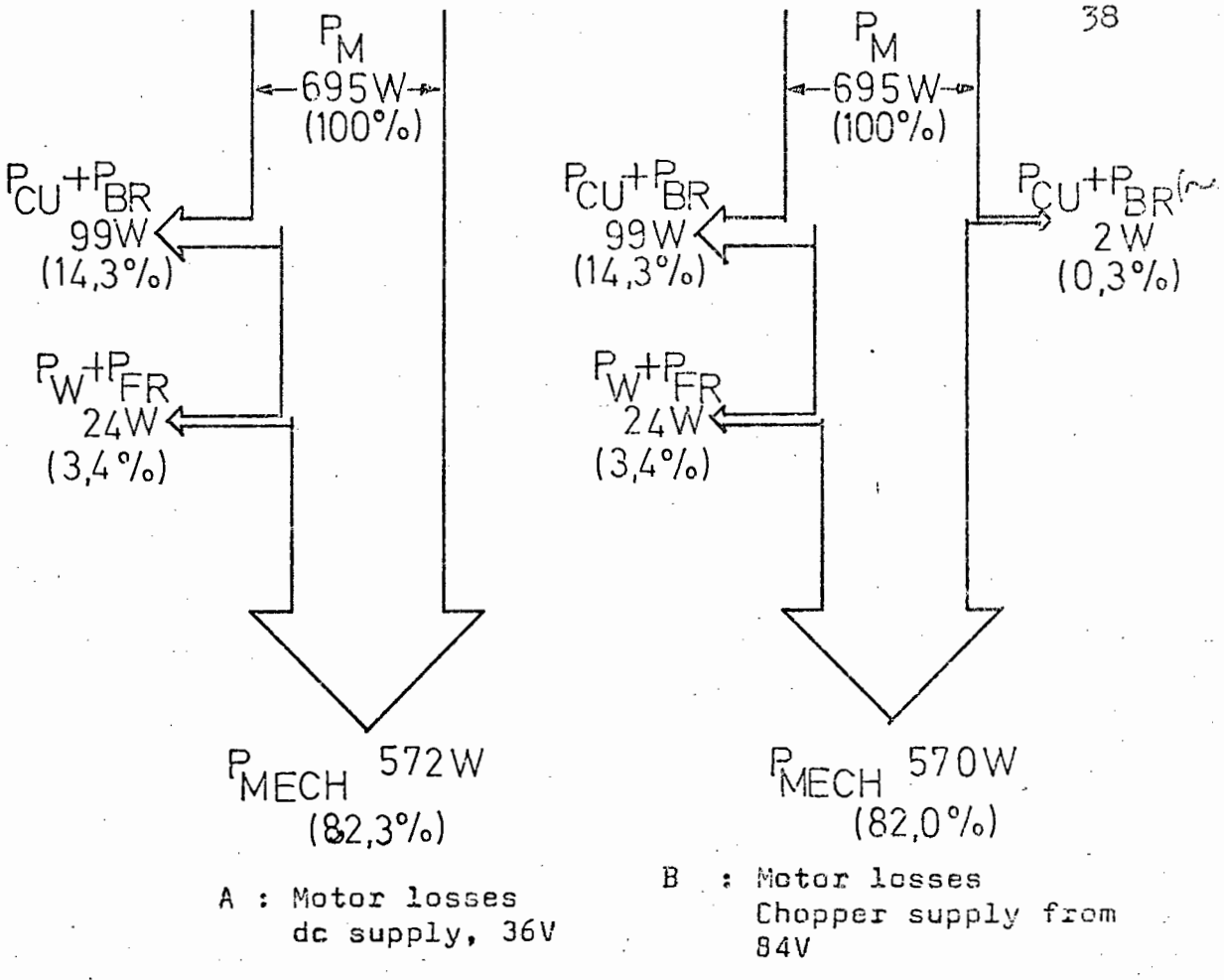

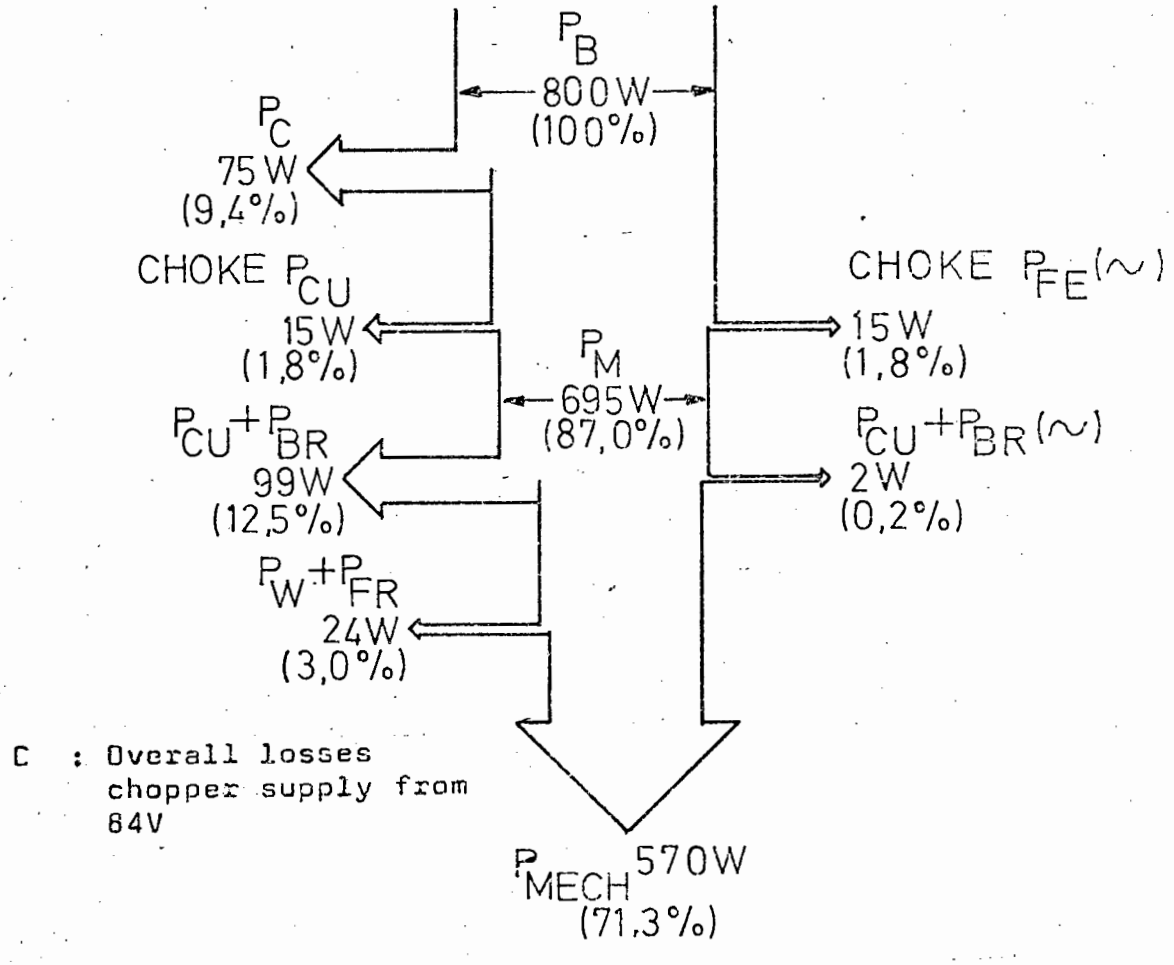

FIGURE 3.8 : SEPARATION OF POWER AND LOSSES IN MOTOR AND CHOPPER

(v) Separation of the total losses occurring in the Chopper and Motor.

To assess the contribution of the individual losses, it is necessary to separate the total losses occurring in the motor, choke and chopper. The motor was run at approximately half speed to obtain the maximum current ripple and the motor current was set at 20A to enhance this effect. To analyse the effect of the chopper on the losses occurring in the motor, it is necessary to deduce the individual losses that occur when the motor is supplied directly from a battery. These losses are shown diagramatically in figure 3.8A.

The quantities represented by the abbreviations are:

P_M = input power to motor

$P_{CU} + P_{BR}$ = copper and brush losses

$P_W + P_{FR}$ = windage and friction losses

P_{MECH} = mechanical output power of motor

Next, the losses occurring in the motor when supplied via a chopper are shown in figure 3.8B. So that these results would be comparable with those of figure 3.8A, the input power to the motor was kept the same in both cases. All the losses occurring in the motor, chopper and choke are shown in figure 3.8C (P_B = power supplied by the battery; P_C = power loss in the chopper). From this it is seen that the additional losses occurring in the motor due to the current form factor amount to only 0,2% of the total input power from the battery, whereas the choke consumes 3,6% of this power. This shows that the designed form factor is too conservative, and to optimise the overall efficiency, there should be more of a compromise between these two losses, by reducing the value of the inductance and by using thicker wire for the windings of the choke to reduce its series

resistance. However, the cost of such improvements should be taken into account.

From figure 3.8C, it is also seen that the chopper consumes 9,4% of the input power. This is because the semiconductors of the chopper have a constant forward voltage drop, causing the chopper power loss to be more appreciable, in relation to the total power consumed, at low motor speeds.

(vi) Voltage and Current Waveforms

Figures 3.9 - 3.11 show voltage and current waveforms recorded during motoring with both low and high values of the per unit mark. It may be seen from the figures how closely the real waveforms resemble the theoretical waveforms which were described previously. It is interesting to note how the peak-to-peak ripple of the motor current remains constant as the average current is increased (figures 39(a) and (b)).
3.9

3.6 SEPARATION OF LOSSES OCCURRING IN A BATTERY VEHICLE DURING ACCELERATION AND CONSTANT SPEED MOTORING.

From the results of the load tests given in the previous section, it is possible to predict the losses occurring in a vehicle control system. Two cases will be considered:

(i) The energy consumed during an acceleration from rest up to a maximum speed of this mode, taken as 50 km/h (14 m/s);

(ii) The power losses occurring while motoring at 50 km/h.

The total vehicle mass is taken as 600 kg, the rolling resistance for this mass is 132 Newtons, and the wind resistance is given by $0,5v^2N$, where v is in m/s. These figures are assumed at present, but will be dealt with in more detail in chapter 8.

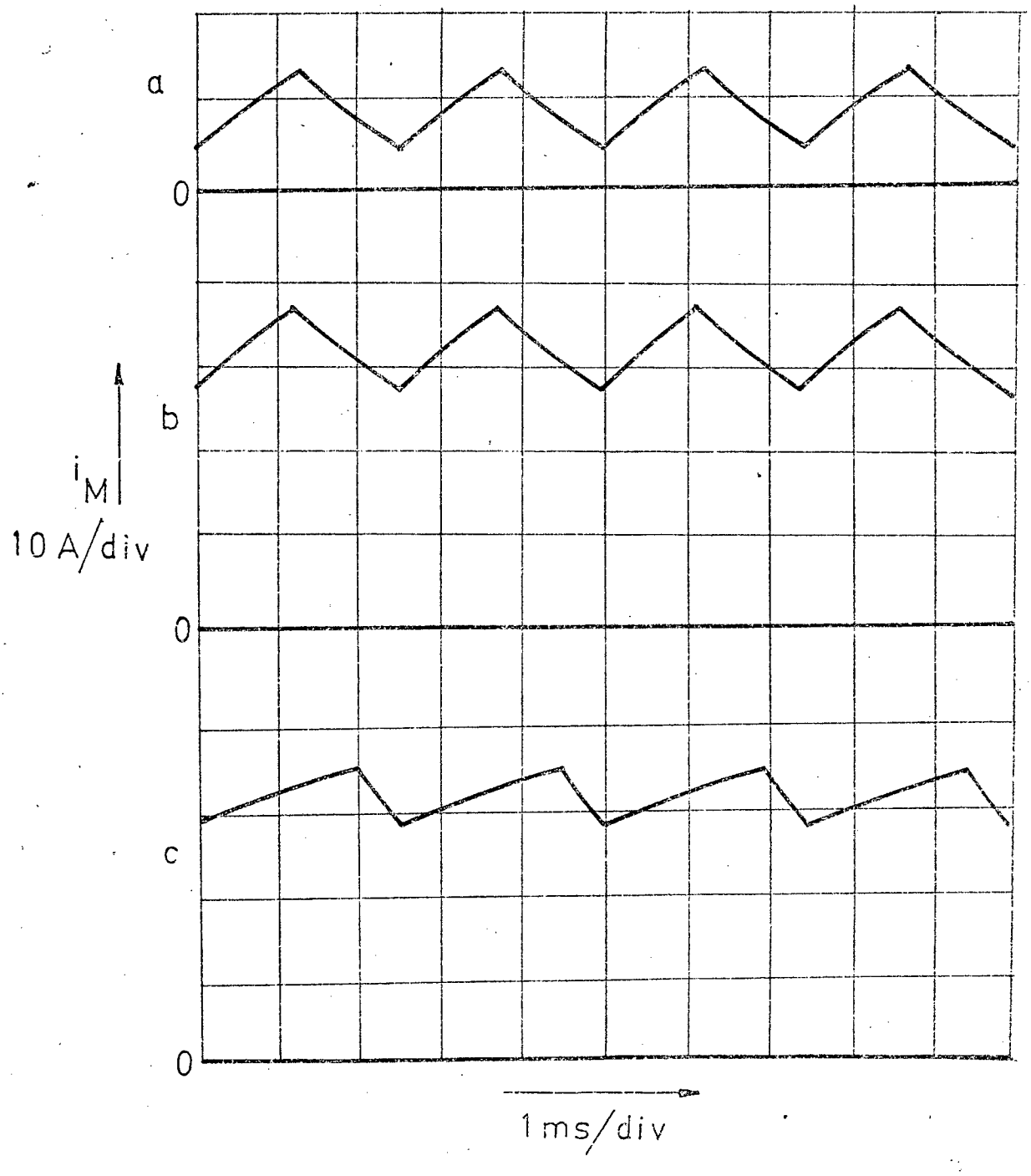

FIGURE 3.9 : MOTOR CURRENT WAVEFORMS

(a) I_M = 10A, 0,5 p.u. Mark
(b) I_M = 37A, 0,5 p.u. Mark
(c) I_M = 37A, 0,8 p.u. Mark

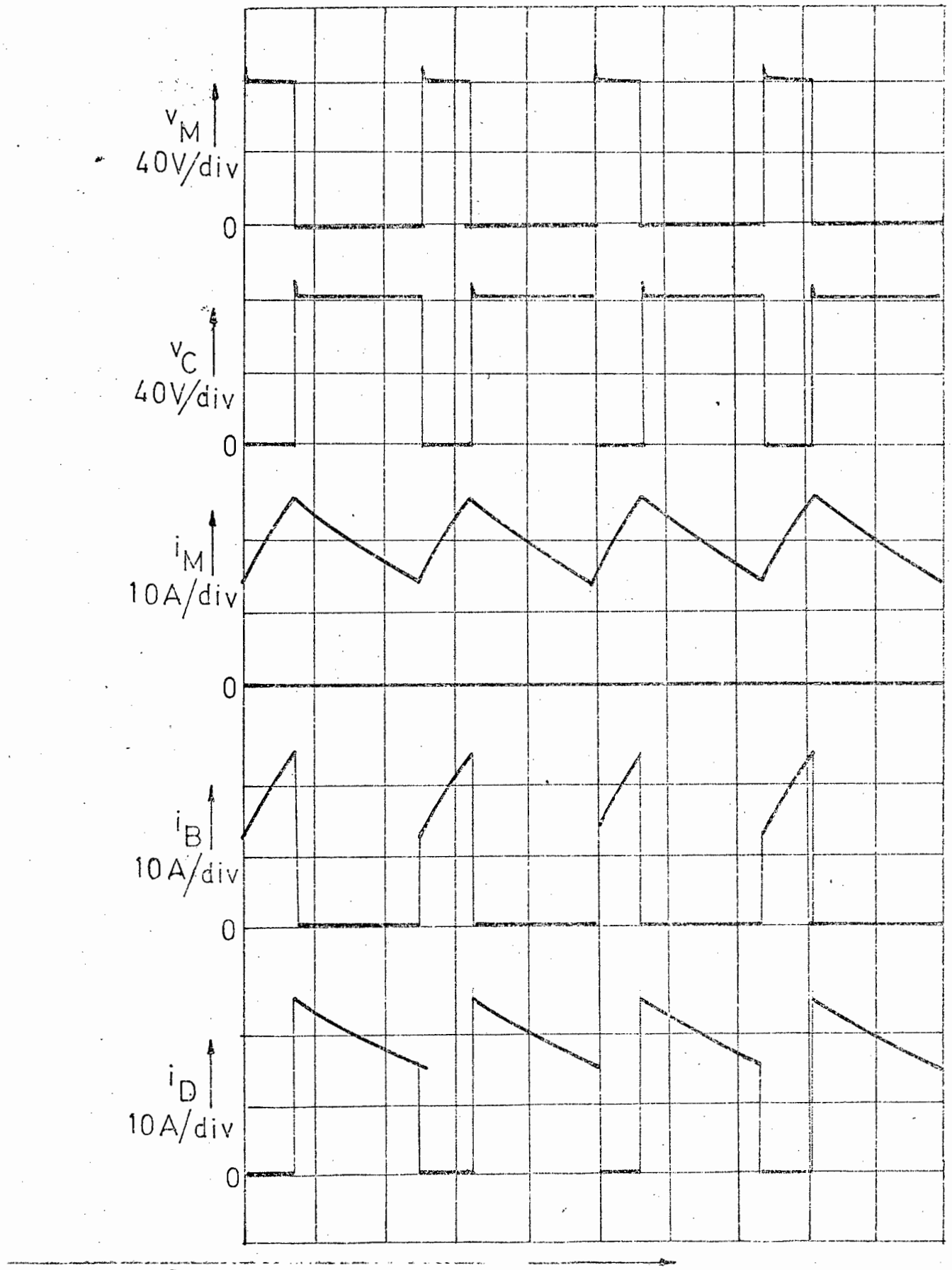

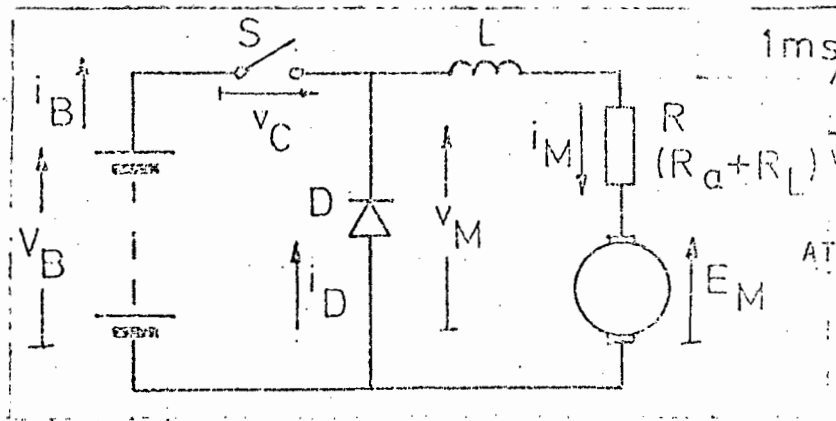

FIGURE 3.10 : VOLTAGE AND CURRENT WAVEFORMS DURING MOTORING AT 400 r.p.m. (0,3 p.u. MARK)

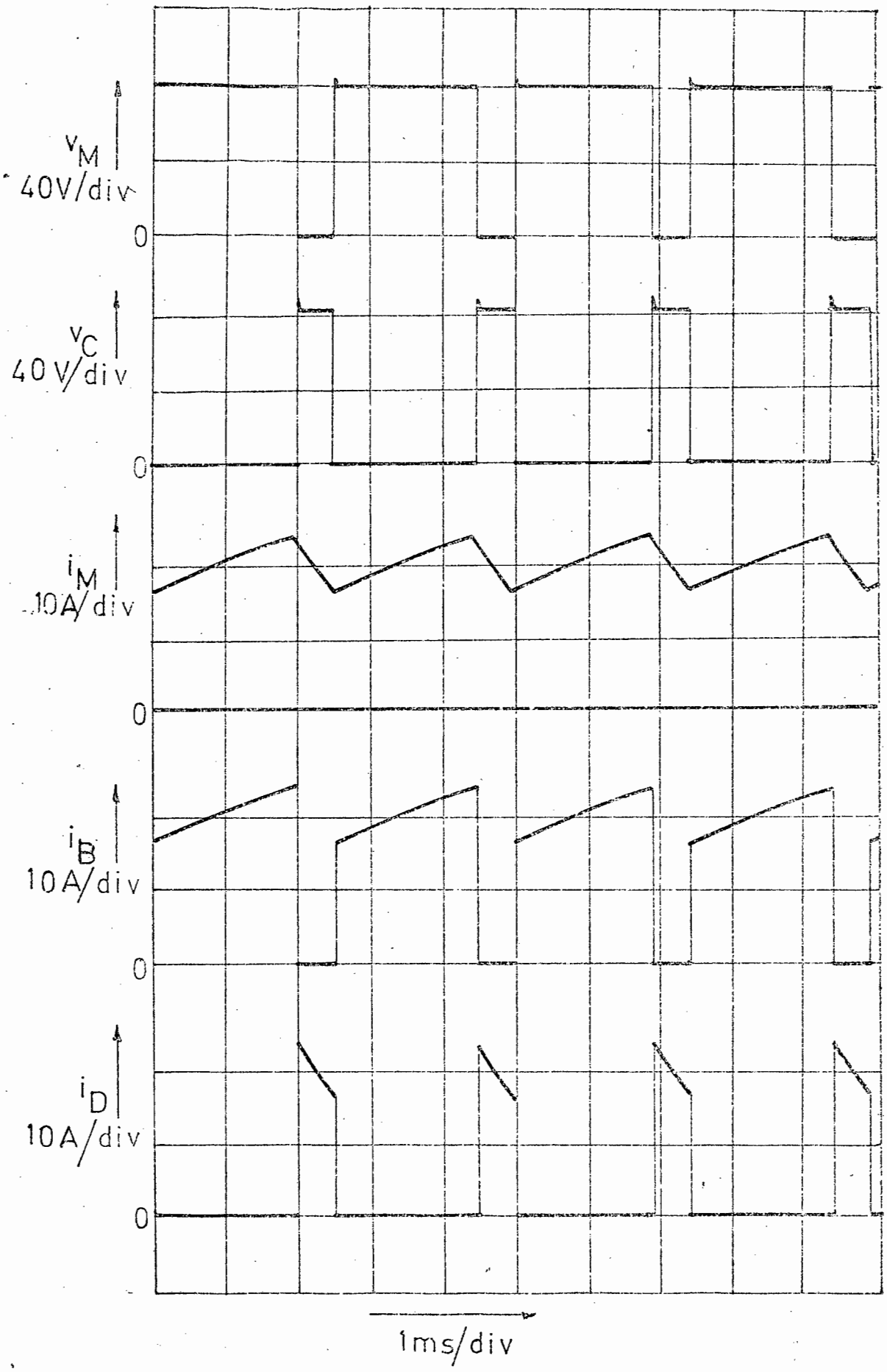

FIGURE 3.11 : VOLTAGE AND CURRENT WAVEFORMS DURING MOTORING AT 1300 r.p.m. (0,8 p.u. MARK)

(i) Energy consumed during a single acceleration.

It is assumed that the vehicle accelerates uniformly from rest, at maximum motor torque, attaining the speed 14 m/s in 20 seconds. The distance covered during this acceleration will therefore be 140 metres. ✓ 0,7 m/s²

(a) Vehicle kinetic energy achieved:

$$E_V = \tfrac{1}{2}\, mv^2 = \tfrac{1}{2} \times 600 \times 14^2/3600$$

$$= \underline{17Wh}$$

(b) Energy lost by overcoming rolling resistance:

$$E_R = 132 \times 140/3600$$

$$= \underline{5Wh}$$

(c) Energy lost by overcoming wind resistance:

$$E_W = 0,5v^2\ ds \quad (s = \text{distance covered})$$

$$= 2 \times 0,5 \times a \int_0^{140} s\ ds \quad (a = \text{acceleration})$$

$$= 0,7 \times 0,5 \times 140^2/3600$$

$$= \underline{2WH}$$

(d) Transmission energy loss:

Assume 10% of the energy that is transmitted is absorbed in the transmission.

Energy transmitted = 24Wh

Energy lost = 2,4Wh

(e) Energy loss occurring in motor:

The average motor efficiency at maximum torque over the entire speed range may be calculated from figure 3.4. The value obtained was 65%.

Therefore, the energy loss occurring in the motor

$$= 35 \times 26,4/65$$

$$= \underline{14,2Wh}$$

(f) Chopper energy loss:

The average power loss in the chopper is proportional to the per unit mark, which is proportional to speed, and in turn, to time.

Therefore, $E_C = \frac{1}{2} P_c \times t$

$= \frac{1}{2} \times 5 \times 37 \times 20/3600$

$= \underline{0,5WH}$

(g) Battery energy supplied

E_B = total of the individual energies

$= \underline{41Wh}$

(h) Comments

The energy distribution for a single acceleration is shown diagramatically in figure 3.12. Once again, it must be pointed out that the efficiency of the motor at low speeds is degraded because the motor was not operated over its rated speed range of 0 - 3000 r.p.m. This accounts for the value of average efficiency of only 65%, given in (a) above. Had the machine been accelerated from 0 = 3000 r.p.m., this value would have been closer to 75%.

From figure 3.12 it is seen that the major portion of the battery energy that is supplied is consumed by the losses of the system. Less than 50% of the battery energy is converted into kinetic energy of the vehicle.

(ii) Power losses occurring at a constant speed of 50km/h.

Using the same values of wind and rolling resistance as given previously, the individual power losses occurring in a vehicle drive system may be predicted.

(a) Power loss occurring in the chopper and motor:

From figure 3.4, it is seen that approximately 5% of the input power is consumed in the chopper and 15% in the motor.

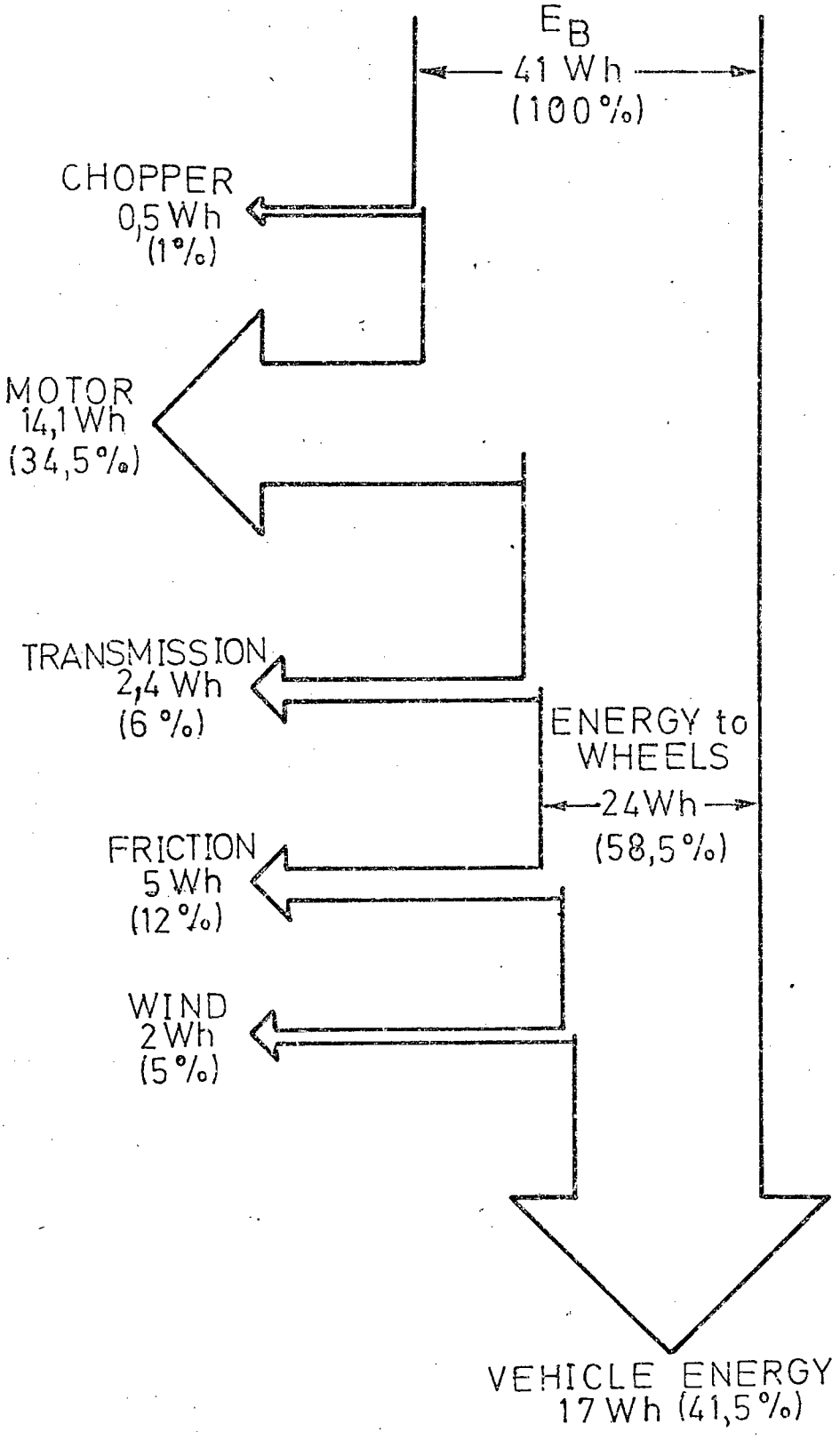

FIGURE 3.12: DIVISION OF ENERGY OCCURING IN A 600 kg ELECTRIC VEHICLE ACCELERATED FROM REST TO 50 km/h.

(b) Power loss occurring in the transmission:

A figure of 10% is assumed.

(c) Friction and wind losses:

The remaining 70% of the input power may be divided in the ratio of the rolling and wind resistances at 50km/h.

Rolling resistance = 132N

Wind resistance = $\frac{1}{2} \times 14^2 = 98N$

Therefore 40% of the input power is required to overcome the friction losses, and 30% is required to overcome the wind resistance. The above data are shown diagramatically in figure 3.13.

3.7 COMMENTS.

The test results presented in this chapter show that the measured and calculated values of average current and current ripple agree to within 10% over a wide range of load current.

The chopper and choke cause a loss in overall efficiency of 8%, of which 3% is attributed to the choke. To optimise the efficiency and cost of the system, there must be a compromise in the battery voltage selected, and between the losses in the motor and in the choke.

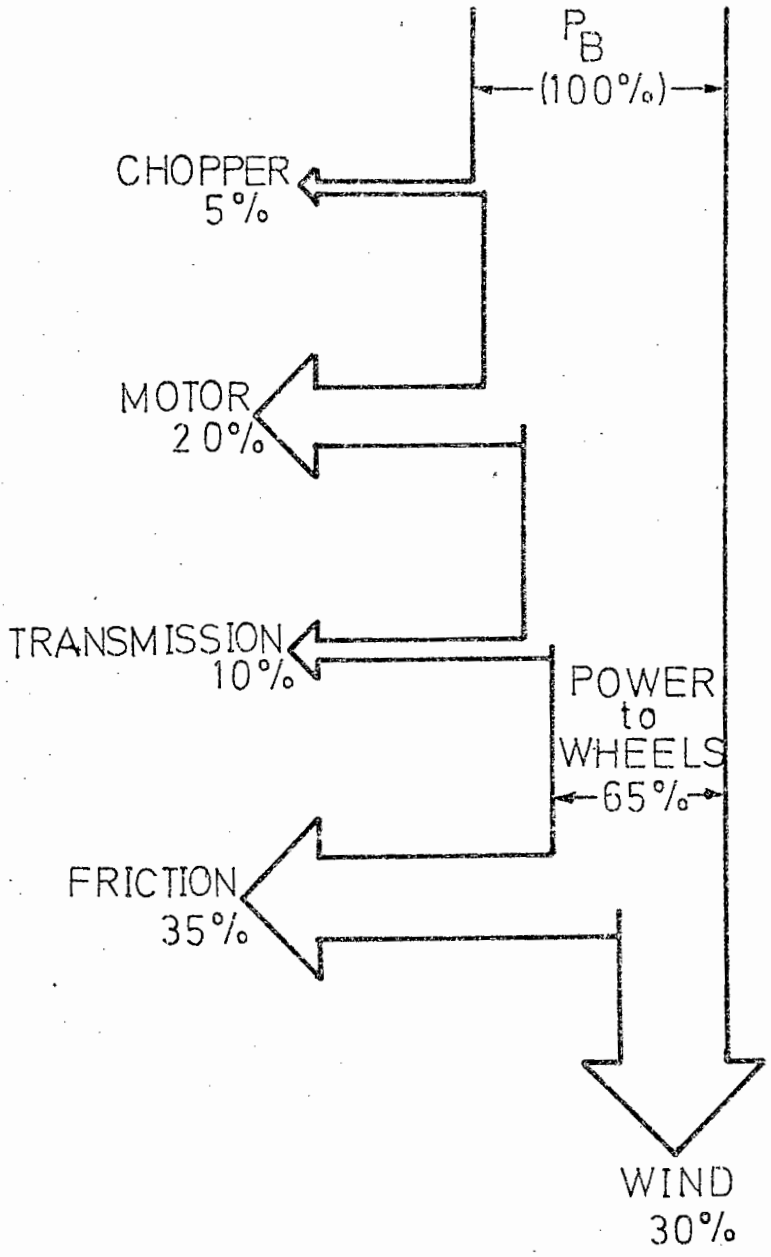

FIGURE 3.13: DIVISION OF POWER LOSSES IN A 600 kg VEHICLE TRAVELLING AT 50 km/h.

CHAPTER 4.

THE PERFORMANCE OF THE MACHINE IN THE MODE OF REGENERATIVE BRAKING OVER THE RANGE $0 \leq E_M \leq V_B$

4.1 INTRODUCTION

The advantages of a regenerative braking system over a mechanical or dynamic braking system were discussed in chapter one. The principle of operation of the circuit, whereby it is possible to return energy to the battery from a lower voltage source, was explained in chapter two. This chapter will present the experimental results of this mode and show that it is possible to increase the range of a vehicle if regenerative braking is used.

4.2 THE CORRELATION BETWEEN THE THEORETICAL AND MEASURED VALUES OF THE AVERAGE MOTOR CURRENT.

Equation 2.23 indicated that the average current was determined by the per unit mark, the back-emf of the machine and the circuit resistance. The average motor current was measured as a function of the p.u. mark with the motor speed kept constant, and the correlation between the experimental and calculated values is shown in figure 4.1. The agreement is better than 5% with both the 4mH and 12mH chokes, but with the 12mH choke, better correlation is obtained at the lower currents, as the current ripple is reduced by a factor of 3. However, over the major portion of the current range the value of I_M is independent of the value of the inductance.

4.3 THE EVALUATION OF THE PERFORMANCE OF THE MOTOR AND CHOPPER IN THE REGENERATIVE BRAKING CONFIGURATION.

To study the performance of the motor and chopper in this configuration, load tests were conducted, and results are shown in figures 4.2 and 4.3.

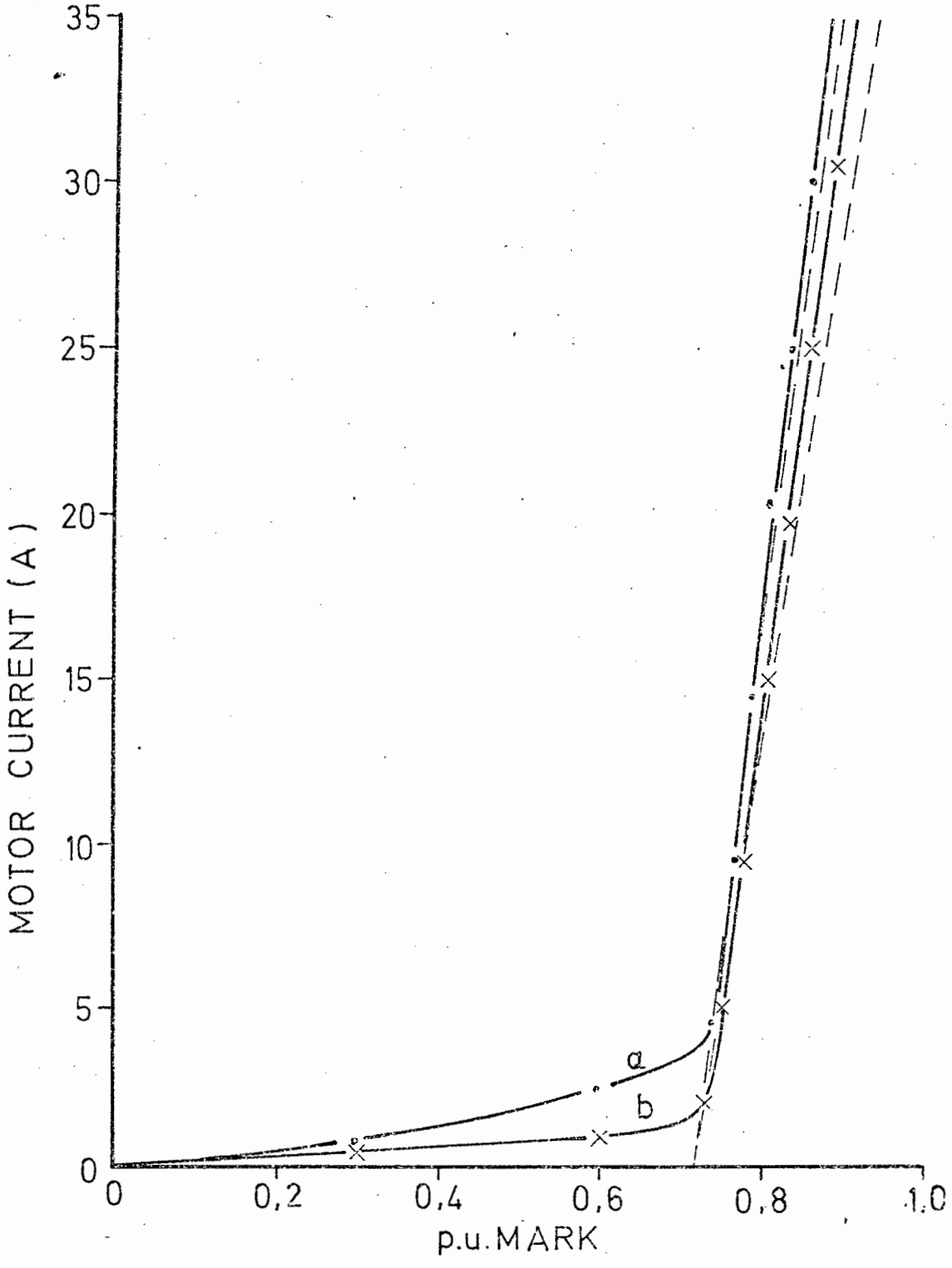

FIGURE 4.1 : DETERMINATION OF AVERAGE MOTOR CURRENT UNDER BRAKING CONDITIONS AT CONSTANT SPEED OF 620 r.p.m.

-------- THEORETICAL CURVE

_____ EXPERIMENTAL CURVE

(a) : 4 mH in series with motor

(b) : 12 mH in series with motor

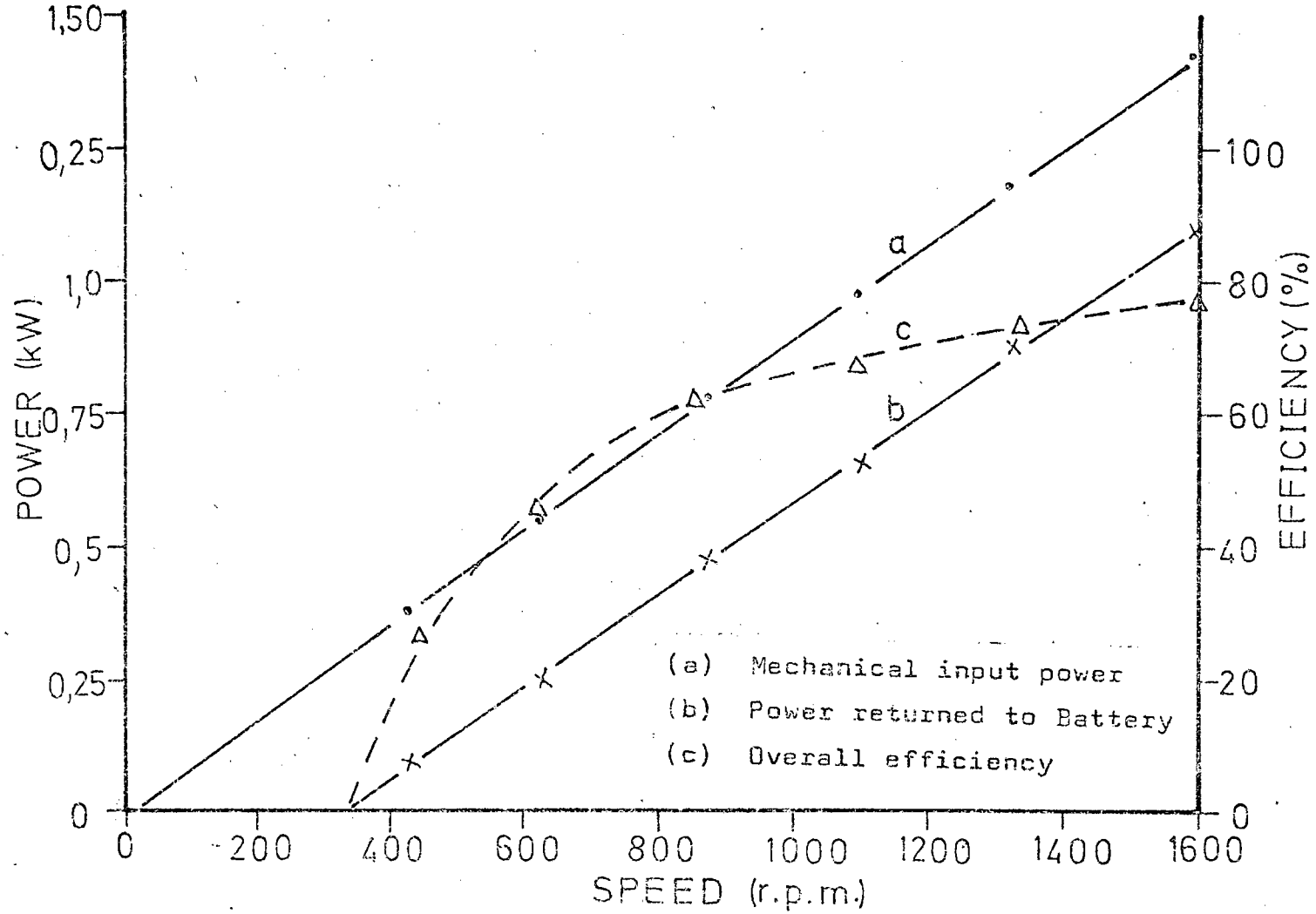

FIGURE 4.2 : PERFORMANCE OF MACHINE WHEN REGENERATIVE BRAKING AT CONSTANT TORQUE (I_M = 20A)

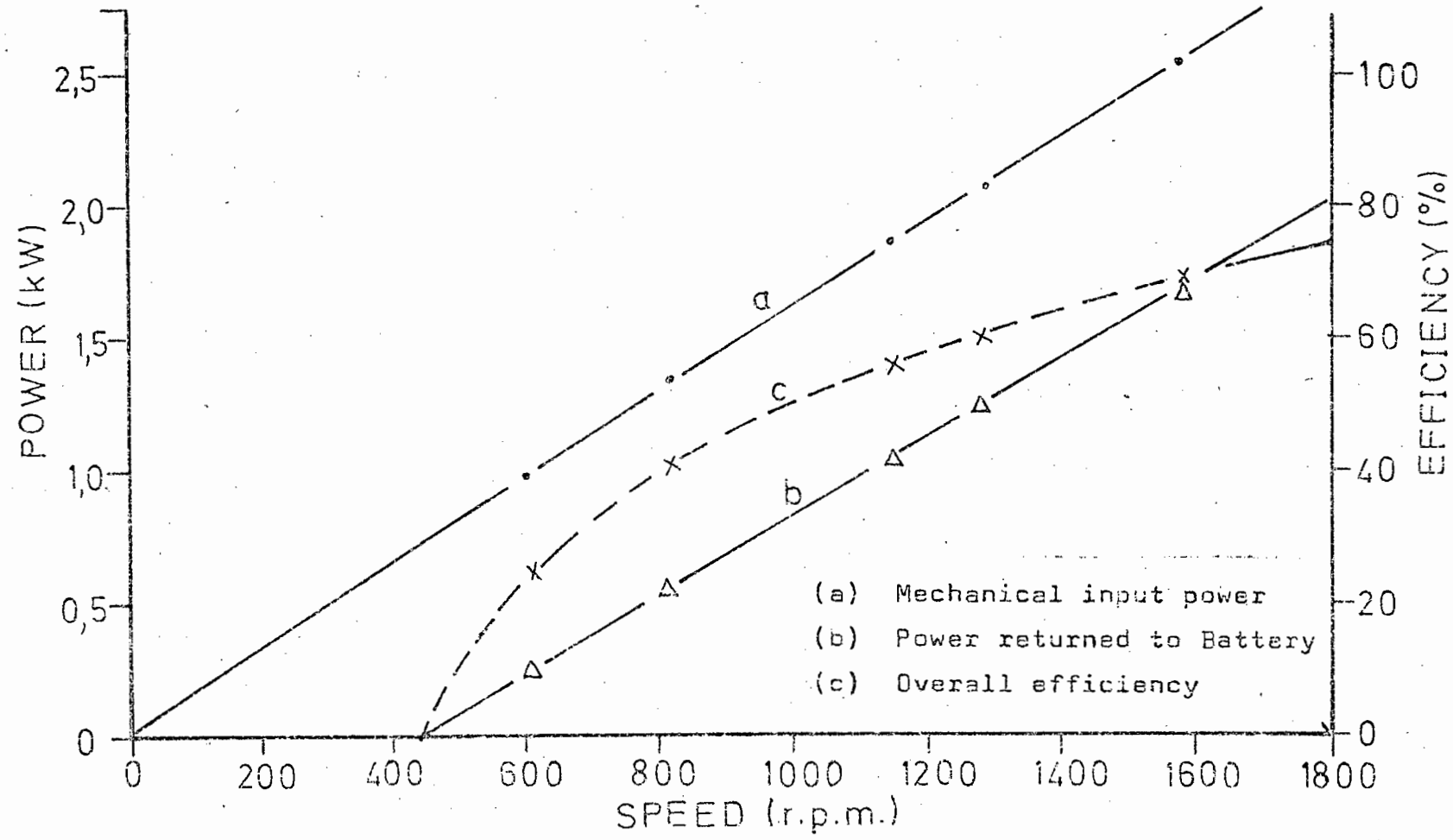

FIGURE 4.3 : PERFORMANCE OF MACHINE WHEN REGENERATIVE BRAKING AT CONSTANT CURRENT OF 37A (i.e. FULL LOAD TORQUE)

(i) Efficiency

The efficiency of regeneration (mechanical to electrical), and the amount of power returned to the battery are shown as functions of speed at constant torque, i.e. constant armature current. The efficiency rises uniformly for speeds above 1000 r.p.m., reaching almost 80% at 1600 r.p.m. As the battery voltage rises when high charging currents are passed into it, the upper speed could have been extended to approximately 2500 r.p.m., at which point the motor back-emf would have exceeded the battery voltage, and the control of the motor current by the chopper would have been lost. At speeds in excess of 2000 r.p.m., efficiencies greater than 80% are possible. The motor was restricted to the range illustrated in figures 4.2 and 4.3 so as to relate the results during braking with those during motoring (figures 3.3 and 3.4).

(ii) Braking at low speeds

To brake the machine when the vehicle is proceeding slowly, it may be necessary to keep the chopper closed in order to achieve the desired braking torque. Under these conditions, all regenerative capability is lost. The back-emf at which this occurs can be calculated from the following equation:

$$E_M = I_M R + V_c \quad \ldots\ldots\ldots\ldots\ldots\ldots\ldots\ldots\ldots\ldots (4.1)$$

where V_c = chopper voltage drop

for example, at 37A:

$$E_M = 37 \times 0{,}45 + 3 = 19{,}6V$$

or N = 468 r.p.m.

From curve (b) of figure 4.3, N = 450 r.p.m., an agreement of 4%. It is important to note that this speed is not a function of the battery voltage, but is a characteristic of the chopper and motor combination. If the motor were operated over its rated speed range

of 0 - 3000 r.p.m., regenerative braking would be effective down to 13% of the maximum speed. In terms of road speed, a vehicle with a top speed of 70km/h, would be able to regenerate down to 9km/h.

(iii) Form factor and circuit losses when braking.

The form factor of the motor current waveform, and the individual losses in the circuit were investigated, but as the results are very similar to those obtained in chapter 3 for motoring, the results are not shown here.

(iv) Waveforms

Typical voltage and current waveforms are shown in figure 4.4.

4.4 THE ADVANTAGES OF REGENERATIVE BRAKING AS ILLUSTRATED BY CYCLIC ACCELERATION AND BRAKING TESTS.

(i) Using a flywheel to store energy

In order to evaluate the amount of energy returned to the battery during regenerative braking, in relation to the energy expended during acceleration of a vehicle over some specified speed range, it is necessary to have some means available of storing energy. A flywheel coupled to the motor does provide such a means, if the flywheel has kinetic energy comparable with that of the vehicle. An indication of the amount of kinetic energy required is shown by the following calculations:

Consider a vehicle with a mass of 600kg and a top speed of 50km/h (14 ms).

At this speed, $E = \frac{1}{2} M_v^2 = \frac{1}{2} \times 600 \times 14^2$

$= 6 \times 10^4$ Joules.

If at this speed the motor was running at 1500 r.p.m., the moment of inertia (J) ~~required by~~ the flywheel would be

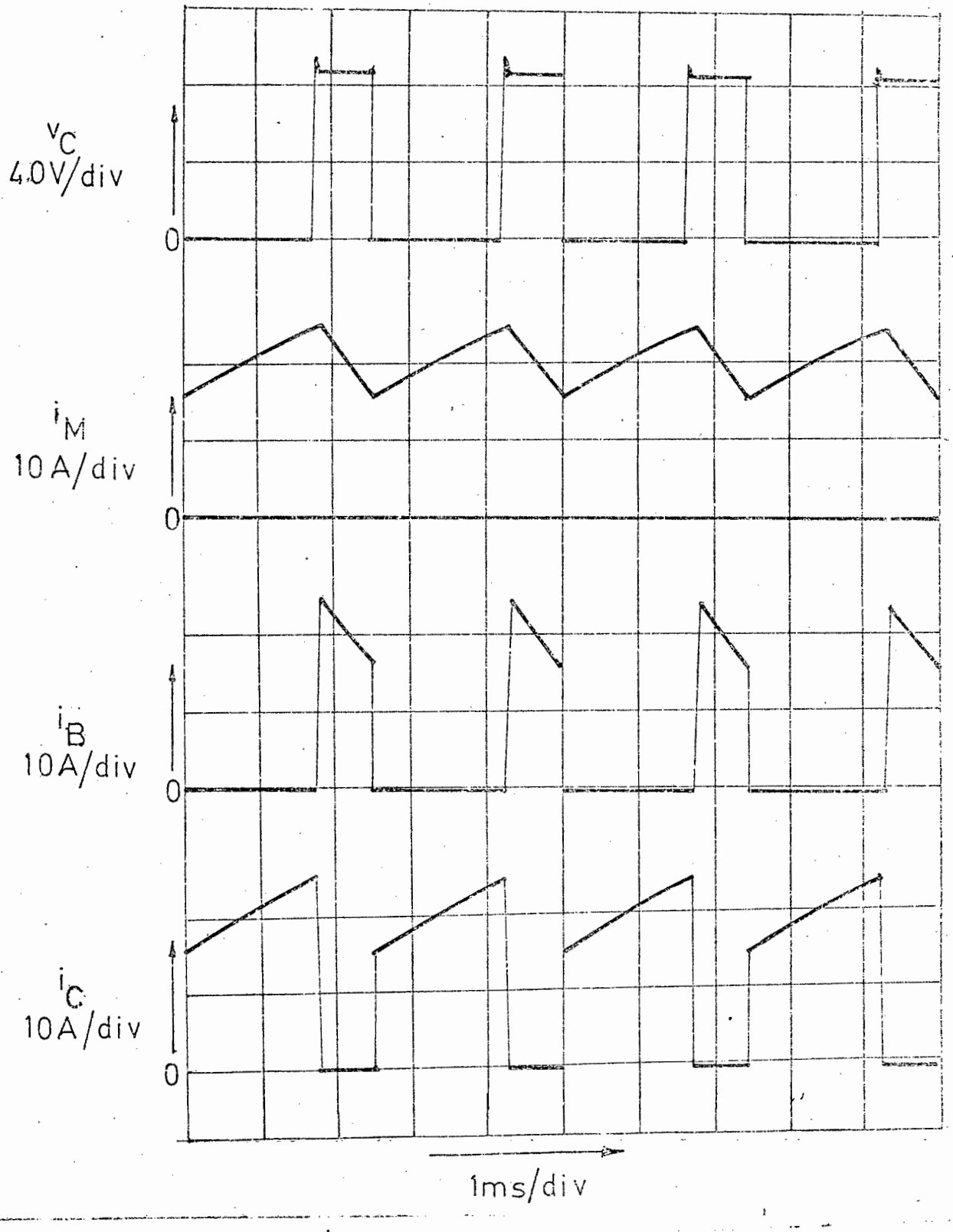

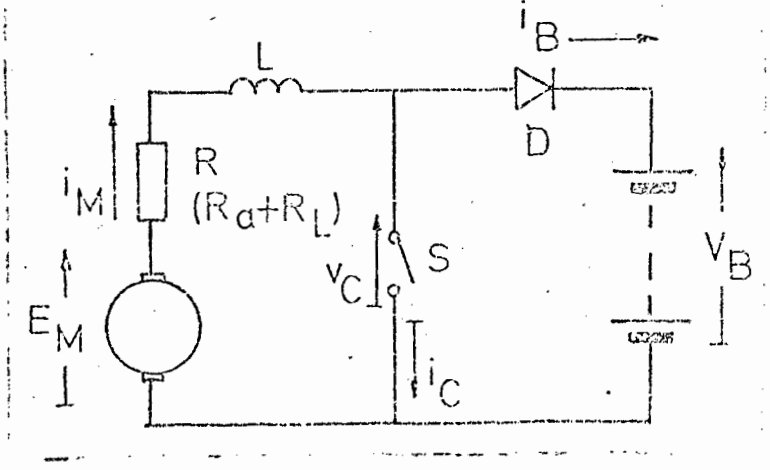

FIGURE 4.4: VOLTAGE AND CURRENT WAVEFORMS DURING REGENERATIVE BRAKING. OVER THE RANGE $E_M \leq V_B$.

$$E = \tfrac{1}{2} J w^2$$

$$J = 12 \times 10^4 / 2{,}5 \times 10^4$$

$$= 4{,}8 \text{ kgm}^2$$

A flywheel of outside diameter 0,62m and mass 100kg would fulfill these requirements. A flywheel of this size could not be found and a smaller one, of the type used on alternators, was used. This had a mass of 64kg., a moment of inertia of 0,95kgm^2, and an outside diameter of 420mm.

(ii) A comparison of the energies used by resistive, chopper and regenerative controllers.

Resistive and chopper controllers were compared by measuring the amount of battery energy required to accelerate the permanent magnet motor and flywheel up to a given speed. The difference between the readings would indicate the saving in energy gaining by using the chopper controller. A similar measurement, taken during regenerative braking, would indicate the percentage of the energy used during acceleration that could be returned during braking. During both acceleration and braking, the motor torque was kept constant.

Figure 4.5 shows the results for two motor torques and two speed ranges. The amount of energy is represented by the height of the blocks, those blocks above the horizontal axis indicating acceleration, and those below indicating braking. For some of the tests, the speed was restricted to the range 500 - 1500 r.p.m. This was to achieve full benefit from the regenerative system, which becomes inoperative below 500 r.p.m., as was explained in section 4.3 (ii).

By using the chopper instead of the resistive controller, the energy consumed during acceleration is reduced by approximately 35%. Under severe stop-start conditions, a chopper controller would offer a greatly increased range for a vehicle. The results indicate that

(ENERGIES GIVEN ARE IN Wh.)

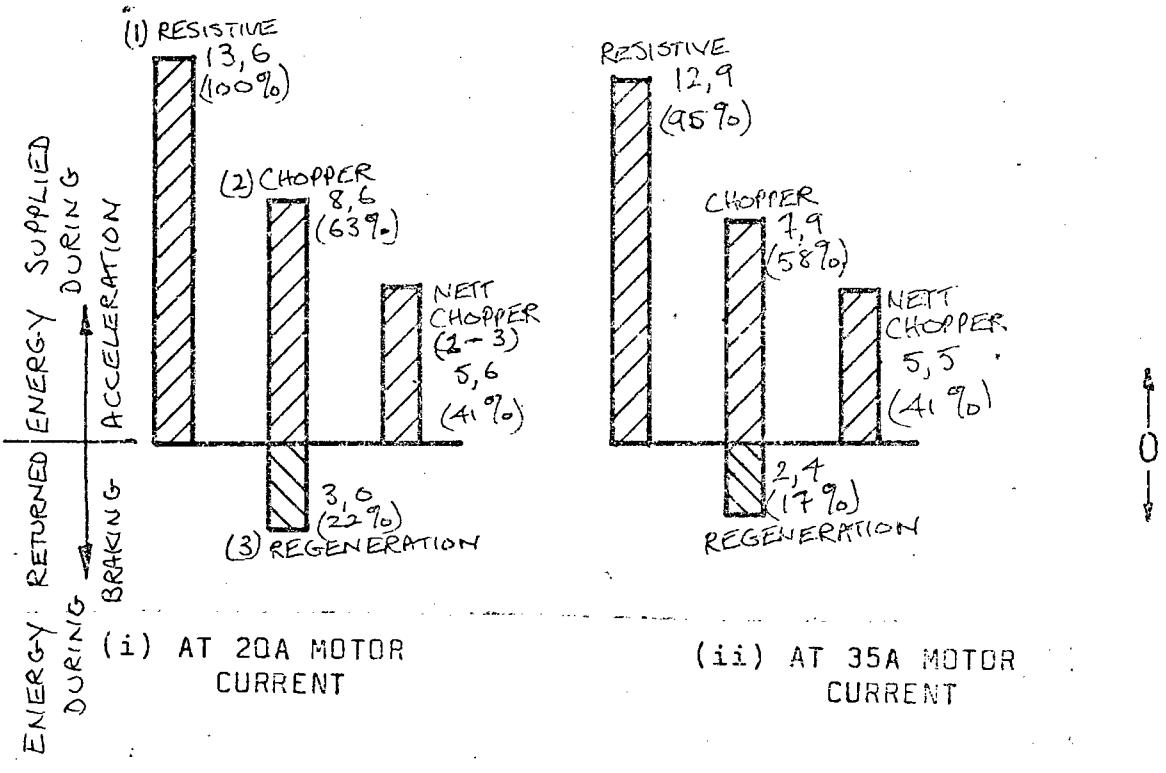

(a) ACCELERATION AND BRAKING OVER THE RANGE 0 - 1500 r.p.m.

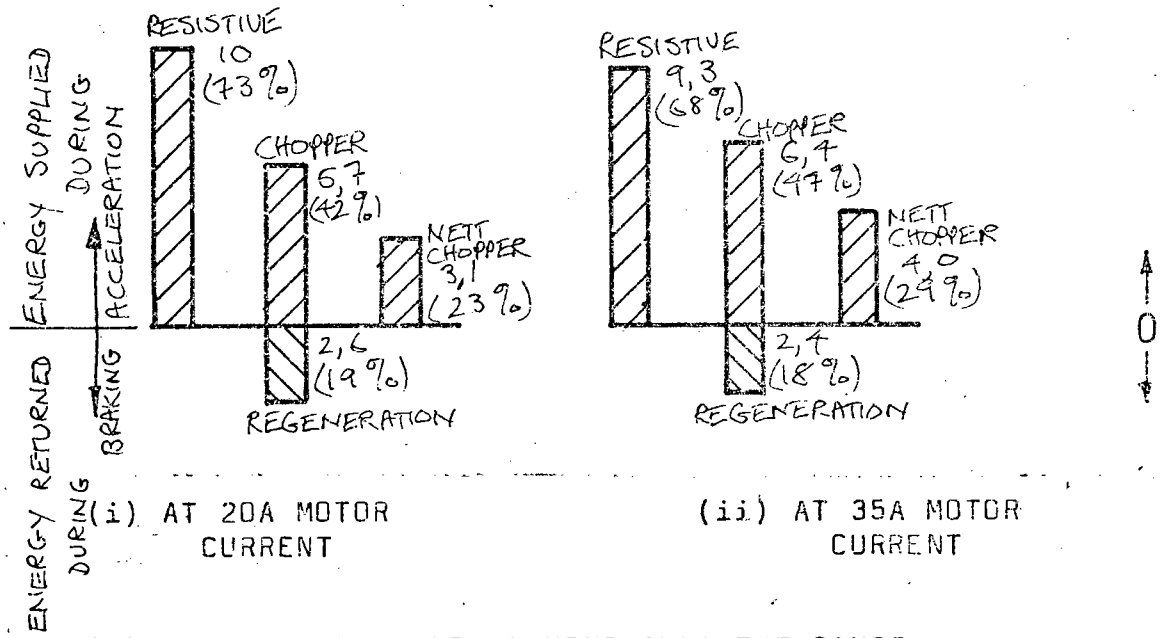

(b) ACCELERATION AND BRAKING OVER THE RANGE 500 - 1500 r.p.m.

FIGURE 4.5 COMPARISON OF ENERGIES SUPPLIED FROM, AND RETURNED TO, THE BATTERY DURING ACCELERATION AND BRAKING, USING RESISTIVE AND CHOPPER CONTROL.

the regenerative braking scheme is able to return approximately 40% of the energy used during the chopper-controlled acceleration. Over a complete acceleration and braking cycle, a regenerative chopper system used approximately 60% less battery energy than a resistive controller. All these results indicate the outstanding advantages offered by a chopper controller incorporating regenerative braking.

4.5 AN ESTIMATE OF THE EFFECTIVENESS OF REGENERATIVE BRAKING WHEN USED IN A VEHICLE.

The effectiveness of the use of a regenerative braking system in a vehicle may be predicted by considering a vehicle in traffic such that it accelerates and brakes three times in each kilometre travelled. After acceleration up to 50km/h over a distance of 140m, the vehicle travels for a while at this speed, then brakes to rest over a distance of 50m. The vehicle therefore covers a total distance of 430m at 50km/h. The energy per kilometre supplied by, or returned to, the battery during each stage may be estimated by the following calculations:

(i) Acceleration from rest to up to 50km/h.

The energy supplied by the battery during a single such acceleration was investigated in section 3.6, and was found to be 41Wh. ✓ Three accelerations would then consume 123Wh. ✓

(ii) Motoring at constant speed.

The power losses occurring in a vehicle drive system were calculated in section 3.7, and it was shown that at 50km/h, the rolling resistance is 132N, and the wind resistance 100N.

(a) Work done against rolling resistance

$$= 132 \times 430/3600 = 15.8\text{Wh}.$$

(b) Work done against wind resistance

$= 100 \times 430/3600 = \underline{12Wh}$

(c) Energy supplied by battery.

Considering the motor, controller and transmission 70% efficient,

$E_B = 27,8 \times 10/7 = \underline{40Wh}.$

(iii) Braking from 50km/h to rest.

At 50km/h, the kinetic energy of the vehicle is 17Wh. After some of this energy is lost overcoming friction and wind resistance, it is passed via the transmission to the motor and chopper, where it is transformed and returned to the battery.

(a) Rolling resistance energy loss

$E_R = 132 \times 50/3600 = \underline{1,8Wh}.$

(b) Wind resistance energy loss

$$E_W = 2 \times a \times 0,5 \int_0^{50} s \, ds$$

$$= 3,3 \times 0,5 \times 50^2/3600 = \underline{1,1Wh}.$$

(c) Transmission energy loss

Energy received by the transmission = 17 - 1,8 - 1,1.

$= \underline{14,1Wh}$

Energy lost in transmission = $\underline{1,4Wh}$.

Energy transmitted to motor = $\underline{12,7Wh}$.

(d) Motor and chopper energy loss

From figure 4.3, the average efficiency of the motor and chopper, over the entire speed range = 46%. This value for braking at maximum torque is low because of the fact that regeneration fails below 400 r.p.m. (13km/h).

Energy loss in motor and chopper = $\underline{6,9Wh}$.

(e) Energy returned to battery

Total energy lost = 11,2Wh.

Therefore, E_B = 5,8Wh (= 17 - 11,2)

In relation to the vehicle's kinetic energy, this is 35%.

Three such brakings will return 17,4Wh to the battery.

(f) Nett energy supplied by the battery.

Total energy supplied by the battery

= 123 + 40 = 163Wh.

Total energy returned to the battery = 17Wh.

As a percentage, this is 11% returned. This figure compares very well with field tests conducted on a battery-powered vehicle [16], which indicated that 10% of the battery energy could be recovered under similar "stop-start" driving conditions. The above figures are shown diagramatically in figures 4.6 and 4.7.

4.6 COMMENTS.

The measured and calculated values of average motor current showed a correlation of better than 5% over a wide range of loads.

It was predicted that, by using a regenerative braking system in a vehicle, about 10% of the battery energy could be returned under "stop-start" driving conditions. Such a system would consume only 55% of the battery energy needed by a resistively controlled and mechanically braked system under the same driving conditions. The advantages of the regenerative braking mode are significiant when seen in terms of a decreased battery size for a vehicle.

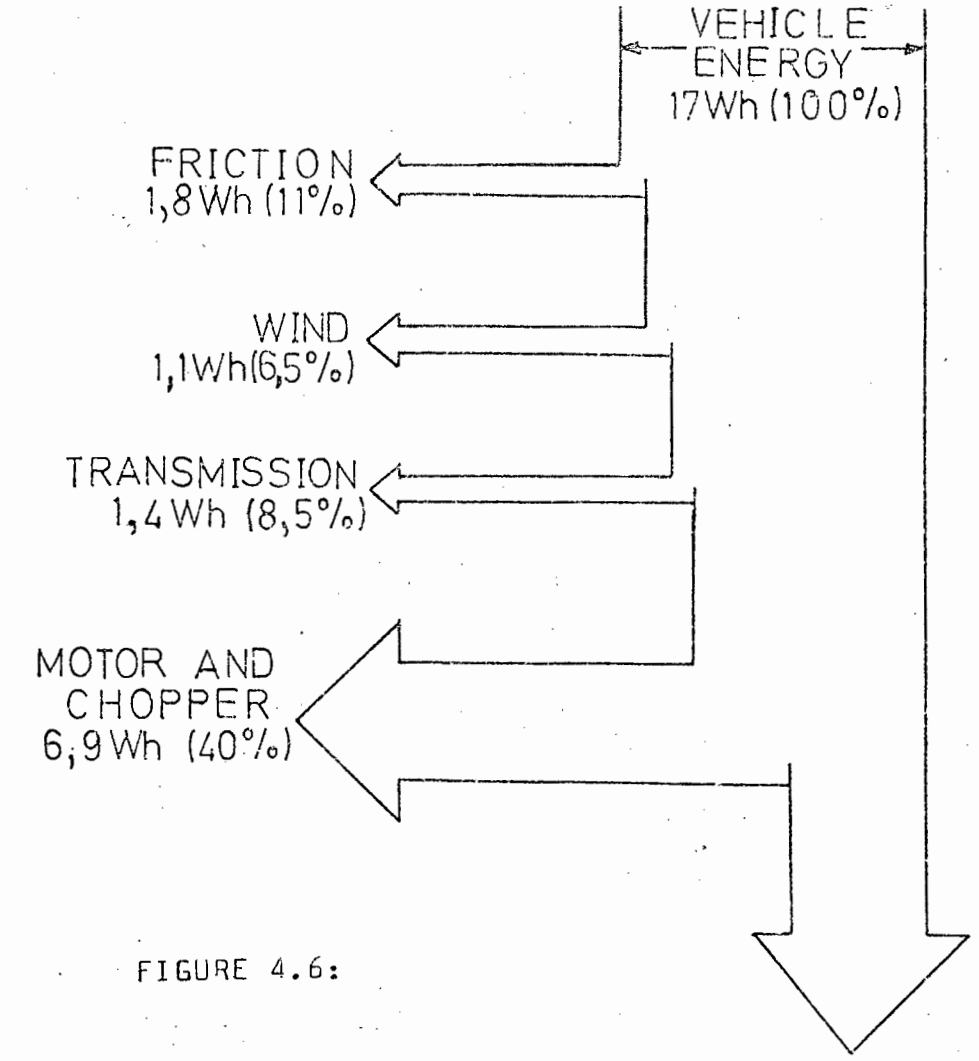

FIGURE 4.6:

DIVISION OF ENERGY OCCURING WHEN A 600 kg VEHICLE IS BRAKED FROM 50 km/h TO REST.

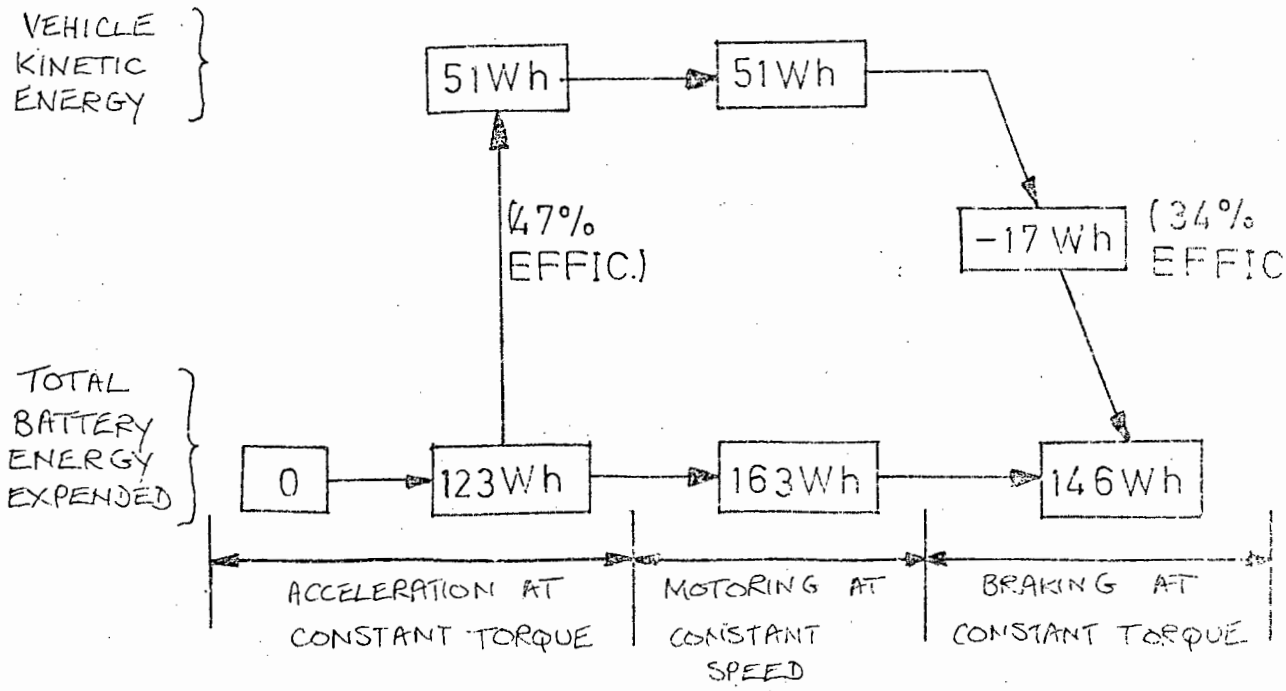

FIGURE 4.7: TRANSFER OF ENERGY DURING STOP-START DRIVING OVER ONE KILOMETRE.

CHAPTER 5.

THE PERFORMANCE OF THE MACHINE IN THE MODES OF MOTORING AND REGENERATIVE BRAKING OVER THE RANGE $E_M \geq V_B$.

5.1 INTRODUCTION

The desirability of having higher speed modes of motoring and braking were outlined in chapter one. These modes would allow the driver to have full control over the vehicle when travelling faster under conditions of reduced torque. As the circuit configurations for these two modes are very similar to those for motoring and braking over the range $0 \leq E_M \leq V_B$, no comparison has been made between the calculated and measured values of average current for those of current ripple, this having been done in chapters three and four.

This chapter will investigate the performance of the permanent magnet motor in the modes of motoring and braking over the range $E_M \geq V_B$.

5.2 THE PERFORMANCE OF THE MOTOR AND CHOPPER IN THE MOTORING CONFIGURATION.

(i) The limitation placed on the maximum battery current.

As the form factor of the motor current of this configuration is much greater than unity at increased speeds, care must be taken to avoid the RMS current rating of the armature being greatly exceeded. This was achieved by limiting the maximum battery current to the full load rating of the armature of the motor, i.e. 37A. In this way, the average value of the motor current will fall with increasing speed and so will compensate for the rising form factor

(ii) Efficiency and power relationships

The efficiency of the motor and chopper were investigated as a function of speed with the battery current kept constant at 37A and

at 20A, and the results are shown in figures 5.1 and 5.2 respectively. For the tests presented in this chapter, it was necessary to reduce the battery voltage to 60V, to keep the voltage appearing across the semiconductor switch to a safe level when the speed of the machine was increased. The speed range then extends from base speed, which is when $E_M = V_B$, to 50% above base speed.

It is seen from the results that the efficiency of the motor is virtually unaffected by the non-continuous current that is flowing in it, and remains essentially constant above 80% over the speed range investigated. The overall efficiency of the motor and chopper is approximately 10% below this figure.

(iii) Form factor of the motor current

As the output power of the motor remains essentially constant over the speed range investigated, the average motor current, and together with it the torque, decreases as a linear function of speed, as shown by curves "a" of figure 5.3 and 5.4. A characteristic similar to that of field weakening is thereby obtained. It is important to note that, although the form factor of the motor current increases to as much as 1,2, ~~and~~ the RMS value of the motor current remains below the average value of the battery current. Since the form factor of the battery current is much lower than that of the motor current, a simplified expression for the RMS value of the motor current, I_M' can be given by:

$$I_M' = \sqrt{I_B I_M} \quad \ldots\ldots\ldots\ldots\ldots\ldots\ldots\ldots (5.1)$$

It is therefore possible to avoid overloading the motor at these increased speeds by limiting the average value of the battery current to that of the current rating of the motor.

(iv) The effect of the inductance of the armature

To allow efficient transfer of energy from the inductor L to the

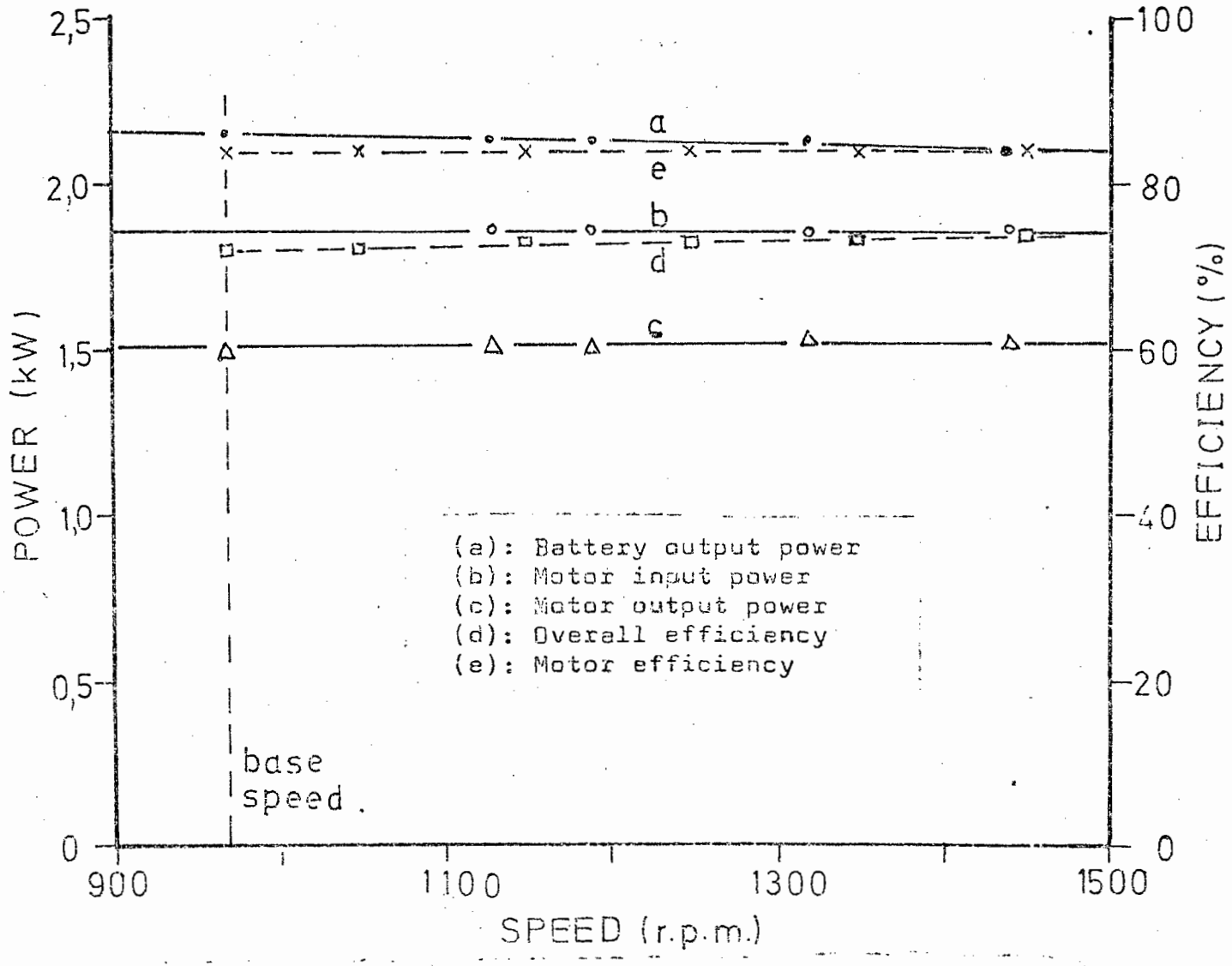

FIGURE 5.1: LOAD CHARACTERISTICS OF MACHINE WHEN MOTORING WITH $E_M > V_B$ AT CONSTANT BATTERY CURRENT OF 37A.

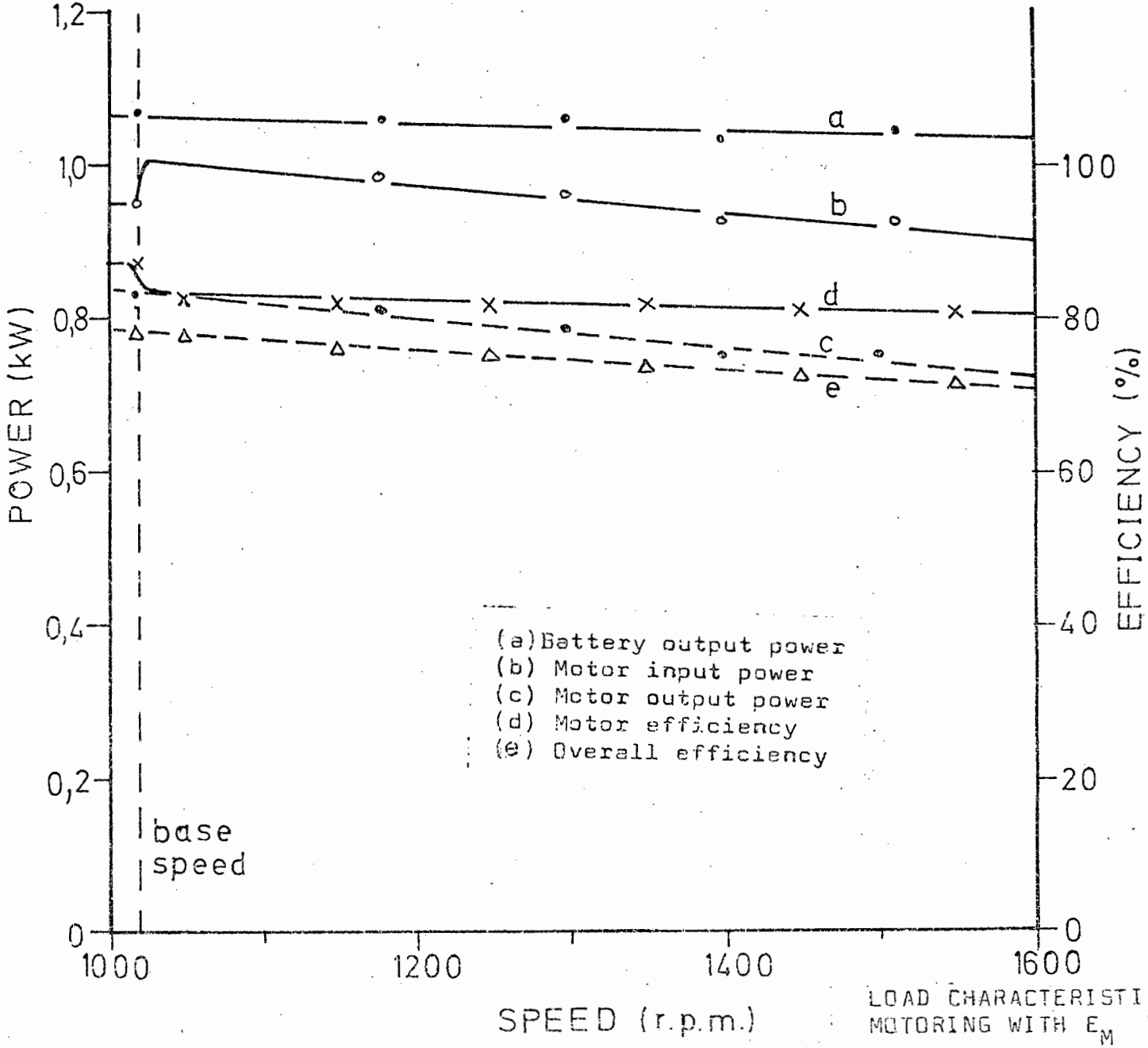

FIGURE 5.2:
LOAD CHARACTERISTICS OF MOTOR WHEN MOTORING WITH E_M V_B AT CONSTANT BATTERY CURRENT OF 20A.

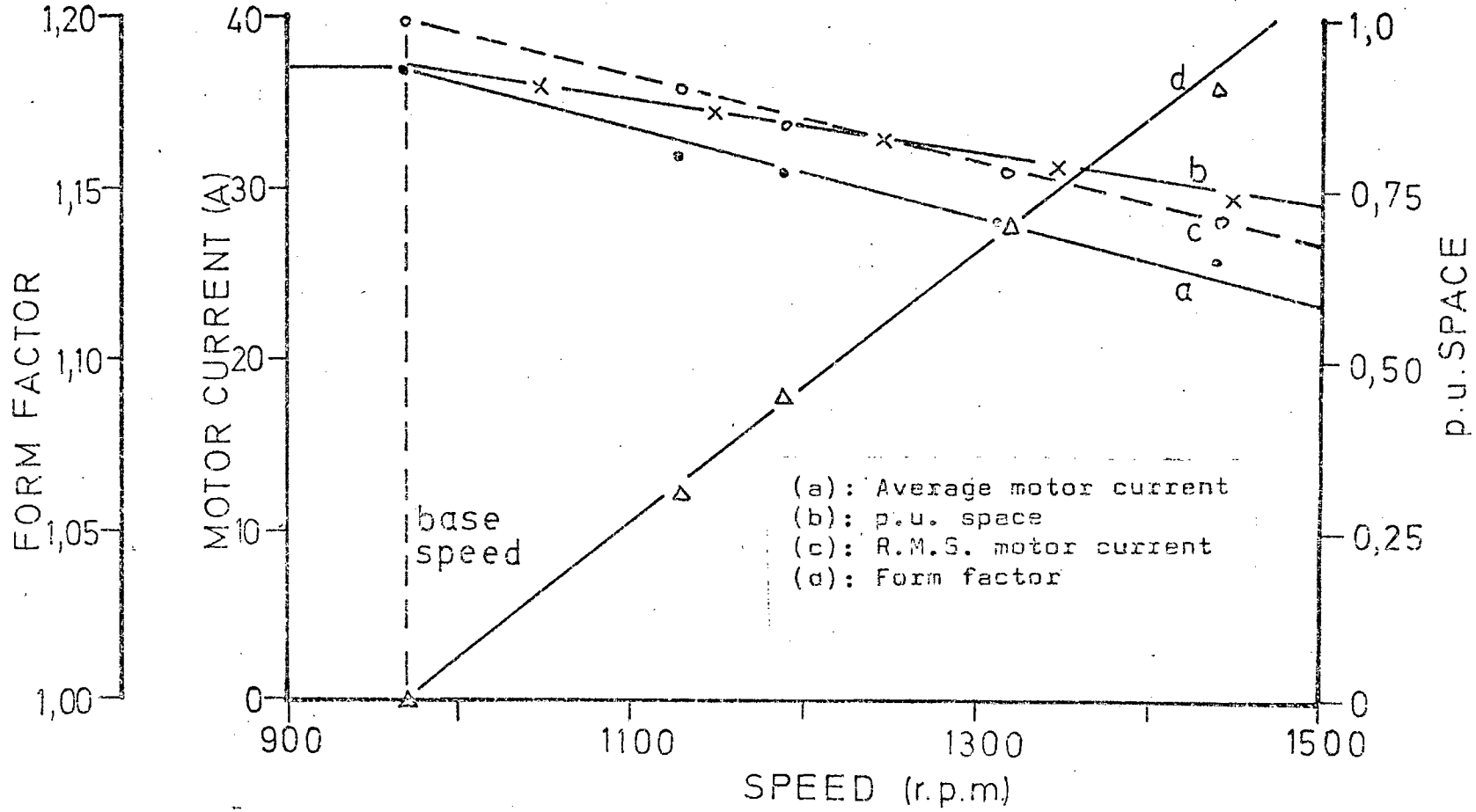

FIGURE 5.3: CURRENT CHARACTERISTICS OF MACHINE WHEN MOTORING OVER THE RANGE $E_M \geq V_B$, AT CONSTANT BATTERY CURRENT OF 37A.

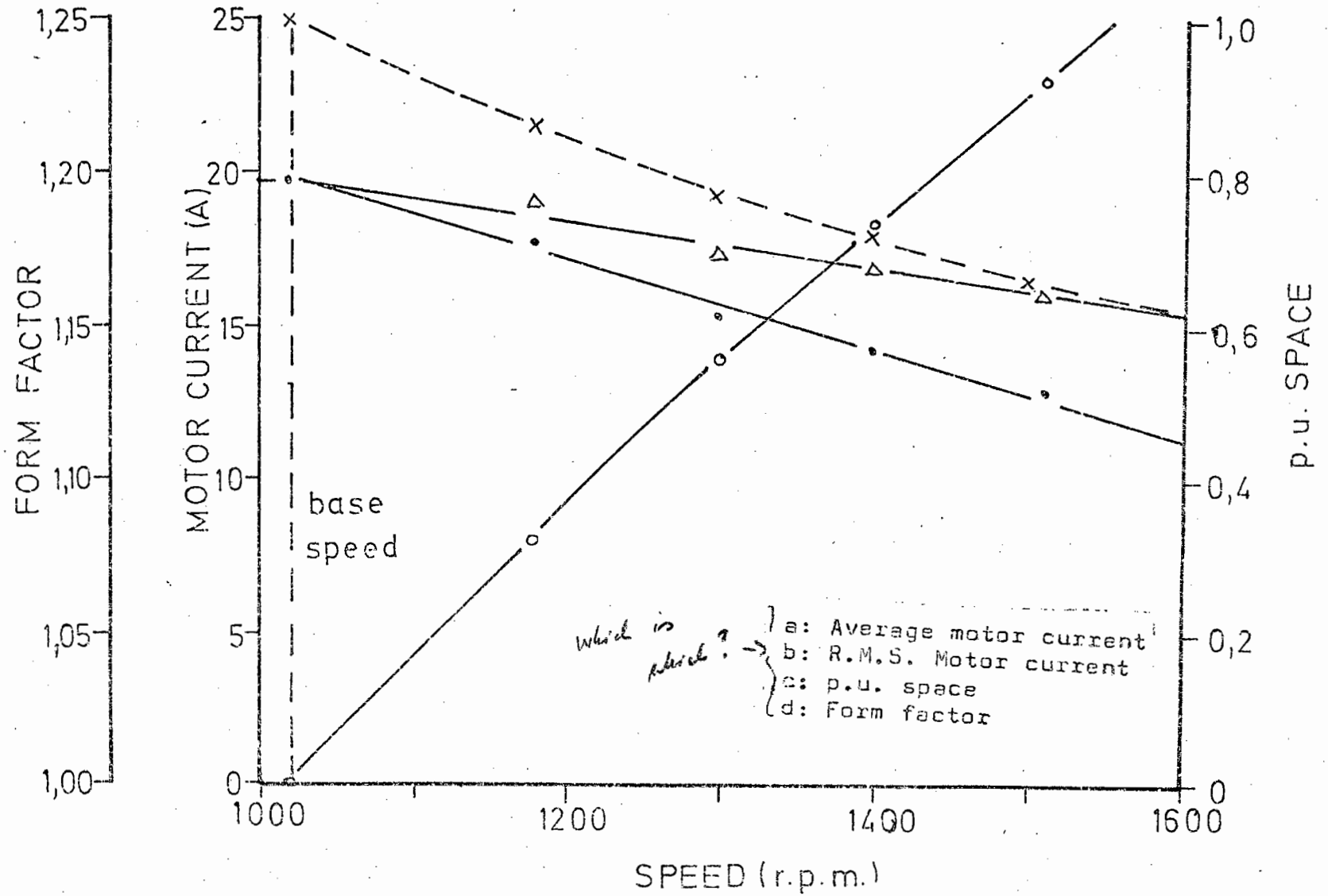

FIGURE 5.4: CURRENT CHARACTERISTICS OF MOTOR WHEN MOTORING OVER THE RANGE $E_M \geq V_B$, AT CONSTANT CURRENT OF 20A.

motor, the inductance of the armature should be as low as possible. The permanent magnet motor was suitable for use in this mode of operation, as a low value of armature inductance was achieved by nature of the disc-type construction of the armature.

(v) Voltage and current waveforms

Typical waveforms for this mode of motoring are shown in figure 5.5.

5.3 THE COMPARABLE PERFORMANCE OFFERED BY A SEPARATELY EXCITED MACHINE, USING FIELD WEAKENING

Field weakening may be employed in a separately excited machine to obtain an increase in maximum speed at reduced torque. It is therefore interesting to compare the performance of this machine with that of the permanent magnet motor/chopper combination of the previous section. The machine tested was a 3kW, 1500 r.p.m. motor. The armature current was kept constant at the rated value of 20A, while the field was progressively weakened. Comparing the results shown in figure 5.6 with those of the previous section (figures 5.1 - 5.4), it is seen that the characteristics of the permanent magnet motor/chopper configuration are very similar to those of conventional field weakening.

5.4 THE EVALUATION OF THE PERFORMANCE OF THE MOTOR AND CHOPPER IN THE REGENERATIVE BRAKING MODE

(i) Practical difficulties.

As the battery voltage rises by about 20% when large charging currents are flowing into it, the upper speed of the machine had to be increased to 2000 r.p.m., and the battery voltage reduced to 48V in order to achieve suitable motor currents during braking. Even under these conditions, it was not possible to realise the

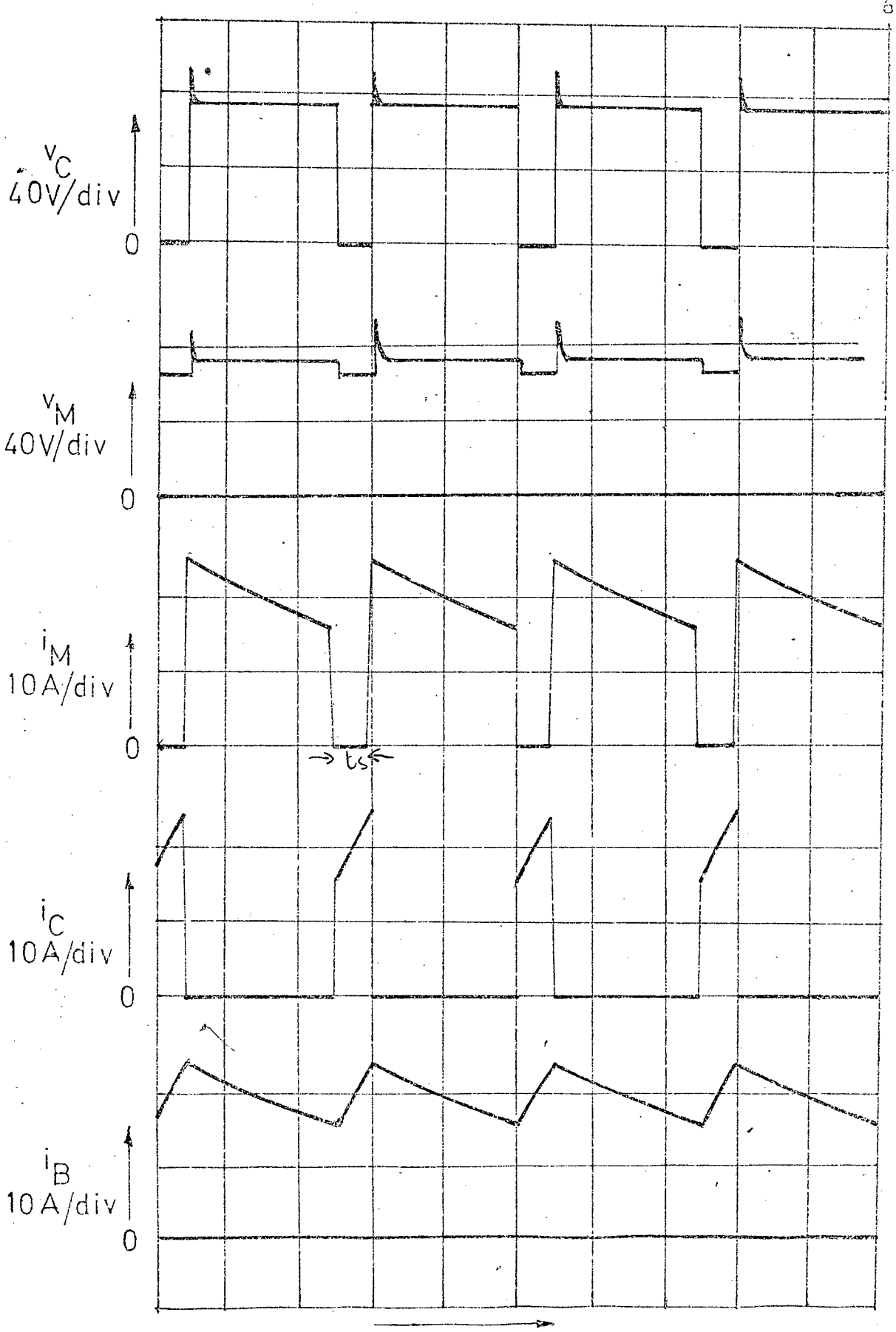

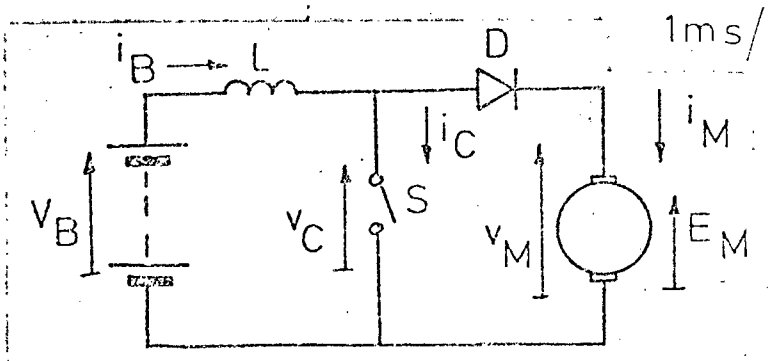

FIGURE 5.5: VOLTAGE AND CURRENT WAVEFORMS FOR MOTORING OVER THE RANGE $E_M \geq V_B$.

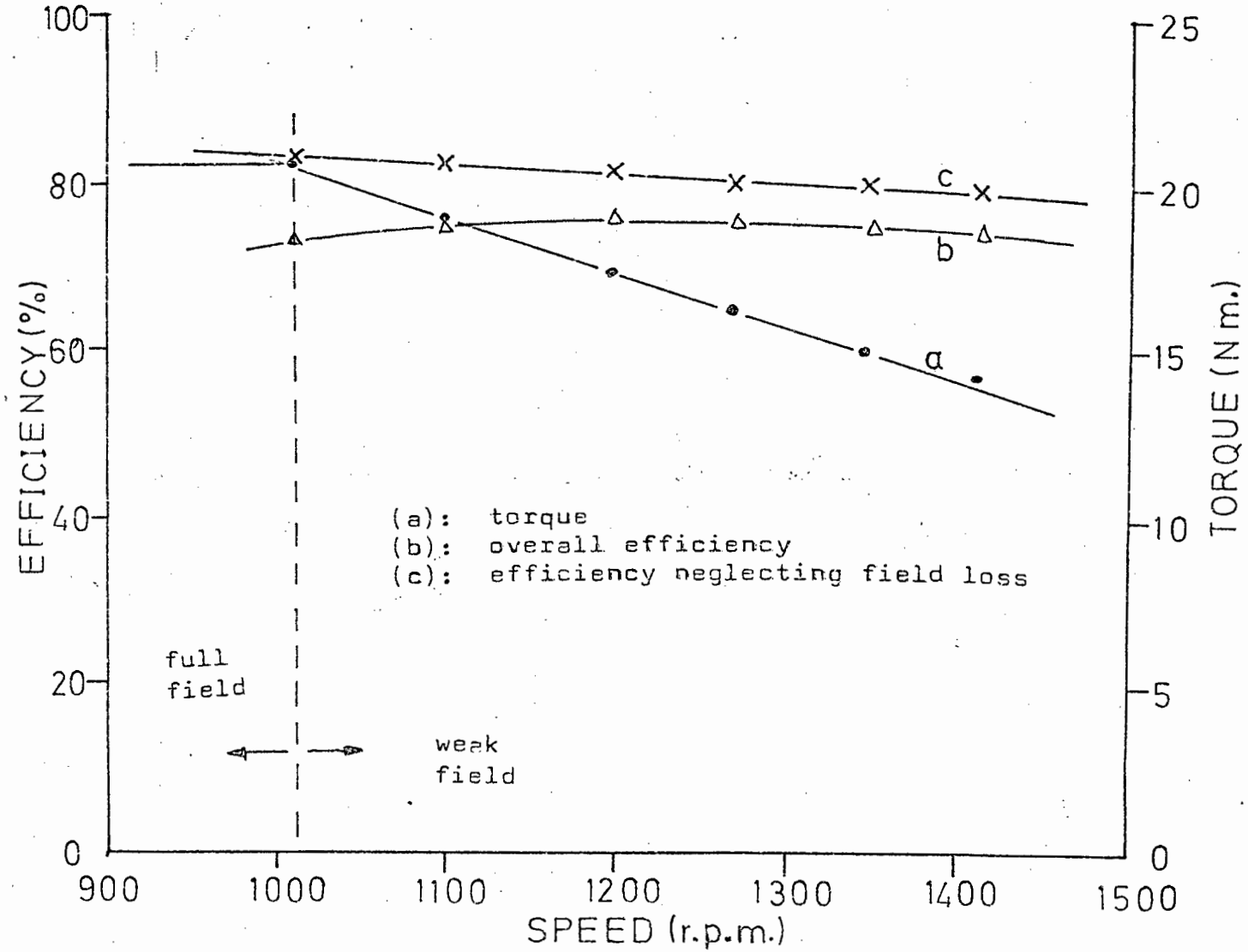

FIGURE 5.6: THE PERFORMANCE OF A SEPARATELY EXCITED MACHINE AT INCREASED SPEEDS USING FIELD WEAKING AT CONSTANT ARMATURE CURRENT.

rated current of 37A.

(ii) The results of the tests.

It was possible to conduct tests in the regenerative braking mode for a motor current of 20A only. The results are shown in figures 5.7 and 5.8. It is seen that only a very limited variation in the p.u. mark was possible ---0,82 to 0,97--- in spite of the reduced battery voltage and increased speed. Consequently the maximum form factor realised was only 1,1.

(iii) Voltage and Current Waveforms

Typical voltage and current waveforms are shown in figure 5.9. The p.u. mark was approximately 0,8.

5.5 COMMENTS ON THE MOTORING AND BRAKING MODES

The performance of the motor and chopper in the mode of motoring when $E_M \geq V_B$ is very similar to that obtainable by field weakening in a conventional shunt motor, and the overall efficiency of the motor/chopper combination is virtually constant for speeds up to 50% above base speed.

However, in the case of the regenerative braking mode, the performance is far from satisfactory, as it is not possible to achieve sufficiently high braking currents in the motor, even at increased speeds. As mentioned previously in section 4,3, it is possible to extend the speed range covered by the mode of regenerative braking when $E_M < V_B$, to cover a speed range up to 50% above base speed. The other configuration for achieving regenerative braking when $E_M > V_B$, which was evaluated in this chapter, may be discarded.

The complete speed range of the vehicle may then be covered by 3 modes: (1) a mode of motoring from standstill up to base speed;

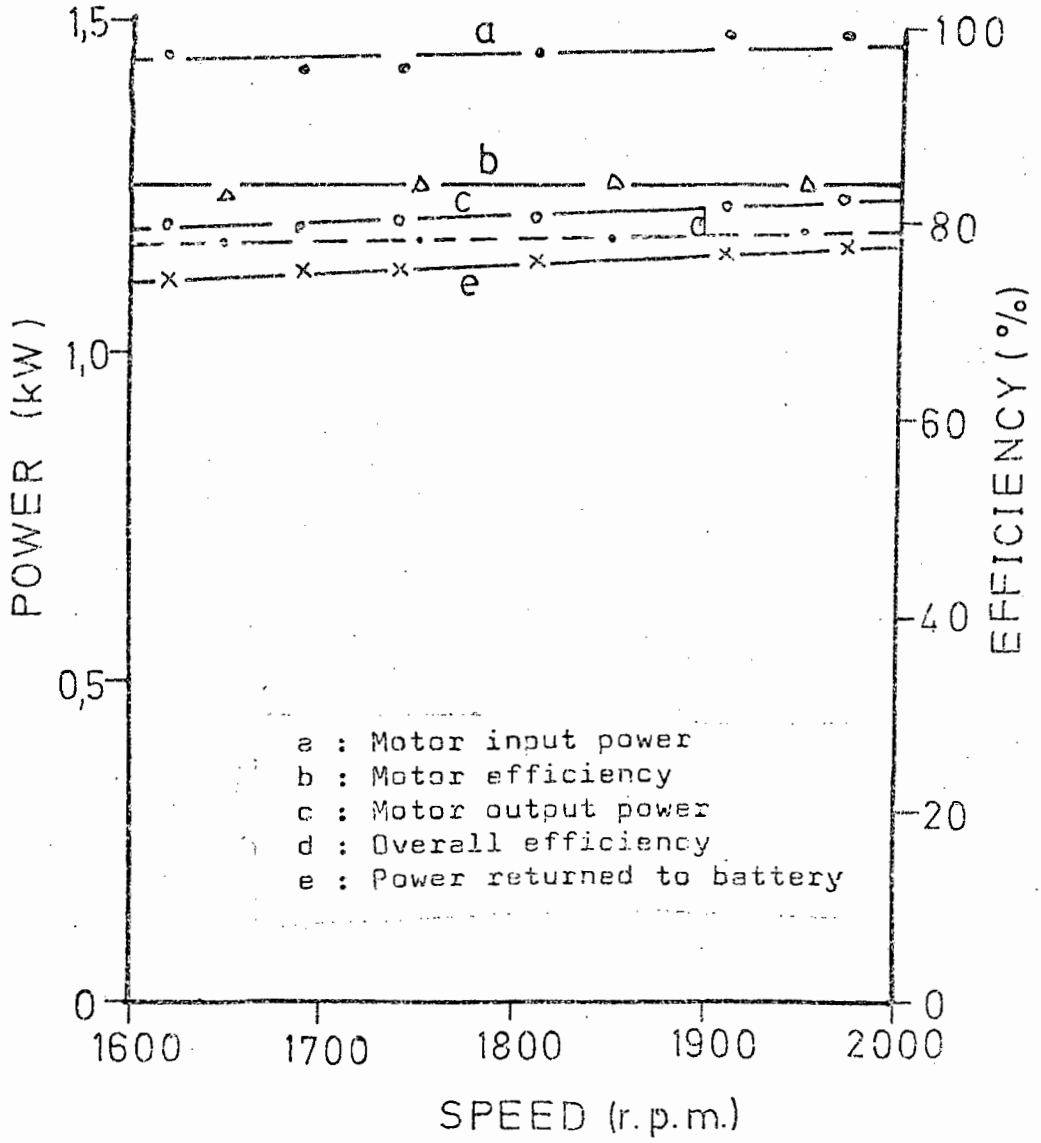

FIGURE 5.7: PERFORMANCE OF MACHINE WHEN BRAKING OVER THE RANGE $E_M \geq V_B$ AT A CONSTANT BATTERY CURRENT OF 20A.

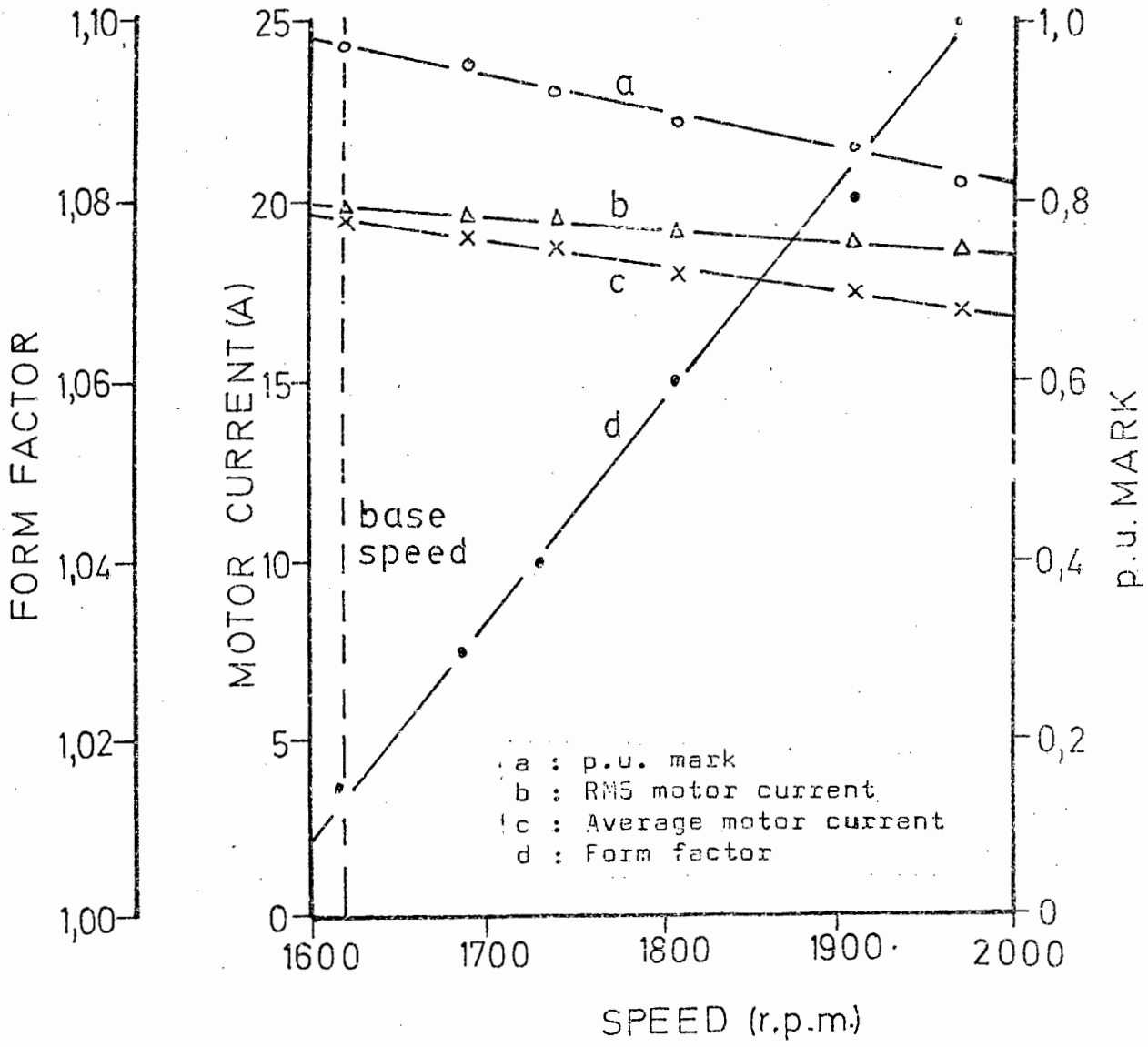

FIGURE 5.8: CURRENT CHARACTERISTICS OF MACHINE WHEN BRAKING OVER THE RANGE $E_M \geq V_B$ AT A CONSTANT BATTERY CURRENT OF 20A.

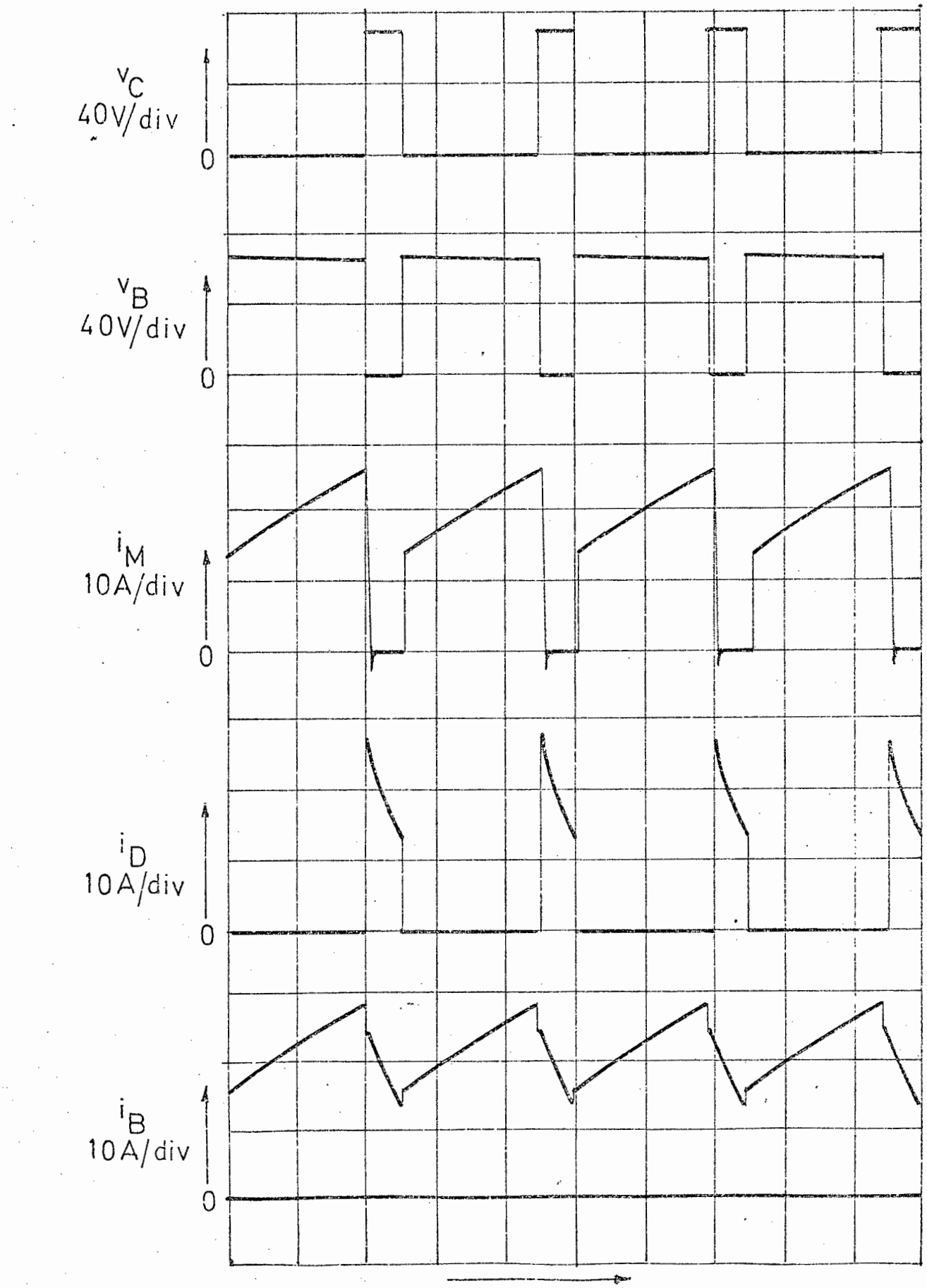

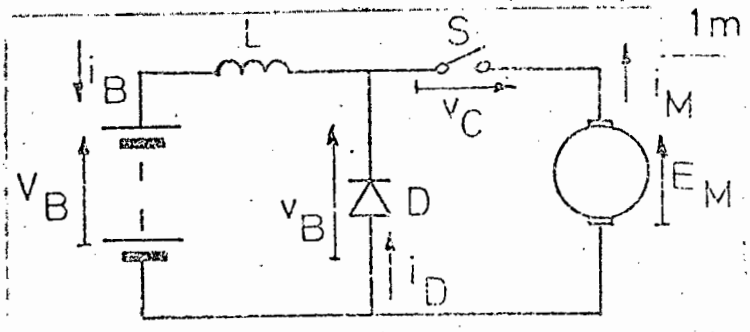

FIGURE 5.9: VOLTAGE AND CURRENT WAVEFORMS DURING REGENERATIVE BRAKING OVER THE RANGE $E_M \geq V_B$.

(2) a second mode of motoring covering the range from base speed to 50% above base speed; (3) one mode of regenerative braking covering the range from 50% above base speed to a few km/h above standstill.

CHAPTER 6.

THE CHOPPER SWITCH.

6.1 INTRODUCTION.

In the preceding five chapters, the chopper was described simply as being a semiconductor switch which operated cyclically, passing current in a series of short pulses. It is now necessary to study in detail the use of various semiconductor devices as choppers, as well as the methods of varying the mark/space ratio.

This chapter will describe the operation of one type of semiconductor chopper using the thyristor.

6.2 THE THREE BASIC FORMS OF SWITCHING

(i) Fixed frequency, variable pulse width [5,25,27,29,30].

As shown in figure 6.1, the speed of the motor (for a given torque) is increased by increasing the pulse width t_m. The average value of the motor voltage is given by:

$$V_M = V_B \, t_m / (t_m + t_s) \quad \ldots\ldots\ldots\ldots\ldots\ldots\ldots\ldots (6.1)$$

As the chopper can be operated at high frequency, near the maximum permissible frequency, (limited by switching losses in the chopper and by reduction of the limits of the M/S ratio obtainaole), the current bandwidth K, for a given torque and inductance is maintained at a low level and has its maximum when $t_m = t_s$, viz at half speed.

(ii) Fixed pulse width, variable frequency [4,9,25,27,30].

By fixing the pulse width at t_m and varying the frequency to obtain a variable voltage, it is possible to simplify the circuitry of the chopper [6,27]. From figure 6.2 the equation describing the average voltage of the chopper in terms of the frequency can be derived and is given by:

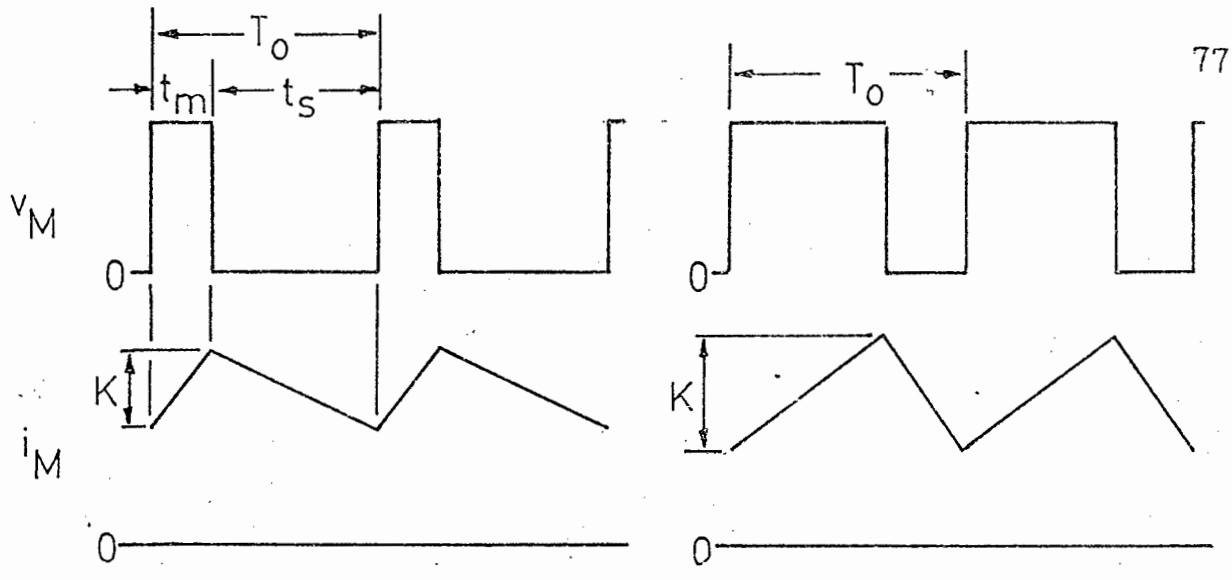

FIGURE 6.1: FIXED FREQUENCY, VARIABLE PULSE WIDTH.

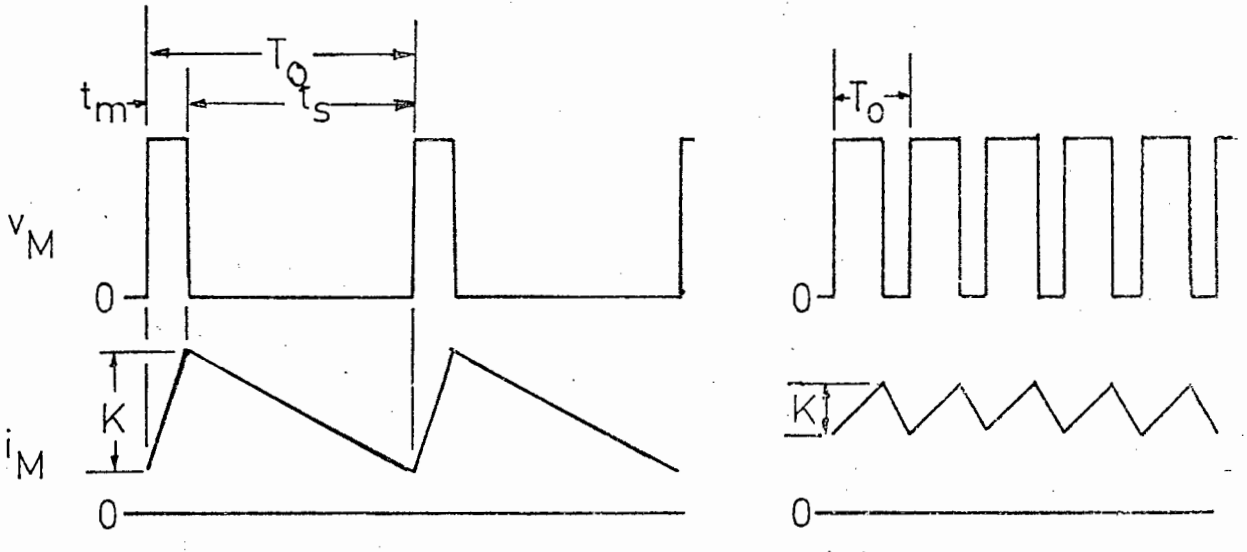

FIGURE 6.2: FIXED PULSE WIDTH, VARIABLE FREQUENCY

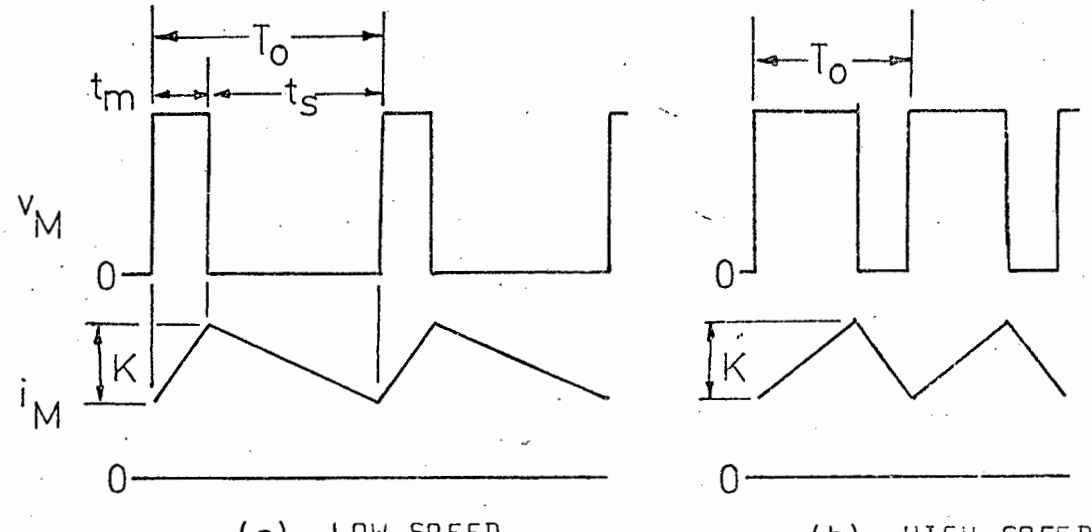

FIGURE 6.3: CURRENT BANDWIDTH CONTROLLED.

$$V_M = V_B t_m f \quad \ldots\ldots\ldots\ldots\ldots\ldots\ldots\ldots\ldots\ldots (6.2)$$

It is seen from equation 6.2 that low speeds will result in low frequencies. As the maximum operating frequency is determined by the same criterion as for the variable pulse width (v.p.w.) chopper, the use of the variable frequency (v.f.) chopper will result in a larger ripple in the motor current at low speeds for a given torque. This is illustrated graphically in figure 6.4, where the ripple factors of the two types of chopper are compared for a motor current of 40 amps, from a battery voltage of 80V. In order to reduce the ripple factor at low speeds to a level comparable to that of the v.p.w. chopper, it is necessary to increase the value of the inductance significiantly, viz from 2mH to 10mH.

(iii) Current bandwidth controlled chopper [1,3,4,7] .

In chopper circuits, where the frequency or pulse width are varied independently, the ripple of the motor current at a given torque varies considerably over the speed range. By making the bandwidth K the controlling element, it is possible to obtain a variable output voltage from the chopper by varying both frequency and pulse width.

The frequency of operation is given by the expression [1] :

$$f = 1/ (t_m + t_s) \quad \ldots\ldots\ldots\ldots\ldots\ldots\ldots (6.3)$$

where

$$t_m = \frac{L}{R} \ln \frac{V_B - E_M - RI_p}{V_B - E_M - RI_V} \quad \ldots\ldots\ldots\ldots (6.4)$$

The principle of the chopper is easily explained with reference to figure 6.3. The controller is set for some bandwidth K, and the switch remains closed for a time t_m, until the predetermined current maximum is reached. The switch then opens for a time t_s until the current falls to the predetermined minimum value. In this way

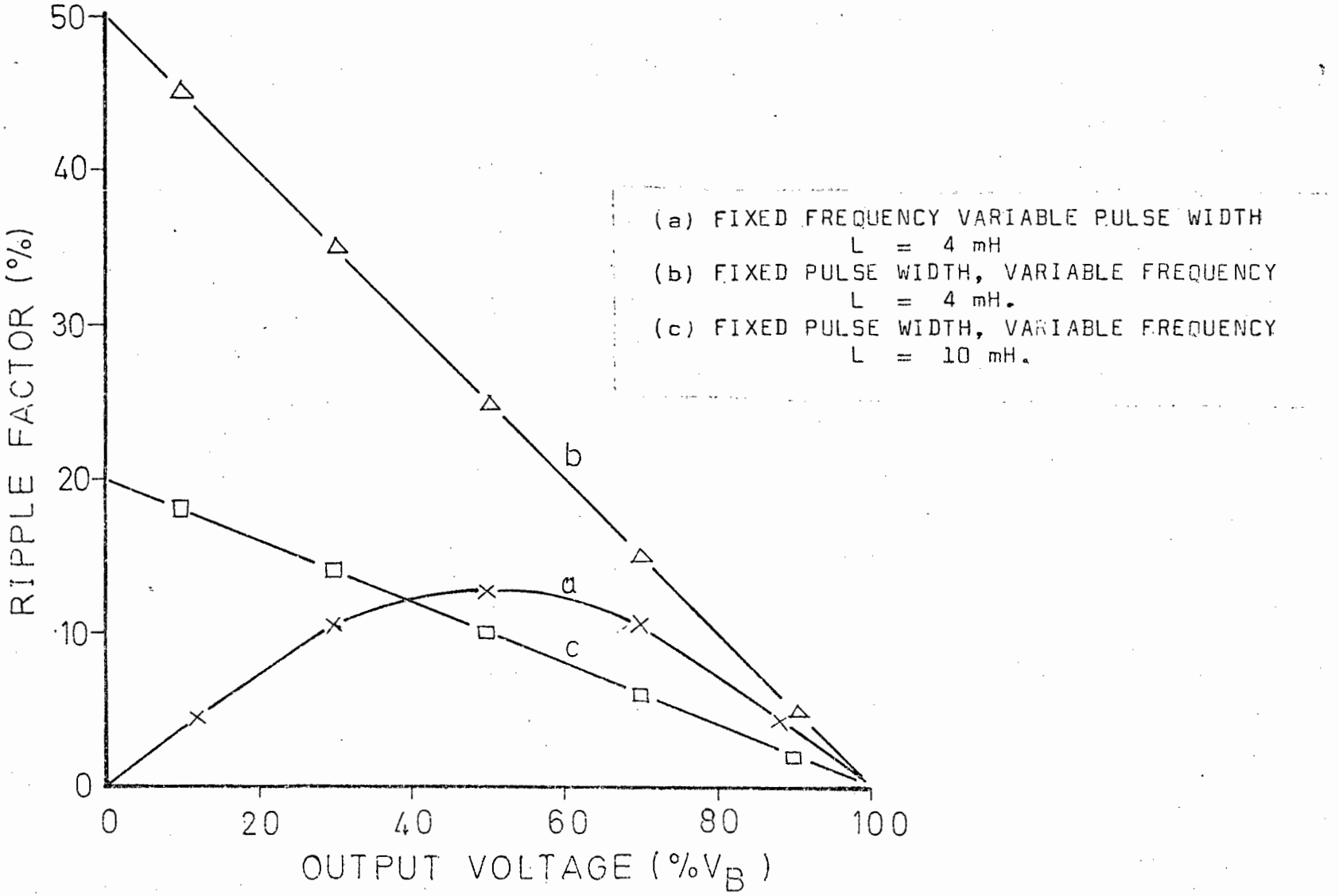

FIGURE 6.4: RIPPLE FACTOR OF TWO TYPES CHOPPER WITH AN UPPER FREQUENCY LIMIT OF 500 Hz. BATTERY VOLTAGE = 80V, MOTOR CURRENT = 40A.

complete control of both form factor and torque is exercised. However, this type of chopper is correspondingly more complex as both minimum and maximum current values must be monitored, whereas current control can be applied to v.p.w. and v.f. choppers by monitoring the maximum value alone.

(iv) The method of switching chosen for use with the permanent magnet motor.

While the current bandwidth control is attractive, it is considered unnecessarily complex, as similar current control can be applied to either the v.p.w. or v.f. choppers by monitoring the peak value of the current waveform alone. Of the two remaining types, the v.p.w. was chosen because of its lower ripple characteristic.

6.3 THE THYRISTOR AS A CHOPPER SWITCH

(i) The basic thyristor chopper

Figure 6.5 illustrates the basic thyristor chopper and motor circuit. Thyristor TH_1 replaces the switch S of figure 2.1 and represents a hypothetical device that can be turned off at will. As a thyristor, in practice, can only be commutated by either allowing the forward current to drop below the value of the holding current, or by applying a reverse voltage bias to the device for the duration of the turn-off time, it is necessary to provide some external circuity to commutate the device.

(ii) Forced commutation

Various techniques of forced commutation are available [25-29], but the method most commonly used, and one of the simplest, is that shown in figure 6.6. This chopper was designed for operation on 100V, with a current capability of 20A, and is described in detail by the author in another thesis [23], but the theory of operation

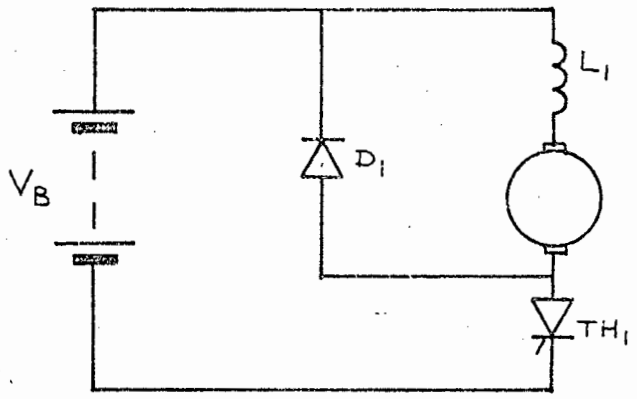

FIGURE 6.5: THE BASIC THYRISTOR CHOPPER

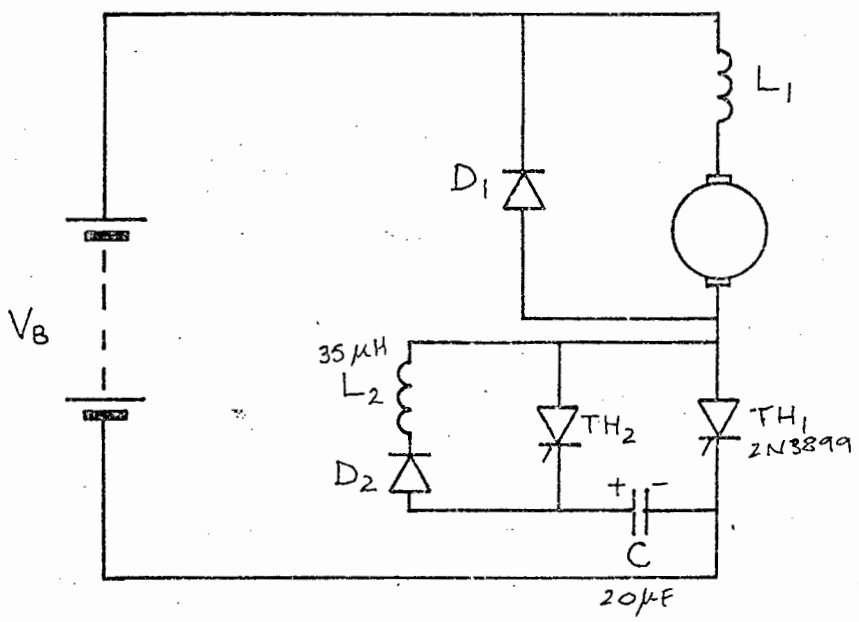

FIGURE 6.6: COMMUTATION CIRCUIT

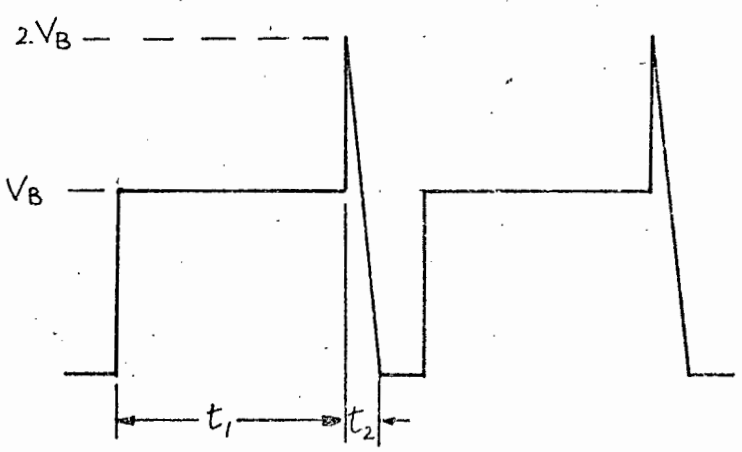

FIGURE 6.7: OUTPUT VOLTAGE WAVEFORM OF CHOPPER

will be briefly described now in the following steps:

(a) Before the main thyristor TH_1 is triggered, the commutating thyristor TH_2 must be triggered, charging up the capacitor C through the load in the polarity shown. When C is fully charged, TH_2 extinguishes.

(b) TH_1 is triggered, allowing the main load current to flow, and at the same time closing loop TH_1, C, L_2 and D_2. C and L_2 resonate, so that the polarity of C is reversed, D_2 blocking any further resonance.

(c) After the required delay (t_r), TH_2 is again triggered, connecting C across TH_1 and so extinguishes it, after which C recharges.

C must be sufficiently large so as to reverse bias TH_1, and to supply the maximum expected load current, for the duration of the turn-off time of TH_1 (t_{off})

$$C \geq t_{off} \, I_M / V_B \quad \ldots\ldots\ldots\ldots\ldots\ldots\ldots\ldots (6.5)$$

A factor of safety of 1,5 - 2,0 is allowed for in the value of C. L must be large enough to reverse bias TH_2 in a time equal to a quarter cycle of oscillation.

$$L \geq t_{off}^2 / {}^2 C \quad \ldots\ldots\ldots\ldots\ldots\ldots\ldots\ldots (6.6)$$

D_2 must be able to withstand the repetitive peak resonant current. TH_2 must be able to withstand the repetitive peak turn-off current. As the duty cycle of TH_2 is very low, it can be of substantially lower current rating than TH_1.

(iii) Waveforms of the thyristor circuit

Voltage and current waveforms are shown in figure 6.8 for the thyristor chopper that is illustrated in figure 6.6.

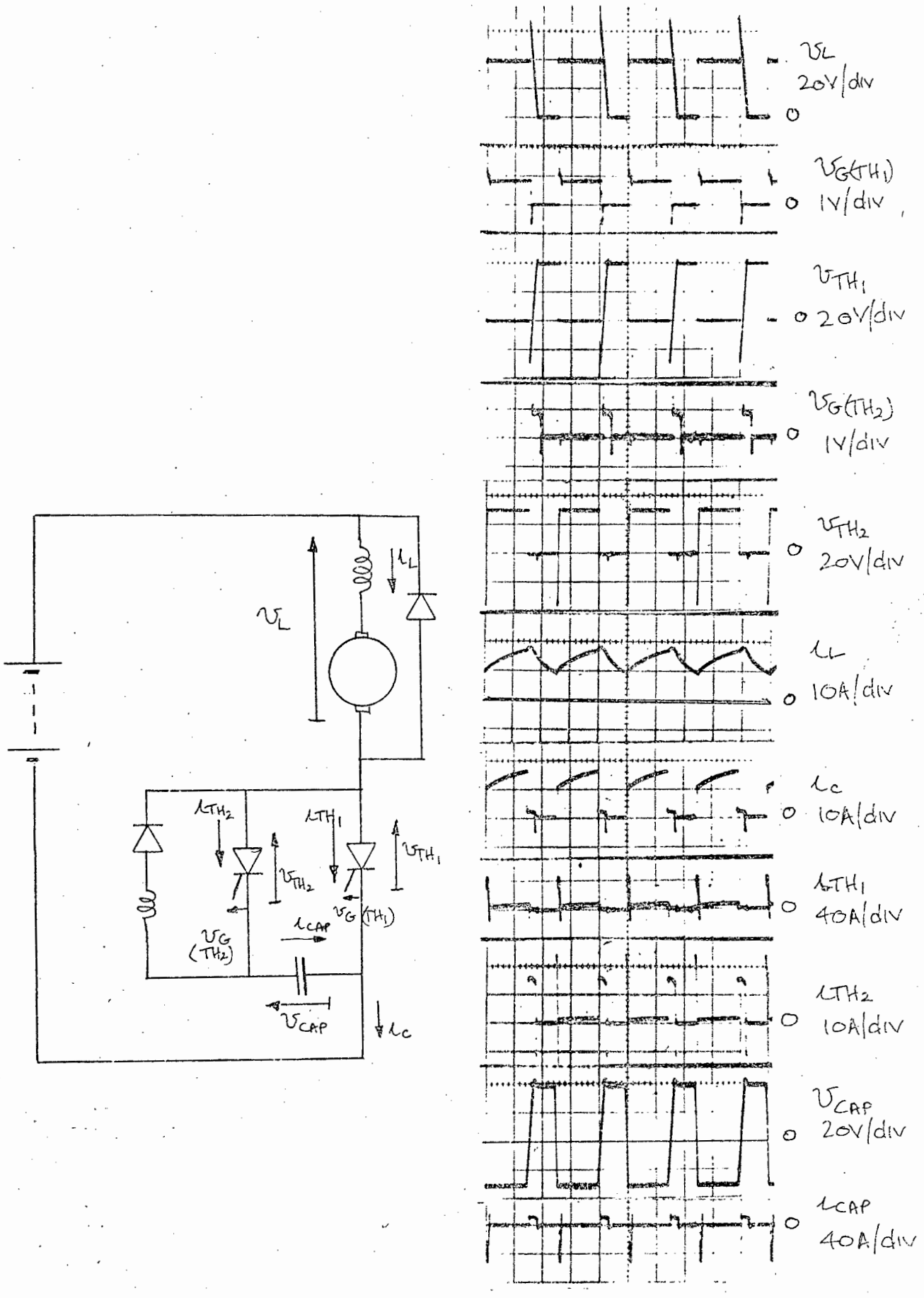

FIGURE 6.8: THYRISTOR CHOPPER WAVEFORMS.

6.4 TRIGGER CIRCUIT FOR THE THYRISTOR CHOPPER

The complete circuit, shown in figure 6.9, is described in detail in reference 23. A ramp generator, consisting of a UJT relaxation oscillator (TR_1) is used in conjunction with the Schmitt trigger (TR_3 and TR_4) to produce variable width rectangular pulses. TH_1 and TH_2 are triggered in time with the leading and trailing edges of the rectangular pulses respectively.

6.5 SUGGESTED STATIC SWITCHING SYSTEMS USING THYRISTORS, FOR SELECTING DESIRED MODES OF OPERATION.

(i) A static controller covering two modes of operation

A thyristor network, which would allow control in the modes of motoring and braking when $E_M \leq V_B$, is shown in figure 6.10. TH_2, C_1, L_2, D_2 form the commutation circuit for TH_1, which is the main thyristor during motoring, with D_3 being the "free-wheel" diode. TH_4, C_2, L_3, D_4 form the commutation circuit for TH_3, which is the main thyristor during regenerative braking with D_1 being the free-wheel diode.

This circuit may be simplified if both commutation circuits share one capacitor, as shown in figure 6.11. The forward voltage drop for either circuit during motoring or braking would be less than 2V.

(ii) A Static controller covering three modes of operation.

In chapter 5, it was shown that full control for the entire speed range of a vehicle could be obtained by using three modes of operation of the motor : motoring below base speed; motoring above base speed; and one mode of regenerative braking. A thyristor switching network which would cover these three modes is shown in figure 6.12. This circuit is considerably more complex than those shown in figure 6.10 and 6.11, because to include the mode of motoring above base

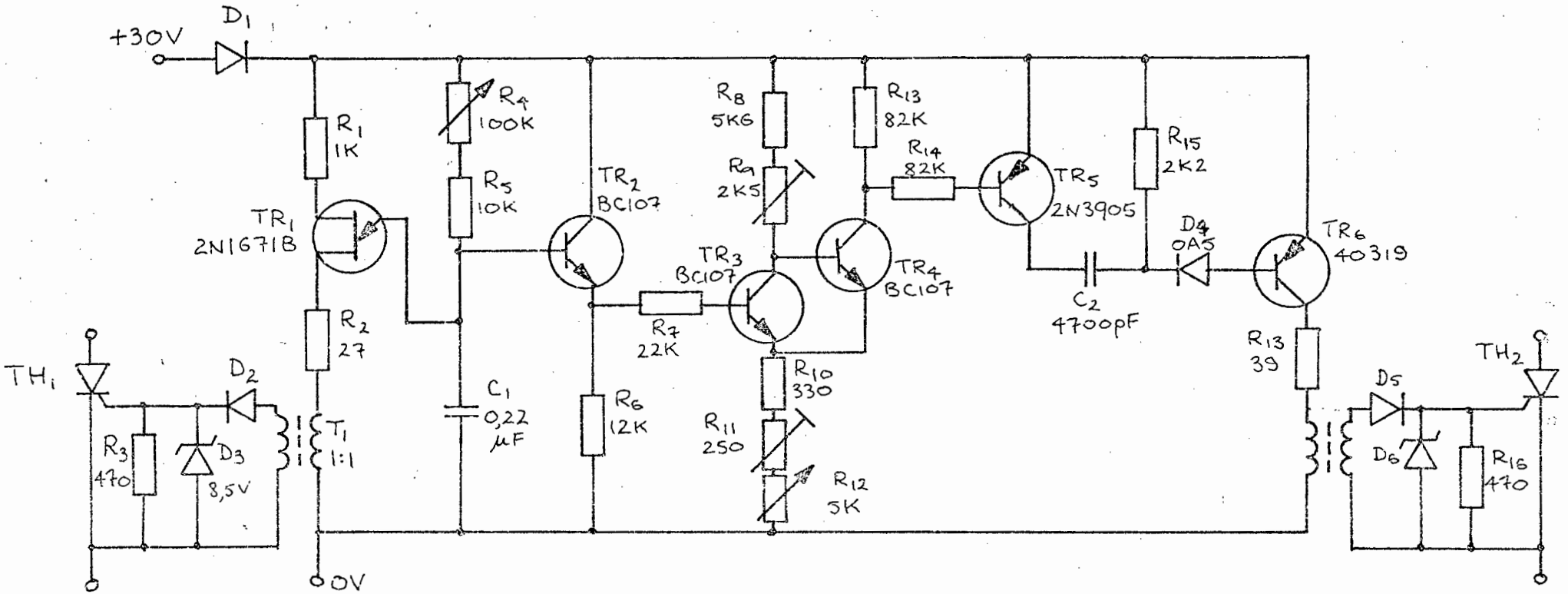

FIGURE 6.9 : THYRISTOR TRIGGER CIRCUIT

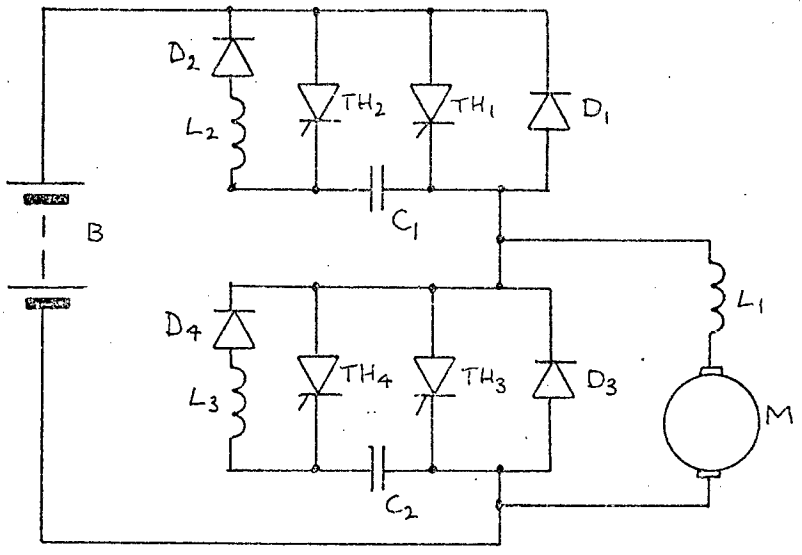

FIGURE 6.10: THYRISTOR SWITCHING NETWORK FOR MOTORING AND BRAKING

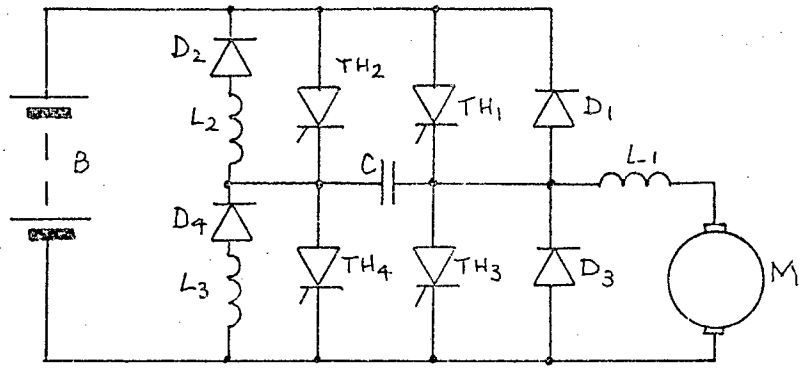

FIGURE 6.11: SIMPLIFIED CIRCUIT

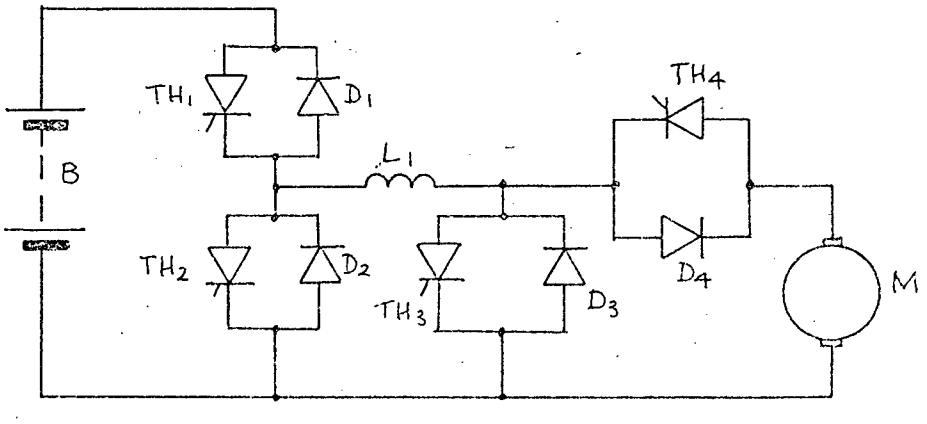

FIGURE 6.12: THYRISTOR NETWORK FOR THREE MODES OF OPERATION.

speed, the motor must be separated from the inductance to achieve the voltage step-up. Each thyristor shown would have a commutation circuit, such as that shown in figure 6.10, and the maximum forward voltage drop of the network would be either a thyristor and a diode (2,5V) or 2 thyristors (3V).

The path followed by the main current during each of the modes is as follows:

(a) Motoring below base speed:

"on" period = B, TH_1, L_1, D_4, M.

"free-wheel" period = L_1, D_4, M, D_2.

(b) Motoring above base speed:

"on" period = B, TH_1, L_1, TH_3.

"free-wheel" period = B, TH_1, L_1, D_4, M.

(c) Regenerative braking:

"on" period = M, TH_4, L_1, TH_2.

"free-wheel" period = M, TH_4, L_1, D_1, B.

(D_3 is a free-wheel diode when TH_4 is commutated and $E_M \geq V_B$)

6.6 COMMENTS ON THE THYRISTOR CHOPPER

The thyristor as a device is robust and is well suited for use as a chopper switch in an electric vehicle drive. However, some of the characteristics of the thyristor chopper should be noted:

(i) The reliability of the chopper operation depends on the ability of the capacitor to successfully commutate the main thyristor.

(ii) From figure 6.7, it is seen that the output voltage of the chopper will be load dependent, for, although the period t_1 is fixed by the mark/space ratio, the period t_2 ---- the discharge and recharge of the capacitor ---- is variable, dependent on the load current.

(iii) Similarly, the mark/space ratio will be restricted at high frequencies, because the minimum "space" period will correspond to time t_2, although this limitation may be avoided by using more complex circuitry to enable the recharging of the capacitor to be independent of the load [29] .

It was decided to investigate other types of choppers and to compare them to the thyristor chopper in terms of efficiency of operation, circuit simplicity and reliability.

CHAPTER 7

TRANSISTOR AND THYRISTOR-TRANSISTOR ARRAY SWITCHES

This chapter will describe the basic transistor chopper, and a static mode selection system using a combination of thyristors and transistors.

7.1 THE BASIC TRANSISTOR CHOPPER

To operate the basic transistor chopper illustrated in figure 7.1, the base of the transistor must be driven sufficiently hard to ensure saturation, which reduces the forward voltage drop to less than one volt (see figure 7.2), and then by removing the base drive, the transistor is turned off. As the voltage applied to the motor will be a rectangular waveform, it will not be load or frequency dependent, as was the case with the thyristor chopper.

7.2 THE TRANSISTOR CHOPPER FOR THE PERMANENT MAGNET MOTOR.

As the 150V voltage rating of the permanent magnet motor was too high for safe operation with a transistor chopper, the battery voltage was decreased by 84V, which reduced the maximum speed of the machine from 3000 r.p.m. to 1800 r.p.m. As single transistors capable of handling the full load motor current of 37A are expensive, the chopper consisted of a number of devices in parallel. A factory-matched array of 3 germanium transistors (MP902) with 150A and 120A rating was tried, but this older type of transistor with its lack of second breakdown capability (see section 106), was not suitable for use with inductive loads and the transistors were damaged by voltage breakdown in spite of protective zener diodes placed between collector and emitter.

Modern silicon transistors intended for switching operation have

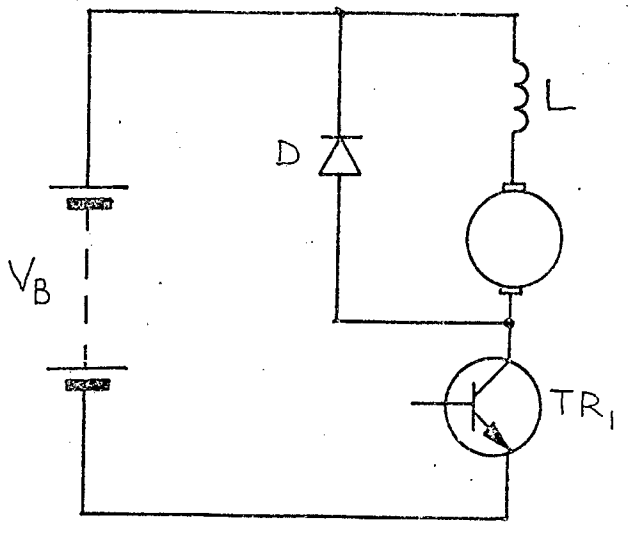

FIGURE 7.1 : BASIC TRANSISTOR CHOPPER

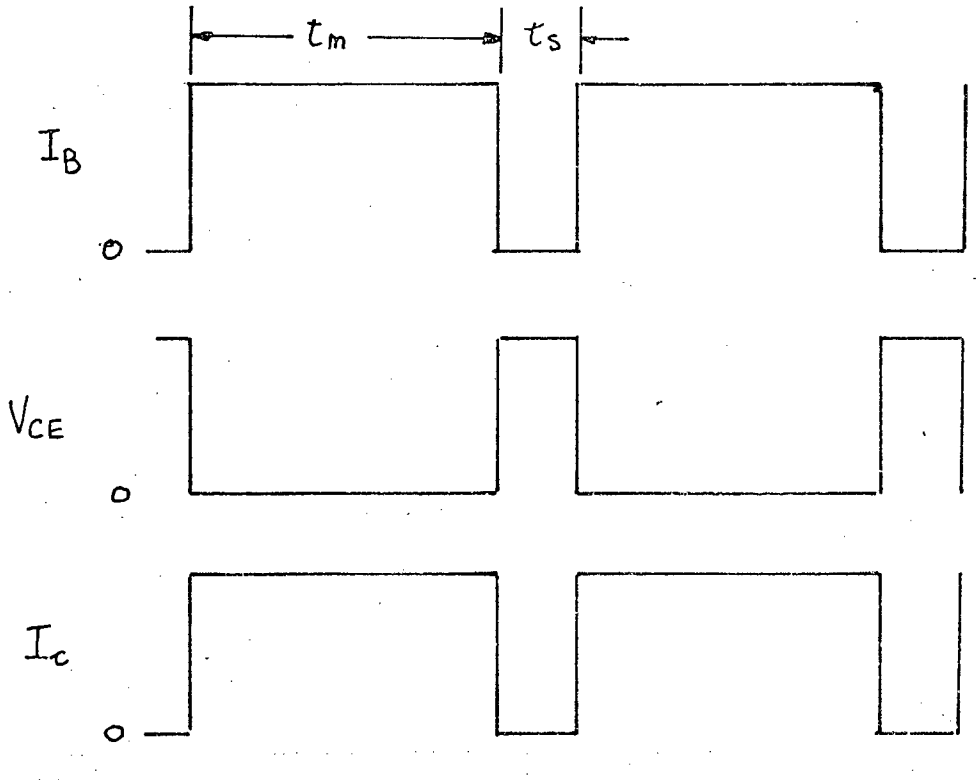

FIGURE 7.2: BASIC TRANSISTOR CHOPPER WAVEFORMS

high second-breakdown capability [37, 38] , and are more suited to inductive circuits. An array consisting of four 2N3773 in parallel was used for the chopper. Each of these transistors have a 30A peak current capability with a 140 volt V_{CE} rating. (see reference 37 for detailed specifications).

7.3 PARALLELING OF TRANSISTORS.

The four transistors, placed in parallel, were selected from a batch of 30, and were matched on the basis of their saturation voltage at a continuous collector current of 10A. A group with their saturation voltage spread over the range 520 - 560 mV was chosen.

In order to assess the current sharing of the transistors when connected in parallel, it was necessary to measure the individual transistor currents. This was done by connecting a 30A ammeter shunt of 3.3. m.ohm resistance in series with each collector as shown in figure 7.3. The emitters were directly coupled together and the collector leads were kept as short and as equal in length as possible. The transistors, mounted on a common heatsink, were saturated by providing a 1A base drive for each device, and with a total of 40A being drawn from the battery, the individual collector currents had a spread of only 6% about the mean value of 10A.

As the saturation voltage is proportional to both the collector current and the case temperature, (see specification sheets - reference 37) a satisfactory current sharing was achieved without the addition of current sharing resistors.

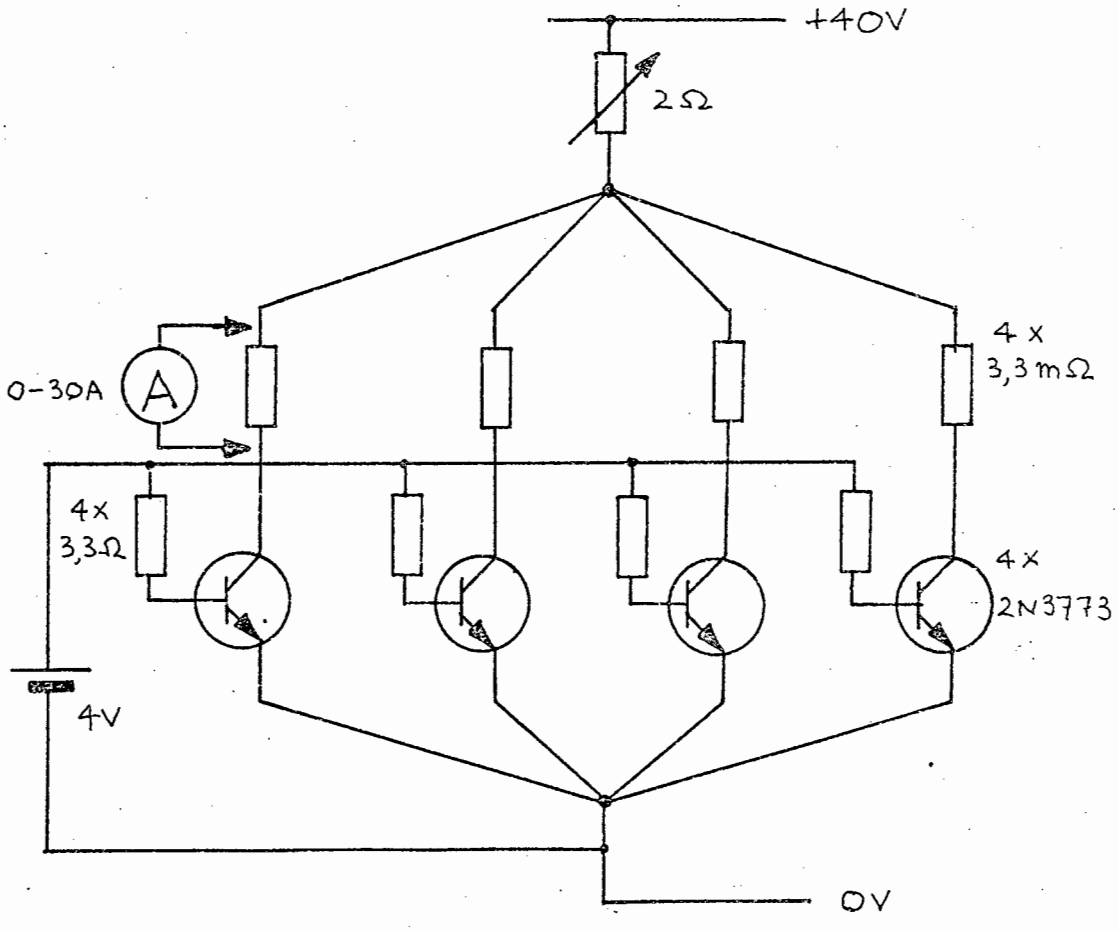

FIGURE 7.3, : CURRENT MONITORING IN PARALLEL ARRAY

7.4 BASE DRIVE TECHNIQUES

Consideration must be given to the most suitable method of driving the bases of the individual transistors of the chopper, so that each transistor will carry an equal share of the total load current. Because of the method in which the transistors were matched, each transistor must be supplied with an equal base drive. The base drive methods must also be evaluated in terms of their ability to saturate the transistors in the array, as this minimises the losses in the chopper.

(i) Darlington Pair

Figure 7.4(a) shows a basic Darlington configuration for achieving a high current gain for the transistor base drive. The main transistor, TR_p, is turned on by connecting the base resistor of the driver transistor, TR_D, to a voltage source greater than $2V_{BE} = 1,5V$. However, the disadvantage of this connection is that TR_p will not saturate as TR_D maintains the collector of TR_p at a higher potential than the base (see appendix for definition of saturation), causing increased losses and heating of TR_p.

This may be overcome by the addition of a series resistor in the collector of TR_p (figure 7.4(b)), so TR_D will drive TR_p fully into saturation. The value of R_C to ensure saturation is given by:

$$V_{CE\ (Sat)_p} + I_{c_p} R_C \geq V_{BE_p} + V_{CE\ (Sat)_D} \quad ...(7.1)$$

However, for parallel operation of power transistors, there must be a driver for each main transistor, to ensure that there is equal base drive in the power transistors.

(ii) Modified Darlington Pair

The main transistor (TR_p) can be driven fully into saturation by connecting the driver transistor to a separate supply (figure 7.5)

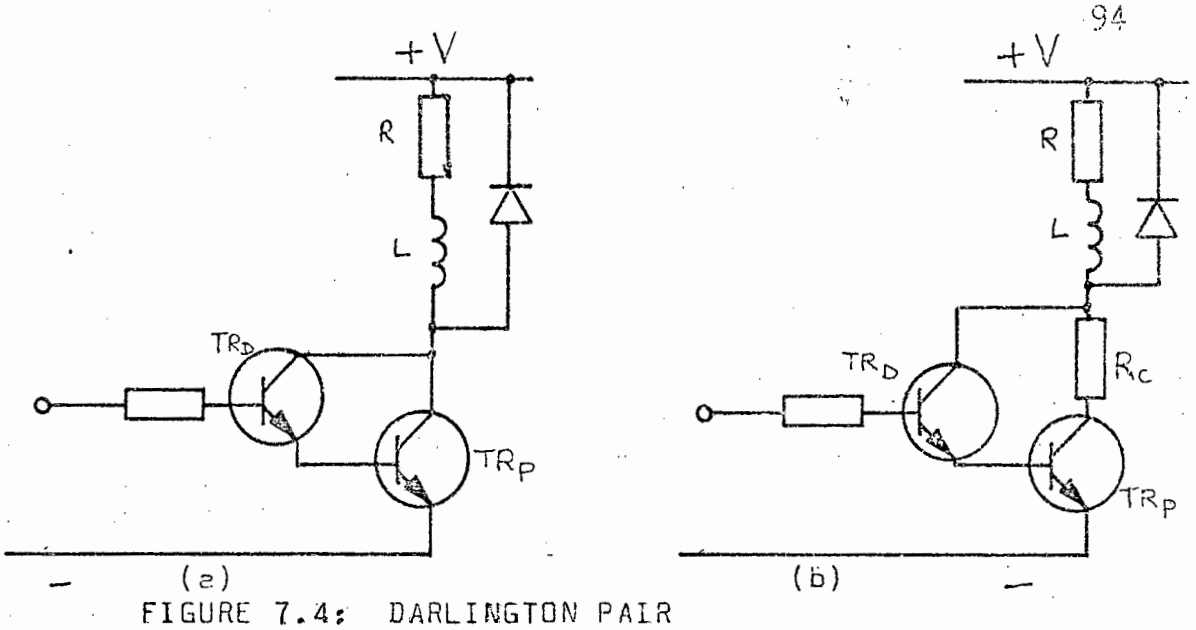

FIGURE 7.4: DARLINGTON PAIR

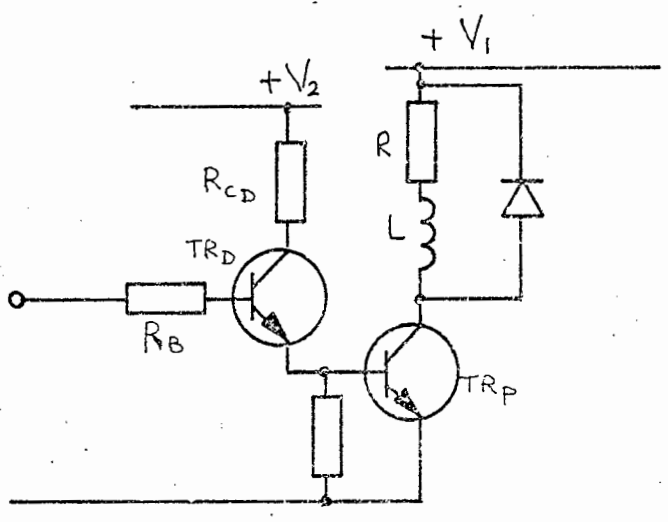

FIGURE 7.5: MODIFIED DARLINGTON PAIR

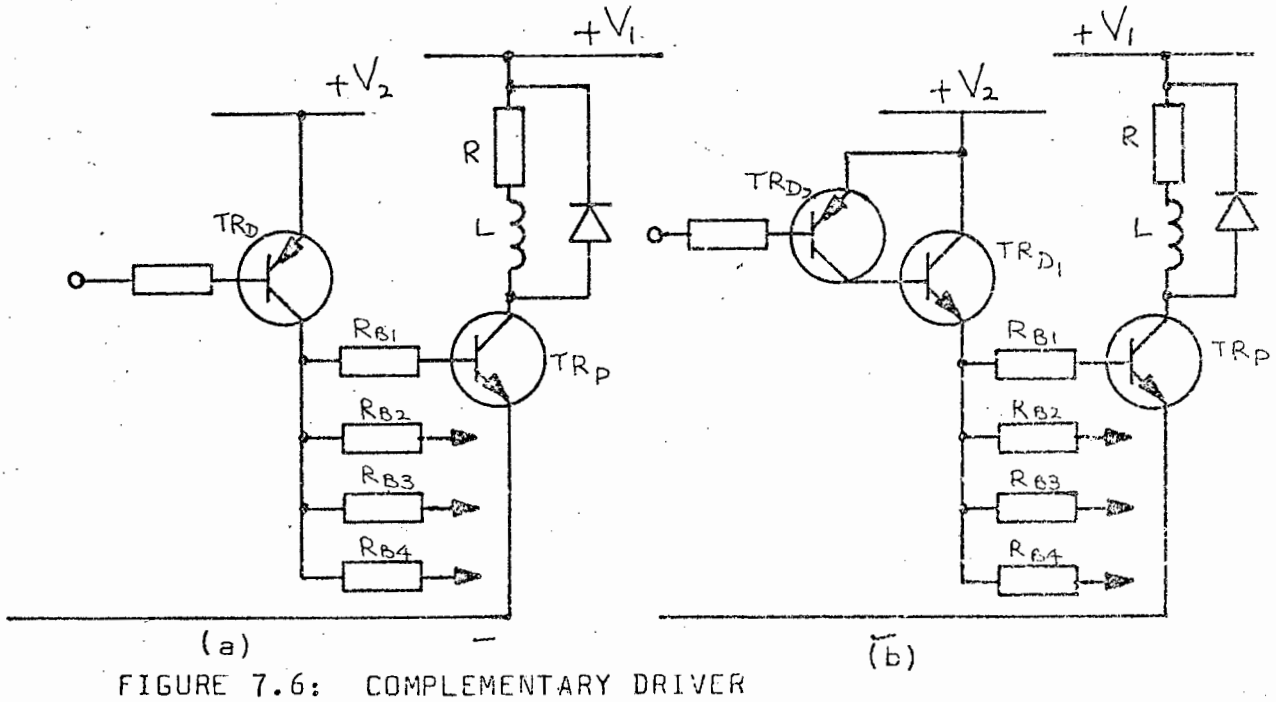

FIGURE 7.6: COMPLEMENTARY DRIVER

By keeping V_2 as low as possible, the power loss in R_{CD} is very little, and for V_2 = 6V this loss is approximately equal to that in R_C of figure 7.4(b). This configuration will allow TR_p to go fully into saturation, provided sufficient base drive is provided. However, as with the previous connection, this configuration is not suitable for a parallel array of transistors as one driver is required for each power transistor, if equal base drive is to be assured.

(iii) Complementary driver

With a PNP driver transistor and a NPN power transistor (figure 7.6) the advantages of the previous connections are maintained, while at the same time providing equal base drive via RB1, RB2, ... to all transistors in a parallel array (RB1 = RB2 ....).
However, when the transistor chopper was built, medium power PNP silicon transistors were difficult to obtain, and so the PNP driver of figure 7.6(a) was replaced by a PNP/NPN Darlington pair as in figure 7.6(b) which gives similar characteristics. It is unimportant that TR_{D1} will then not saturate, as the power consumed by the base drive of the main transistors is not large. It should also be noted that using the circuits of figure 7.6(a) and (b) the base waveform of TR_D must be inverted to produce the same output in TR_p as previously.

7.5 THE TRANSISTOR CHOPPER POWER CIRCUIT

(i) Circuit description

The implementation of a practical chopper for the permanent magnet motor is shown in figure 7.7. Although the chopper is shown connected for the mode of motoring below base speed, it may equally well be used in the other modes by appropriate reconnection of the

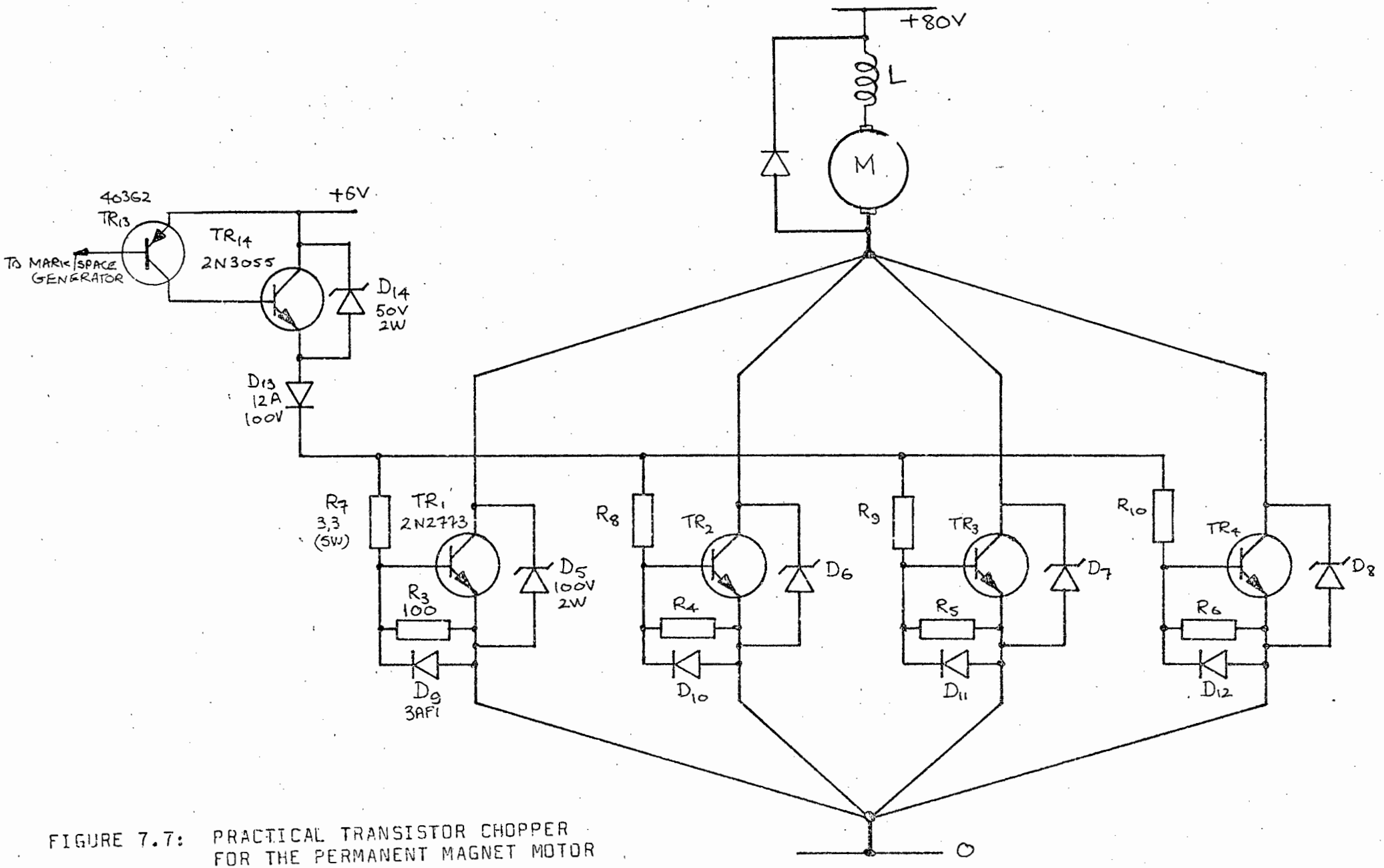

FIGURE 7.7: PRACTICAL TRANSISTOR CHOPPER FOR THE PERMANENT MAGNET MOTOR

chopper, motor, inductance and battery. The bases of the 4 parallel 2N3773 transistors were driven by a single 2N3055 transistor through 3,3 ohm resistors, from a separate 6V supply, providing 1A peak base current for each transistor. The base drive transistors were connected in the complementary configuration described in section 7.4(iii). Circuit details of the mark/space generator are given in section 7.7.

Protection for each transistor from voltage transients was provided by a 100V, 2W Zener diode connected between each collector and emitter, and a diode connected in anti-parallel with each base-emitter junction provided reverse voltage protection. The 100 ohm resistor connected between base and emitter was chosen from the specification sheets [37] as giving both increased V_{CE} rating and second-breakdown capability.

(ii) Switching waveforms of the transistor chopper

Some difficulties were encountered with the switching characteristics of the chopper shown in figure 7.7. From the switching waveforms shown in figure 7.8 for a collector current of 20A, it is seen that during turn-off, a step occurs in the collector-emitter voltage that is not present in the base current waveform. As this causes the turn-off losses to be approximately three times the turn-on losses, the total losses in the transistors, including switching and saturation losses, will be increased by approximately 25% above the calculated values of 7W per transistor (see Appendix for the calculations).

7.6 A SOLID STATE POWER CIRCUIT FOR SELECTING TWO MODES OF OPERATION

To change from one mode of operation to another when using the

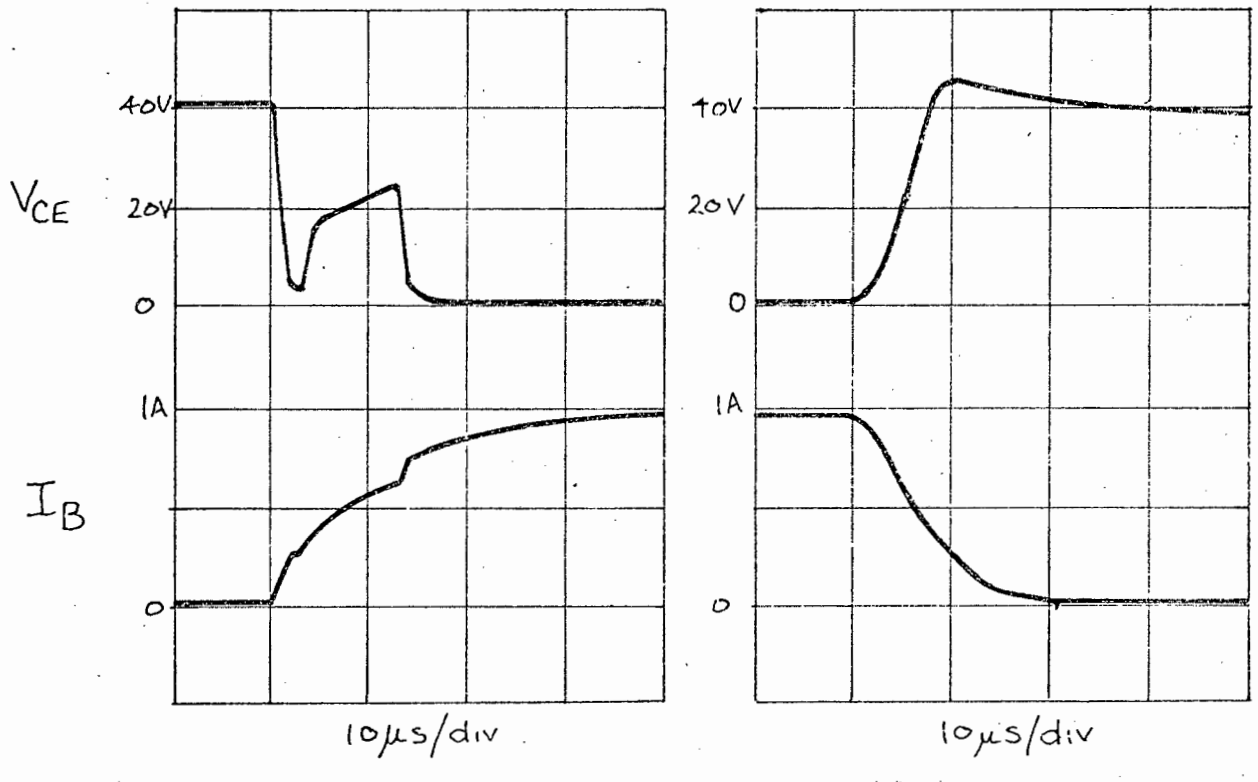

(a) TURN-ON (b) TURN-OFF

FIGURE 7.8: TRANSISTOR SWITCHING WAVEFORMS

transistor chopper just described, it is necessary to physically reconnect the circuit components. A power circuit will now be described which enables the motor to operate in either of two modes by appropriate gating of solid state switches.

(i) Circuit description

Because of the low leakage currents of silicon transistors when in cut-off (I_{CEO} = 2 mA for 2N3773), it is possible to use the parallel array of transistors described in the previous section as a line switch for thyristors, which have a holding current in the range 8-80 mA [44]. Figure 7.9 illustrates how two thyristors and the transistor array may be used as a fully electronic changeover switch for the modes of motoring and regenerative braking when $E_M \leq V_B$. Changeover is effected by the appropriate triggering of either TH_1 or TH_2 once the "on" thyristor has been commutated by the transistors. R_1 and R_2 are inserted to supply the thyristor being triggered with latching current.

The principle of operation of the circuit may be followed by considering the main current path for each of the two modes:

(a) Motoring:

on period = B, TH_1, L, M, D_3, TR_1.

free-wheel period = L, M, D_3, D_2.

(b) Braking:

on period = M, L, TH_2, TR_1, D_4.

free-wheel period = M, L, D_1, B, D_4.

(ii) The losses in the semiconductor components

During the "on" period in either the motoring or braking modes, the load current flows through the transistor, a diode and a thyristor. The maximum power loss in the semiconductors will occur

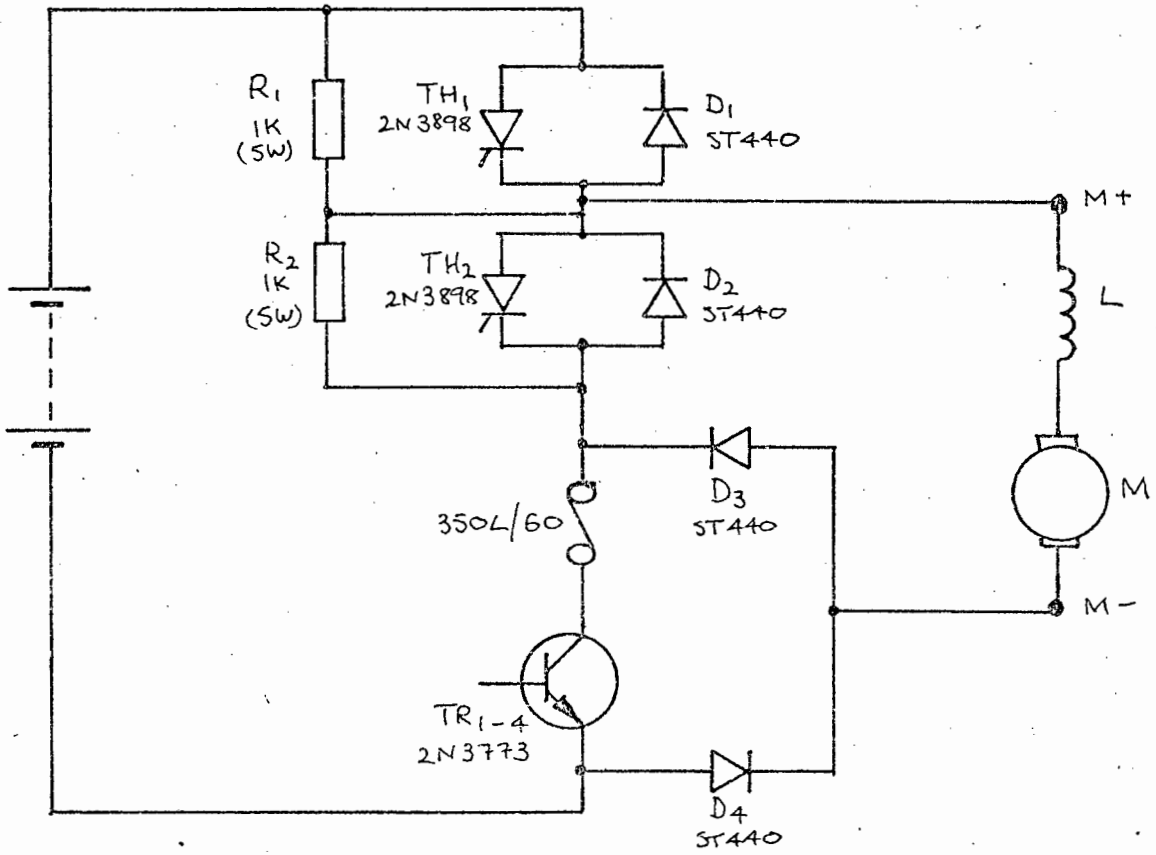

FIGURE 7.9: A HYBRID THYRISTOR/TRANSISTOR POWER CIRCUIT FOR BOTH MOTORING AND BRAKING.

at full load current and at a p.u. mark close to unity.

The calculated power loss in each of the semiconductors is:

Transistors : 22W (19%)

Thyristor : 55W (48%)

Diode : 37W (33%)

The total power loss is therefore 114W, corresponding to 3,7% of the input power from the battery.

7.7 CONTROL CIRCUIT FOR THE SOLID STATE CHANGEOVER SWITCH

To implement the operation of the solid state changeover switch, the necessary control circuitry which consists of a mark-space generator, thyristor trigger circuits and interlocking logic, must be incorporated into the system.

(i) Block diagram

The complete block diagram for the two mode motor control system is shown in figure 7.10. The relaxation oscillator, Schmitt trigger and inverter comprise the mark-space generator, which sets the on/off ratio of the power transistors. The gating of the correct thyristor for a particular mode is controlled by the logic and timing pulses from the mark-space generator.

(ii) Mark/Space Generator

A variable frequency saw tooth generator is produced by varying the charging current of a capacitor in a UJT relaxation oscillator (TR_5, figure 7.11). C_1, R_{11} and R_{12} were chosen from the manufacturer's data sheets [41] for the UJT used. When operating off a 10V supply, the voltage across C_1 varies linearly between 1V and 6V as shown in figure 7.12. If the capacitor is charged with constant current

$$I_c = C\, dv_c/dt \quad \ldots\ldots\ldots\ldots\ldots\ldots\ldots\ldots\ldots\ldots\ldots\ldots (5.1)$$

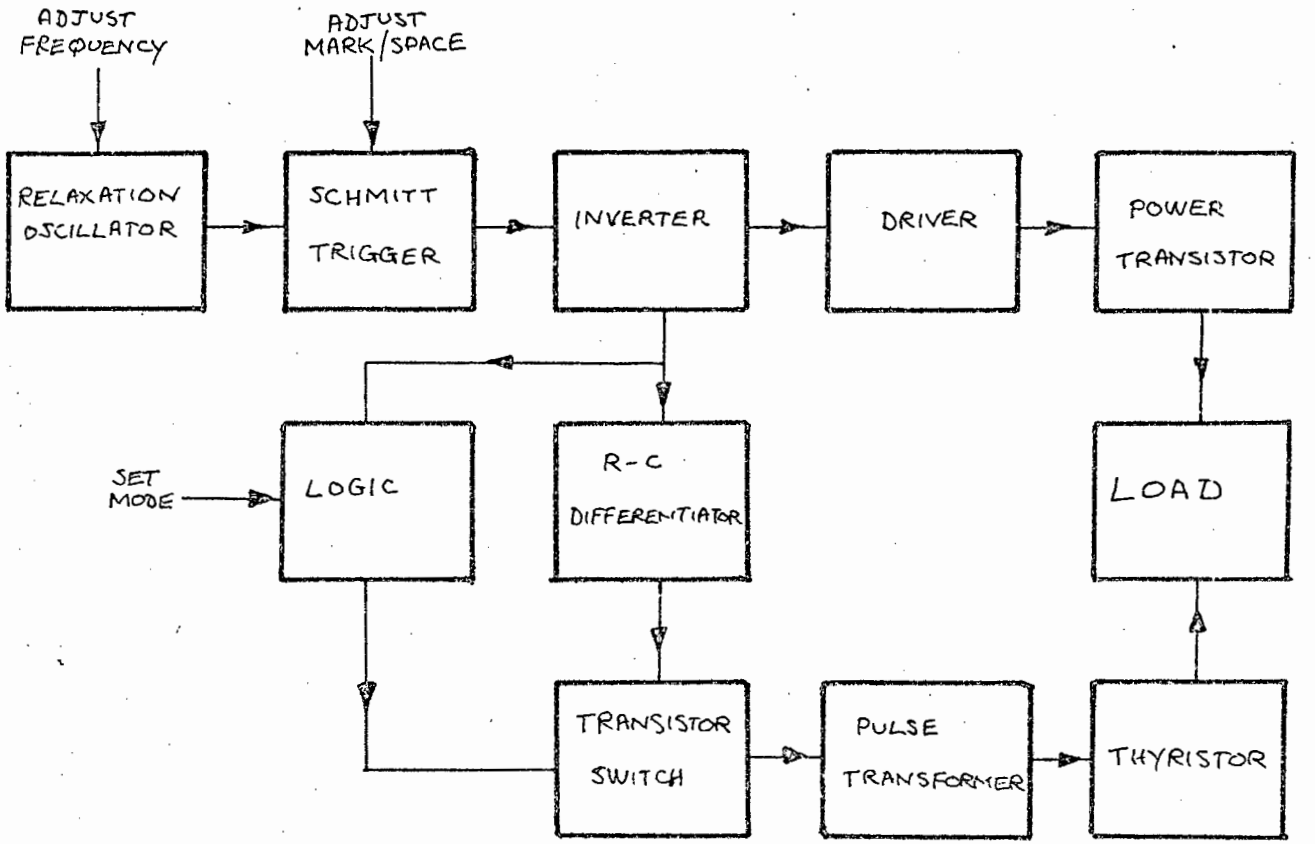

FIGURE 7.10: BLOCK DIAGRAM OF THE THYRISTOR/TRANSISTOR CHOPPER

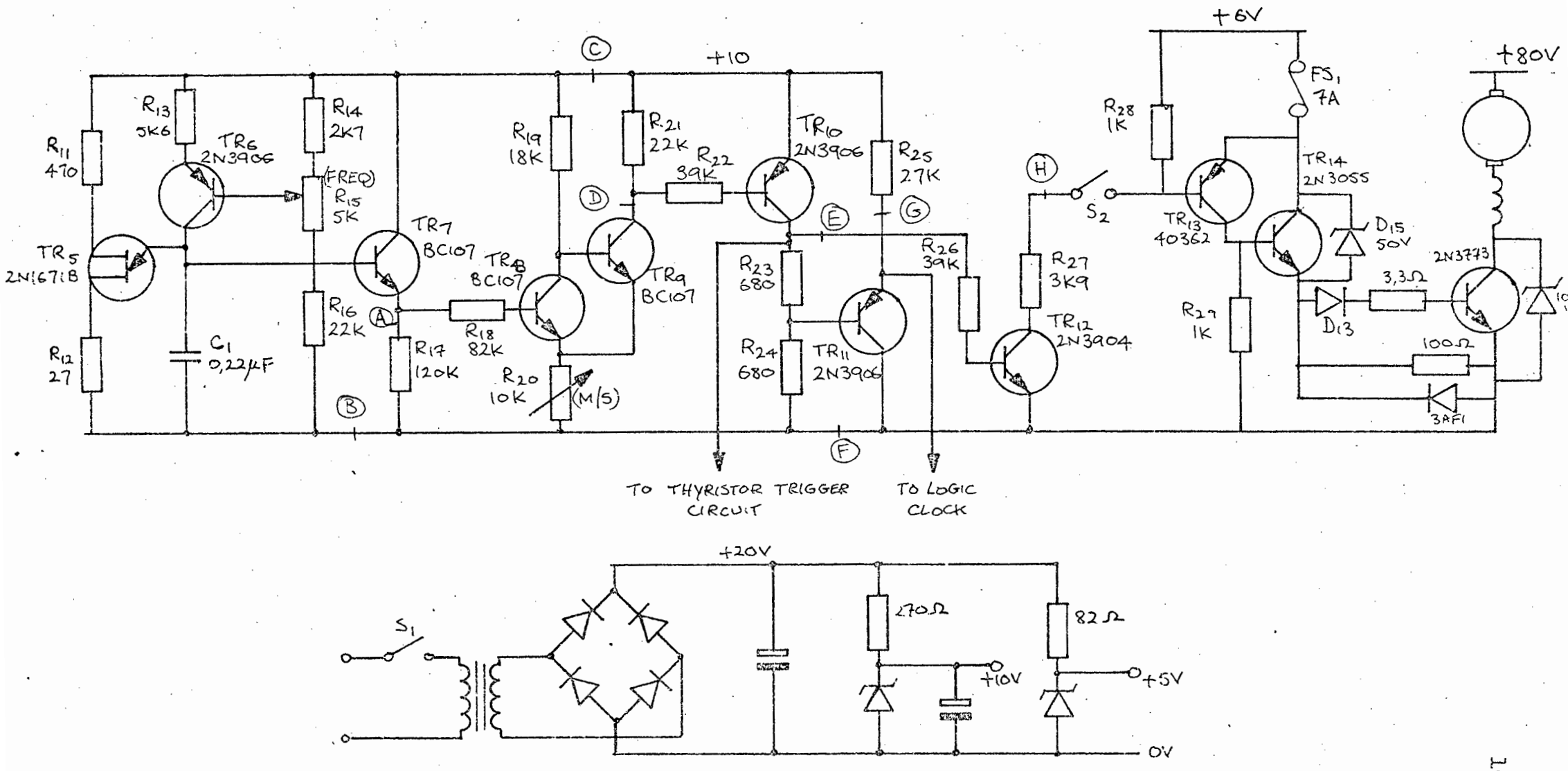

FIGURE 7.11: CIRCUIT DIAGRAM OF VARIABLE PULSE WIDTH GENERATOR AND TRANSISTOR DRIVER

where v_c is the voltage across the capacitor.

For a frequency of 50 Hz, I_c = 55 microamps

For a frequency of 500 Hz, I_c = 550 microamps

This current is regulated using an emitter follower circuit consisting of TR_6 and R_{13} and a potential divider consisting of R_{14} and R_{15} and R_{16}.

The switching level of the Schmitt trigger (TR_8 and TR_9) is variable between 0 and 6 volts, by means of R_{20}. As the output of the Schmitt trigger, taken between the 10V rail and the collector of TR_9 produces voltage pulses of limited and varying amplitude as shown in figure 7.12, it is necessary to take this output through an inverter to obtain the full voltage swing between the rails.

The output of this inverter is then passed on to the driver stage (TR_{12} - TR_{14}) and to an RC differentiator that produces trigger pulses for the thyristors.

The output of the inverter is a convenient point to generate a clock pulse for the logic which is fully described in section 7.7.(iv) Making R_{22} = R_{23} = 680 ohms the level of 5V required by the TTL is obtained. As the normal state of TTL logic is the "1" level, it is necessary to have the transistor switch TR_{11} to switch the clock to the "0" level.

The driver stage was supplied from a 6V battery, in order to keep the base drive losses at a minimum. The PNP/NPN pair of TR_{13} and TR_{14} was used to replace a medium power silicon PNP transistor. Assuming a forced beta of 10, the main power transistors (TR_1 - TR_4) were each supplied with just over one amp (peak) base drive. TR_{12} is then required to carry approximately 50 mA. S_2 completely isolates the last stages of the driver circuit, keeping the main transistors on the off state.

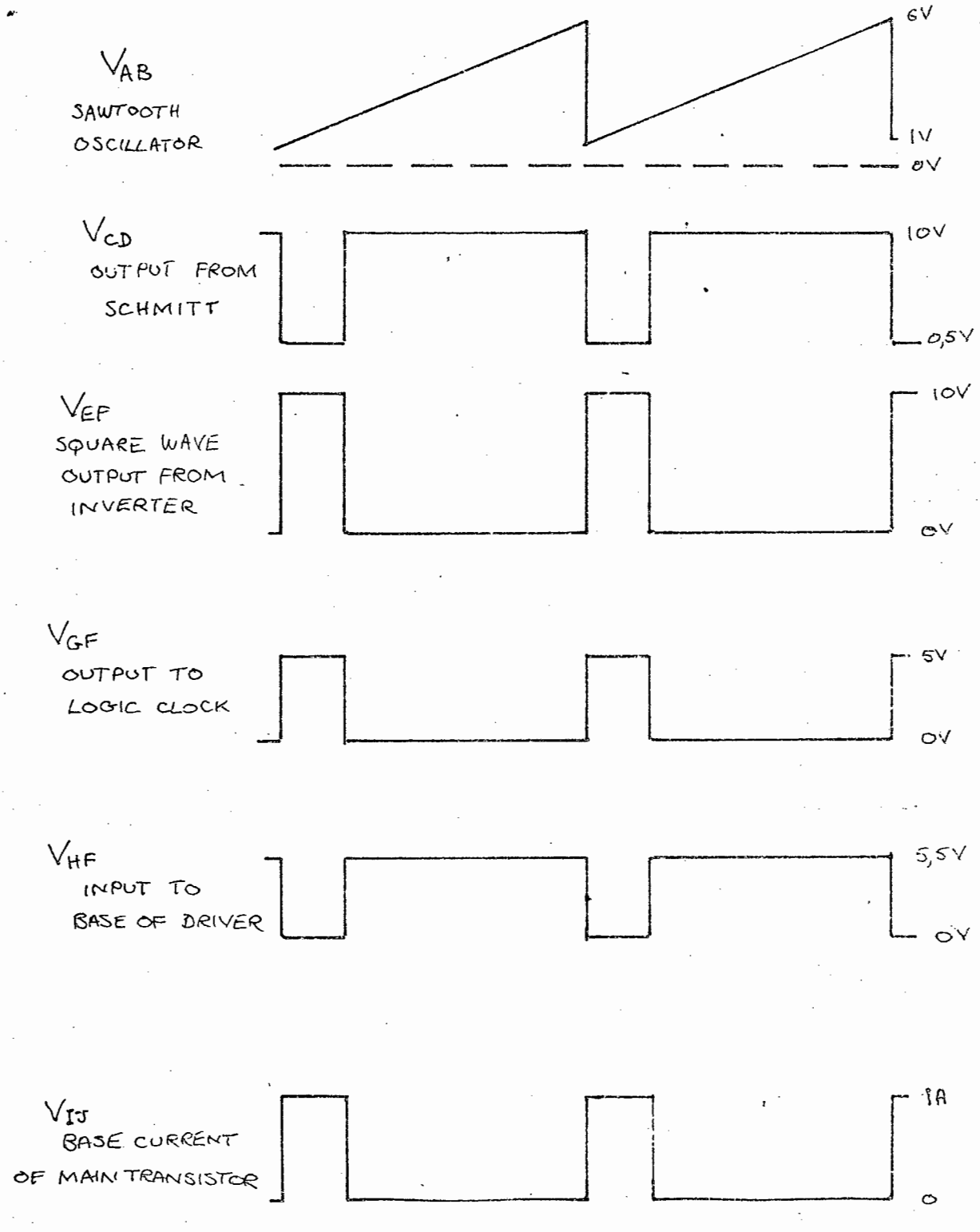

FIGURE 7.12: VOLTAGE WAVEFORMS OF VARIABLE PULSE WIDTH GENERATOR. (1/5 MARK/SPACE)

D_{14}, a 12A 200V silicon diode, protects the power transistors against reverse V_{BE} damage and D_{15}, a 50V 2W Zener diode, protects TR_{14} against any excessive voltage spikes between the collector and emitter.

(iii) Trigger circuit for thyristors

Thyristors 1 and 2 of figure 7.9 are triggered by voltage pulses generated from the square wave transistor driver, obtained from the collector of TR_{10}. Pulse triggering of thyristors requires that the gate be overdriven by a pulse of current much larger than the dc gate current required to trigger the device. The use of a large current pulse reduces variations in turn-off time, minimizes effect of temperature variations on triggering characteristics, and makes possible short switching times. The minimum requirement for the pulse width is that it should be wide enough for the thyristor anode current to achieve latching value. However, a more conservative design would require the pulse width to be at least equal to the turn-on time of the thyristor [33] .

Square waves with fast rise and fall times applied to C_2 of figure 7.13, produce voltage pulses across R_{29} with time constant RC. As the turn-on time of the thyristors used was 2 microseconds, a time constant of 10 microseconds would ensure triggering. With R = 2K7 ohm and C = 4,7nF, a time constant of 13 microseconds was obtained.

As only the positive pulses, as shown in figure 7.14 are required, (this being when the power transistors are being switched from the "off" to "on" state) the negative pulse is eliminated by D_{16}. The parallel connection of D_{16} used here was found to be more effective than the more common series connection.

The spacing between the positive and negative pulses is

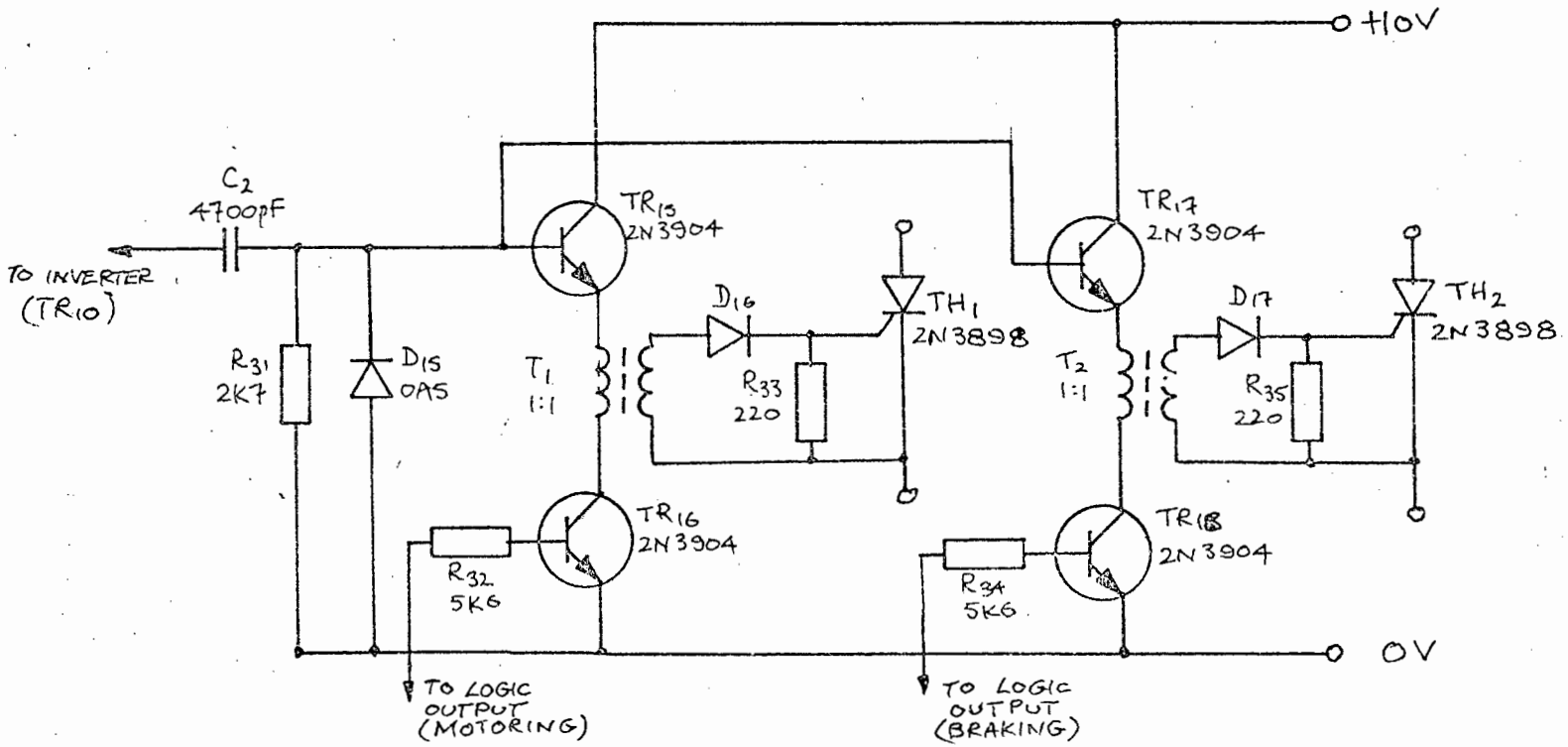

FIGURE 7.13 : TRIGGER CIRCUIT FOR THYRISTORS

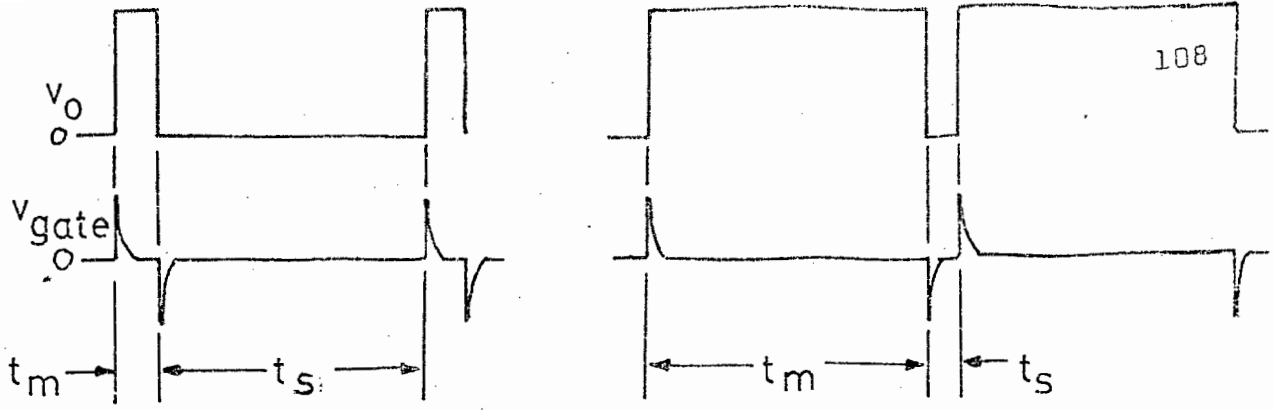

(a) LOW MARK/SPACE

(b) HIGH MARK/SPACE

FIGURE 7.14 : SPACING OF THYRISTOR TRIGGER PULSES

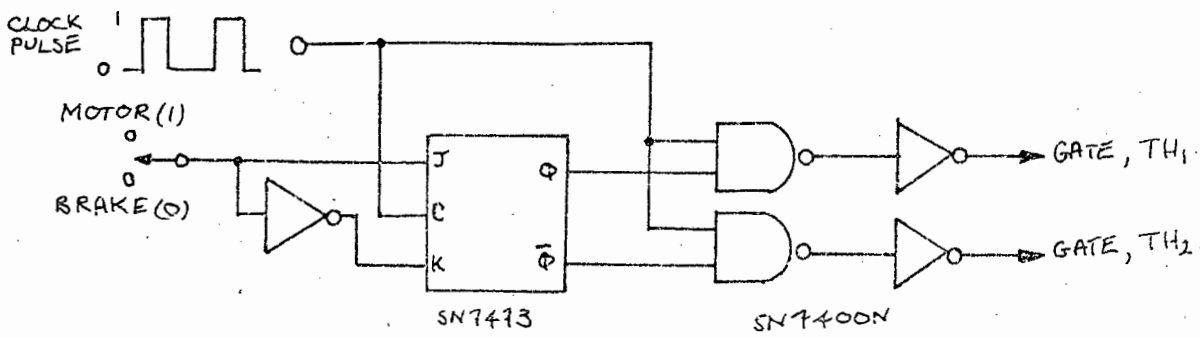

FIGURE 7.16 : LOGIC CONTROLLING THE GATING OF THE THYRISTORS

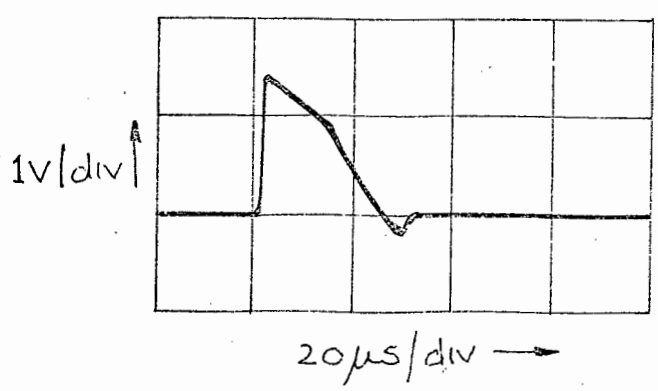

FIGURE 7.15 : A TRIGGER PULSE FOR THYRISTORS

important as it determines the upper and lower limits of the mark/space ratio (t_m/t_s). If the spacing between the positive and negative pulses is less than 6 RC (i.e. before the capacitor current has effectively reached zero) the amplitude of the pulses is reduced, this reduction becoming more marked as the spacing is decreased. The minimum off-time (t_s) at 400 Hz was set to 100 microseconds, giving an upper mark/space ratio of 19:1, or output voltage = 95% of maximum. The lower m/s was similarly determined by the value of t_m such that the positive pulse was of sufficient amplitude to turn on the respective thyristor. Thus a range of voltage from 5% to 95% of the battery voltage can be generated.

To provide dc isolation between the trigger circuit and the two thyristors, pulse transformers were used. These were wound on ferrite pot-cores with 100 turns of 42 SWG wire on both primary and secondry. Low impedance drive was provided for the transformers by TR_{15} and TR_{17}, and the selection of the desired thyristor for use is determined by the state of switches TR_{16} and TR_{18}, which are driven by the output of the logic. D_{16} and D_{17} provide reverse voltage protection for the thyristor gates and R_{30} and R_{31} provide a low impedance (220 ohm) link between gate and cathode. The shape and magnitude of the gate pulse is shown in figure 7.15.

(iv) Logic control of the triggering of TH_1 and TH_2

For the proper functioning of the static changeover switch, consisting of the two thyristors and the transistor commutator, the following requirements are necessary when changing from one mode to another:

(a) The thyristors must not be triggered simultaneously, otherwise a directly short will be placed across the battery.

(b) The second thyristor must not be triggered until the thyristor that was conducting, has been commutated.

By using the J-K flip-flop in the circuit in figure 7.16, both these requirements are satisfied.The desired mode is selected by connecting the "J" input of the flip-flop to a "I" for motoring, or to a "0" for braking. Identical levels cannot appear at the outputs of the flip-flop, and in addition, the flip-flop cannot change state until the clock level falls to zero, which corresponds to the main transistors being turned off. The outputs of the two NOT gates are connected via 5K6 resistors to the bases of TR_{16} and TR_{18}, figure 7.13, which control the operation of the pulse transformers T_1 and T_2.

7.8 A COMPARISON BETWEEN THYRISTOR AND TRANSISTOR/THYRISTOR HYBRID CHOPPERS.

The principles of operation, and the basic design procedures have been outlined for the two types of choppers --- the capacitor-commutated thyristor chopper, and the chopper which uses both thyristors and transistors as switching elements. The two types of choppers will now be compared in terms of their power loss and output voltage characteristics, and their suitability for use in a motor controller will be evaluated.

(i) Power loss

Figures 7.17(a) and (b) show the losses in a transistor/thyristor hybrid chopper and in a capacitor commutated thyristor chopper as a function of the average chopper current.

From the power loss at 0,8 p.u. mark shown in figure 7.17(a) the losses of the individual semiconductors in the hybrid chopper shown in figure 7.9 would be:

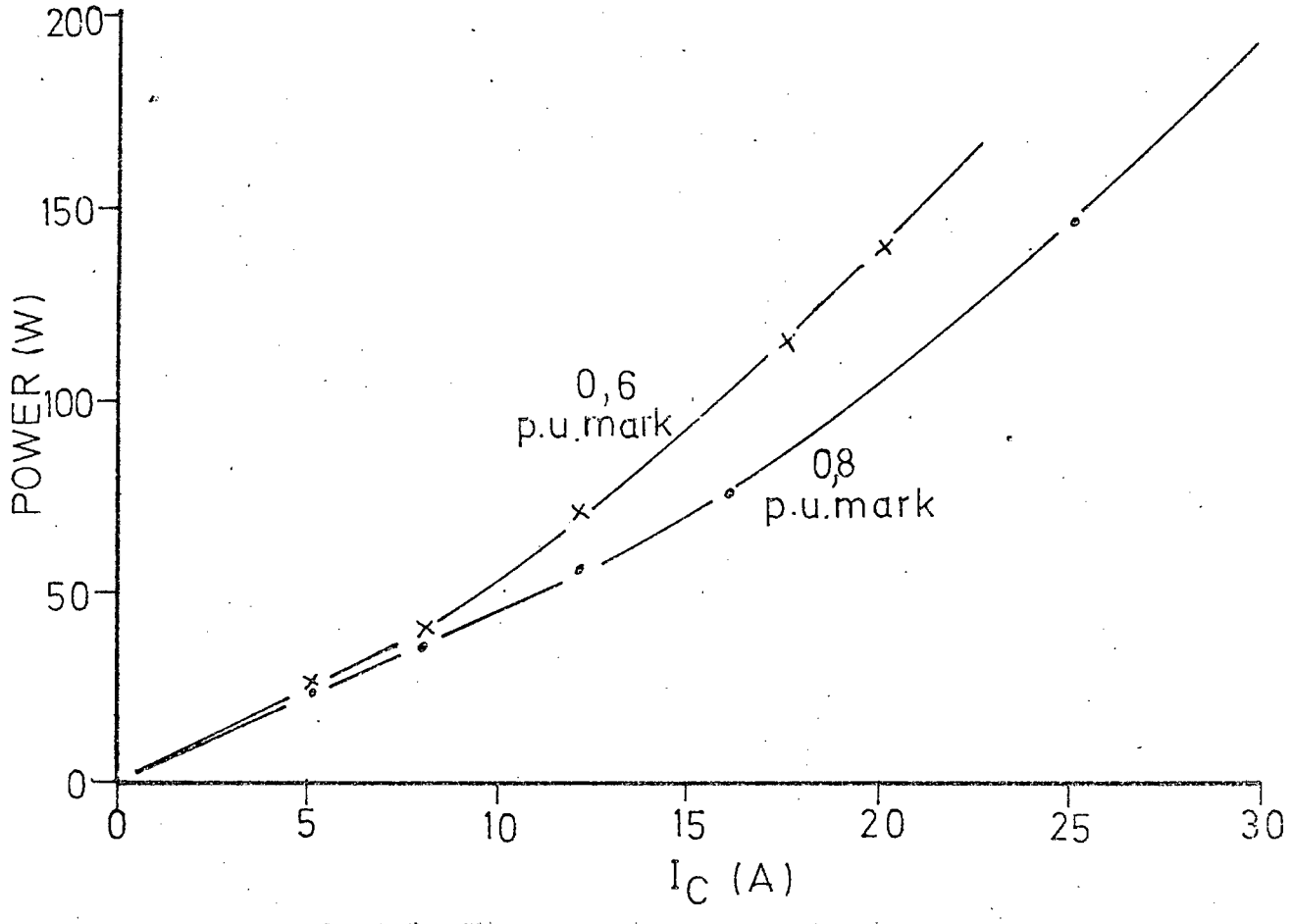

(a) TRANSISTOR/THYRISTOR CHOPPER

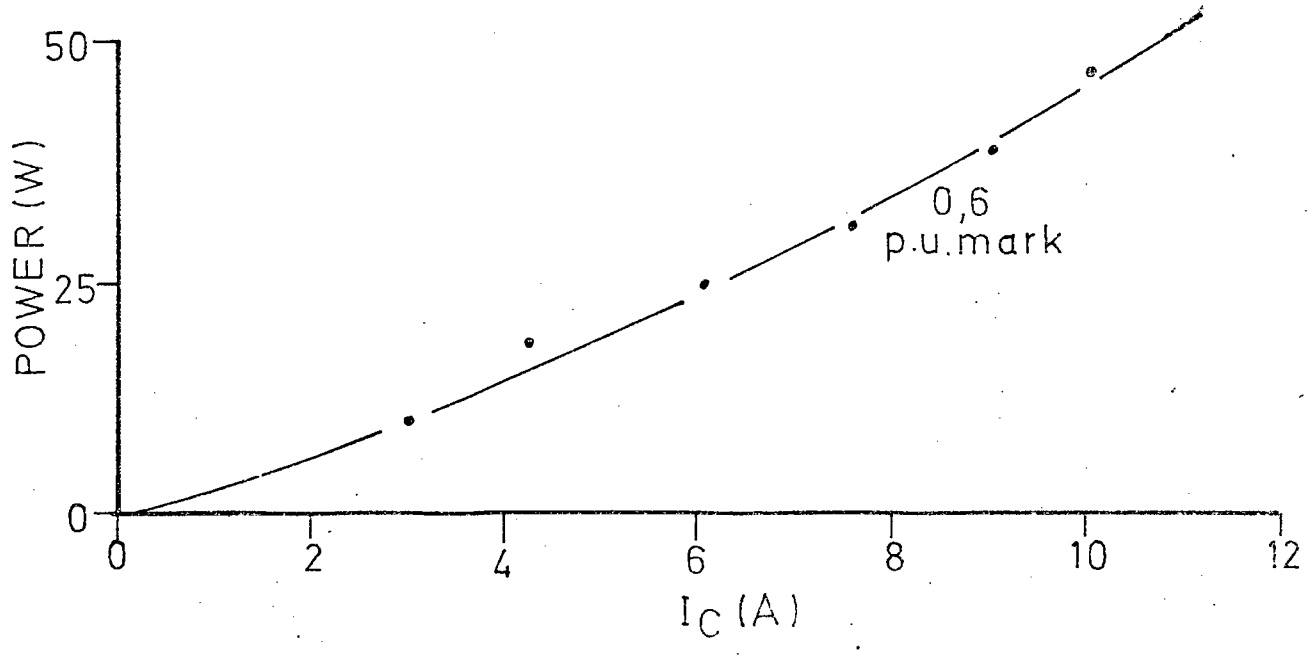

(b) THYRISTOR CHOPPER

FIGURE 7.17: COMPARISON OF POWER LOSSES OCCURRING IN CHOPPERS AT 400 Hz.

TH_1 : 40%; TR : 30%; D_3: 25%; D_2: 5%

From the measurements of the power loss in the thyristor chopper, it may be deduced that the commutation and switching losses account for approximately half the total power losses, if a forward voltage drop of 1,5V is assumed. At the same current and per unit mark, the transistor/thyristor chopper has approximately 50% more power loss than the thyristor chopper. This is because the hybrid chopper has 3 semiconductors in series during the "ON" period, causing a voltage drop of 3V as compared to approximately 1,5V for a similar thyristor chopper, as shown in figure 6.10, which also enables two modes of operation to be selected.

(ii) Output voltage characteristics

The effect of the capacitor commutation pulse in the voltage waveform of the thyristor chopper is shown in figures 7.18 - 7.20. The width of the commutation pulse is dependent on the load current - i.e. the rate at which the capacitor recharges. Over any one period then, the chopper output voltage has two components - one proportional to the p.u. mark, and the other inversely proportional to the load current.

The output voltage of the hybrid chopper, on the other hand, is virtually uneffected by load current or frequency of operation, because of rectangular shape of the output voltage.

7.7 THE APPLICATION OF THE TRANSISTOR/THYRISTOR CHOPPER IN A VEHICLE DRIVE SYSTEM.

The use of a two mode transistor/thyristor hybrid chopper in a vehicle drive system instead of a two mode thyristor chopper would reduce the overall efficiency by approximately 2%, for a battery voltage of less than 100V.

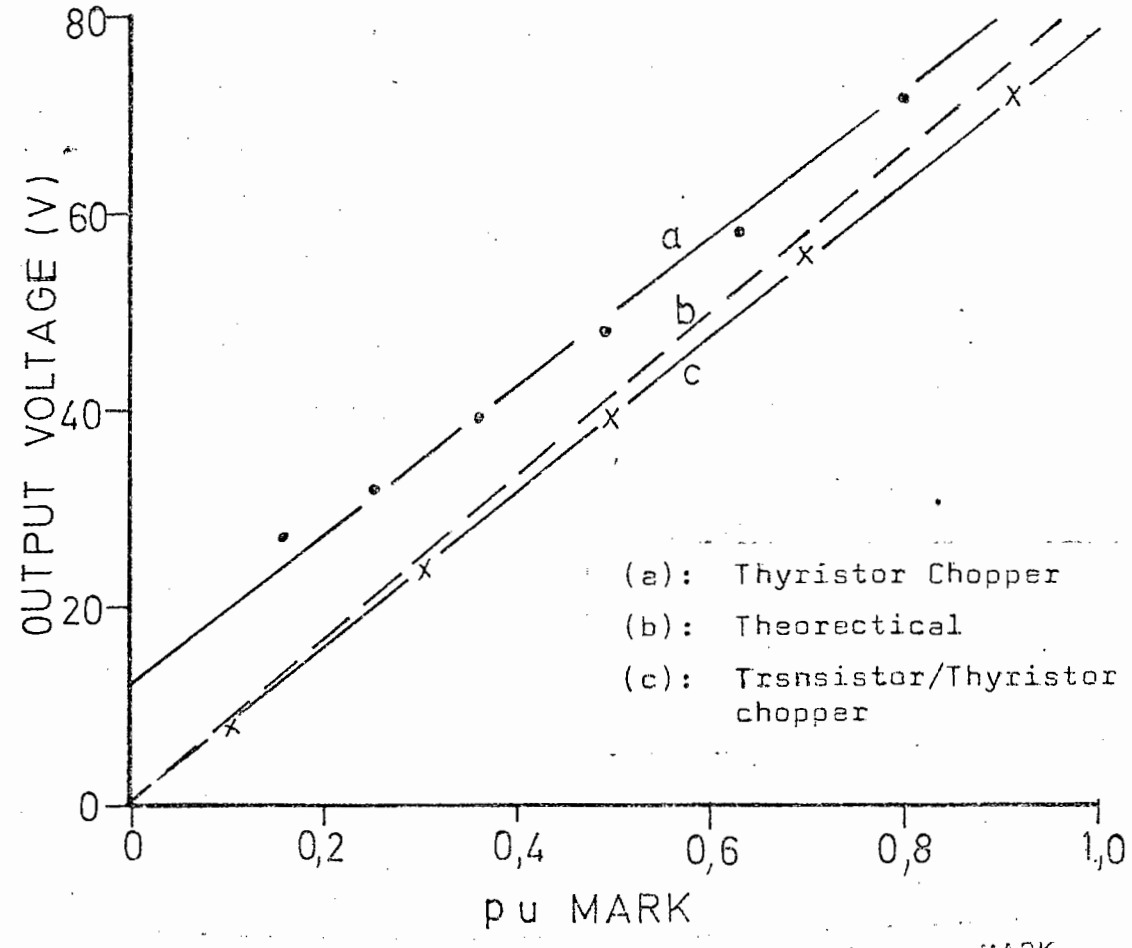

FIGURE 7.18 : RELATIONSHIP BETWEEN p.u. MARK AND OUTPUT VOLTAGE

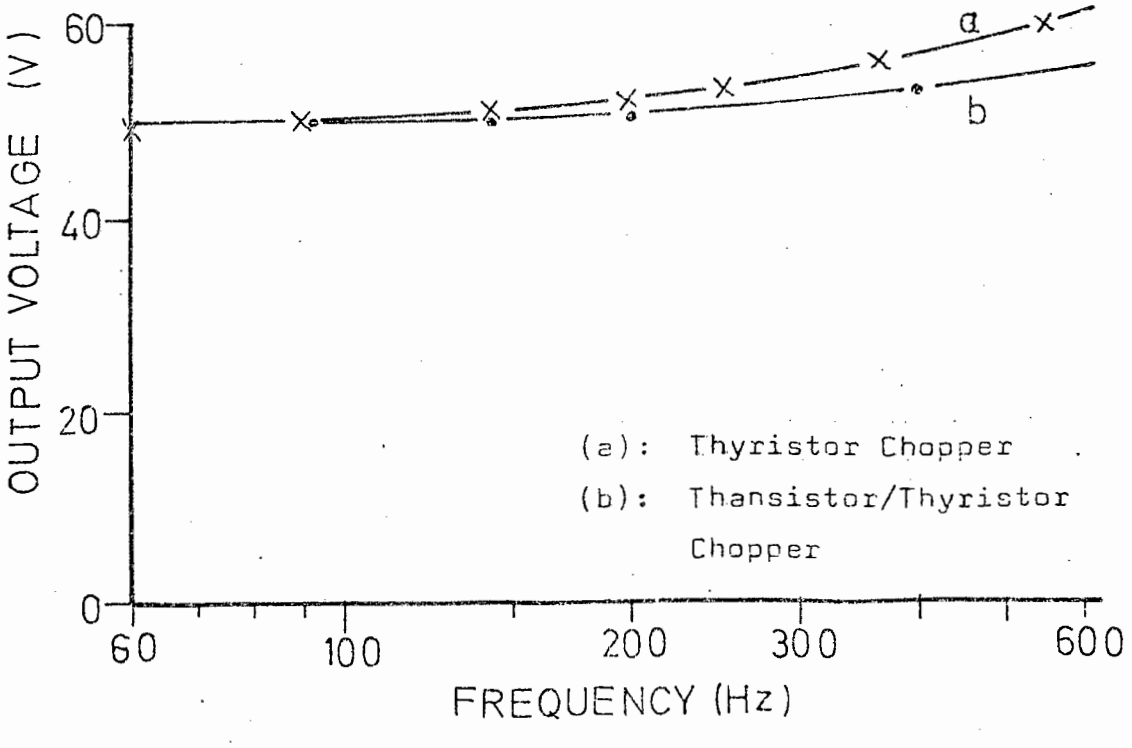

FIGURE 7.19 : RELATIONSHIP BETWEEN FREQUENCY AND OUTPUT VOLTAGE AT CONSTANT MARK/SPACE

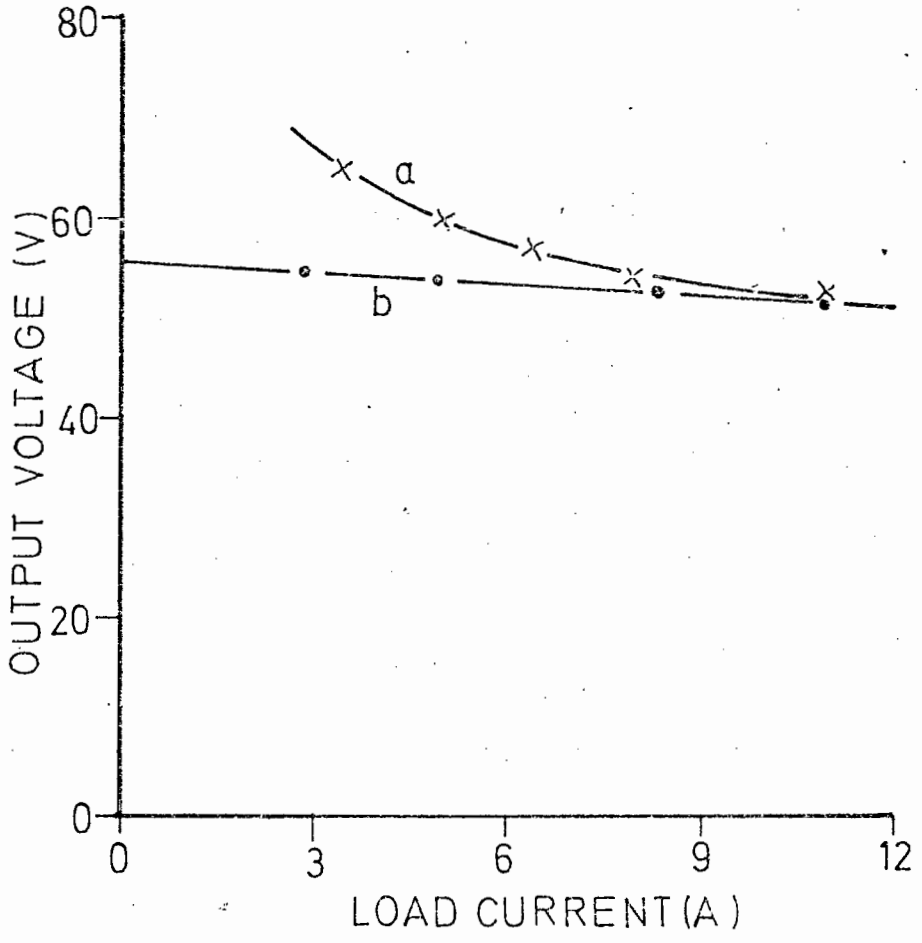

FIGURE 7.20 : INFLUENCE OF LOAD CURRENT ON THE OUTPUT VOLTAGE OF CHOPPERS AT 400 Hz AND CONSTANT MARK/SPACE

(a): Thyristor Chopper

(b): Transistor/thyristor chopper

No simple circuit could be devised for selecting three modes of operation using a transistor as a line switch for thyristors, as in the two-mode changeover switch described in this chapter. The only method of accomplishing static switching for all 3 modes is to use the thyristor switching array shown in figure 6.12.

The transistor as a device is not as suited to traction drives as is the thyristor, as the transistor has a lower breakdown voltage and a lower peak/average current capability than the thyristor. Although the surge current capability of a chopper containing transistors can be raised by increasing the current rating of the transistors, this creates an average current rating which is much higher than is required.

Weber [32] suggests a factor of safety of 3 in the current rating of the transistors. For a 200A motor circuit, he uses 10 transistors of 60A rating in parallel. This still does not match the surge current rating of thyristors which is usually 10 times that of the average current rating.

CHAPTER 8

ENERGY AND POWER CONSIDERATIONS FOR THE ELECTRIC VEHICLE

8.1 INTRODUCTION

In designing a drive system for an electric vehicle, the maximum speed and range must be selected, as these determine the power and energy requirements of the motor and the storage system respectively. As the energy density(kWh/kg) of storage cells is at present 1000 times less than that obtainable from chemical fuels, careful consideration should be given to the choice of the most suitable energy storage arrangement.

This chapter will therefore investigate the various storage systems, and an attempt will be made to estimate the size of the motor and battery suitable for a small vehicle which has an empty mass (mass of vehicle without batteries) of approximately 400kg.

8.2 TYPES OF ENERGY STORAGE SYSTEMS

The most widely used secondary cells at present are the lead/acid; nickel/cadmium (or iron) and silver/zinc, of which the lead/acid is by far the most popular, for a number of reasons which will be discussed later. Recently the fuel cell has made a competitive stand in this field and high temperature cells, sodium/sulphur (Ford Motor Co.) and lithium chlorine (General Motors), offering greatly increased energy densities, are under development, but as yet have not been produced commercially [20, 48] .

8.3 FUEL CELLS

Although the same basic laws of electro-chemistry apply to storage batteries and fuel cells, one major point of difference is that whereas in storage batteries the oxidant and fuel are kept

inside the reaction cells, in the case of fuel cells, both of these materials are stored outside and are fed in continuously when current is required. Arrangements are also made to remove the reaction products from the site of the reaction as rapidly as possible, thereby eliminating one of the main factors causing polarisation in storage batteries. Figure 8.1 shows the family of discharge voltage curves at different current ratings for a conventional lead/acid battery. The effect of polarisation is shown in the "knee" of the discharge curves.

Since the oxidant and the fuel, usually oxygen and hydrogen or hydrazine ($N_2 H_4$), are held outside the reaction cell, when exhausted they can quickly be replenished in much the same way as fuel is added to the tank of a motor car. In this respect, fuel cells have an obvious advantage over storage batteries, which generally require several hours of recharge, however, energy cannot be returned to the fuel cell with a regenerative braking scheme as in the case with other cells. The life of the fuel cell is largely determined by the rate at which the electrolytes deteriorate, as is the case with storage batteries [20, 21] .

8.4 COMPARISON OF STORAGE SYSTEMS

The open-circuit terminal voltages of the cells considered are noteworthy: 2.0V for lead/acid; 1.3V for nickel/cadmium; 1.6V for silver/zinc; and 1.2V for the oxygen/hydrogen fuel cell. This means to obtain a battery of any given voltage, the number of cells required is in the ratio 4:6:5:7, indicating a practical advantage of the lead/acid system.

Figure 8.2 shows the energy densities at different rates of discharge of the various systems. These curves indicate that, for

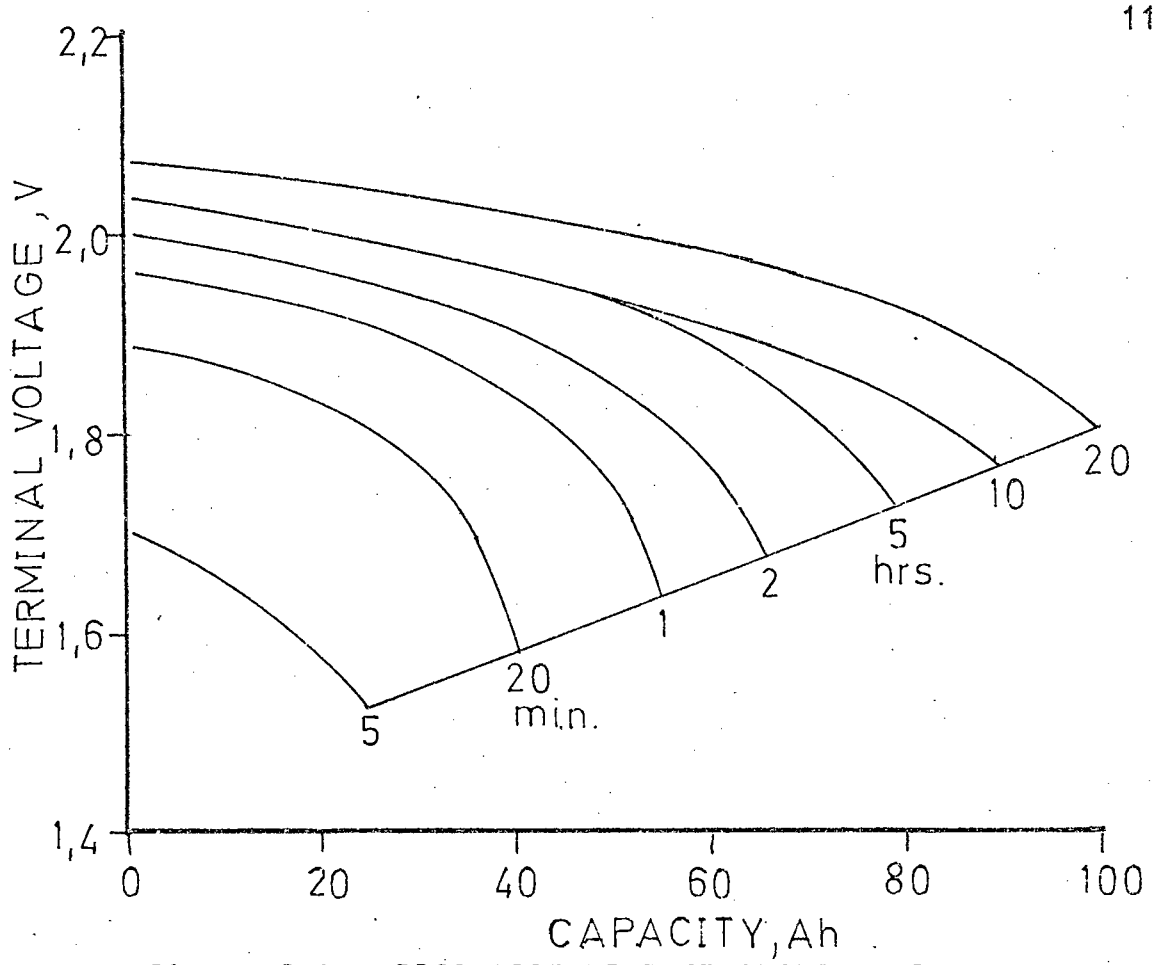

Figure 8.1: DISCHARGE VOLTAGE CURVES AND CAPACITY AVAILABILE AT VARIOUS RATES OF DISCHARGE FOR A 100 Ah LEAD-ACID BETTERY [21] .

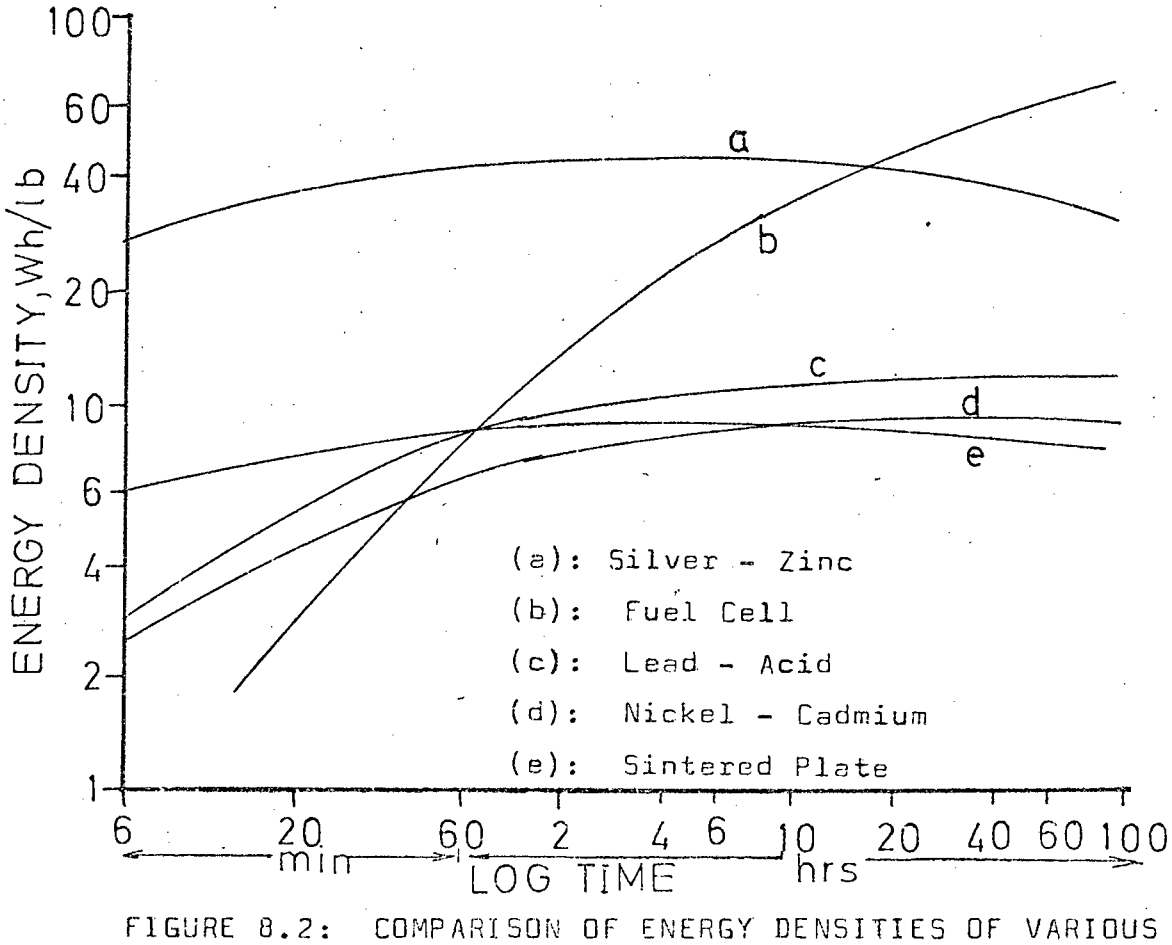

FIGURE 8.2: COMPARISON OF ENERGY DENSITIES OF VARIOUS SYSTEMS AT DIFFERENT RATES OF DISCHARGE 21 .

durations of less than 1 hour, the lead/acid and nickel cadmium batteries have a higher energy density than fuel cells. At discharge rates of about 4 hours, i.e. those commonly associated with traction, the fuel cell begins to show superiorty. A detailed analysis of the possible application of fuel cells to electric cars has been made by Poulston and Kirkley [22] . Although the silver/zinc battery has an energy density four times that of a lead/acid battery, the high cost and limited reversibility rules out the silver/zinc system for most commercial applications. Therefore, the low cost, high degree of reversibility and high current densities possible, make the lead/acid system a popular choice, and the use of this battery will be assumed in the calculations to follow.

8.5 THE RELATIONSHIP BETWEEN THE VEHICLE AND BATTERY MASSES.

The range of a vehicle travelling at a constant speed is a function of the stored energy contained in the battery. As the stored energy capacity is increased, by adding larger cells, the range is progressively increased until a stage is reached when the range/unit vehicle mass becomes a maximum, and any further increase in the size of the batteries does not achieve a corresponding increase in range. This optimum size of the battery occurs approximately when the battery and vehicle masses are equal. This may be illustrated as follows:

If we have vehicle mass = M_V, and battery mass = M_B

Rolling friction is proportional to the total mass

$$F_R = k_1 (M_V + M_B)$$

Assuming the energy capacity of a battery is proportional to mass (i.e constant kWh/kg)

$$E_B = k_2 M_B$$

At slow speeds, wind resistance may be neglected, therefore the work done against friction over a distance d is

$$E_R = k_1 (M_V + M_B) d$$

If the energy of the battery is fully expended

$$d = \frac{k_2 M_B}{k_1 (M_V + M_B)}$$

Range/unit mass $d' = \frac{k_2 M_B}{k_1 (M_V + M_B)^2}$

this is a maximum when

$$M_V = M_B$$

This means for a vehicle with a mass of 400 kg for instance, the battery mass should also be 400 kg to achieve optimum energy utilisation. However, a battery of this size would be very unwieldly in a small vehicle and in commercially produced vehicles, the battery is considerably smaller, usually about half the mass of the vehicle alone. The approximate ranges obtainable with the two sizes of batteries will be investigated in the next section.

8.6 ESTIMATION OF THE MOTOR POWER AND BATTERY CAPACITY

(i) The values chosen for Wind and Rolling Resistances

To calculate the power requirements of the motor, it is necessary to know suitable values for the Rolling Resistance (F_R) and wind Resistance (F_W).

Rolling Resistance: Lindgreen [18] and Hills [17] give values of 220N/t (47 lbf/ton) and 150N/t (33 lbf/ton) respectively. The former was chosen for calculations

$$F_R = 220 \text{ N/t} \qquad \ldots\ldots\ldots\ldots\ldots\ldots\ldots\ldots\ldots\ldots (8.1)$$

Wind Resistance : Both Hill and Lindgreen give values of

$$F_W = 0{,}05\ AS^2 \quad N \qquad \text{.....(8.2)}$$

where A is in m^2

and S is in km/h

(ii) Calculation of the Motor size

(a) Battery and Vehicle masses equal

$M_B = M_V = 400$ kg.

Therefore, $F_R = 220 \times 0{,}8 = 176N$

Consider maximum continuous vehicle speed to be 60km/h.

If frontal area $= 1m^2$, $F_W = 0{,}05 \times (60)^2 = 180N$.

Output power of motor $= 356 \times 60 \times 1000/3600$

$= 5{,}9$ kW

Allowing for motor and controller efficiency of 80%,

Input power $= 7{,}4$ kW

Energy stored in battery $= 25$ Wh/kg $\times$ 400 kg

$= 10$ kWh

Discharge time at 60 km/h $= 1{,}35$ hours

Range = 80 km

(b) Battery mass half that of vehicle

$M_V = 400$ kg, $M_B = 200$ kg

$F_R = 200 \times 0{,}6 = 132N$

At 60 km/h, $F_W = 180N$

Output power of motor $= 312 \times 60/3{,}6 = 5{,}2$ kW

Allowing for motor and controller efficiency,

Input power $= 6{,}5$ kW.

Energy stored in battery $= 25 \times 200 = 5$ kWh

Discharge time $= 0{,}77$ hours

Range = 46 km

The results of the calculated performance of the vehicle using the smaller battery agree closely with the specifications of electric cars in use at present [19, 51] .

(iii) The influence of the Vehicle Speed on the Power requirements.

Figure 8.3 shows the drive power required by the vehicle as a function of road speed. It can be seen that the power required to propel the vehicle at 100 km/h is nearly four times that required at 60 km/h, due mainly to wind resistance. It would seem then, that in order to keep the cost of the vehicle low by keeping the size of the motor and batteries to a minimum, the maximum speed of an urban commuter-type vehicle will be in the region of 60 - 80 km/h.

(iv) The Effect of the Battery capacity on the Vehicle range

From the above formulae, the vehicle range may be calculated as a function of the battery capacity. If the energy density of the battery is taken as a fixed value of 25 Wh/kg, the capacity and mass may be taken as being synonymous. From figure 8.4, it is seen that an increase in the battery mass does not produce a corresponding increase in the vehicle range, because the rolling resistance is proportional to the gross vehicle mass. The maximum value of range/unit gross mass occurs approximately when the vehicle and battery masses are equal. If the battery mass is increased beyond this point, extra range is obtained by sacrificing operating efficiency. A useful range of 70 - 110 km at 50 km/h may be economically obtained by using a battery system with a mass between 200 and 400 kg.

This range will be reduced by 20 - 40% when the vehicle is used in urban stop-start traffic, because of the lower energy conversion efficiency that is obtainable during acceleration. This was illustrated in chapter 3.

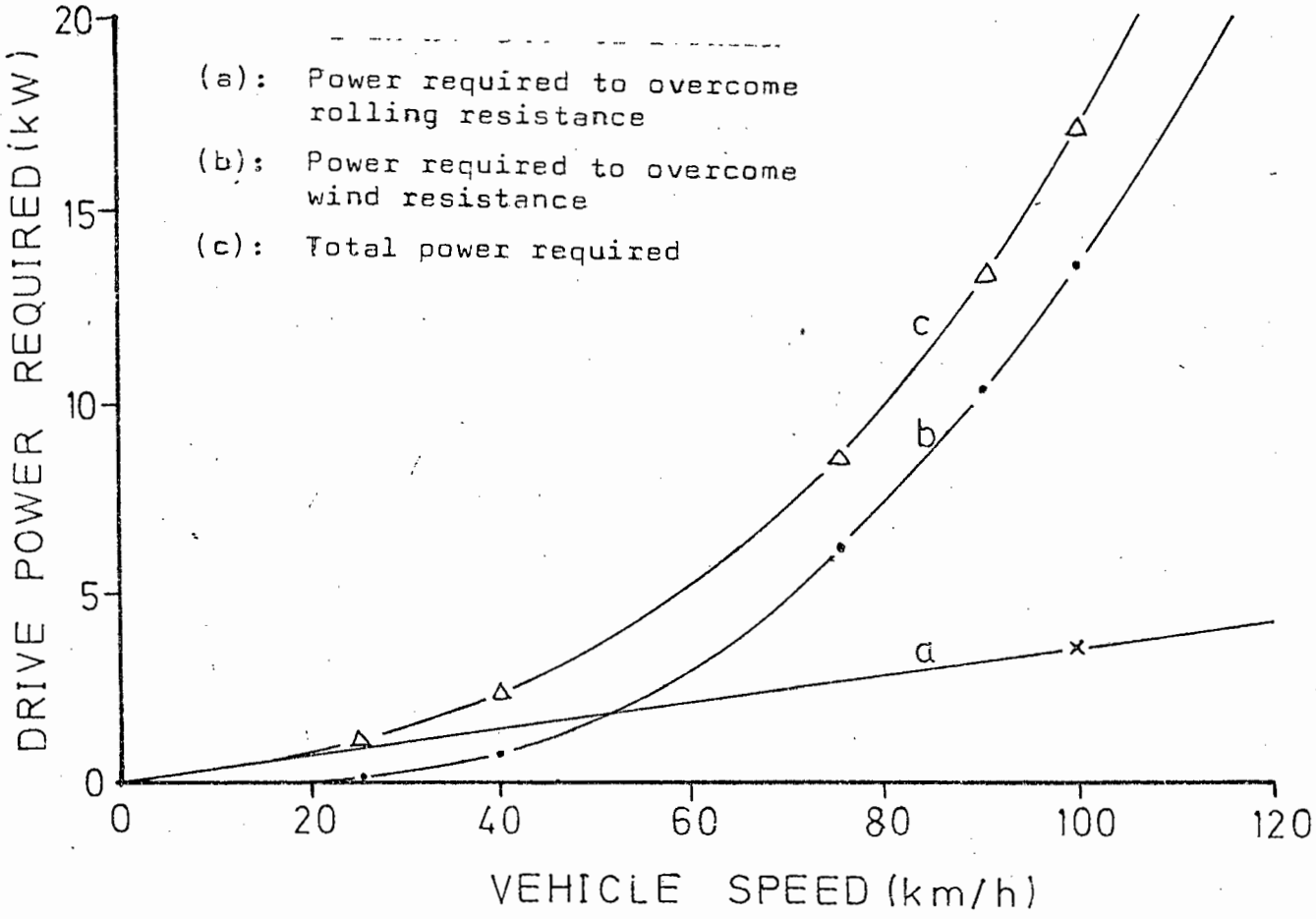

FIGURE 8.3: RELATIONSHIP BETWEEN DRIVE POWER REQUIREMENTS AND VEHICLE SPEED FOR A TOTAL VEHICLE MASS 600 kg.

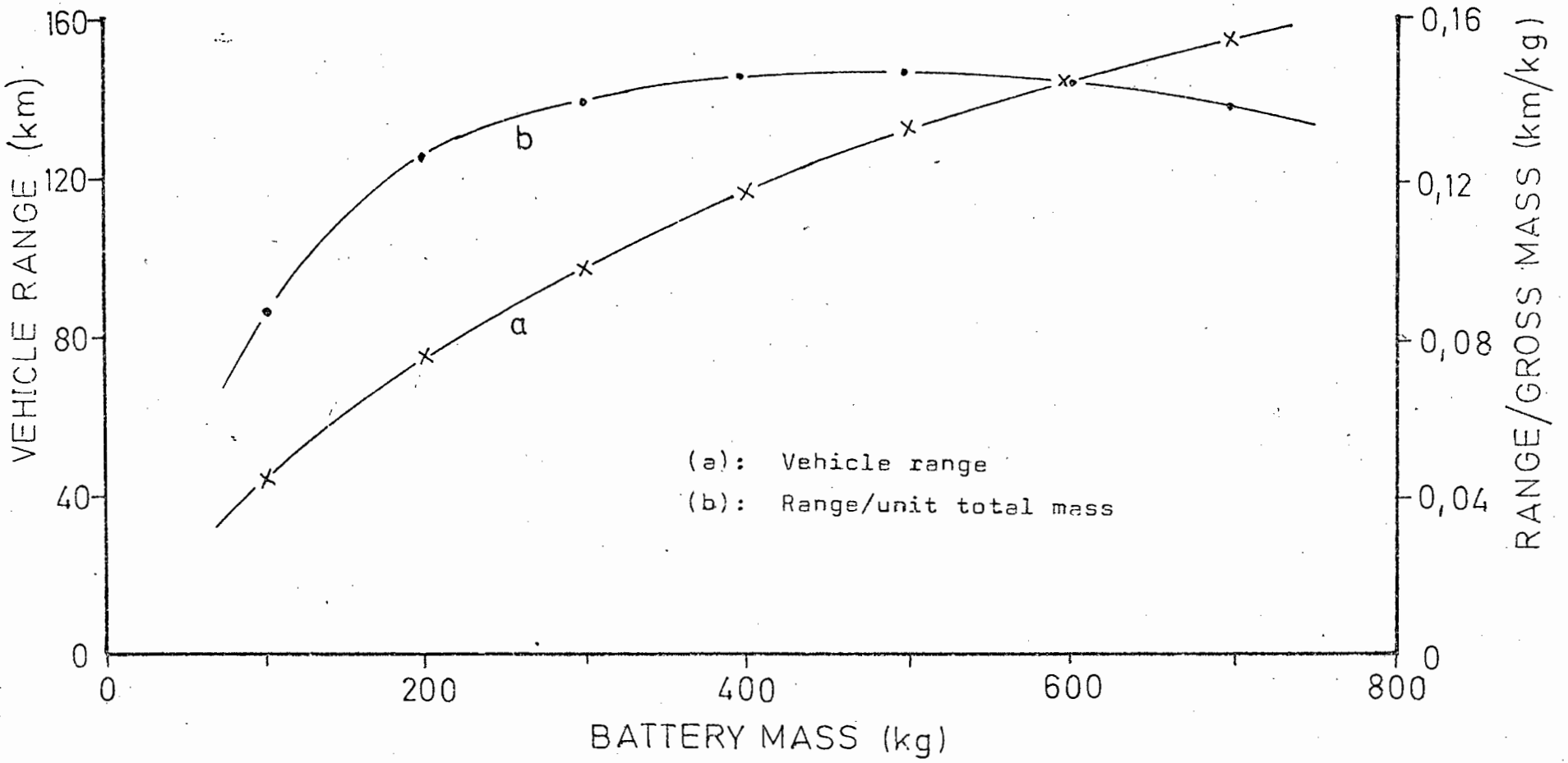

FIGURE 8.4: EFFECT OF BATTERY SIZE ON THE VEHICLE RANGE AT 50 km/h
EMPTY VEHICLE MASS = 400 kg.

8.7 FUTURE IMPROVEMENTS IN STORAGE SYSTEMS.

The major disadvantage of the electric vehicle is the low range that is obtainable from a single charge of the battery, as shown in the above calculations. Although the specific energy density of lead/acid batteries has risen recently from 25 to 33 Wh/kg [53], Barak predicts that this figure is unlikely to rise above 44 Wh/kg, which would give a range of no more than 100 km at 60 km/h.

The use of Sodium Sulphur cells offers an increase in the energy density to above 100 Wh/kg. A drive system using these batteries has been tested in a vehicle [48], but there must be much improvement before such a system can be produced commercially. Another method of improving the range is to adopt a hybrid system [52, 53, 54] where a clean running i.c. engine, such as a Stirling engine, supplements the battery energy. Because of the space requirements and cost of such system, this method is usually limited to larger vehicles such as buses.

For the urban commuter, simpler methods of improving the range would be to provide recharging facilities in cities, for example at parking meters, or a battery exchange scheme at garages, where it would be possible to obtain a fully charged set of batteries in return for the discharged set.

CHAPTER 9

A PROPOSED VEHICLE CONTROL SYSTEM AND ITS EVALUATION

The individual elements of a vehicle drive system have been examined in the previous chapters: the operation of the motor and chopper in each of the modes; the design and performance of thyristor and transistor choppers; and the energy and power considerations for a required vehicle range and speed. The results obtained in these chapters will now be used in the proposal and evaluation of a practical vehicle control system, for a small vehicle with empty mass of approximately 400 kg.

9.1 THE MODES OF OPERATION OF THE MOTOR

From the results of the experimental tests of the proposed modes, presented in chapters 2 to 5, it was found that 3 modes of operation could provide efficient control of the motor over a wide speed range.

(i) Motoring below base speed ($0 \leq E_M \leq V_B$)

This mode would provide control at the rated torque of the motor, from standstill up to a speed where $E_M = V_B$. At this point, the vehicle speed would be 60 km/h, which would enable the vehicle tc move with the other urban traffic, which is usually restricted to this speed in built-up areas.

(ii) Motoring above base speed ($E_M \geq V_B$)

The speed of the vehicle may be increased above the base speed of 60 km/h by employing this second mode of motoring. However, as the form factor of the motor current in this mode increases with speed, the average current must be progressively decreased with speed to avoid exceeding the RMS current rating of the motor. Therefore this mode is primarily intended for allowing the vehicle

to travel above 60 km/h down a hill, or wherever the torque demand on the motor decreases. The speed can be increased to 90 km/h, which is the upper speed limit for the braking mode.

(iii) Regenerative Braking

By using a regenerative braking system, the stored vehicle energy may be converted into battery energy instead of being wastefully disipated as heat if mechanical or dynamic braking was employed. Regenerative braking enables the range of the vehicle to be increased by approximately 10%, depending on the driving conditions. As the terminal voltage of the batteries rises by 20% under charging, one mode of regenerative braking would cover the speed range from 90 km/h down to 10 km/h, where it would be necessary to use the mechanical brakes of the vehicle. If the top speed is not limited to 90 km/h, the back emf of the motor will be so much greater than the battery voltage that this mode of braking will no longer have control over the motor current.

The range of operation of each of the modes is shown diagramatically in figure 9.1.

9.2 THE MOTORS AND BATTERIES

From figure 8.3, it is seen that the power recuired to propel a 600 kg vehicle at 60 km/h is 5 kW. To provide differential action for the rear wheels, two motors, each with an output power of 2,5 kW, should be connected in series. If permanent magnet motors are used, their full load efficiency would be over 90% and their combined mass approximately 30 kg.

A lead acid battery system with a mass of 200 kg has been chosen for the 400 kg vehicle as a trade-off between vehicle range and

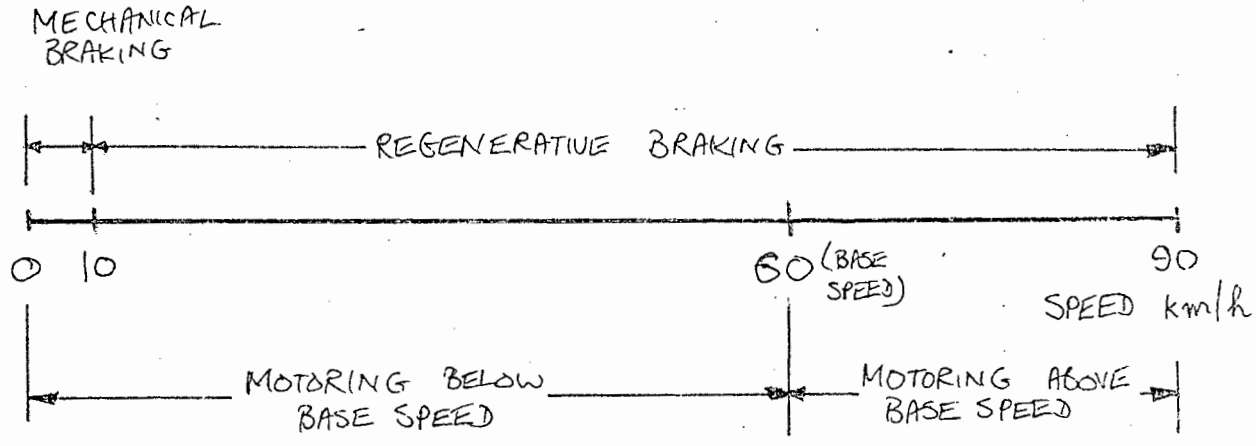

FIGURE 9.1: THE SPEED RANGES OF THE THREE MODES

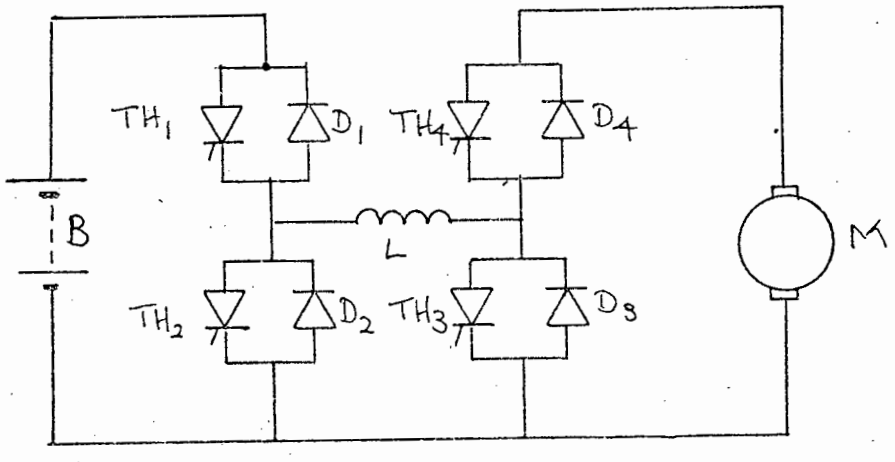

FIGURE 9.2: THE THREE MODE CHOPPER CIRCUIT

battery cost and volume. The capacity of this battery system would then be 5 kWh, for an energy density of 25 Wh/kg. If the battery voltage is increased above 100V, too many cells are required, which increases the price of the batteries. On the other hand, if the voltage is reduced below 60V, the load current becomes excessive and the voltage drop of the chopper and choke (5 -6V) is approximately 10% of available voltage. A system voltage of 80V is a compromise between these two limits. The battery capacity would then be 70 Ah at a two hour rate, giving the vehicle a range of approximately 50 km at a continuous speed of 60 km/h.

To assist the driver in determining the state of charge of his batteries, it is useful to equip the vehicle with some sort of "fuel guage". This may take the form of an energy meter or a simple electronic circuit [57] . These indicators may also be used for switching off the charger when the battery is fully charged. To facilitate charging, the vehicle is fitted with a battery charger which may be connected to the mains outlet in the owner's garage, or to a recharging point located near a parking meter in the city centre.

Summary of drive specifications

Vehicle and Drive system	Total mass 600 kg Chopper controlled Regenerative braking Maximum speed at full load: 60 km/h Maximum speed at reduced load: 90 km/h Range: 50 km at 60 km/h
Motors	2 dc permanent magnet motors in series, one on each rear wheel; each motor 36V, 2500W, 3000 r.p.m. Mass: 15 kg each.
Batteries	Lead-acid accumulators 80V, 70Ah at 2 hr.rate Mass: 200kg.

9.3 THE CHOPPER POWER CIRCUIT

A solid state changeover switch, which enabled either the modes of regenerative braking or motoring below base speed to be selected, was described and evaluated in chapter 7. By using a transistor as a series commutator for two thyristors, either mode could be selected by the triggering of the appropriate thyristor. The necessary logic was incorporated to prevent the false triggering of either thyristor. Although this chopper proved reliable, and the circuitry was simple, this method had several disadvantages:

(i) The forward voltage drop was higher than that of a comparable thyristor chopper, causing unnecessary wastage of energy.

(ii) The method of using a series commutator for the thyristors could not easily be extended to a three-mode selector.

(iii) Because of its voltage and current ratings, the transistor is not as suited for use in traction drives as is the thyristor.

Therefore, to implement the modes of operation suggested in section 9.1, a thyristor switching network, as shown in figure 9.2, is proposed.

(i) Principle of Operation

The principle of operation of the chopper shown in figure 9.2 may be outlined by considering the path followed by the main load current during the "ON" and "free-wheel" periods in each of the three modes.

(a) Motoring (above) base speed

"ON" period: B, TH_1, L, D_4 and M.

"free-wheel" period: L, D_4, M and D_2

(b) Motoring above base speed

"ON" period: B, TH_1, L, and TH_3.

"free-wheel" period: B, TH_1, L, D_4 and M.

(c) Regenerative braking

"ON" period: M, TH_4, L and TH_2.

"free-wheel" period: M, TH_4, L, D_1 and B.

In addition, D_3 is a free-wheel diode used when TH_4 is commutated.

The maximum forward voltage drop due to the semiconductors would be either that of two thyristors (3V) or else that of one thyristor and one diode (2,5V).

(ii) Commutation Circuits

Figure 9.3 illustrates the basic chopper circuit of figure 9.2 with the commutation circuits added. Capacitor C_1 commutates both TH_1 and TH_2 and C_2 thyristors TH_3 and TH_4. The operation of the circuit may be outlined as follows:

Consider the left-hand bank of semiconductors. All the thyristors are off and the motor is stationary. TH_{1C} is triggered, charging up capacitor C_1 through L_1, D_4 and the motor. Plate a is therefore charged positive with respect to plate b. When TH_1 is triggered, C_1 resonates with L_2, reversing the polarity on the capacitor. D_{1C} prevents any futher resonance. TH_1 may then be commutated by triggering TH_{1C} which connects C_1 across TH_1, reverse biassing it. C_1 then recharges through TH_{1C}. Once C_1 has recharged, it may be used to commutate TH_2 by triggering TH_{2C}.

Simalarly, before TH_3 or TH_4 are triggered, C_2 must be charged by triggering TH_3.

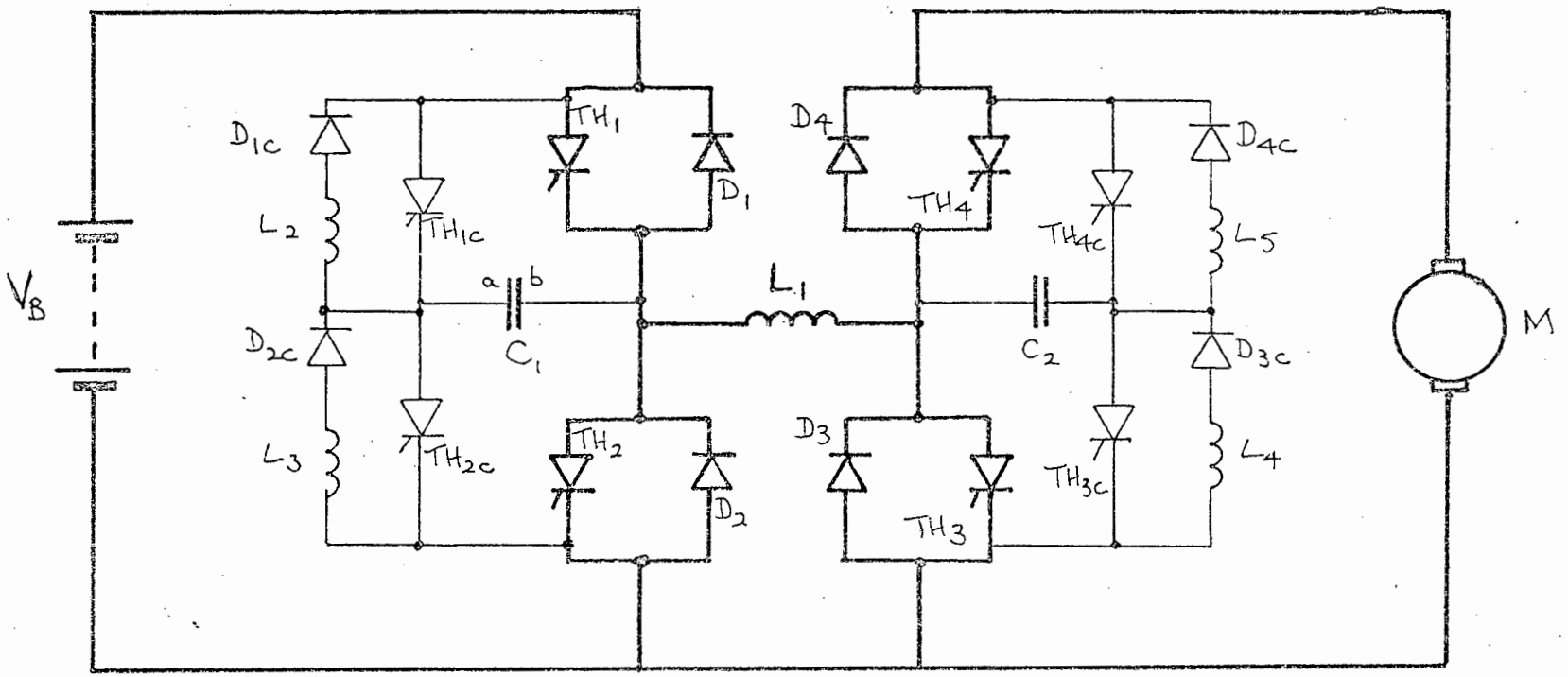

FIGURE 9.3: THE COMPLETE CHOPPER CIRCUIT, SHOWING THE COMMUTATION CIRCUITS.

(iii) The Thyristor Trigger Circuits

Figure 9.4 illustrates the trigger circuits for the main and commutation thyristors. The main thyristors are turned on by connecting the "ON" pulse to the bases of the transistors TR_1 - TR_4. This allows a pulse of current to pass through the primaries of the isolating transformers, which have their secondaries connected to the gates of TH_1 - TH_4. Those thyristors which are not required for a particular mode are prevented from receiving a trigger pulse by the inhibit transistors, TR_5 - TR_8, which are turned on by raising the respective inhibit input to a logic "1" level.

Similarly, the commutation thyristors are triggered by the "OFF" pulse which is connected to transistors TR_9 - TR_{12}. This pulse is gated to the correct thyristors by transistors TR_{13} - TR_{16}.

(iv) Forward and Reverse Control

A practical vehicle control system should include a method of enabling the vehicle to move forwards or backwards. Figure 9.5 illustrates a method of achieving this. The motor is connected between two changeover contactors F and R. When the solenoid is de-energised, the contacts F_1 and F_2 are closed, as shown in the diagram, and the changeover switch is in the forward position. Therefore the solenoid will consume no power when the vehicle is travelling forwards. If the solenoid is energised, contacts R_1 R_2 will close and the motor will turn in the opposite direction.

Contactors were chosen in place of semiconductor devices because their forward voltage drop is approximately 10% of that of a comparable semiconductor device. As the contactors are switched only a few times during each vehicle trip, the wear on them will be low and they should not require maintainance during the life of the vehicle.

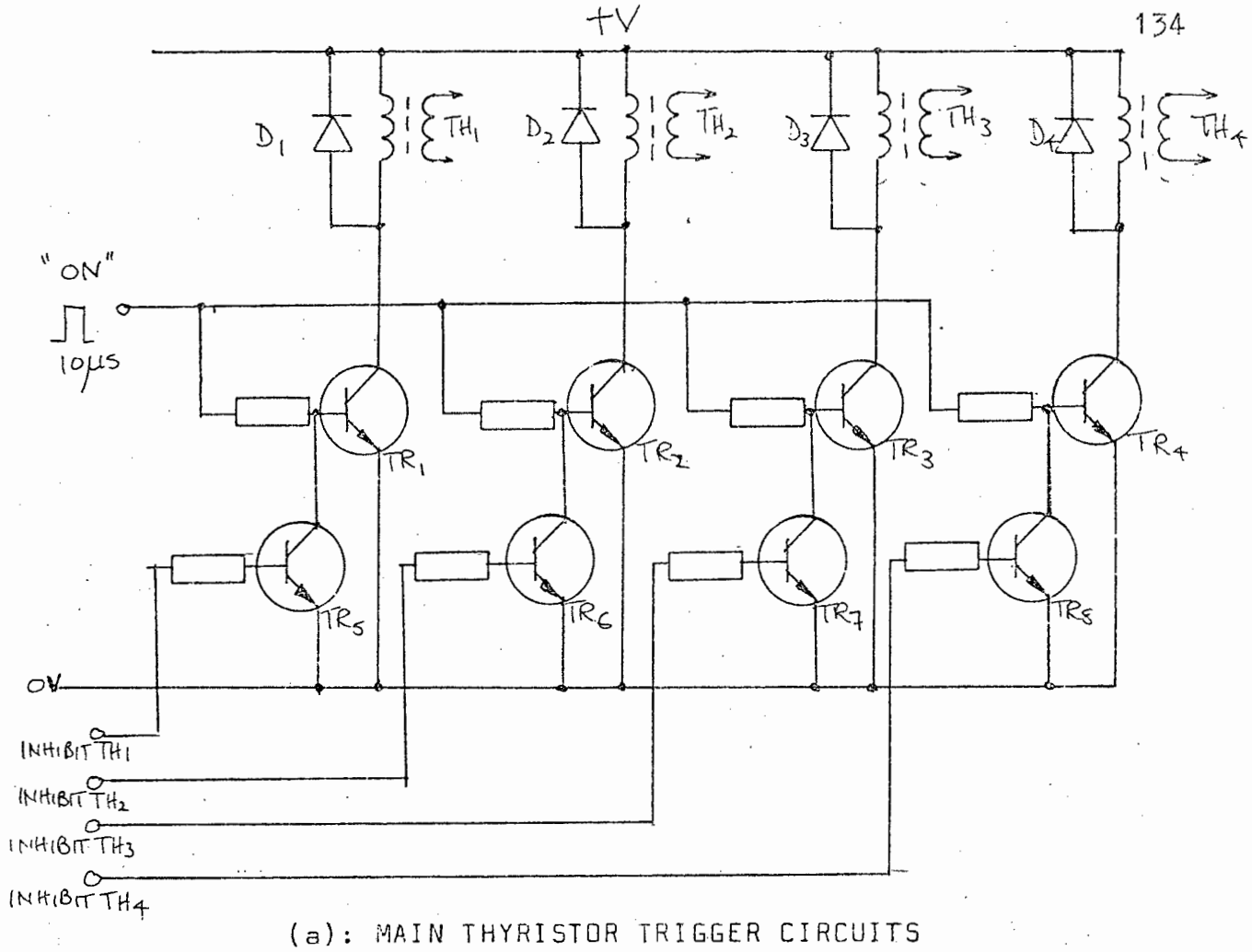

(a): MAIN THYRISTOR TRIGGER CIRCUITS

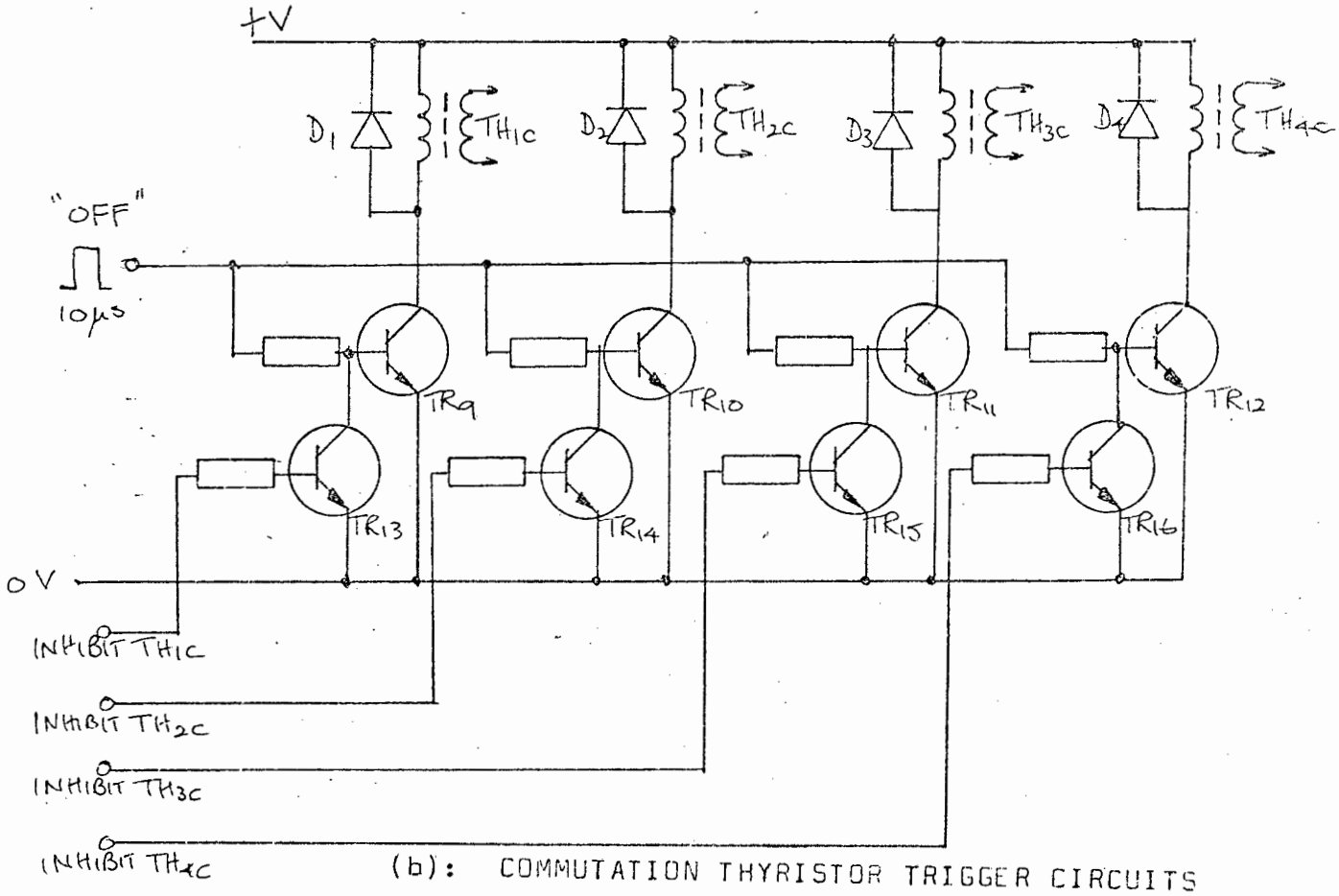

(b): COMMUTATION THYRISTOR TRIGGER CIRCUITS

FIGURE 9.4: THYRISTOR TRIGGER CIRCUITS.

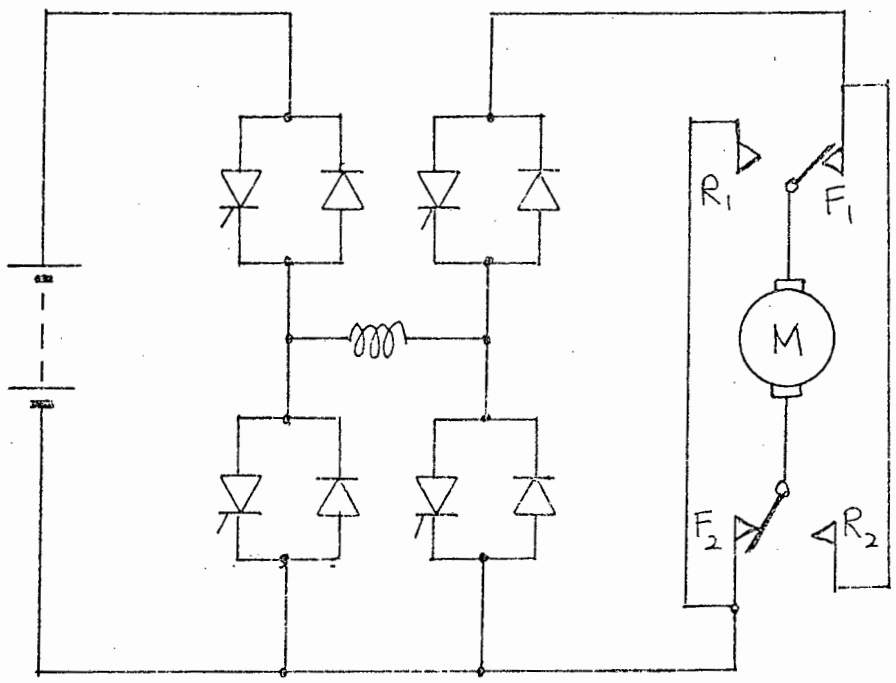

FIGURE 9.5: MODIFICATION OF THE BASE CHOPPER OF FIGURE 9.2 TO INCORPORATE A REVERSE CONTROL.

The interlocking citcuitry for controlling the contactors F and R is described in section 9.6.

(v) The Ratings of the Chopper components

The Main Thyristors and Diodes

The current rating of thyristors TH_1 - TH_4 and diodes D_1 - D_4 would need to be approximately 120A to carry the full load motor current of 80A, plus the peak caused by the current ripple. To protect the devices against voltage transients, the voltage rating of the thyristors and diodes should be 400V. The thyristors should have fast turn-off times to allow a wide range in the mark-space ratio.

The Commutation Circuit

As the duty cycle of the commutating thyristors is low, the current rating of these devices can be much lower than that of the main thyristors. A device, capable of 25A average and 400V, would be suitable. The commutating capacitor must be able to supply the full load current while reverse biassing the main thyristor, for the duration of the thyristor turn-off time.

$$C \geq \frac{It}{V_B} = \frac{100 \times 20 \times 10^{-6}}{80}$$

$$= 25\ \mu F$$

Allowing factor of safety of 2, a 50μF, 200V capacitor would be suitable. The capacitor must be able to withstand the peak resonant current, and must have low internal losses.

To enable the per unit mark to be reduced to 5%, the commutating capacitor must be reversed in approximately 2% of the chopper period. The value of inductance that will achieve this when the chopper frequency is 400 Hz is 5μH. The peak resonant current is then approximately 240A. The commutation circuit diode must have a rating of not less than 25A, 400V.

Form factor, choke and chopper frequency

These three parameters are selected together because of their effect on each other. By increasing the chopper frequency, the value of the inductance for achieving a particular current ripple is proportionately reduced. However, as the switching loss of the chopper and the iron losses of the choke increase with frequency, a compromise must be found between these two conflicting requirements. A value of 400 Hz was chosen as being the highest practicable frequency.

To optimise the overall efficiency, there must also be a compromise between the losses in the motor armature due to the current form factor and the losses in the choke, bearing the cost and mass of choke in mind. For an inductance of 1 mH, the maximum form factor at full load current will be 1,015, which will cause the efficiency of the motor to drop by approximately 0,5% at half speed when the form factor will be greatest.

By using "C" cores with thin laminations and heavy guage wire for the windings, the losses of the choke may be kept to approximately 80W at full load curremt, corresponding to less than 1% of the input power to the motor. A choke with this performance will cost in the region of 10% of the cost of the motors.

9.4 CONTROL CHARACTERISTICS

A most important aspect of the vehicle drive system is the correct choice of the control characteristic, as this forms the interface between the driver and the power circuitry which controls the motors. Either of two characteristics may be chosen --- constant speed or constant torque.

A constant speed characteristic is attractive for motoring as it

allows the driver to maintain an even vehicle speed, even though the gradient of the road may change. However, the driver has no direct control over the torque of the motor, except by virtue of the current limit which must be provided to protect the motor from overload. Therefore to achieve a uniform acceleration rate, the driver would have to continuously alter the speed demand setting until the desired speed was reached. A torque controller, on the other hand, would provide both a direct control of the acceleration rate, so affording a smooth ride for the driver and passengers, and an inherent current protection for the motor. A particular torque setting would maintain a constant vehicle speed providing the gradient of the road did not change.

Similarly, for passenger comfort, it would be desireable to have a uniform retardation rate. This is most easily achieved by having a torque control and not a speed control characteristic. The driver would select the desired rate of retardation, and not the speed to which he wished to slow down. The characteristic of a torque controller would be very similar to that of a mechanical braking system, as is normally used in an i.c. engined vehicle.

It is desireable from the driver's point of view to have the same characteristic for both motoring and braking, for then the controls of the vehicle would have the same "feel" during acceleration and braking. It is therefore proposed that a torque control characteristic be used for all modes of operation. Evidence of the suitability of this characteristic is to be found in the literature [1,6,28,46].

9.5 IMPLEMENTATION OF THE DESIRED CONTROL CHARACTERISTIC

(i) Accelerator and Brake Pedals

It would be an advantage if both the acceleration and braking demands could be controlled by means of a single pedal, as suggested by Berman [46] . However, this would be very difficult to implement, if one considers that it is essential to have a mechanical braking system which is coupled to the controlling pedal. This is necessary for the following reasons: to provide additional braking in emergencies; to provide braking at very low speeds (less than 10 km/h), when the electrical brakes will have little effect; to provide a back-up system in the case of failure of the electrical brakes.

It is therefore proposed that there be two separate control pedals - one for motoring and one for braking. Each pedal will be ganged to a potentiometer, so that the torque demand will be proportional to the angle of the pedal, with the maximum setting of each pedal corresponding to the rated torque of the motor. In addition, near the end of the travel of the brake pedal, the mechanical brakes of the vehicle will be brought into action. For safety, actuation of the brake pedal will override any commands from the accelerator pedal.

(ii) Current Monitor

As the motors proposed for the vehicle drive are constant flux machines, the motor torque may be determined by the measurement of the average value of the armature current, which may be obtainable from the instantaneous value by simple processing in a wave shaping circuit [30] .

A low resistance, non-inductive shunt may be used for this purpose, but it is considered undesireable because of the power dissipation; lack of isolation from the power circuitry, and the

dependence of the polarity of the output voltage on the direction of current flow, therefore making it necessary to invert the voltage when in the braking mode.

Other devices which may be used are the Hall effect device [42, 58, 59, 60] and the magnetoresistor [58, 61], two semiconductor devices which react to the absolute value of magnetic flux density, and consume negligible power. The Hall effect device is a 4 terminal package, two terminals being for the power supply and the other two for the voltage output. Sensitivities of the order of 10 - 60 $mV/Wb/m^2$ are obtainable.

The magnetoresistor is a semiconductor device which has its dc resistance proportional to the magnetic flux density. The zero field resistance is typically 500 ohm and an increase of the order of 20% is possible in a flux density of $0,5 wb/m^2$. By passing 10 mA through the device, a voltage variation of more than 1V is therefore possible. In addition, as the magnetoresistor is a two terminal device, it does not require any bias supply, and is particularly suitable for remote sensing. This device was therefore considered to be the most suitable for use as a current monitor.

Figure 9.6 shows a practical method of mounting the magnetoresistor. The device is placed in the air-gap of the core of the series choke L which carries the main load current. By connecting the magnetoresistor to a constant current source, as shown in figure 9.7, the voltage change across the device is directly proportional to the resistance change caused by the application of the magnetic field. A thermistor compensates for the temperature coefficient of the magnetoresistor. The positive voltage offset due to the zero field resistance of the magnetoresistor may be adjusted by the amplifier A_1.

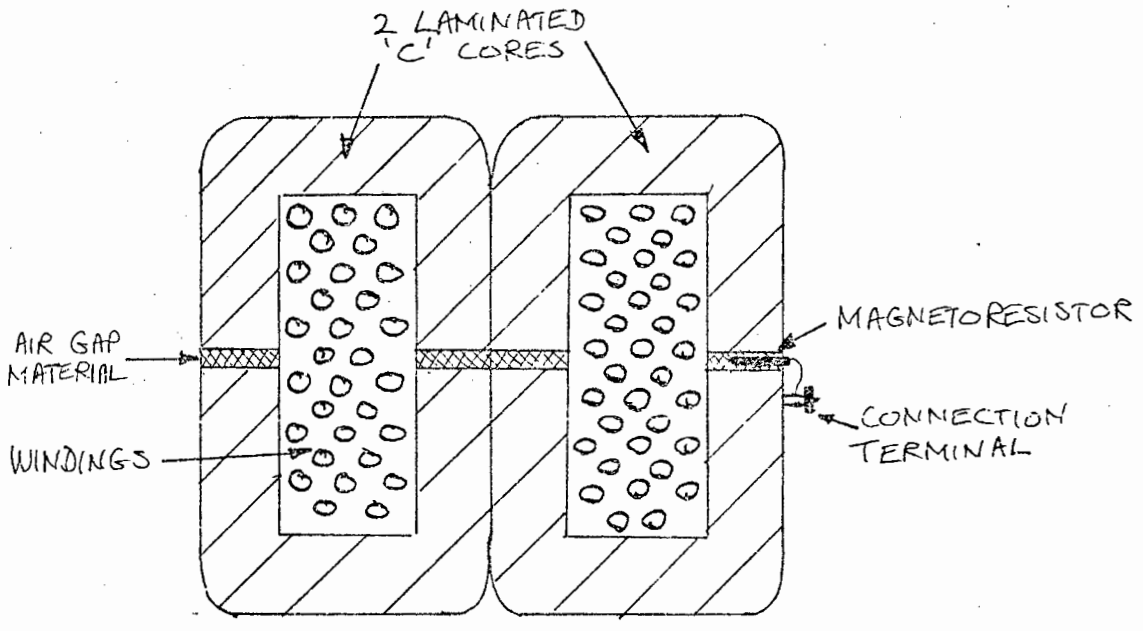

FIGURE 9.6: MOUNTING OF THE MAGNETORESISTOR IN SERIES INDUCTANCE

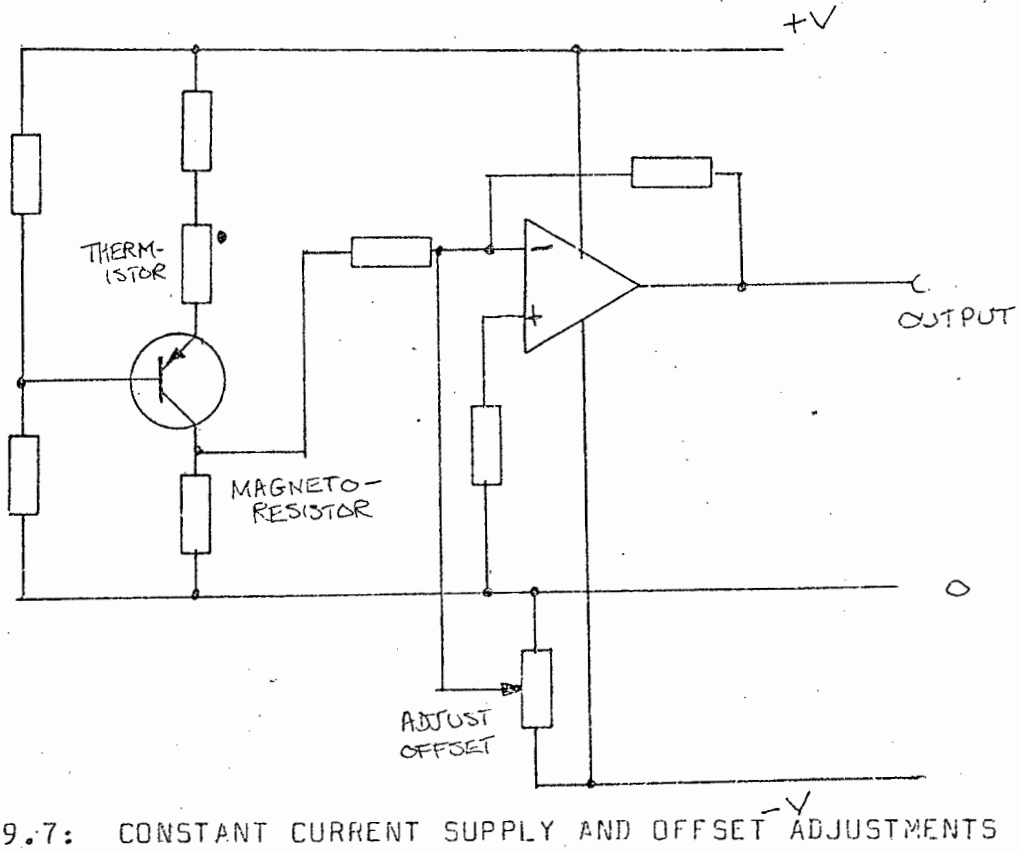

FIGURE 9.7: CONSTANT CURRENT SUPPLY AND OFFSET ADJUSTMENTS FOR MAGNETORESISTOR.

(iii) Implementation of Torque Feedback

To implement a constant torque characteristic, the average value of the current, obtained from the current monitor, is compared against the demand signal, set by the position of the accelerator or pedal brake, in a current error amplifier. The output of the amplifier controls the mark-space ratio so that the desired value of torque is maintained. As there are two torque demands that may be connected to the current error amplifier - one from each of the pedals - the correct demand must be chosen by the logic after examination of the various parameters in the control circuit.

To achieve stable operation of the feedback system, the correct signal must be obtained from the current monitor for each of the three proposed modes. For the modes of braking and motoring below base speed, this presents no problem, as the motor current is continuous and the average value may easily be obtained. However, when motoring above base speed, the motor current is no longer continuous, but in a series of pulses of duration t_m, causing the form factor to increase. To avoid exceeding the RMS current rating of the motor, the available torque must be decreased as the speed is increased above base speed. If the motor is supplied with constant power from the battery, the output torque will fall linearly with speed. As the battery voltage is fixed, this constant power characteristic may be realised by monitoring the average value of the battery current while motoring above base speed. If the current monitoring device is mounted in the series inductance, which is positioned in the chopper circuit as shown in figure 9.2, this changeover will be accomplished automatically when the mode of motoring is changed. As the average values of the motor and battery currents are equal at the base speed, no discontinuities in the

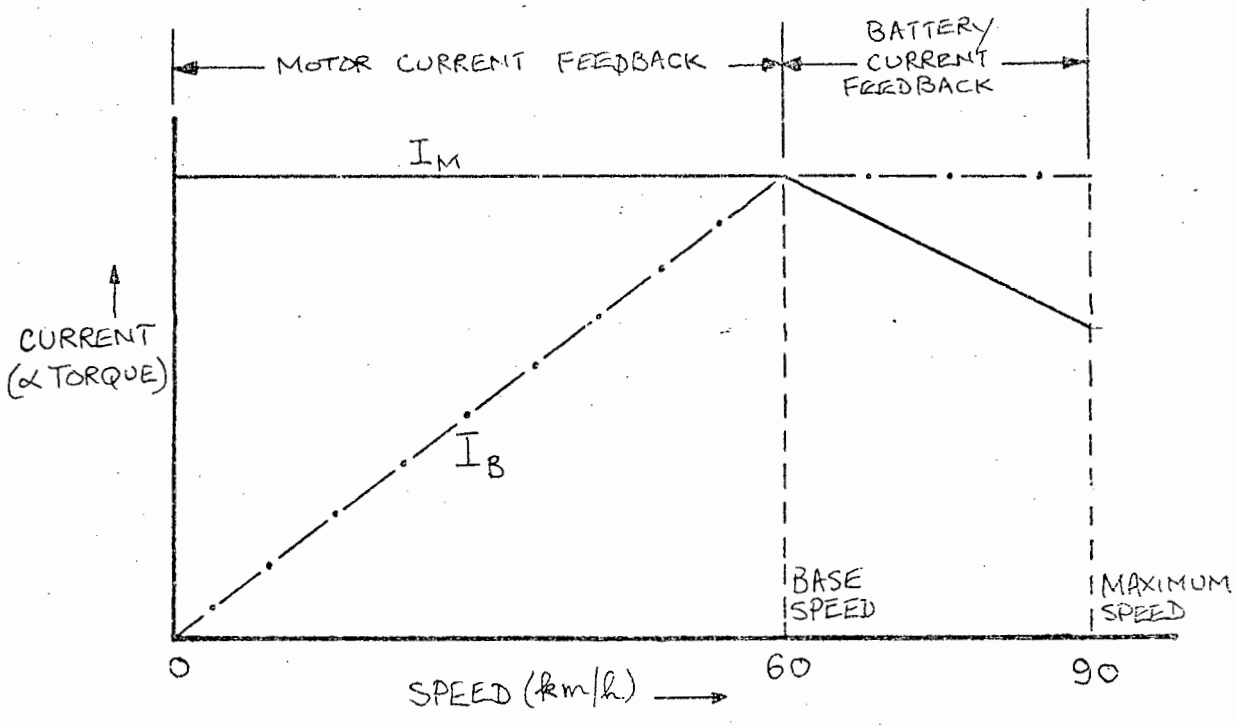

FIGURE 9.8: TORQUE FEEDBACK REQUIREMENTS FOR MOTORING ABOVE AND BELOW BASE SPEED

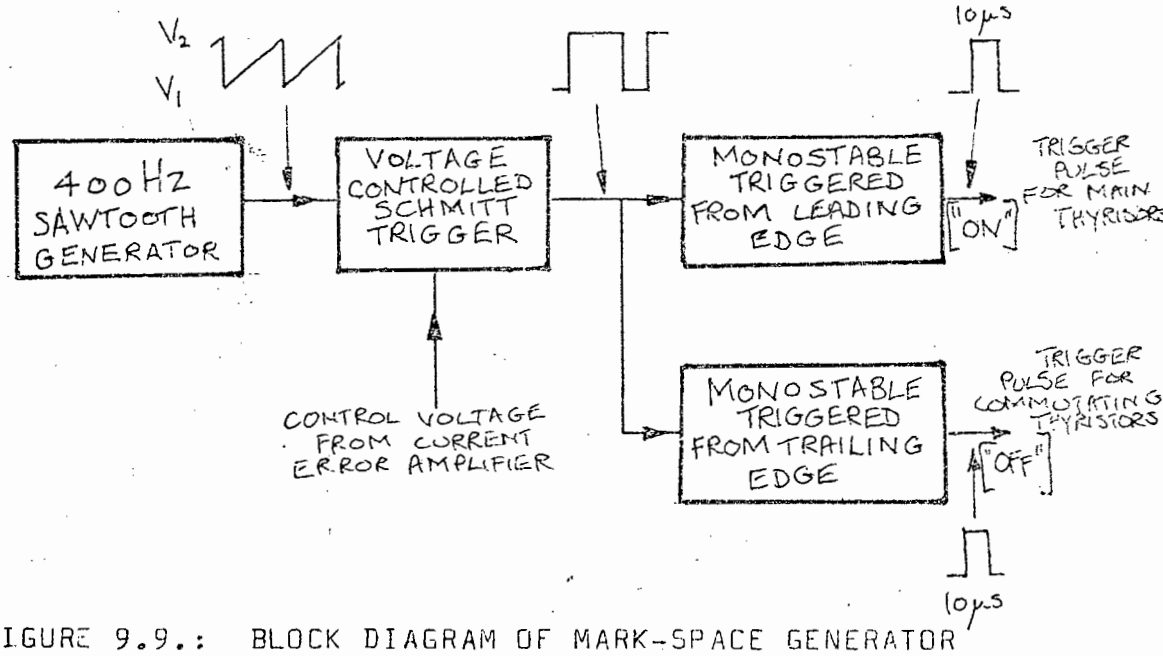

FIGURE 9.9.: BLOCK DIAGRAM OF MARK-SPACE GENERATOR

feedback signal will occur. The feedback arrangements for motoring are shown diagramatically in figure 9.8.

(iv) Mark - Space Generator

The block diagram of the mark-space generator is shown in figure 9.9. A saw-tooth waveform, with a repetition rate of 400 Hz, sweeps between two voltage levels V_1 and V_2. A Schmitt trigger switches on anywhere on the rising edge of the saw-tooth, set by the voltage output of the current error amplifier, and switches off on the falling edge. The "ON" trigger pulse for the main thyristors is triggered by the positive edge of the Schmitt output, and the "OFF" trigger pulse for the commutating thyristors is triggered by the negative edge of the Schmitt output.

9.6 IMPLEMENTATION OF MODE SELECTION BY MEANS OF THE ASSOCIATED LOGIC.

(i) Principle of operation of the comolete control system

A complete drive system, showing both the power unit and the associated controls and logic, is given in figure 9.10. For the sake of simplicity, the commutation circuits for the main thyristors have been omitted. A typical cycle, starting from rest, may be described as follows:

The key switch S_1, is closed. This operates the sequencing circuit shown in figure 9.11 which closes the main contactor, connecting the battery to the power control unit. Simultaneously, a second pulse is passed to the logic circuits which inhibits the triggering of all the main thyristors and triggers the commutation thyristor TH_{1C}, allowing the commutation capacitor C_1 to charge up. The vehicle is now ready to move off. If the brake pedal is released, S_2 will be closed and the logic circuit will command the feedback

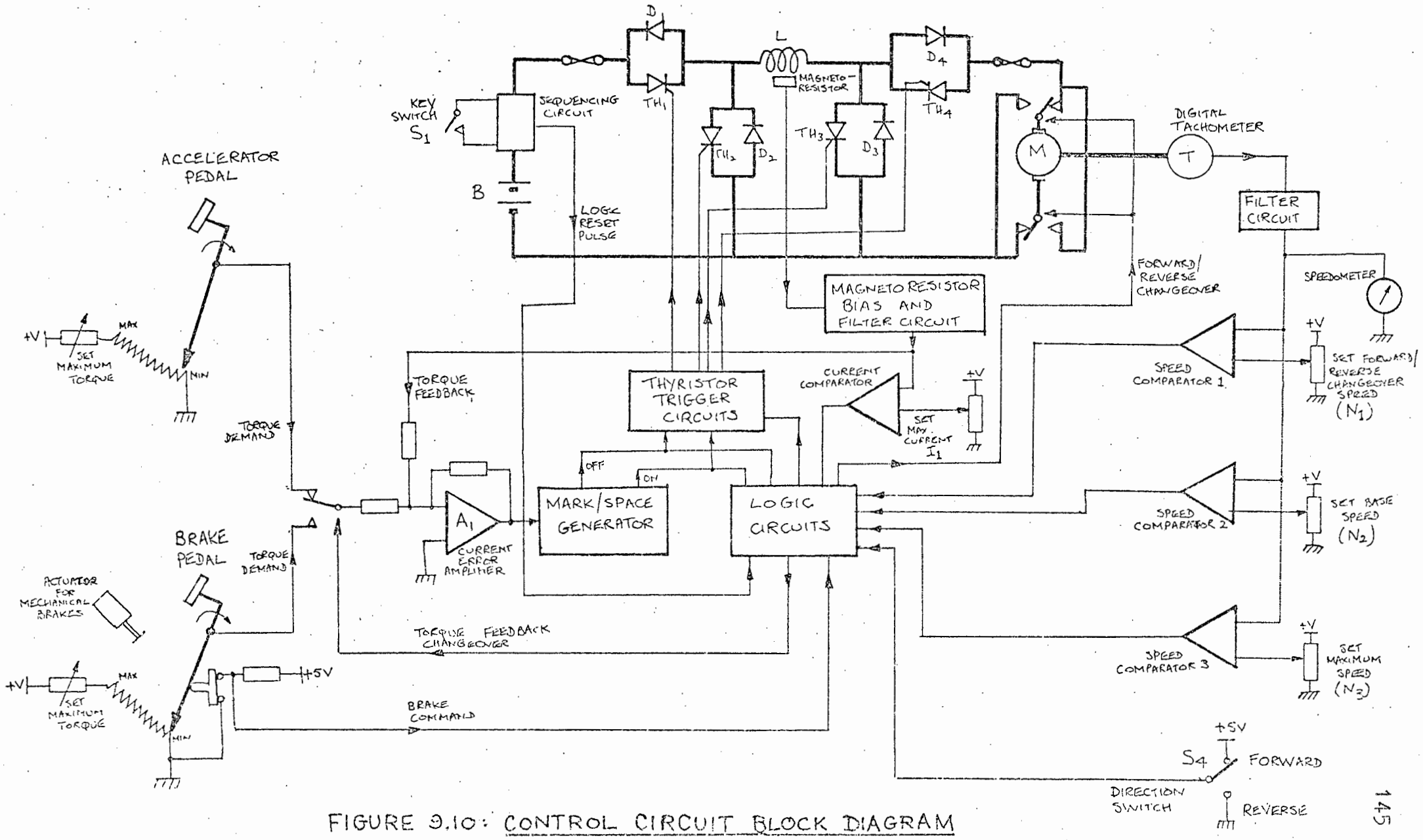

FIGURE 9.10: CONTROL CIRCUIT BLOCK DIAGRAM

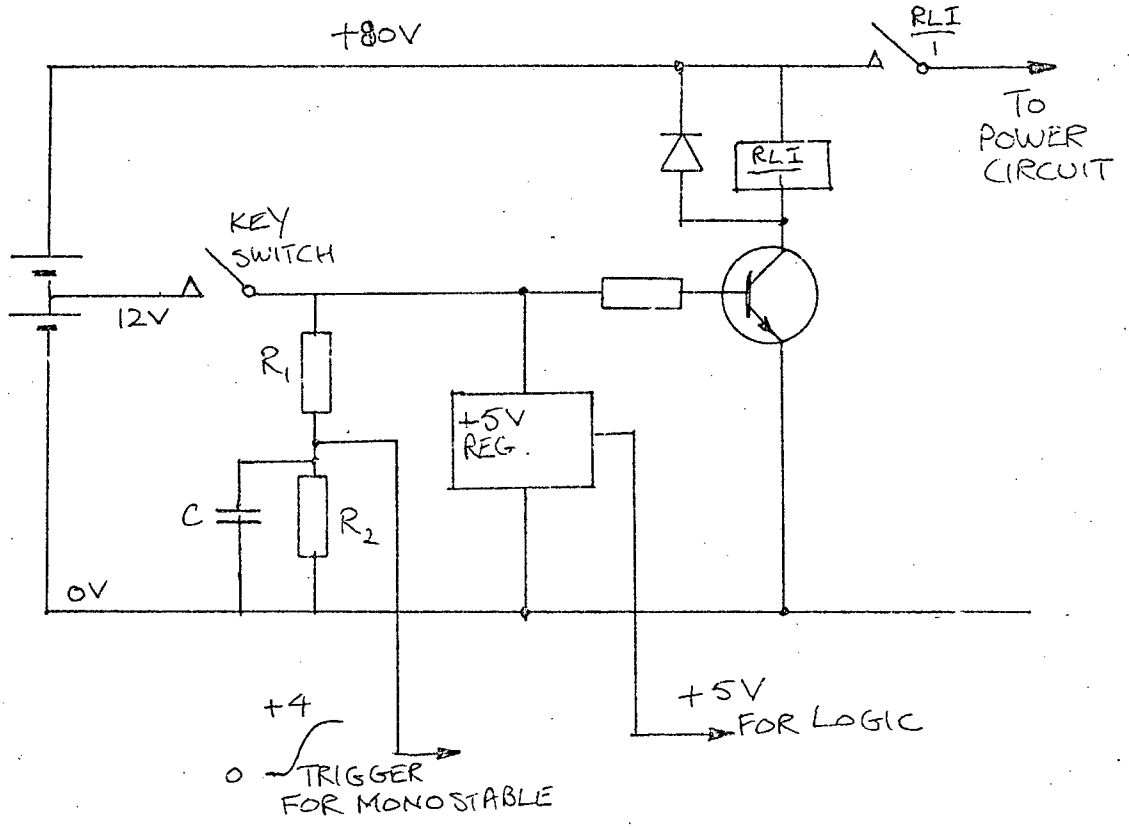

FIGURE 9.11: SEQUENCING CIRCUIT

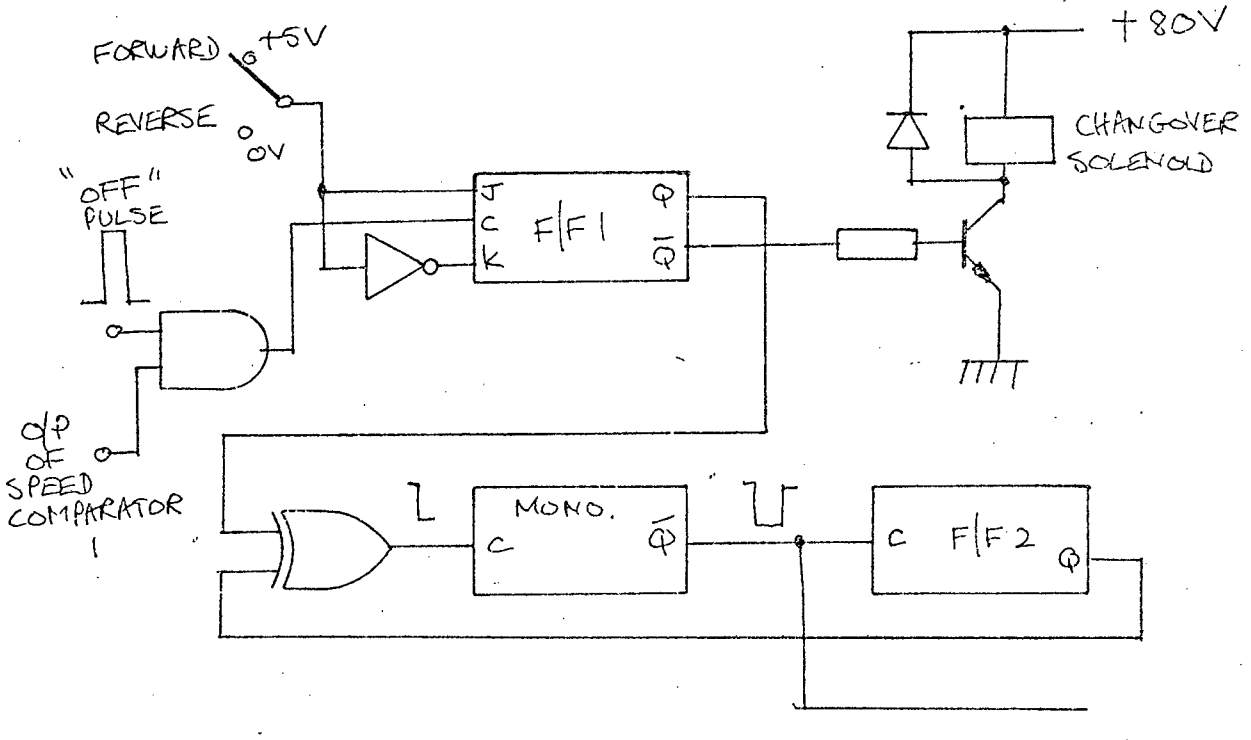

FIGURE 9.12: FORWARD AND REVERSE LOGIC.

switch S_3, to be set to the motoring position. A torque demand from the accelerator pedal is compared with the current feedback signal from the magnetoresistor, MR and produces an output from the error amplifier A_1, which controls the ON/OFF ratio of the mark/space generator. TH_1 is cyclically turned on and off so that the current remains at the desired level.

If the vehicle accelerates to base speed, N_2, the circuit may change over into the mode of motoring above base speed ($E_M \geqq V_B$). Thyristor TH_1 is left on, while TH_3 is operated in a chopper mode. The vehicle can accelerate in this mode until the maximum battery current is reached. If the vehicle slows down because of a change of gradient of the road, the motor will remain connected in this mode until the current rises to 10% above the rated value, at which point the logic will change the configuration back to motoring below base speed.

If instead, however, the vehicle travels down a slope so that it continues to accelerate, TH_4 will be triggered when a speed N_3, corresponding to 90 km/h, is reached, limiting any further acceleration. The reason for doing this was explained earlier.

If at anytime the brake pedal is depressed, S_2 is opened, and the logic will allow TH_2 and TH_4 to be triggered once TH_1 and TH_3 have been commutated. Simultaneously, the feedback switch S_3 is changed to the braking position and the torque is controlled by means of the brake pedal. Near the end of the travel of the brake pedal, the mechanical brakes are activated, assisting in the braking effort.

(ii) Operation of the Forward and Reverse Switch

Figure 9.12 shows a method of implementing the forward/reverse switch. The solenoid for the contactor is driven by the output of the flip-flop F/F_1, which follows the setting of S_1 - 1 state

for forward, 0 state for reverse - when the F/F is clocked by the "OFF" pulse. However, this pulse will only be gated through to the F/F when the output of speed comparator 1 is high, which occurs when the speed is below 5 km/h. Wherever F/F_1 changes state, a monostable is triggered which inhibits the triggering of the main thyristors for a period of 100 ms, to allow the contactors to change over.

(iii) Implementation of the Associated Logic

The conditions necessary for the triggering of each thyristor are defined as follows:

TH_1:
1) Brake Pedal Off
And 2) Speed below N_2 (base speed)
And 3) TH_2 off
And 4) TH_4 off

TH_{1C}:
1) Speed below N_2
And 2) TH_1 on
And 3) TH_3 off

TH_2:
1) Brake pedal on
And 2) TH_1 off
And 3) TH_3 off

TH_{2C}:
1) TH_2 on

TH_3:
1) Brake pedal off
And 2) Speed above N_2
And 3) Current below I_1 (10% above rated current)
And 4) TH_2 off
And 5) TH_4 off
And 6) Speed below N_3 (Maximum speed)

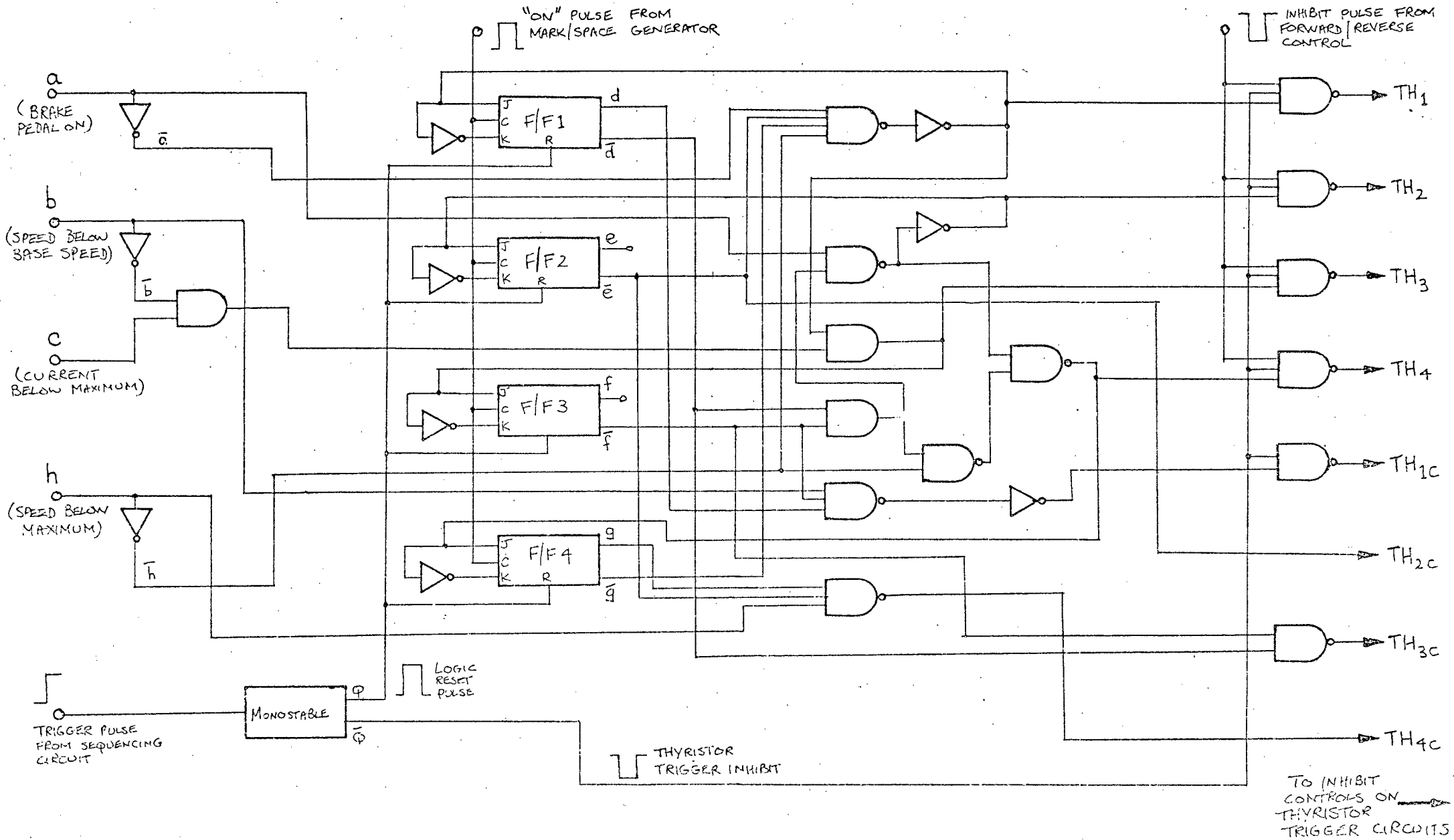

FIGURE 9.13: LOGIC SCHEME FOR MODE SELECTION

TH_{3C}:
1) TH_3 on
OR 2) TH_1 on (to allow the commutating capacitor to charge up)

TH_4 :
1) Brake pedal on OR speed above N_3
AND 2) TH_1 off
AND 3) TH_3 off

TH_{4C}:
1) TH_2 off
AND 2) TH_4 on
AND 3) Speed below N_2

From this, the various inputs to the logic may be defined. Using positive logic notation, where the "on" state corresponds to a logic 1, the eight inputs required are:

a = Brake pedal on
b = Speed below N_2
c = Current below I_1
d = TH_1 on
e = TH_2 on
f = TH_3 on
g = TH_4 on
h = Speed below N_3

The conditions for triggering of each thyristor may therefore be rewritten as:

$TH_1 : \bar{a}.\ \bar{e}.\ \bar{g}.\ h$; $TH_{1C} : b.\ d.\ \bar{f}$

$TH_2 : a.\ \bar{d}.\ \bar{f}$; $TH_{2C} : e$

$TH_3 : \bar{a}.\ \bar{b}.\ c.\ \bar{e}.\ \bar{g}.\ h$; $TH_{3C} : f + d$

$TH_4 : a.\ \bar{d}.\ \bar{f} + \bar{h}.\ \bar{d}.\ \bar{f}$; $TH_{4C} : \bar{e}.\ g.\ h$

A logic scheme for implementing these conditions is shown in figure 9.13. The state of each of the main thyristors is indicated by the state of the relavent flip-flop (F/F1 - F/F4), which are clocked by the "ON" pulse from the mark-space generator. These

flip-flops are all reset to the off state by the monostable M_1 which is triggered when the key switch is closed. This reset pulse also inhibits the triggering of the main thyristors while allowing the commutating Capacitor C_1 (figure 9.3) to charge up.

When changing from motoring to braking, and vice versa, there is no free-wheel period to allow the current to decay to zero before triggering the next set of thyristors. This is to achieve the changeover as quickly as possible. The system used by Berman [47], where there is a delay of 350 ms when changing from motoring to braking is undesireable, because if the vehicle is travelling at 60 km/h, a distance of 5,8 m will be covered before the brakes take effect.

(iv) Speed measurement using a digital tachometer

As three inputs to the logic circuit are outputs from speed comparators, it is necessary to have a tachometer connected either to one of the motors, as shown in figure 9.10, or to one of the road wheels.

A simple and inexpensive tachometer may be constructed by using a magnetoresistor and a toothed disc, as shown in figure 9.14. The magnetoresistor is glued to a small permanent magnet and placed 1 - 2 mm away from the surface of the disc. When a tooth passes the magnetoresistor, the resistance changes, causing TR_1 to switch on and off, which triggers a monostable multivibrator. The voltage appearing across C_1 is the average voltage of the train of pulses.

A system such as this offers an advantage over a photo-transistor system, because it is insensitive to dust and dirt which may interfere with the operation of photo-transistor.

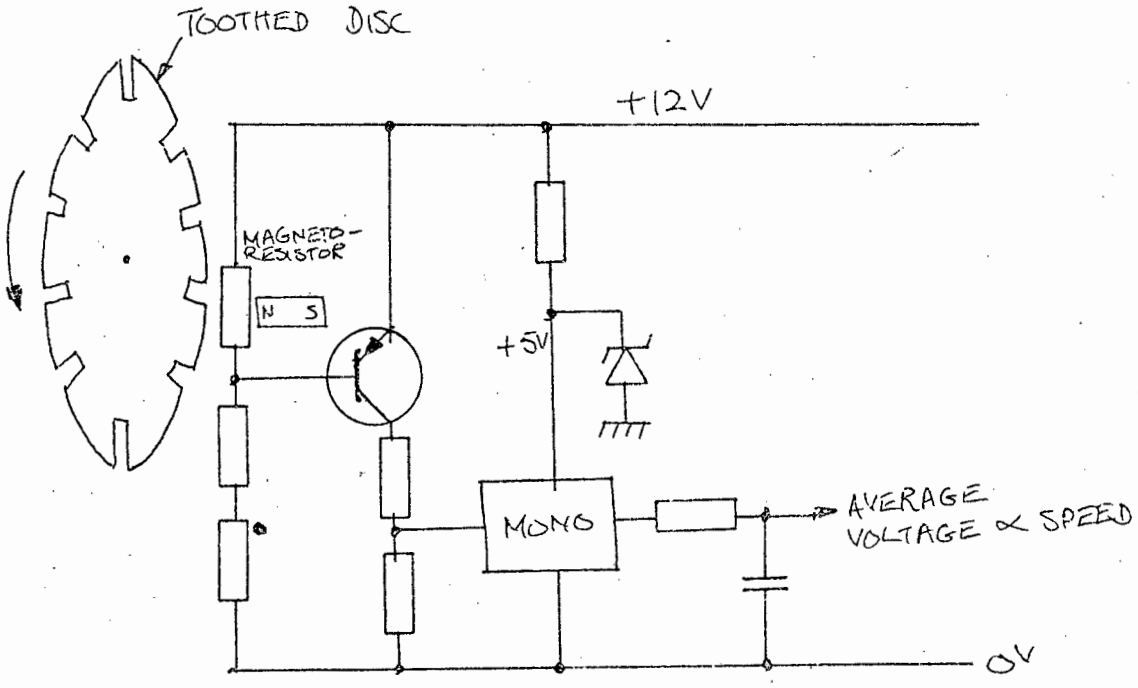

FIGURE 9.14: DIGITAL TACHOMETER

9.7 EVALUATION OF THE PROPOSED SYSTEM

(i) Power loss in the chopper circuit.

As the battery voltage is only 80V, any voltage drops caused by the chopper circuit, consisting of the semiconductor devices and the choke, will have a significant effect on the overall efficiency of the drive system. Therefore one criterion for evaluating the proposed control system is the estimated power loss in the chopper circuit in each of the three modes of operation.

From the circuit diagram of the chopper power circuit shown in figure 9.2, it can be seen that in each of the three modes, the load current in the "ON" state passes through the inductor L and two semiconductors (two thyristors or one thyristor and one diode). In the "off" state the free-wheel current also passes through L and two semiconductors (2 diodes or one thyristor and one diode).

If the motor was producing its rated output power, the chopper power circuit would consume 7,5 - 8,0% of the power being passed through it. This power loss may be divided amongst the components of the power circuit as follows:

Switching thyristor:4,0%; Choke 2,0% and the remaining semiconductor 1,5 -2,0%,depending on whether it was a diode or a thyristor. The corresponding power loss in a basic one mode chopper circuit consisting of a single switching thyristor, as series choke and a freewheel diode, would be approximately 6% of the input power. Therefore, the proposed three-mode controller will consume only 1,5 - 2% more power than the simplest chopper circuit.

(ii) Efficiency of the proposed chopper and motor combination.

The efficiency of the chopper and motor combined will be approximately 85 - 90% in each of the three modes. From the results

of the tests described in chapters 3 to 5, it is estimated that this value of efficiency will be nearly constant over the speed range of 50 - 90 km/h.

For the motoring configuration, this efficiency is very close to that obtained by using a series motor and chopper controller [46]. However the merit of the proposed system will be appreciated in the regenerative braking configuration where the overall efficiency will be approximately 20% greater than that obtainable by using a series motor. This will allow a correspondingly larger amount of energy to be returned to the battery, which will increase the maximum range obtainable for a given size battery.

(iii) Economic Considerations

In assessing the market potential of an electric vehicle for commuter use, its price should be compared with that of a similar sized internal combustion engined vehicle, as this will be one of the deciding factors for most consumers wishing to purchase a vehicle. The cost of an electric vehicle with the proposed control scheme will be in the region of R3000, as compared with R2000 for a similar sized i.c. engined vehicle. The cost of the electric vehicle may be divided as follows:

Batteries : 13%

2 Motors : 27%

Chopper power circuit : 12%
(power semiconductors and choke)

Controller (pedals, logic, etc.) : 6%

The remaining 42% covers the cost of the body structure and the manufacturing costs. As the potential market for an electric car of this type is very large, the development costs may be recovered with little effect on the selling price of the vehicle.

From the division of costs, it is seen that the cost of the chopper power circuit and controller form a minor portion of the total price. Therefore a change in the complexity of the control and power circuitry would not alter the overall price of the vehicle by more than 10%. The price differential between the electric and the conventional car will decrease as manufacturers are forced to meet anti-pollution requirements. Because of the longer expected life of the electric vehicle, the selling price of a second-hand vehicle will be proportionately higher than for a conventional car. The price differential will also be offset by the ever increasing running costs of the i.c. engined vehicle, because of price rises of fuels and oils due to world-wide shortages. At present, the running costs of electric vehicles is 30% below that of conventional vehicles [15] .

Apart from the motor brushes, the only component of the electric drive system that should need replacement is the batteries, which have a life of approximately 1000 charge/discharge cycles. Therefore, every 4 to 5 years the batteries will need to be replaced at a cost of approximately R250, allowing for the scrap value of the batteries.

(iv) Summary

The permanent magnet motors, combined with the proposed 3 mode controller, offer a high efficiency system which will operate over a wide speed range. The additional power lost in the chopper circuit due to its complexity is fully compensated for by the improved performance in the regenerative braking mode.

As the cost of the chopper circuit forms a minor portion of the total cost of the vehicle, the implementation of the proposed system will cause only a slight increase of the price of an electric vehicle. Although the initial cost of an electric vehicle will probably be

50% greater than that of a comparable petrol engined car, this will be compensated for by the lower running cost and longer life of an electric vehicle.

C O N C L U S I O N

The results of the load tests on the permanent magnet motor in each of the four proposed modes indicate that the speed range of the mode of regenerative braking when $E_M \leq V_B$ may be extended up to 50% above base speed, thus dispensing with the mode of regenerative braking which was proposed for operation above base speed.

The efficiency of the motor and chopper in the remaining three configurations is greater than 80% at full load. By using a permanent magnet motor in place of a conventional series motor, the mass of the machine may be reduced by 33%, and a higher operating efficiency is possible, especially in the mode of regenerative braking, where the efficiency may be increased by up to 20%.

The advantages of a regenerative braking system were illustrated when the motor was coupled to a flywheel to simulate the inertia of a vehicle, and it was found that approximately 40% of the energy used during acceleration could be returned to the battery during braking. Allowing for the additional losses occurring in a vehicle drive, it is estimated that approximately 10% of the expended energy could be recovered by the battery, resulting in a greater vehicle range for a given battery capacity.

In order to improve the overall efficiency of the drive system, and to avoid an unnecessary increase in cost, there must be a compromise between the additional motor copper losses (due to the current form factor), the losses in the choke and the chopper frequency.

A system of mode selection, using a series transistor switch

for an array of thyristors, was found to be unsatisfactory because of the amount of power lost in the semiconductors. A more efficient method, using a group of capacitor - commutated thyristors, was suggested. A proposed vehicle control scheme illustrated how power semiconductor devices may be interfaced with low power logic to form a complete system.

The long term economic advantages of electric cars would be appreciated most by the fleet owner who hires vehicles to the public for travelling short distances in the city centre. Unless the stored energy capacity can be substantially increased by some revolutionary development in storage batteries, the electric car will not appeal to the general public as a replacement for the small internal combustion engined vehicle.

CHAPTER 10 : APPENDIX

10.1 MATHEMATICAL ANALYSIS OF CHOPPER OPERATION.

10.1 (i) MOTORING

(a) In figure 10.1, the battery voltage and motor back-emf are represented by V_1 and V_2 respectively, with V_1 greater than V_2. In series with the back-emf of the motor is inductor of value L henries, with resistance R_L ohms, and the armature resistance R_a. The total circuit resistance is then $R_a + R_L = R$. If the switch S is closed at t=0 when $i(0+) = 0$, the current will rise exponentially according to equation:

$$i(t) = \frac{V_1 - V_2}{R} (1 - e^{-Rt/L}) \quad \text{----------(10.1)}$$

This is illustrated graphically in figure 10.2(a)

(b) If S is now opened when $I = \frac{V_1 - V_2}{R}$, the following differential equation exists

$$L \frac{di}{dt} + iR = V_2$$

with initial condition $i(0+) = - \frac{V_1 - V_2}{R}$

Taking laplace transform:

$$sL\, i(s) - L\, i(0+) + R\, i(s) = V_2/s$$

$$sL\, i(s) + (V_1 - V_2)(L/R) + R\, i(s) = V_2/s$$

giving

$$i(s) = \frac{V_2}{R} \left(\frac{1}{s} - \frac{1}{s + R/L}\right) - \left(\frac{V_1 - V_2}{R}\right) \left(\frac{1}{s + R/L}\right)$$

Taking inverse laplace,

$$i(t) = \frac{V_2}{R} - \frac{V_1}{R} e^{-Rt/L} \quad \text{----------(10.2)}$$

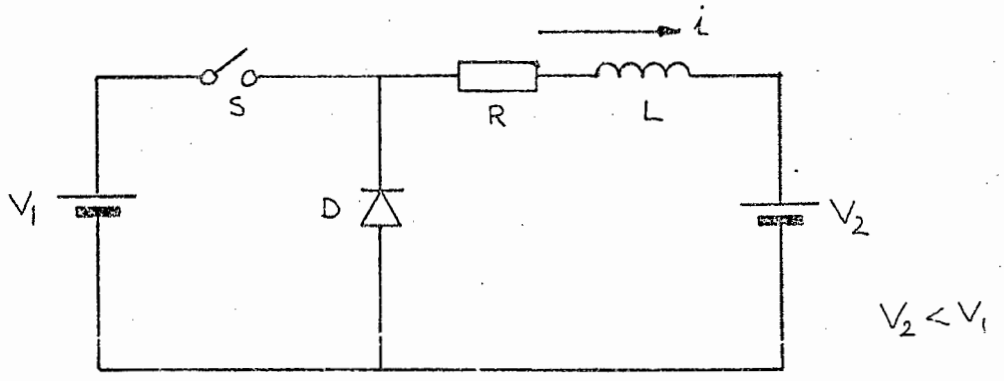

FIGURE 10.1: CIRCUIT CONFIGURATION FOR MOTORING.

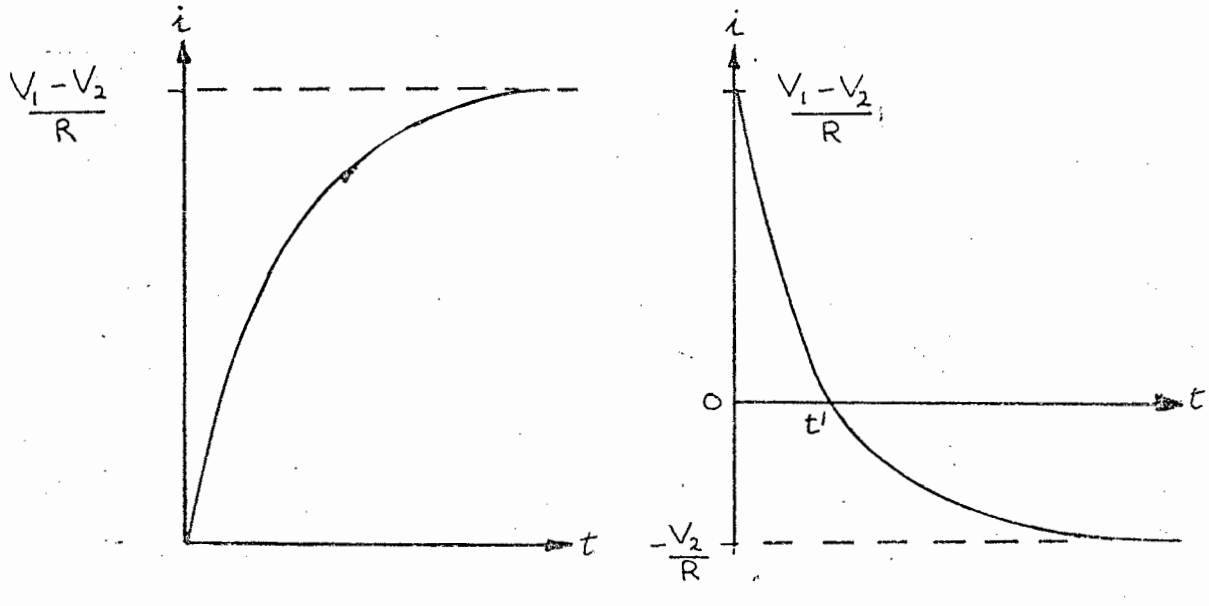

FIGURE 10.2: CURRENT WAVEFORMS FOR OPENING AND CLOSING OF SWITCH S FOR MOTORING.

Taking V_1 as the reference voltage,

$$i(t) = \frac{V_1}{R} e^{-Rt/L} - \frac{V_2}{R} \quad \text{----------(10.3)}$$

The curve of equation 10.3 illustrated in figure 10.2(b), shows that the current will fall to zero after a time t' and then reverse in direction. The reversal will be prevented by the diode D. Time t' is given by

$$t' = L/R \ln (V_1/V_2) \quad \text{----------(10.4)}$$

(c) The switch is closed for an interval t_m when $i(0+) = I_o$, where

$$I_o = \frac{V_1 - V_2}{R} (1 - e^{-Rt_o/L})$$

During this interval t_m, the current will increase by Δi_m, as shown in figure 10.3(a) from I_o to I_1

$$I_1 = \frac{V - V_2}{R} (1 - e^{R(t_o + t_m)/L})$$

$$\Delta i_m = I_1 - I_o$$

$$\Delta i_m = \frac{V_1 - V_2}{R} (e^{-Rt_o/L}) \quad \text{----------(10.5)}$$

This is as expected. The term

$$1 - e^{-Rt_m/L}$$

is an exponentially increasing term, dependent on t_m and the term

$$\frac{V_1 - V_2}{R} e^{-Rt_o/L}$$

is an exponentially decreasing term, dependent on t_o. therefore, for a given t_m, the closer we move to the

zero axis (i.e. the smaller t_o is), the larger i_m is, but the smaller I_o and I_1 are, - i.e. the smaller the average value of i over the time t_m.

(d) The switch is opened for an interval t_s figure 10.3(b) when i (0+) = I'_o, given by

$$I'_o = \frac{V_1}{R} e^{Rt'_o} - \frac{V_2}{R}$$

After an interval t_s, I'_o will decrease to I_2, where

$$I_2 = \frac{V_1}{R} e^{-R(t'_o + t_s)/L} - \frac{V_2}{R}$$

$$\Delta i_s = I'_o - I_2$$

$$\Delta i_s = \frac{V_1}{R} e^{Rt'_o/L} (1 - e^{-Rt_s/L}) \quad \text{---------(10.6)}$$

(e) If S is operated cyclically, with period $(t_m + t_s)$, the current waveform will become repetive, and the average value will reach steady-state when $\Delta i_m = \Delta i_s$, as shown in figure 10.4

To find I_v in terms of t_m and t_s, consider first curve 1

$$I_o = \frac{V_1 - V_2}{R} (1 - e^{-Rt_o/L})$$

giving $e^{Rt_o/L} = 1 - \frac{RI_o}{V_1 - V_2}$ ----------(10.7)

considering curve 2,

$$I_2 = \frac{V_1}{R} e^{-R(t'_o + t_s)/L} - \frac{V_2}{R}$$

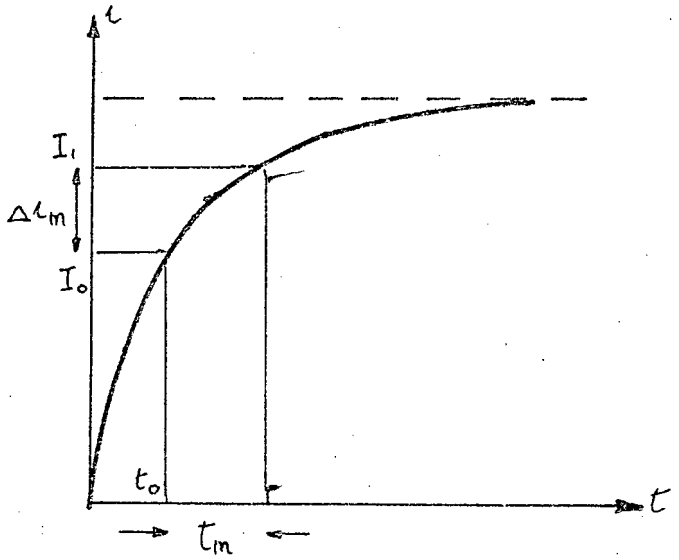

(a) S CLOSED

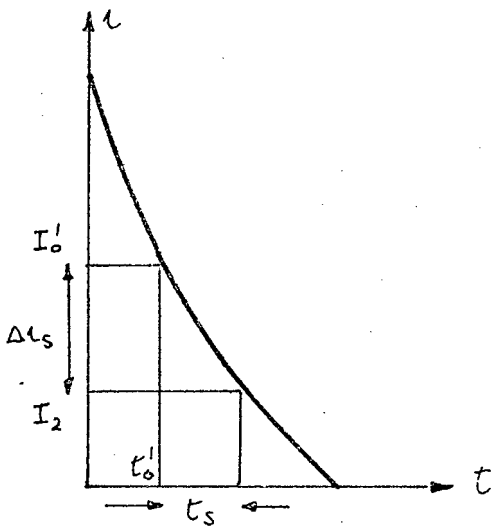

(b) S OPENED

FIGURE 10.3 : TRANSIENT OPERATION

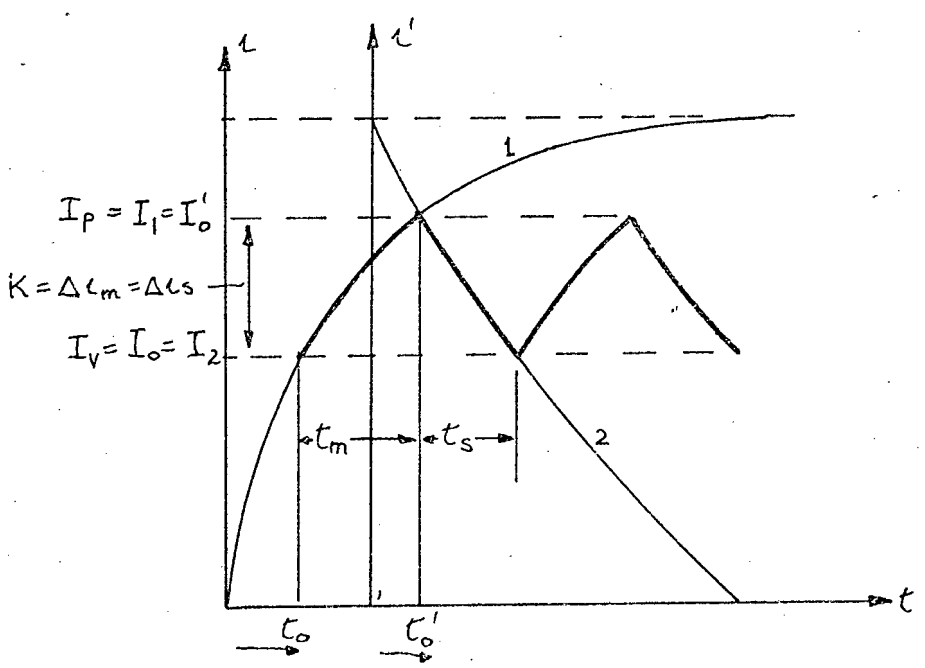

FIGURE 10.4 : STEADY-STATE CYCLIC OPERATION

giving $e^{-Rt_o'/L} = \left(\frac{RI_2 + V_2}{V_1}\right) e^{Rt_s/L}$ ----------(10.8)

Now $\Delta i_m = \frac{V_1 - V_2}{R} e^{-Rt_o/L} (1 - e^{-Rt_m/L})$ ----------from(10.5)

substituting for $e^{-Rt_o/L}$ from (10.7) gives

$$\Delta i_m = \left(\frac{V_1 - V_2}{R} - I_o\right) (1 - e^{-Rt_m/L}) \text{ ----------(10.9)}$$

$$\Delta i_s = \frac{V_1}{R} e^{-Rt_o'/L} (1 - e^{-Rt_s/L}) \quad \text{from 10.6}$$

substituting for $e^{-Rt_o'/L}$ from (10.8) gives

$$\Delta i_s = \left(I_2 + \frac{V_2}{R}\right) (e^{Rt_s/L} - 1) \text{ ----------(10.10)}$$

For steady state conditions,

(i) $\Delta i_m = \Delta i_s$

(ii) $I_o = I_2 = I_v$

Hence equating (10.9) and (10.10)

$$\left(\frac{V_1 - V_2}{R} - I_v\right) (1 - e^{-Rt_m/L}) = \left(I_v + \frac{V_2}{R}\right) (e^{Rt_s/L} - 1)$$

Solving for I_v gives

$$I_v = \frac{\frac{V_1 - V_2}{R} (1 - e^{-Rt_m/L}) - \frac{V_2}{R} (e^{Rt_s/L} - 1)}{e^{Rt_s/L} - e^{-Rt_m/L}} \text{ ----------(10.11)}$$

(f) To find I_p when S is operated cyclically, consider first curve 1:

$$I_1 = \frac{V_1 - V_2}{R} (1 - e^{-R(t_o + t_m)/L})$$

giving: $e^{-Rt_o/L} = \left(1 - \frac{I_1 R}{V_1 - V_2}\right) e^{Rt_m/L}$ -------(10.12)

considering curve 2,

$$I_o' = \frac{V_1}{R} e^{-Rt_o'/L} - \frac{V_2}{R}$$

giving: $e^{-Rt_o'/L} = \frac{RI_o'}{V_1} + \frac{V_2}{V_1}$ ----------(10.13)

Now $\Delta i_m = \frac{V_1 - V_2}{R} e^{-Rt_o/L} (1 - e^{-Rt_m/L})$ From (10.5)

substituting for $e^{-Rt_o/L}$ from (10.12) gives

$$\Delta i_m = \left(\frac{V_1 - V_2}{R} - I_1\right) (e^{Rt_m/L} - 1) \text{ ----------(10.14)}$$

Similarly, $\Delta i_s = \frac{V_1}{R} e^{-Rt_o'/L} (1 - e^{-Rt_s/L})$ from (10.6)

substituting for $e^{-Rt_o'/L}$ from (10.13) gives:

$$\Delta i_s = \left(I_o' + \frac{V_2}{R}\right) (1 - e^{-Rt_s/L}) \text{ ----------(10.15)}$$

For steady state conditions

(i) $\Delta i_m = \Delta i_s$

(ii) $I_1 = I_o' = I_p$

equating (10.14) and (10.15)

$$\left(\frac{V_1 - V_2}{R} - I_p\right) (e^{Rt_m/L} - 1) = \left(I_p + \frac{V_2}{R}\right) (1 - e^{-Rt_s/L})$$

solving for I_p gives

$$I_p = \frac{\frac{V_1 - V_2}{R} (e^{Rt_m/L} - 1) + \frac{V_2}{R} (e^{-Rt_s/L} - 1)}{e^{Rt_m/L} - e^{-Rt_s/L}} \text{ ------(10.16)}$$

(g) As the period of the chopper is much less than the time constant of the circuit ($T_o \ll L/R$), it is possible to simplify equations (10.11) and (10.16) by using a Taylor expansion for exponentials, where

$$e^{-Rt/L} = 1 - Rt/L + \tfrac{1}{2}(Rt/L)^2 \text{ ----------(10.17)}$$

$$e^{Rt/L} = 1 + Rt/L + \tfrac{1}{2}(Rt/L)^2 \text{ ----------(10.18)}$$

Substituting equations (10.17) and (10.18) into (10.11) and (10.16), we have

$$I_v = \frac{\frac{V_1-V_2}{R}\, Rt_m/L - \tfrac{1}{2}(Rt_m/L)^2 \quad -\frac{V_2}{R}\, Rt_s/L + \tfrac{1}{2}(Rt_s/L)^2}{Rt_s/L + Rt_m/L + \tfrac{1}{2}(Rt_s/L)^2 - \tfrac{1}{2}(Rt_m/L)^2} \text{ --(10.19}$$

$$I_p = \frac{\frac{V_1-V_2}{R}\, Rt_m'/L + \tfrac{1}{2}(Rt_m/L)^2 \quad -\frac{V_2}{R}\, Rt_s/L - \tfrac{1}{2}(Rt_s/L)^2}{Rt_s/L + Rt_m/L + \tfrac{1}{2}(Rt_m/L)^2 - \tfrac{1}{2}(Rt_s/L)^2} \text{ -(10.20)}$$

(h) The average value of the current flowing through R, L and V_2 (motor circuit) over the period $t_m + t_s$ is given by

$$I_{AV} = \frac{I_p + I_v}{2} \text{ ----------(10.21)}$$

This assumes that the waveform can be considered linear over these intervals

Neglecting the terms

$$\tfrac{1}{2}\ (Rt_s/L)^2 \ - \tfrac{1}{2}\ (Rt_m/L)^2 \quad \text{and}$$

$$\tfrac{1}{2}\ (Rt_m/L)^2 \ - \tfrac{1}{2}\ (Rt_s/L)^2$$

$$I_{AV} = \frac{1}{R}\left(\frac{V_1 t_m}{t_m + t_s} - V_2\right) \text{----------(10.22)}$$

It is interesting to note that this is independent of the value of L and is proportional to tm (for fixed (V_1, V_2).

(i) The current bandwidth is given by the difference between current maxima and minima

$$K = I_p - I_v \text{----------(10.23)}$$

From (10.19) and (10.20) the bandwidth is found to be

$$K = \frac{(V_1 - V_2)\ (t_m)^2 + V_2\ (t_s)^2}{L\ (t_m + t_s)} \text{----------(10.24)}$$

This is a maximum when $t_m = t_s = \tfrac{1}{2}\ T_o$

$$K_{MAX} = \frac{V_1\ T_o}{4\ L} \text{----------(10.25)}$$

and

$$r_{MAX} = \frac{V_1}{8\ I_{AV}}\ fL \text{----------(10.26)}$$

where $r = \dfrac{I_p - I_v}{I_p + I_v} = \dfrac{K}{2I_{AV}}$

10.1 (ii) REGENERATIVE BRAKING

(a) In figure 10.5, the battery voltage and motor back-emf represented by V_1 and V_2 respectively, with V_1 greater than V_2. The resistance of the armature and the choke are R_a and R_L respectively, the total resistance, $R = R_a + R_L$.

If the switch S is closed when $i(0+) = 0$, the current will rise exponentially according to the equation

$$i(t) = V_2/R \ (1 - e^{-Rt/L}) \quad \text{----------(10.27)}$$

This is illustrated graphically in figure (10.6(a))

(b) If S is now opened when $I = V_2/R$, the following differential equation exists

$$L \frac{di}{dt} + iR = V_1 - V_2$$

with initial condition $i(0+) = -V_2/R$

Taking laplace transform,

$$sLi(S) - L\, i(0+) + Ri(s) = (V_1 - V_2)/s.$$

$$sli(S) + V_2\, L/R + Ri(s) = (V_1 - V_2/s.$$

giving

$$i(s) = \frac{V_1 - V_2}{R} \left(\frac{1}{s} - \frac{1}{s + R/L}\right) - \frac{V_2}{R} \left(\frac{1}{s + R/L}\right)$$

Taking inverse laplace

$$i(t) = \frac{V_1}{R} (1-e^{-Rt/L}) - \frac{V_2}{R} \quad \text{----------(10.28)}$$

The curve of equation 10.28, illustrated in figure 10.6(b), shows that the current falls to zero after a time t' given by

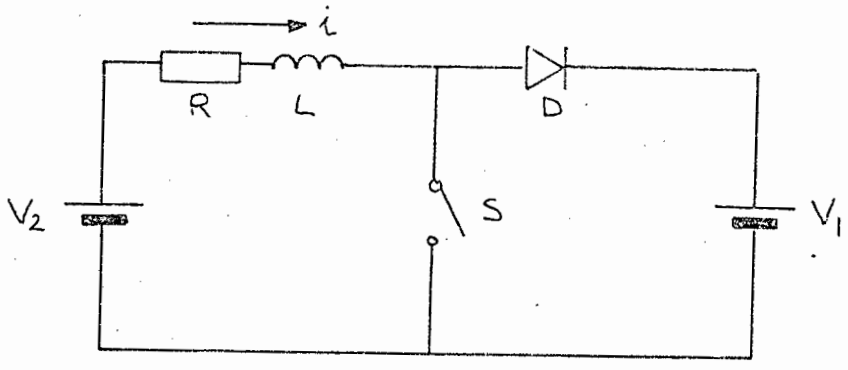

FIGURE 10.5 : CIRCUIT CONFIGURATION FOR REGENERATIVE BRAKING

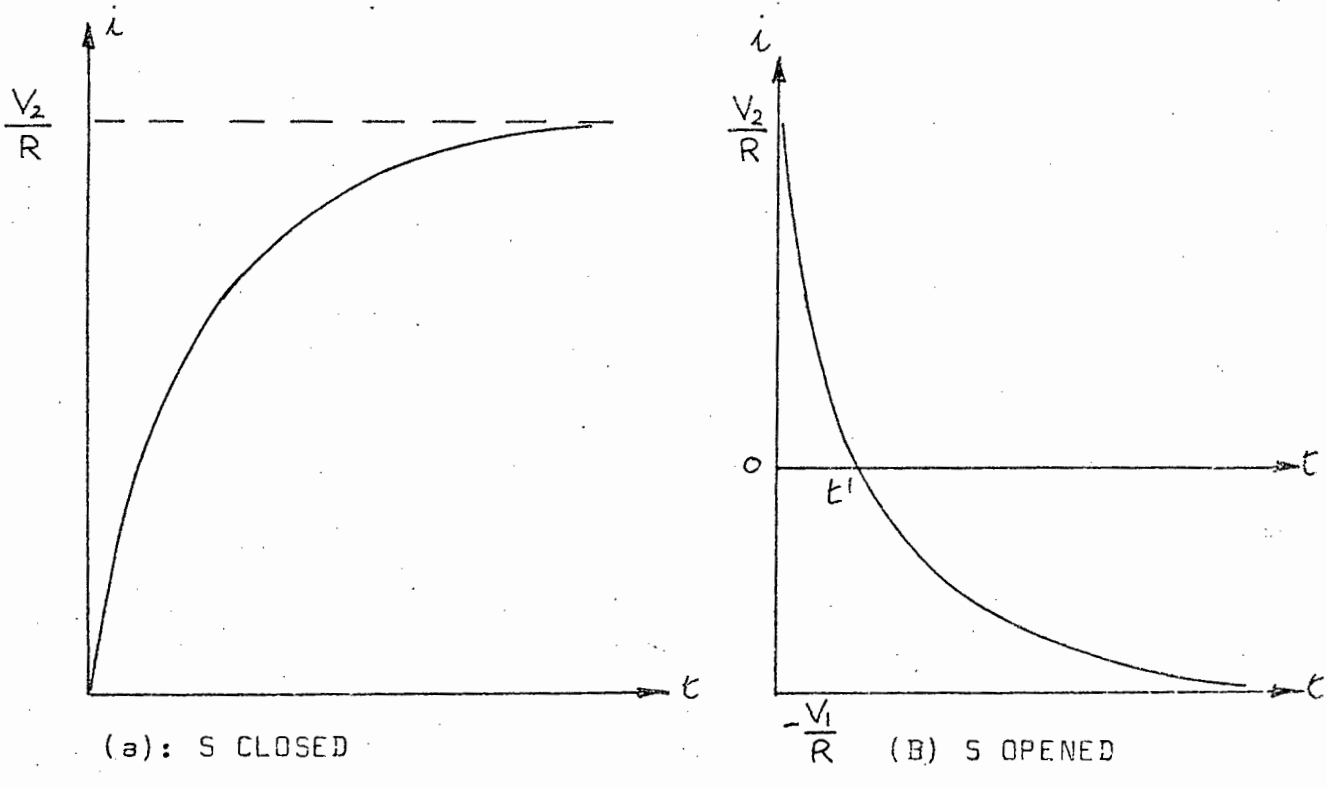

FIGURE 10.6: CURRENT WAVEFORMS FOR OPENING AND CLOSING OF SWITCH S FOR BRAKING

$$t' = L/R \ln \left(\frac{V_1}{V_1 - V_2}\right) \quad \text{----------(10.29)}$$

The current then reverses, in direction, but this is prevented in the circuit of figure 10.5 by diode D.

(c) The switch is closed at a time t_o for an interval t_m when $i(0+) = I_o$ where

$$I_o = V_2/R \ (1 - e^{- Rt_o/L})$$

During this interval the current will increase by Δi_m from I_o to I_1 (figure 10.3 (a))

$$I_1 = V_2/R \ (1 - e^{- R(t_o+t_m)/L})$$

$$\Delta i_m = I_o - I_1$$

$$\Delta i_m = \frac{V_2}{R} \ e^{- Rt_o/L} \ (1 - e^{- Rt_m/L}) \quad \text{----------(10.30)}$$

(d) The switch is opened at time t_o' for an interval t_s when $i(0+) = I_o'$, where

$$I_o' = \frac{V_2}{R} - \frac{V_1}{R} \ (1 - e^{- Rt_o'/L})$$

During this interval, the current will fall by Δi_s from I_o' to I_2 (figure 10.3 (b))

$$I_2 = \frac{V_2}{R} - \frac{V_1}{R} \ (1 - e^{- R(t_o' + t_s)/L})$$

$$\Delta i_s = \frac{V_1}{R} \ e^{- Rt_o'/L} \ (1 - e^{- Rt_s/L}) \quad \text{--------(10.31)}$$

where $\Delta i_s = I_o' - I_2$

(e) If S is operated cyclically, with period $(t_m + t_s)$, the current waveform will become repetitive, and the average value will reach steady-state when $\Delta i_m = \Delta i_s$, as shown in figure 10.4.

To find I_v in terms of t_m and t_s, first consider curve 1:

$$I_o = \frac{V_2}{R} \left(1 - e^{-Rt_o/L}\right)$$

giving

$$e^{-Rt_o/L} = I - \frac{RI_o}{V_2} \qquad \text{----------(10.32)}$$

next, consider curve 2:

$$I_2 = \frac{V_2}{R} - \frac{V_1}{R} \left(1 - e^{-R(t'_o + t_s/L}\right)$$

giving

$$e^{-Rt'_o/L} = \left(1 - \frac{V_2 - RI_2}{V_1}\right) e^{Rt_s/L} \qquad \text{---------(10.33)}$$

Now $\Delta i_m = \frac{V_2}{R} e^{-Rt_o/L} \left(1 - e^{-Rt_m/L}\right)$ ---from (10.30)

substituting for $e^{-Rt_o/L}$ from (10.32) gives

$$\Delta i_m = \left(\frac{V_2}{R} - I_o\right) \left(1 - e^{-Rt_m/L}\right) \qquad \text{----------(10.34)}$$

Similarly, $\Delta i_s = \frac{V_1}{R} e^{Rt'_o/L} \left(1 - e^{-Rt_s/L}\right)$ from (10.31)

substituting $e^{-Rt'_o/L}$ from (10.33) gives

$$\Delta i_s = \left(\frac{V_1 - V_2}{R} + I_2\right) \left(e^{Rt_s/L} - 1\right) \qquad \text{---------(10.35)}$$

For steady-state conditions

(i) $i_m = i_s$

(ii) $I_o = I_2 = I_v$

Hence equating (10.34) and (10.35)

$$\left(\frac{V_2}{R} - I_v\right)\left(1 - e^{-Rt_m/L}\right) = \left(\frac{V_1 - V_2}{R} + I_v\right)\left(e^{Rt_s/L} - 1\right)$$

giving

$$I_v = \frac{\frac{V_2}{R}\left(1 - e^{-Rt_m/L}\right) - \frac{V_1 - V_2}{R}\left(e^{Rt_s/L} - 1\right)}{e^{Rt_s/L} - e^{-Rt_m/L}} \quad \text{--(10.36)}$$

(f) To find I_p when S is operated cyclically, consider first curve 1 (figure 10.4):

$$I_1 = \frac{V_2}{R}\left(1 - e^{-R(t_o + t_m)/L}\right)$$

giving $e^{-Rt_o/L} = \left(1 - \frac{I_1 R}{V_2}\right) e^{Rt_m/L}$ ----------(10.37)

next, considering curve 2:

$$I_o' = \frac{V_2}{R} - \frac{V_1}{R}\left(1 - e^{-Rt_o'/L}\right)$$

giving $e^{-Rt_o'} = 1 - \frac{V_2 + RI_o'}{V_1}$ ----------(10.38)

$$i_m = \frac{V_2}{R} e^{-Rt_o/L}\left(1 - e^{-Rt_m/L}\right) \quad \text{from (10.30)}$$

substituting for $e^{-Rt_o/L}$ from (10.37), gives

$$i_m = \left(\frac{V_2}{R} - I_1\right)\left(e^{Rt_m/L} - 1\right) \text{----------(10.39)}$$

also, $i_s = \frac{V_1}{R} e^{-Rt'_o/L} (1 - e^{-Rt_s/L})$ (from 9.31)

substituting for $e^{-Rt'_o/L}$ (from 9.38), gives

$$i_s = \left(\frac{V_1 - V_2}{R} + I'_o\right)\left(1 - e^{-Rt_s/L}\right) \text{ ---------(10.40)}$$

For steady-state conditions,

(i) $i_m = i_s$

(ii) $I_1 = I'_o = I_p$

equating (10.39) and (10.40), we have

$$\left(\frac{V_2}{R} - I_p\right)\left(e^{Rt_m/L} - 1\right) = \left(\frac{V_1 - V_2}{R} + I_p\right)\left(1 - e^{-Rt_s/L}\right)$$

Solving for I_p gives

$$I_p = \frac{\frac{V_2}{R}\left(e^{Rt_m/L} - 1\right) - \frac{V_1 - V_2}{R}\left(1 - e^{-Rt_s/L}\right)}{e^{Rt_m/L} - e^{-Rt_s/L}} \text{ -----(10.41)}$$

(g) As the period of the chopper (T_o) is much less than the time constant of the circuit (T_o L/R), it is possible to simplify equations (10.36) and (10.41) by using Taylor expansion for exponentials, as given in equations (10.17)and (10.18)

Substitution into (10.36) and (10.41) gives

$$I_v = \frac{\frac{V_2}{R}\left(Rt_m/L - \frac{1}{2}(Rt_m/L)^2\right) - \frac{V_1 - V_2}{R}\left(Rt_s/L + \frac{1}{2}(Rt_s/L^2)\right)}{Rt_m/L + Rt_s/L - \frac{1}{2}(Rt_m/L)^2 + \frac{1}{2}(Rt_s/L)^2} \text{ ---(10.42)}$$

$$I_p = \frac{\frac{V_2}{R}\left(Rt_m/L + \frac{1}{2}(Rt_m/L)^2\right) - \frac{V_1 - V_2}{R}\left(Rt_s/L - \frac{1}{2}(Rt_s/L)^2\right)}{Rt_m/L + Rt_s/L + \frac{1}{2}(Rt_m/L)^2 - \frac{1}{2}(Rt_s/L)^2} \text{ ---(10.43)}$$

(h) The average value of the current flowing through R, L and V_2 (motor circuit) over the period $t_m + t_s$ is given by

$$I_{AV} = \tfrac{1}{2} (I_p + I_v) \text{ ----------(10.44)}$$

This assumes that the rise and fall of the waveform can be considered linear over these intervals

Neglecting the terms

$$\tfrac{1}{2} (Rt_s/L)^2 - \tfrac{1}{2} (Rt_m/L)^2 \quad \text{and}$$

$$\tfrac{1}{2} (Rt_m/L)^2 - \tfrac{1}{2} (Rt_s/L)^2$$

the average value of the current is given by

$$I_{AV} = 1/R \left(\frac{V_1 t_m}{t_m + t_s} - (V_1 - V_2)\right) \text{ ----------(10.45)}$$

Equation (10.45) is similar in form to that for motoring (10.22) and is likewise independent of the value of L.

(i) The current bandwidth is given by the difference between the maximum and minimum current values.

$$K = I_p - I_v \text{ ----------(10.46)}$$

From (10.42), and (10.43) the bandwidth is found to be

$$K = \frac{V_2 t_m^2 + (V_1 - V_2) t_s^2}{L (t_m + t_s)} \text{ ----------(10.47)}$$

This is a maximum when $t_m = t_s = \tfrac{1}{2} T_o$

$$K_{MAX} = \frac{V_1 T_o}{4 L} \text{ ----------(10.48)}$$

$$\text{and } r_{MAX} = \frac{V_1}{8 I_{AV} fL} \text{ ----------(10.49)}$$

It is interesting to note that although equations (10.24) and (10.47), for the current bandwidths in motoring and braking, differ slightly in their form, the equations for the maximum ripple factor - (10.26) and (10.49) are identical.

This shows that under the same conditions of load current and m/s ratio, identical waveforms exist in both motoring and braking.

10.2 CALCULATION OF I_{AV} AND I_{RMS} FROM THE CURRENT WAVEFORM.

10.2(i) Continuous current

Referring to figure 10.7,

$$(a)\ I_{AV} = 1/(t_m + t_s)\left\{ \int_{-t_m}^{0} \left(I_p + \frac{Kt}{t_m}\right) dt + \int_{0}^{t_s} \left(I_p - \frac{Kt}{t_s}\right) dt \right\}$$

$$= 1/(t_m + t_s)\left\{ \left[I_p t + \frac{Kt^2}{2t_m} \right]_{-t_m}^{0} + \left[I_p t - \frac{Kt^2}{2t_s} \right]_{0}^{t_s} \right\}$$

$$I_{AV} = \tfrac{1}{2}\,(I_p + I_v) \qquad \text{----------(10.50)}$$

$$(b)\ I_{RMS} = 1/(t_m + t_s)\left\{ \int_{-t_m}^{0} \left(I_p + \frac{Kt}{t_m}\right)^2 dt + \int_{0}^{t_2} \left(I_p - \frac{Kt}{t_s}\right)^2 dt \right\}$$

$$= 1/(t_m + t_s)\left\{ \left[I_p^2 t + \frac{I_p K t^2}{t_m} + \frac{K^2 t^3}{3t_m^2} \right]_{-t_m}^{0} + \left[I_p^2 t - \frac{I_p K t^2}{t_s} + \frac{K^2 t^3}{3t_s^2} \right]_{0}^{t_s} \right\}$$

$$I_{RMS} = \sqrt{1/3\ (I_p^2 + I_p I_v + I_v^2)} \qquad \text{----------(10.51)}$$

(c) Form Factor (f.f.)

$$f.f. = I_{RMS} / I_{AV} \qquad \text{----------(10.52)}$$

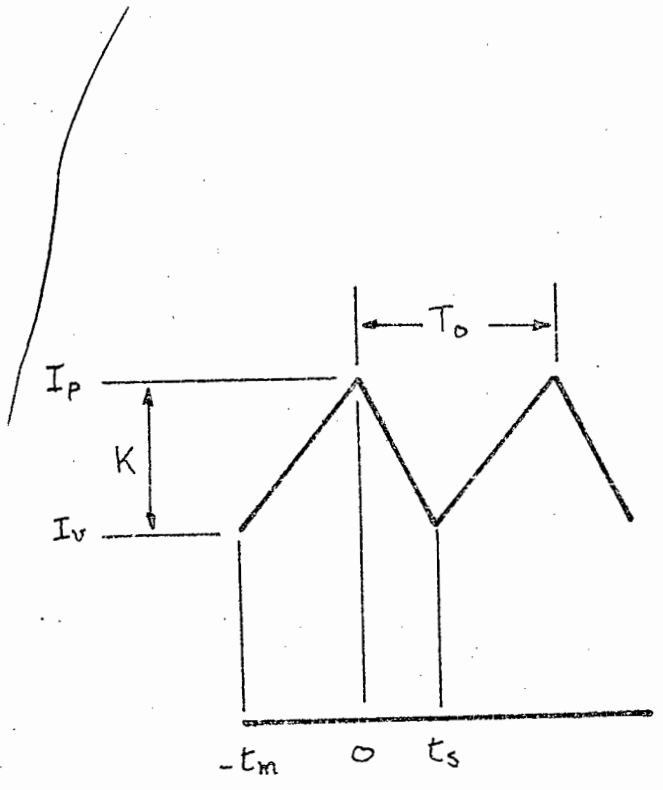

FIGURE 10.7 : CONTINUOUS CURRENT WAVEFORM

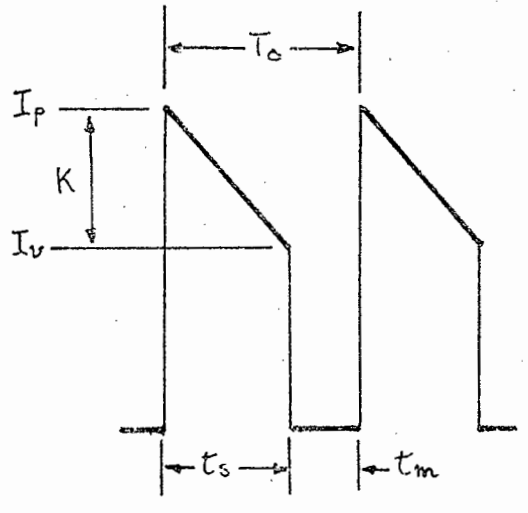

FIGURE 10.8 : NON-CONTINUOUS CURRENT WAVEFORM

$$f.f. = \sqrt{I_{RMS}^2 / I_{AV}^2}$$

$$= \sqrt{4/3 \; \frac{I_p^2 + I_p I_v + I_v^2}{(I_p + I_v)^2}}$$

$$= \sqrt{4/3 \left[1 - \frac{I_p I_v}{(I_p + I_v)^2} \right]}$$

$$= \sqrt{1 + 1/3 \; r^2} \qquad \text{----------(10.53)}$$

10.2(ii) NON-CONTINUOUS CURRENT

In order to distinguish between the currents for for the two waveforms, the average and RMS values of the non-continuous current will be referred to as I'_{AV} and I'_{RMS} respectively.

Referring to figure 10.8,

(a) $$I'_{AV} = \frac{1}{T_o} \int_o^{t_s} \left(I_p - \frac{Kt}{t_s} \right) dt$$

$$= \frac{1}{T_o} \left[I_p t - \frac{Kt^2}{2t_s} \right]_o^{t_s}$$

$$I'_{AV} = \frac{t_s}{2T_o} (I_p + I_v) \qquad \text{----------(10.54)}$$

$$= \frac{t_s}{T_o} I_{AV} \qquad \text{----------(10.55)}$$

(b) $$I'_{RMS} = \frac{1}{T_o} \int_o^{t_s} \left(I_p - \frac{Kt}{t_s}\right)^2 dt$$

$$= \frac{1}{T_o}\left[I_p^2 t - \frac{KI_p t^2}{t_s} + \frac{K^2 t^3}{3t_s^2}\right]_o^{t_s}$$

$$= \frac{t_s}{3T_o}\left(I_p^2 + I_p I_v + I_v^2\right) \text{ ---------(10.56)}$$

$$= \frac{t_s}{T_o} I_{RMS} \text{ ----------(10.57)}$$

(c) Form Factor (f.f.)

$$f.f.' = \frac{I'_{RMS}}{I'_{AV}}$$

$$= \frac{T_o}{t_s}\frac{I_{RMS}}{I_{AV}} \text{ ----------(10.58)}$$

10.3 THE TRANSISTOR AS A SWITCH [31 - 34]

10.3 (i) THE COMMON EMITTER (CE) CHARACTERISTICS.

The transistor, when used as a switch can be divided into 3 regions of operation

(i) the saturation region

(ii) the cut-off region

(iii) the active region

These regions are illustrated in figure 10.9 on the common emitter characteristics of a typical power transistor, 2N3773 [35]

The regions of particular interest are the saturation region and the active region. the transistion through the active region in switching operation should be accomplished as quickly as possible to avoid excessive dissipation (see section 10.3(iv)

10.3(ii) THE CE SATURATION REGION

The saturation region may be defined as the one where:

(i) both the collector and emitter junctions are forward biassed

(ii) the collector current is approximately independent of the base current.

When a trsnsistor is in saturation, further increases in base current affect the saturation voltage only slightly

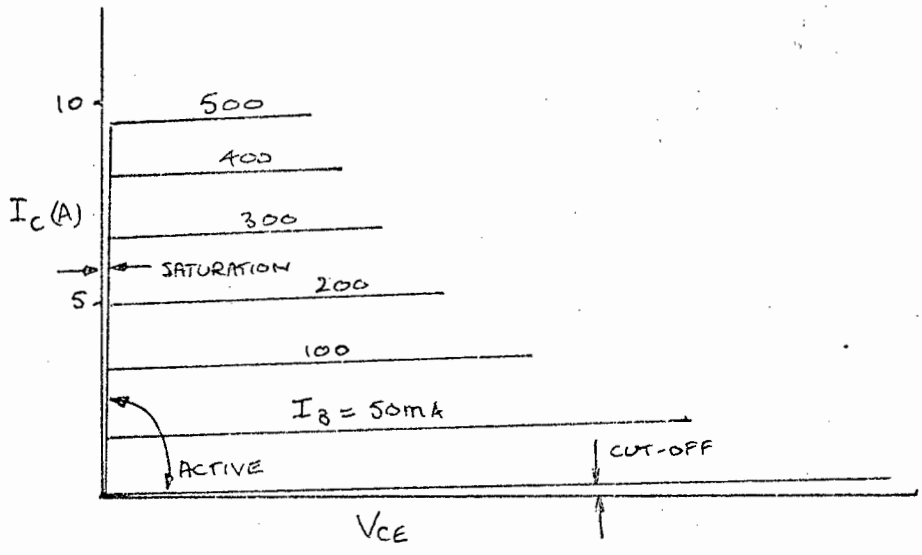

FIGURE 10.9 : THE THREE REGIONS OF TRANSISTOR OPERATION

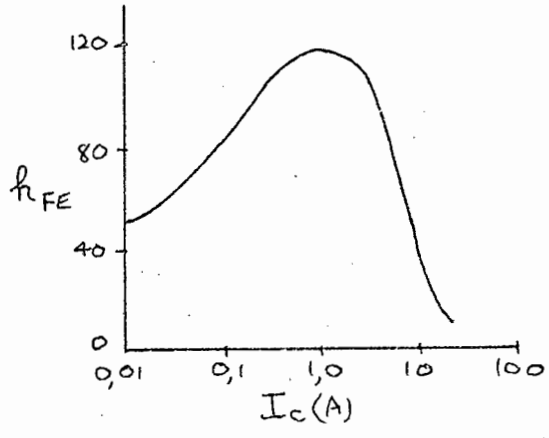

FIGURE 10.10 : VARIATION OF DC FORWARD CURRENT TRANSFER RATIO WITH COLLECTOR CURRENT

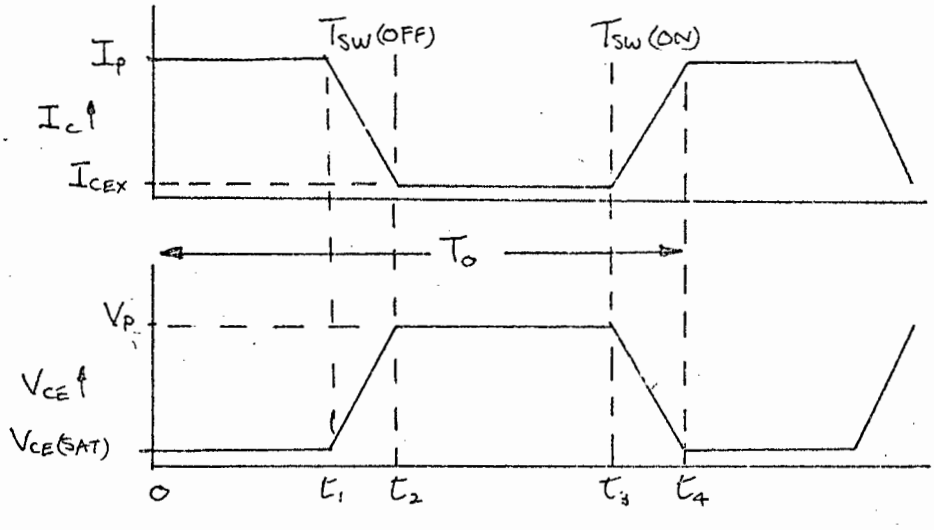

FIGURE 10.11 : SWITCHING WAVEFORMS OF A TRANSISTOR

10.3 (iii) d.c. CURRENT GAIN

A parameter of interest in connection with the switching transistor is the ratio of collector to base currents (I_c/I_b), known as the d.c. forward-current transfer ratio, h_{FE}. It is this ratio which determines the base drive necessary to ensure saturation for a given collector current. A conservative design is to provide the corresponding base drive. The variation of h_{FE} with I_c is shown in figure (10.10) for 2N3773 power transistor.

10.3 (iv) Power dissipation of a transistor in switching service [33]

Dissipation can be divided into four sections

(i) average dissipation

(ii) saturation dissipation

(iii) cut-off dissipation

(iv) switching transient dissipation

Average dissipation is the average power that must be handled over a complete cycle of operation, and basically determines the heatsink requirements for a given transistor case temperature. Where a transistor is continiously turning on and off, the average power can be expressed by the following equation

$$P_{AV} = 1/T_o \int_0^{t_1} V_{CE}(sat)\, I_c(sat)\, dt$$

$$+ 1/T_o \int_{t_1}^{t_2} V_{CE}(t)_{off}\, I_c(t)_{off}\, dt$$

$$+ 1/T_o \int_{t_2}^{t_3} V_{CE}(off)\, I_c(off)\, dt$$

$$+ 1/T_o \int_{t_3}^{T_o} V_{CE}(t)_{on}\, I_c(t)_{on}\, dt$$

Where T_o = total switching time (period)

$0 - t_1$ = transistor on time

$t_2 - t_1$ = turn-off time

$t_3 - t_2$ = transistor off time

$T_o - t_3$ = turn-on time

In order to simplify the above expression to calculate the average power, some assumptions can be made (the idealised waveforms are shown in figure 10.11):

(i) base power is neglible

(ii) Collector voltage and current waveforms vary linearly with time during the switching intervals.

$$P_{AV} = 1/T_o \int_0^{t_1} I_p \, V_{CE}(sat) \, dt$$

$$+ 1/T_o \int_{t_1}^{t_2} I_p \left(1 - \frac{t}{T_{SW}(off)}\right) V_p \left(\frac{t}{T_{SW}(off)}\right) dt$$

$$+ 1/T_o \int_{t_2}^{t_3} I_{CEX} \, V_p \, dt$$

$$+ 1/T_o \int_{t_3}^{t_4} I_p \left(\frac{t}{T_{SW}(on)}\right) V_p \left(1 - \frac{t}{T_{SW}(on)}\right) dt$$

simplifying, this gives

$$P_{AV} = 1/T_o \left(I_p \, V_{CE}(sat) \, T_{ON} + I_{CEX} \, V_p \, T_{OFF} \right)$$

$$+ 1/6T_o \left(I_p \, V_p \, T_{SW}(off) + I_p \, V_p \, T_{SW}(on)\right) \text{-----(10.58)}$$

If in addition, $T_{SW}(on) = T_{SW}(off) = T_{SW}$, then

$$P_{AV} = 1/T_o \left(I_p \, V_{CE}(sat) \, T_{ON} + I_{CEX} \, V_p \, T_{OFF} + 1/3 \, I_p \, V_p \, T_{SW}\right)$$

(10.59)

10.4 HEAT TRANSFER [40] .

(i) Basic principles

In a semiconductor power device, heat is generated in the semiconductor material, and from there is transfered to the outside case of the device, then via heatsink to the surrounding air.

The heat flow through heat conductors is analagons to the flow of electric current through electric conductors. In this analogy, the thermal resistance (R_{th} in deg. C/W) corresponds to the electrical resistance (R in ohms).

Figure 10.12 shows the heat path from the junction to the ambient air as a series connection of 3 thermal resistances:

$R_{th\ j-c}$: Thermal resistance from junction to case. Its value is found in data sheets of the particular semiconductor device.

$R_{th\ c-h}$: Thermal resistance from case to heatsink, resulting from imperfect contact between case and heatsink. Its value can also be found in data sheets.

$R_{th\ h-a}$: Thermal resistance between heatsink and the surrounding air. Its value depends on the design of the heatsink and whether forced ventilation is used or not.

According to figure 10.12, the following formula can be used in heatsink calculations

$$T_j - T_{amb} = P\ (R_{th\ j-c} + R_{th\ c-h} + R_{th\ h-a}) \quad (10.50)$$

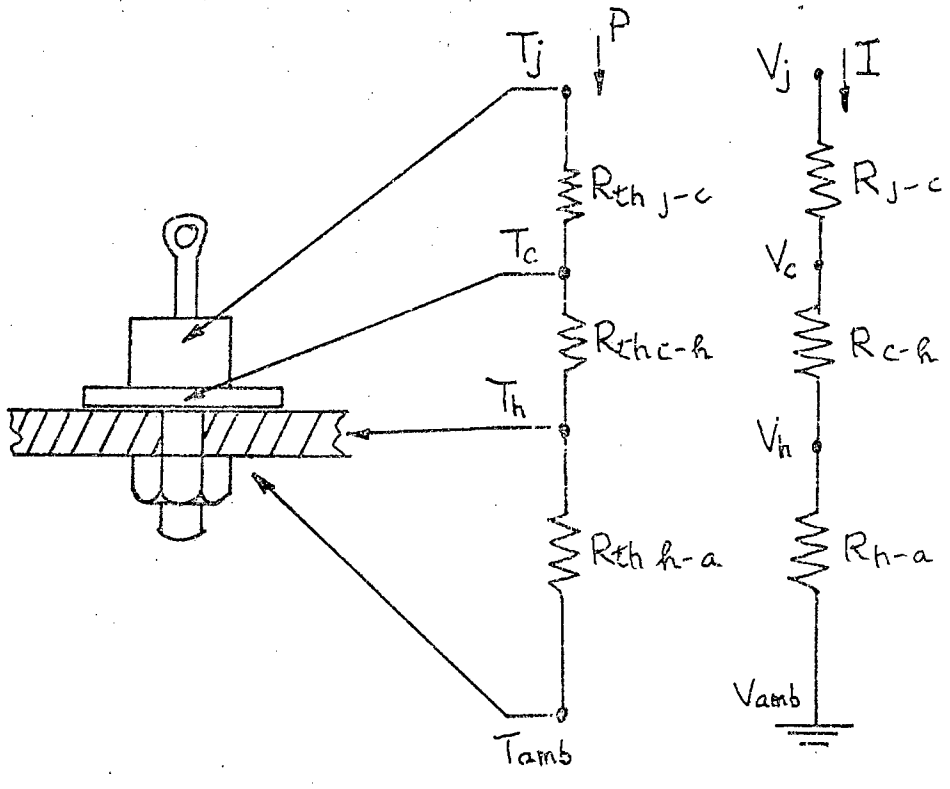

FIGURE 10.12 : ANALOGY BETWEEN HEAT AND ELECTRICAL CONDUCTION

(ii) Power losses and heatsinking for the semiconductors of the two mode transistor - thyristor chopper.

(a) Transistors

Considering each transistor alone:

$$P_{AV} = \frac{I}{T_o} I_p V_{CE}(sat) T_{ON} + I_{CE}(sat) V_p T_{OFF} + 1/3 I_p V_p T_{SW}$$

$$= 400 \quad 10 \times 0{,}5 \times 2{,}5 \times 10^{-3} + 1/3 \times 10 \times 84 \times 20 \times 10^{-6}$$

$$= 400 \quad 12{,}5 \times 10^{-3} + 5{,}6 \times 10^{-3} \quad \text{ignoring the cut-off losses}$$

$$= 7{,}24 W$$

50 mm of type 56290 heatsink (Phillips) 40 has

$$R_{th\ h-a} = 3{,}5 \text{ deg.c/w for 7W dissipation}$$

each transistor fitted with a mice washer with

$$R_{th} = 0{,}5 \text{ deg.c/W}$$

With an ambient temperature of 50 deg.c,

$$T_j - 50 = 7{,}24 \ (3{,}5 + 0{,}5 + 1{,}17) = 37$$

Hence T_j = 87 deg.C., which is safe

(b) Diodes (type ST440, 40A)

$$R_{th\ j-c} = 1{,}0 \text{ deg.c/W}; \quad R_{th\ c-h} = 0{,}2 \text{ deg.c/W}$$

At 37A average current, forward voltage drop

= I V (i.e. P = 37W)

Consider worst case of T_j = 200 deg.c

T_{AMB} = 50 deg.c

$$200-50 = 37 \ (1{,}0 + 0{,}2 + R_{th\ h-a})$$

giving $R_{th\ h-a} = 2{,}8$ deg. c/W

100 mm.of Phillips type 56290 has $R_{th\ h-a} = 2{,}1$ deg.c/W (at 37W)

(c) Thyristors (type 2N3898)

The specification sheets for the thyristor 44 indicated that for a thyristor mounted on 100 mm. of the above heatsink, and in an ambient temperature of 40 deg.c, the maximum safe forward current is 18A. This appeared to be very conservative, as the case temperature of the thyristors at an average forward current of 35A was lower than that of the other semiconductors.

10.5 VOLTAGE BREAKDOWN IN TRANSISTORS

(i) Avalanche breakdown [34, 35] .

Avalanche breakdown is a characteristic of the transistor alone and occurs at high voltages because of the avalanche multiplication of the leakage current. The breakdown region is attained when this current rises abruptly, and large changes in current accompany small changes in applied voltage. The transistor is then destroyed by excessive dissipation in the pellet.

(ii) Reach - Through [34, 35, 41] .

Another mechanism by which a transistor's usefulness may be terminated is known as reach-through and results from the increased width of the collector-junction transition region with increased collector-junction voltage. As the voltage applied across the junction increases, the transition region penetrates deeper into the collector and base. Since the base is very thin, it is possible, that at moderate voltages, the transition region will have spread completely across the base to reach emitter, effectively shorting the collector and emitter. Reach-through does not result in permanent damage to the transistor, provided there is sufficient source impedence to limit the transistor dissipation to safe values. In a particular transistor, the voltage limit is determined by reach-through or breakdown, whichever occurs at the lower voltage.

Silicon devices, as typified by grown diffused, mesa, planar and planar epitaxial structures do not exhibit this characteristic. The phenomenon of reach_through is most prevalent in alloy devices having thin base regions.

(iii) Second Breakdown [34, 35, 39]

Second Breakdown (s/b) is a potentially destructive phenonemom that occurs especially in large-area power transistors operated at

high voltage and current levels. S/b results when the energy absorbed by the transistor is focussed into a small area, causing localised heating that may melt a minute hole in the transistor pellet. The start of S/b is characterised by an abrupt decrease in collector-to-emitter voltage, with a small dynamic resistance in the breakdown region.

This phenonemon may be categorised into two classes:

(a) forward-biased emitter-to-base second breakdown, which occurs when the transistor is operated in the active region.

(b) reverse-biased emitter-to-base second breakdown, which occurs during the turn-off mode of transistor operation.

(a) Forward-biased second breakdown (FB S/b) [35, 37] .

The severity of S/b in the active region depends on the operating collector-to-emitter voltage, duration of applied voltage and transistor temperature.

(b) Reverse second breakdown (RB S/b) [35, 37, 39] .

This form of S/b is of greater importance as the energy required to induce S/b when the transistor is turning off is much lower than that required in the forward-bias mode. RB S/b usually occurs in circuits that involve the switching of inductive loads (inverters, switching regulators), and the RB S/b energy capability increases with a decrease in inductance. Protection for the transistor is afforded by the addition of Zener diodes, diode clamps and R - C networks. An analysis of the action of each type is provided by Locher [39] .

10.6 VOLTAGE BREAKDOWN IN THYRISTORS [25].

(i) Reverse Voltage Breakdown

In the reverse direction (anode negative with respect to cathode), the thyristor behaves like a convential rectifier diode. If the reverse voltage ratings (repetitive PRV or non-repetive PRV) are substantially exceeded, the device will go into avalanche breakdown and may destroy itself.

(ii) Forward Voltage Breakdown

A thyristor can be turned on in the absence of gate drive by exceeding the forward voltage ratings for a given temperature. The thyristor will not be damaged under these conditions unless the forward current rating or the allowable di/dt rating is exceeded.

10.7 CALIBRATION OF METERS (see figure 10.13 for procedure)

(i) Energy Meter.

FREQ. (Hz)	CURRENT (A)	SPEED (r.p.m./A)	ERROR %
d.c.	0,5	13,20	- 4,0
	1,0	13,65	- 0,8
	2,0	13,50	- 2,6
	4,0	13,95	+ 1,5
	6,0	14,20	+ 3,0
70	0,5	13,35	- 3,0
	1,0	13,60	- 2,3
	2,0	13,30	- 3,4
	4,0	13,85	+ 0,7
	6,0	14,10	- 2,2
500	0,5	13,35	- 3,0
	1,0	13,95	+ 1,5
	2,0	14,0	+ 1,8
	4,0	14,30	+ 4,0
	6,0	14,30	+ 4,0

Rated speed = 13,75 r.p.m./A

TABLE 10.1 CALIBRATION OF D.C. ENERGY METER (Siemens - Schuckert, 220V, 5A, 1kWh = 3750 revolutions of disc).

(ii) Wattmeter

MANUFACTURER : WESTON

RANGES : VOLTAGE: 50V (75 max)/100V (150V max)

CURRENT: 50A (75A max)/100A (150A max)

SPECIFICATIONS: MEASUREMENTS OF POWER FROM DC TO 133 Hz AT ACCURACY OF 1/4% OF FULL SCALE VALUE

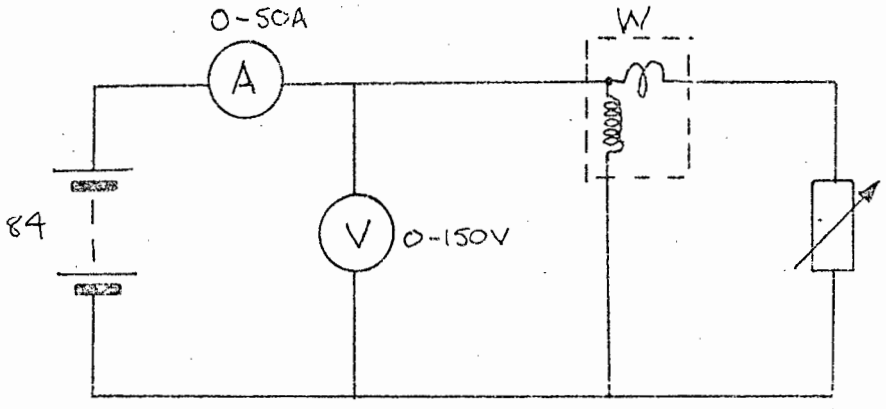

FIGURE 10.13(a): CALIBRATION OF WATTMETER AT DC.

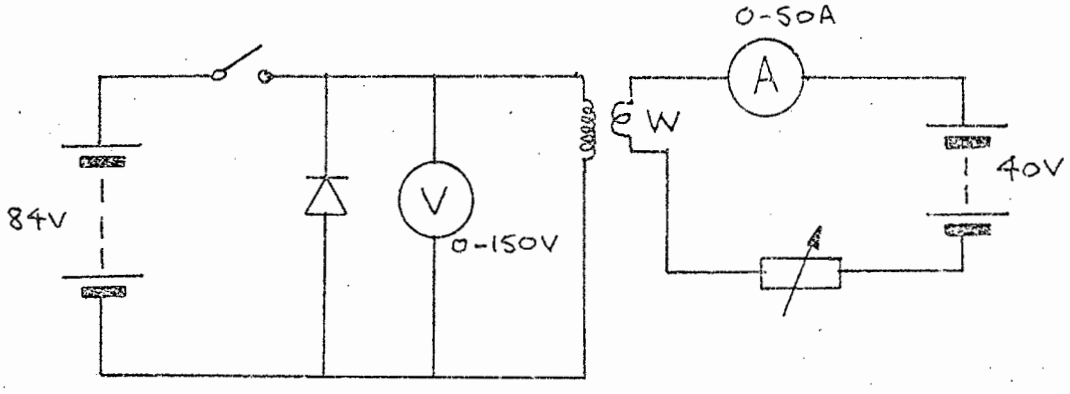

FIGURE 10.13(b): CALABRATION OF WATTMETER FOR DC CURRENT, CHOPPER VOLTAGE.

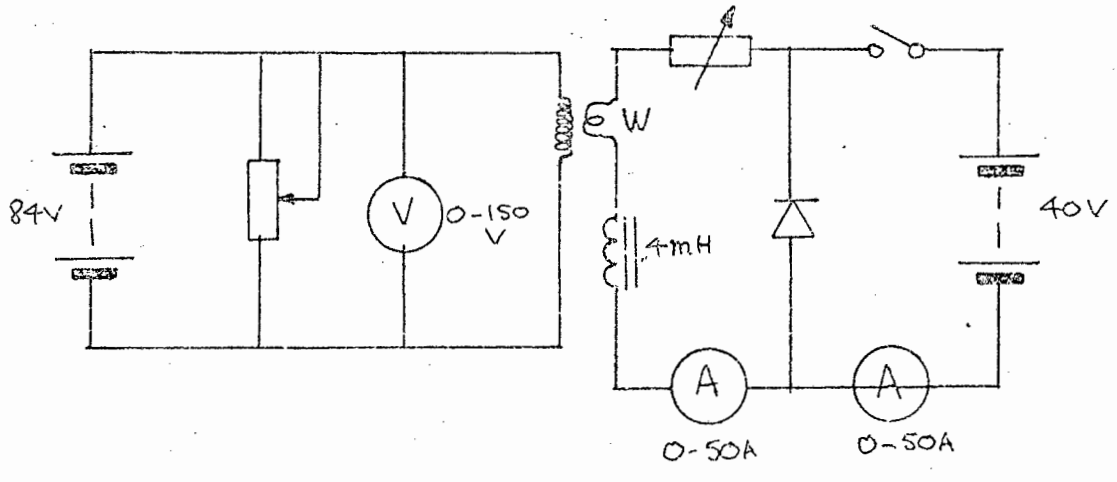

FIGURE 10.13(c): CALIBRATION OF WATTMETER FOR DC VOLTAGE, CHOPPER CURRENT.

Wattmeter		Volts	Amps	Watts Calc.	% diff from Wattmeter
read (W)	x S.F. (W)			(W)	
500	250	35,8	7,0	250,6	+ 0,2
1000	500	33,2	15,1	501	+ 0,2
1500	750	30,1	25,1	755	+ 0,6
2000	1000	25,1	40,3	1000	+ 0
2500	1250	63,2	19,8	1250	+ 0

TABLE 10.2 CALIBRATION OF WATTMETER AGAINST VOLTMETER/AMMETER ON 50V, 50A RANGES (2,5 kW) FOR d.c.

Wattmeter		Volts	Amps	Watts Calc	% diff from Wattmeter
read (W)	X.S.F. (W)	(V)	(A)	(W)	
1040	520	15	35	525	+ 1,0
1080	1040	30	35	1050	+ 1,0
3100	1550	45	35	1575	+ 1,3
4170	2085	60	35	2110	+ 1,3

TABLE 10.3 CALIBRATION OF WATTMETER FOR CONSTANT dc CURRENT, CHOPPED VOLTAGE (400 Hz, 50V, 2.5 kW FULL SCALE)

Wattmeter		Volts	Amps	Watts Calc	% diff from Wattmeter
read (W)	X.S.F. (W)	(V)	(A)	(W)	
980	495	50	10	500	+ 1
1970	985	50	20	1000	+ 1,5
2950	1475	50	30	1500	+ 1,3

TABLE 10.4 CALIBRATION OF WATTMETER FOR CONSTANT VOLTAGE, CHOPPED CURRENT AT 1:1 m/s RATIO, 400 Hz, 50V, 50A, 2.5 kW FULL SCALE

10.8 COMPARISON BETWEEN SHUNT AND SERIES CONNECTIONS UNDER REGENERATIVE BRAKING

(i) Description of motor

Two identical motors of the following specifications were mounted back to back

Manufacturer: Veritys Ltd., Aston

Voltage: 220V

Amps: 6,6A

HP: 1,5

Speed: 1450 r.p.m.

As there was no means of obtaining a direct measurement of shaft torque, this was done indirectly by summation of losses.

For each machine the field and armature resistance (hot) were: 4,7 ohms, and 4,6 ohms respectively.

As the machines were considered identical, it was assumed that the total friction, windage and iron loss would be equally shared. These losses for one machine at various speeds are shown in Table 10.5.

(ii) Tests performed

As no dynamometer was available, the mechanical power P_{MECH}, was evaluated by a summation of losses

$$P_{MECH} = P_{IN} - P_{CU} - P_{BR} - P_{O}$$

where

P_{IN} = the input power

P_{CU} = the armature copper loss

P_{BR} = brush loss

P_{O} = the no load losses

As the battery voltage is fixed, the power returned to the

battery is the product of the battery voltage and the average value of the battery current.

$$P_B = V_B \, I_B$$

The connection diagram for the tests is shown in figure 10.14

(a) constant torque ($0,75T_{FL}$) by keeping the drive motor field and armature currents fixed: power and efficiency were measured as functions of speed.

(b) Constant speed (600 r.p.m.); power and efficiency were measured as functions of torque.

The results of these tests are shown in figure 1.1.

SPEED (r.p.m.)	NO LOAD LOSS FOR ONE MACHINE (W)
980	30
800	22
610	16
420	10
250	5
160	3

TABLE 10.5 FRICTION WINDAGE AND IRON LOSS AS A FUNCTION OF SPEED.

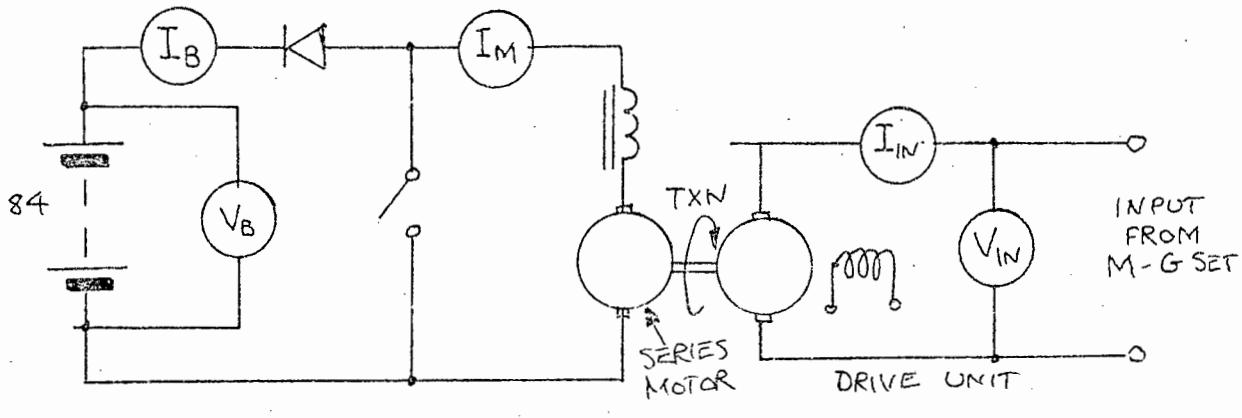

FIGURE 10.14: REGENERATIVE BRAKING TEST ON SERIES

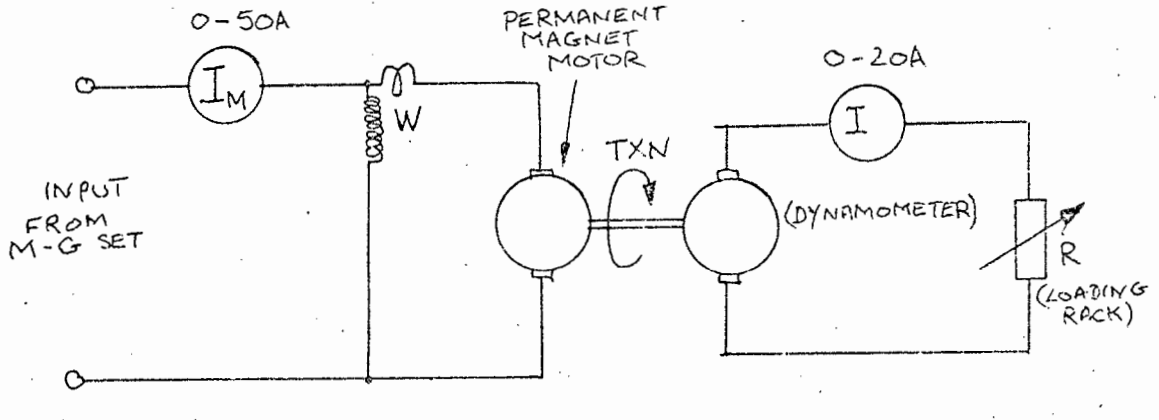

FIGURE 10.15: DC LOAD TEST ON PERMANENT MAGNET MOTOR

10.9 THE CHARACTERISTICS OF THE PERMANENT MAGNET MOTOR

(i) Specifications

MANUFACTURER:	Cie Electro-Mechamique, Dijon, France.
TYPE:	MV26/500057
VOLTAGE:	150V
CURRENT:	37A (continuous)
	200A (pulse)
TORQUE:	16 N.m.
SPEED:	3000 r.p.m.
OUTPUT POWER:	5,0 kW
E/N:	42,0 volts/1000 r.p.m.
T/I:	0,397 Nm/A
MASS:	30 kg
SPECIFIC OUTPUT:	167 W/kg
ARMATURE RESISTANCE:	0,28 ohms
at 25^{o} c	
INERTIA:	36000 g cm^2
MECHANICAL TIME CONSTANT:	4 ms
OUTSIDE DIAMETER:	312 mm
OUTSIDE LENGTH:	134 mm

(ii) General Description

The unusual shape of the motor is shown in the photograph of figure 10.19. The frame consists of a short, finned cylinder and two flat circular end-plateson which are mounted the permanent magnets. These are short and cylindrical and there are approximately 6 on each end-plate. The armature, in the form of a disc only 4mm thick, passes between the magnets. The brushes

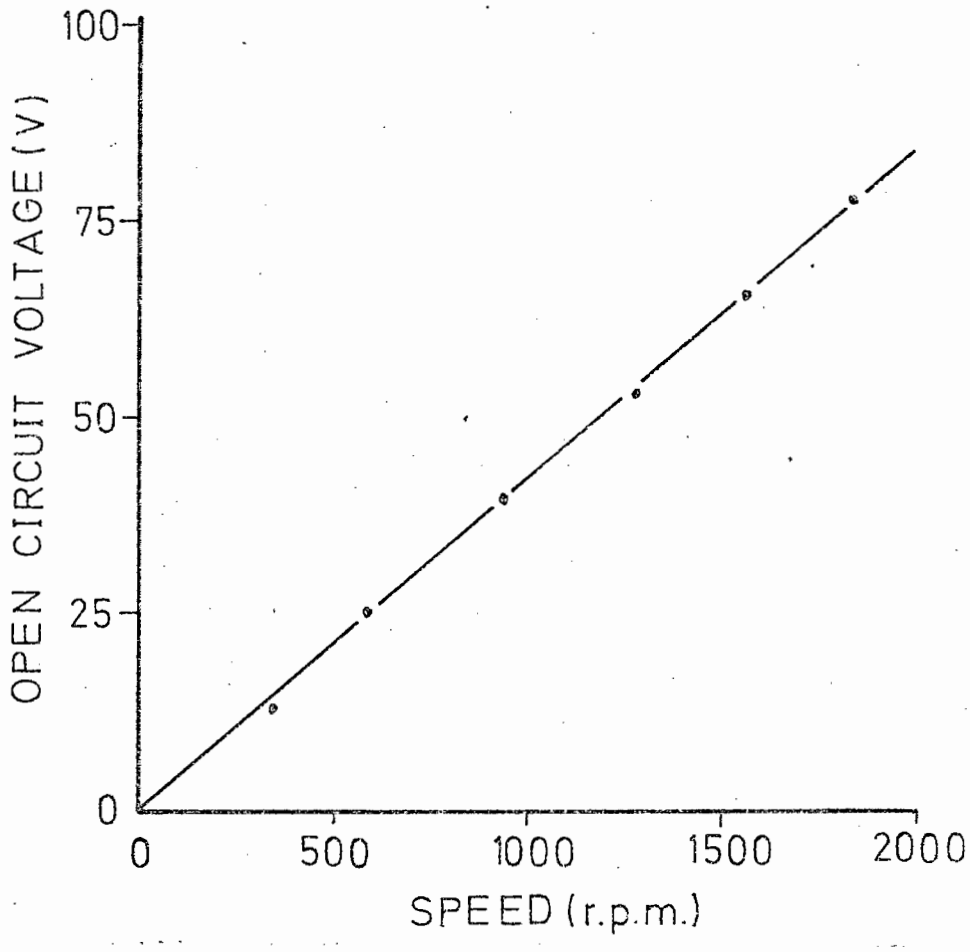

FIGURE 10.16 : OPEN CIRCUIT CHARACTERISTIC OF MOTOR

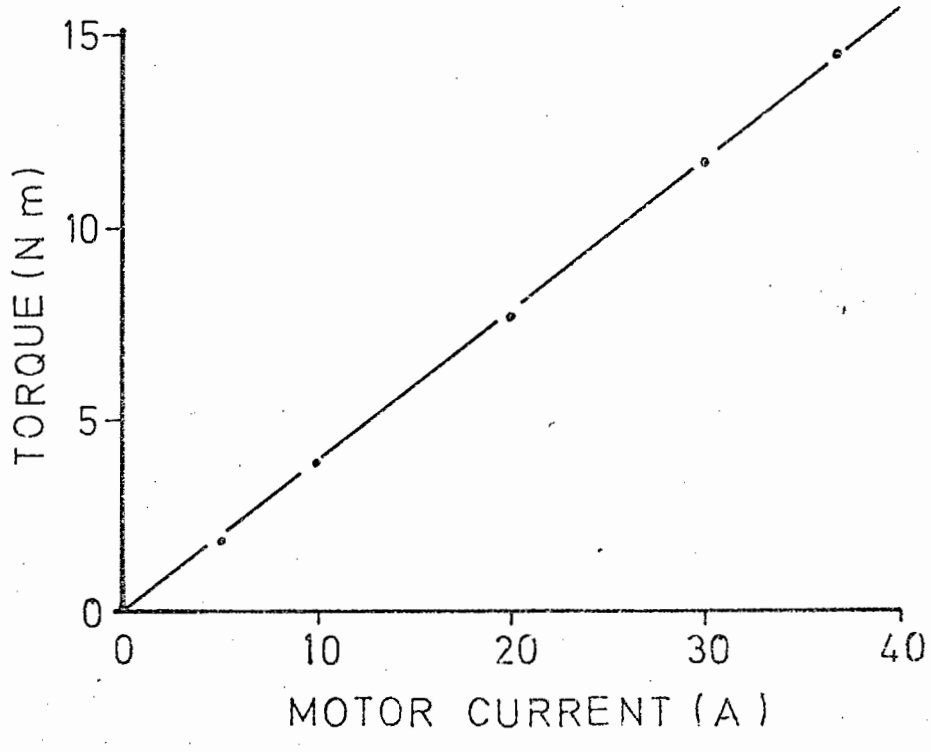

FIGURE 10.17 : TORQUE - CUR ENT RELATIONSHIP FOR MOTOR.

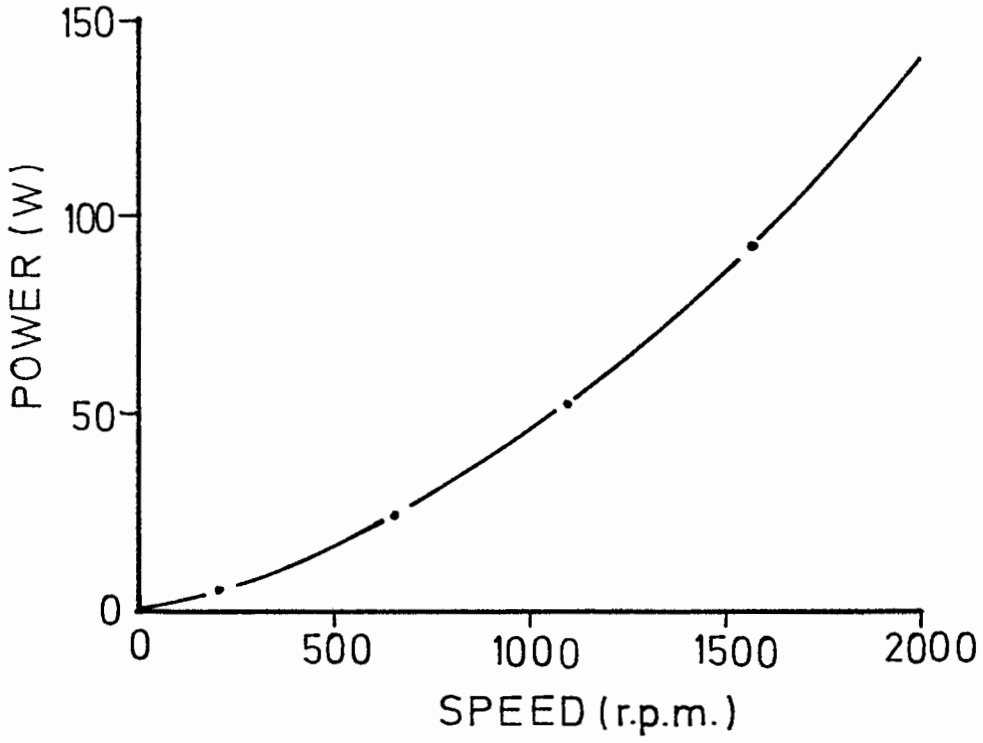

FIGURE 10.18: FRICTION AND WINDAGE POWER LOSS AT NO LOAD

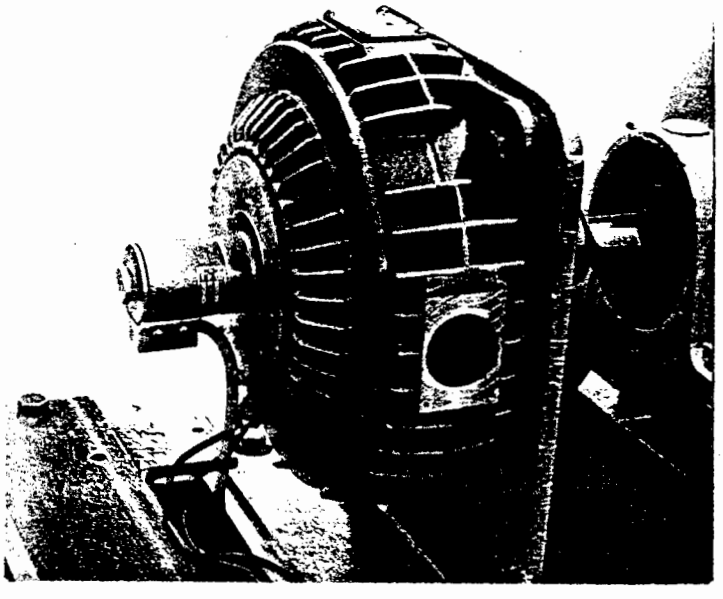

FIGURE 10.19 : THE 5kW PERMANENT MAGNET MOTOR

bear directly on the exposed copper conductors.

(iii) Open circuit characteristics

The open-circuit voltage of the machine, when run as a generator, was measured with a dc voltmeter. This voltage, as a function of the speed is given in figure 10.16. The back-emf per 1000 r.p.m. = 42,0 volts.

(iv) Torque - Amp characteristics.

The shaft torque, as measured on a dynamometer brake, is given as a function of the dc current in figure 10.17. The test was conducted at 1000 r.p.m. and the machine was supplied from a Ward-Leonard system. The torque per unit current = 0,397 Nm/A, which is 10% less than the quoted value.

(v) No-load loss

With the machine uncoupled from the brake, the no-load input power was measured as a function of speed, and the results are given in figure 10.18. The copper loss at the levels used, was neglected as it amounted to less than 5% of the no-load power.

(vi) Load tests at constant torque

The speed of the motor - the latter being driven by a Ward-Leonard system, - was varied while keeping the motor current i.e. torque) constant. The input power, P_{IN}, was measured using a wattmeter and the output power, P_{MECH} = Torque x Speed. The connection diagram is shown in figure 10.15, and the results are shown in figures 10.20 and 10.21.

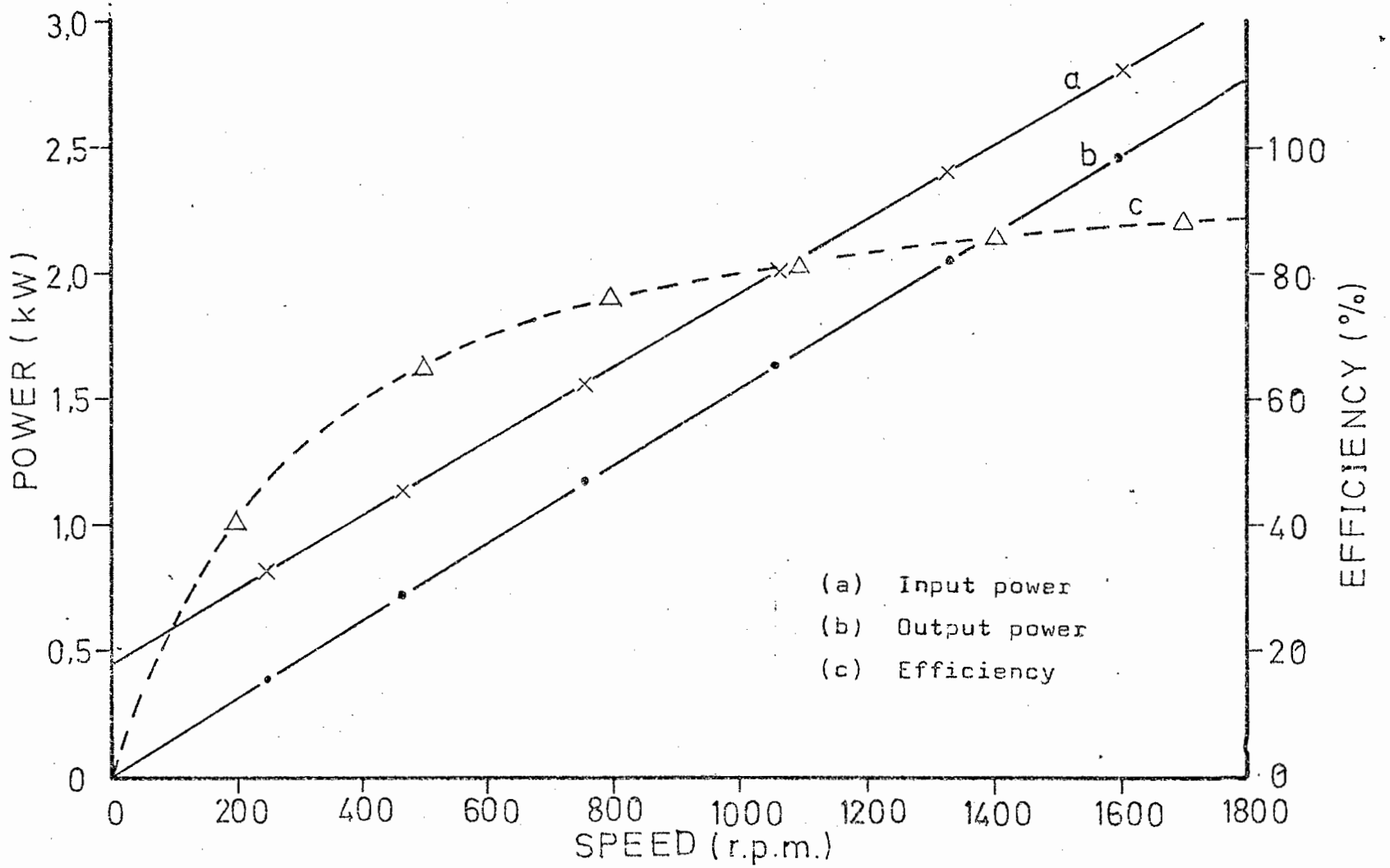

FIGURE 10.20 : PERFORMANCE OF MACHINE UNDER MOTORING AT CONSTANT ARMATURE CURRENT OF 37A (M - G SET)

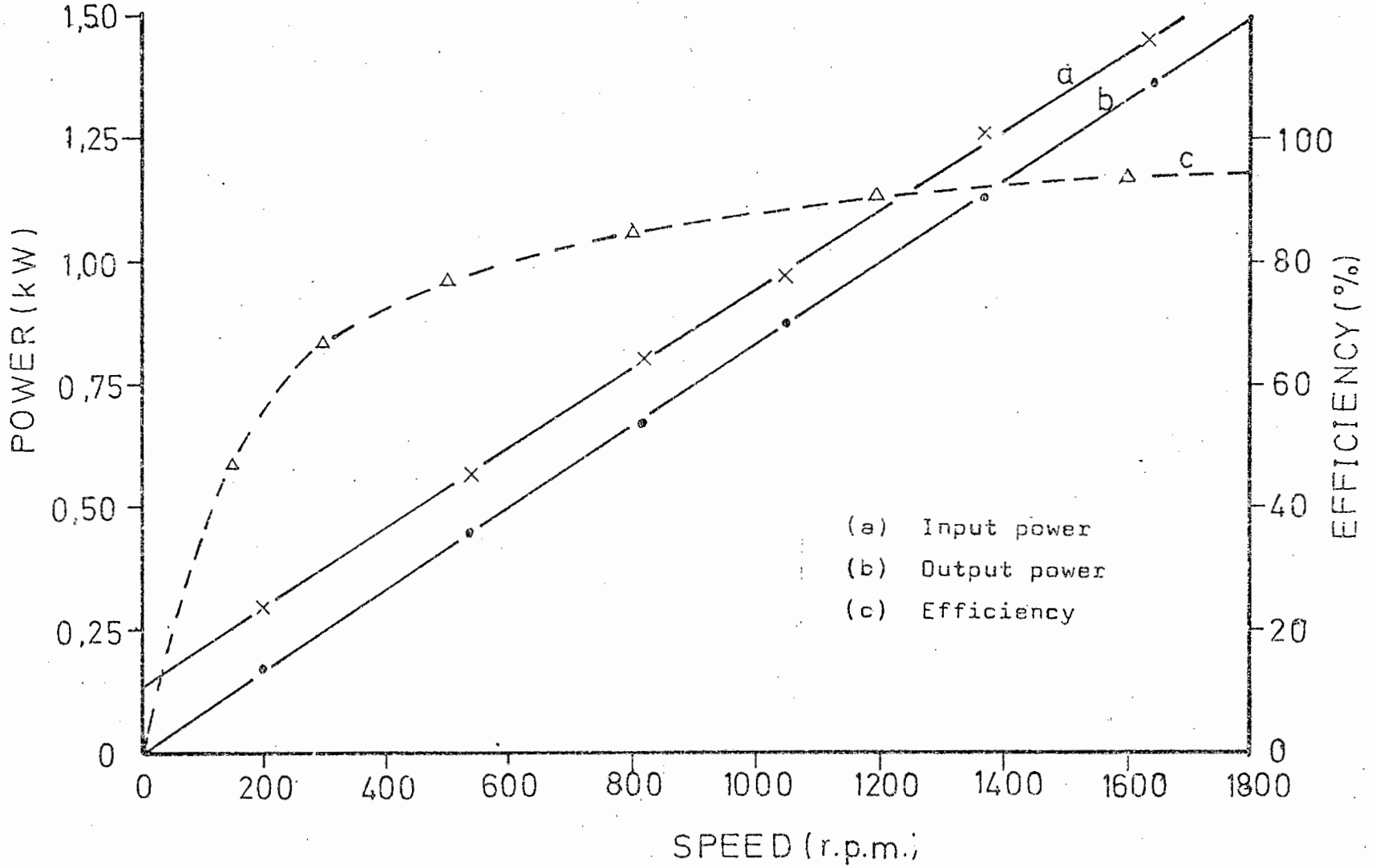

FIGURE 10.21: PERFORMANCE OF MACHINE UNDER MOTORING AT CONSTANT CURRENT OF 20A SUPPLIED FROM M - G SET

10.10 MOTOR CURRENT PREDICTIONS DURING MOTORING AND BRAKING

(Chopper frequency = 400 Hz)

(i) Prediction of average motor current during motoring at a fixed speed. (refer to figure 3.1 for results)

Measurement: The average motor current (as measured on a dc ammeter) was plotted as a function of the p.u. mark (measured on an oscilloscope) for both a 4 mH and a 12 mH choke connected in series with the motor, with the speed of the motor fixed at 1330 r.p.m.

Calculation: The total circuit resistance,

$R = R_a + R_L + R_{leads}$, where

$R_a = 0{,}30$ ohm; $R_{leads} = 0{,}10$ ohm

$R_L = 0{,}05$ ohm (4mH choke); $R_L = 0{,}15$ ohm (12 m_H choke)

N = 1330 r.p.m., therefore E = 54,0V.

$V_B = 79V$, and allowing for semiconductor voltage drops,

$V_B = 76V$.

$I_M = 1/R\ (76\ t_m/T_o - 54)$

$I_M = 0$ for $t_m/T_o = 54/76 = 0{,}71$

(ii) Prediction of average motor current for braking at a fixed speed.

(results given in figure 4.1)

Measurement: The average motor current (as measured on a dc ammeter) was plotted as a function of the p.u. mark (measured on an oscilloscope) for both a 4 mH and a 12 mH choke connected in series with the motor with the speed of the motor held constant at 620 r.p.m.

Calculation: N = 620 r.p.m., therefore E = 25,2V.

Allowing for semiconductor voltage drops, $V_B = 90V$

$I_M = 1/R\ (90\ t_m/T_o - (90 - 25{,}2))$

$I_M = 0$ when $t_m/T_o = 64{,}8/90 = 0{,}72$

(iii) Prediction of motor current ripple during motoring.

(Results shown in figure 3.2)

The peak-to-peak motor current (bandwidth K) was monitored on an oscilloscope while the p.u. mark was varied, keeping the average value of the motor current (measured on a c.c. ammeter) constant. Three values of average current was chosen - 37A, 20A, 10A. The percentage ripple was found from $r = K/I_M$.

This value of ripple was compared to that obtained by calculation, using equations 2.17 and 2.18

10.11 LOAD TESTS ON MOTOR WITH CHOPPER (BELOW BASE SPEED).

All tests conducted at 400 Hz.

(i) Efficiency test during motoring.

(Results shown in figures 3.3 and 3.4)

The input power to the chopper ($V_B \times I_B$), the input power to the motor (P_M), and the output of the motor (Torque XN) were measured as functions of speed with the armature current constant (constant torque).

Two values of armature current were chosen - 37A (14,5 Nm) and 20A (7,8 Nm)

The torque was measured using the dynamometer brake, shown in figure 10.22. The efficiency was calculated from the power curves.

(ii) Form factor during motoring.

(Results shown in figure 3.5)

With the motor current kept constant, the peak to peak current ripple was measured on an oscilloscope for various speeds. From this, the form factor was computed as a function of speed.

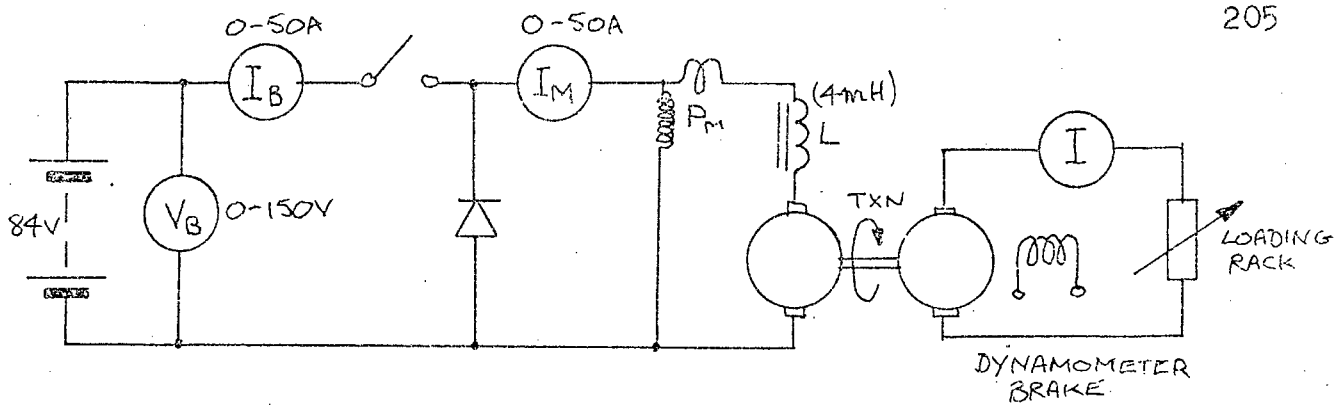

FIGURE 10.22: CHOPPER LOAD TEST ON MACHINE WHEN MOTORING BELOW BASE SPEED.

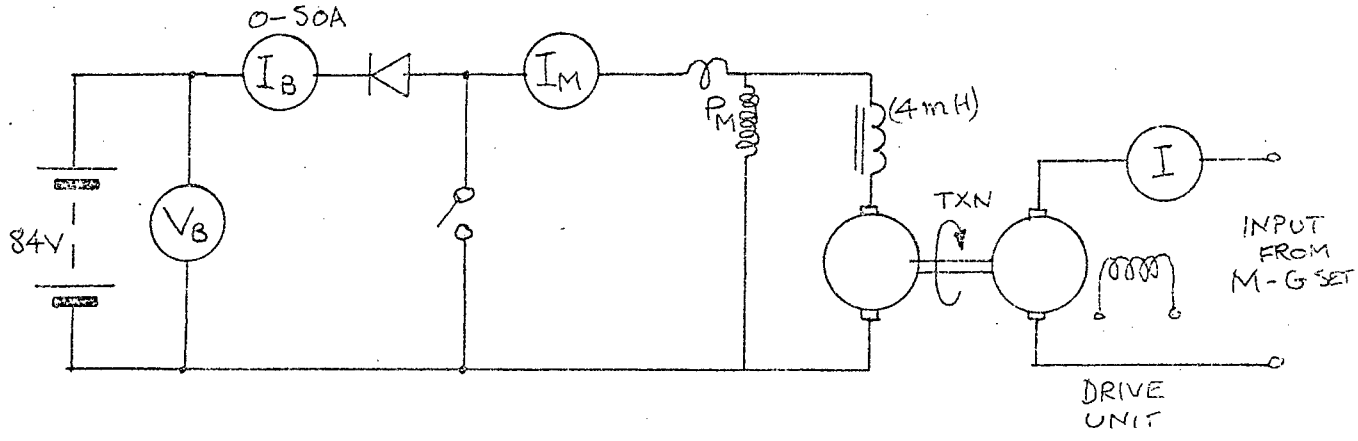

FIGURE 10.23: CHOPPER LOAD TEST ON MACHINE WHEN BRAKING BELOW BASE SPEED.

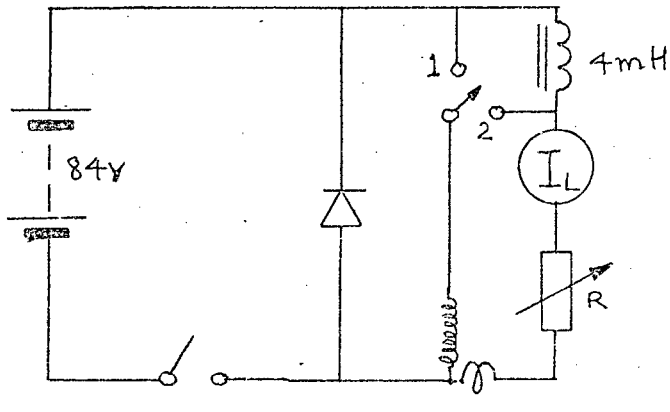

FIGURE 10.24: MEASUREMENT OF POWER LOSS IN CHOKE

(iii) Current multiplication

(Results shown in figure 3.6)

These curves were computed from the readings taken during the load tests described in section 10.11 (1).

(iv) Power loss in a 4mH choke.

(Results shown in figure 3.7).

Firstly, the dc I^2R power loss was measured at various currents using the wattmeter. Secondly, the choke was connected to the chopper (operating on 400 Hz), as shown in figure 10.24, and with the p.u. mark set to 0,5, R was varied to obtain the required current. The power loss in L is the difference between the wattmeter readings with the one end of the voltage coil connected alternately to 1 and 2 (P_1 & P_2) then: $P_L = P_1 - P_2$.

(v) Efficiency during regenerative braking.

(Results shown in figures 4.2 , 4.3).

The shaft input power, motor output power and power returned to the battery were measured as functions of speed, with armature current kept constant, using the connection shown in figure 10.23. The two values of armature current chosen were 37A (15,5 Nm) and 20A (8,5 Nm). The efficiency was calculated from the power curves.

10.12 LOAD TESTS FOR MOTORING AND BRAKING ABOVE BASE SPEEDS.

(Tests conducted at 400 Hz)

(i) Power measurements during motoring

(Results shown in figures 5.1 , 5.2)

The chopper input power, motor input and output powers and the p.u. mark were measured as functions of the motor speed, using the connection shown in figure 10.25. The speed was varied from base

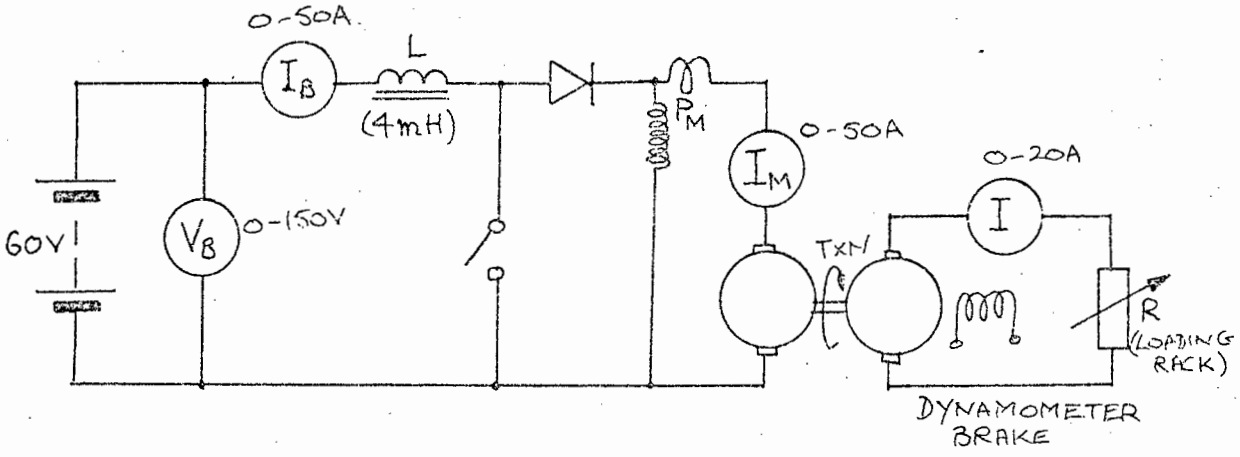

FIGURE 10.25: CHOPPER LOAD TEST ON MACHINE WHEN MOTORING BELOW BASE SPEED.

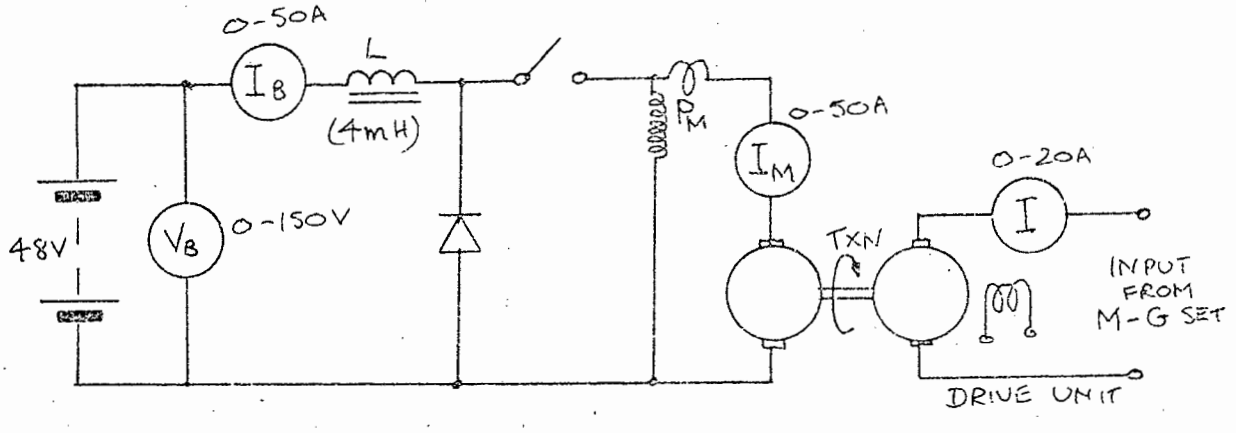

FIGURE 10.26: CHOPPER LOAD TEST ON MACHINE WHEN BRAKING ABOVE BASE SPEED.

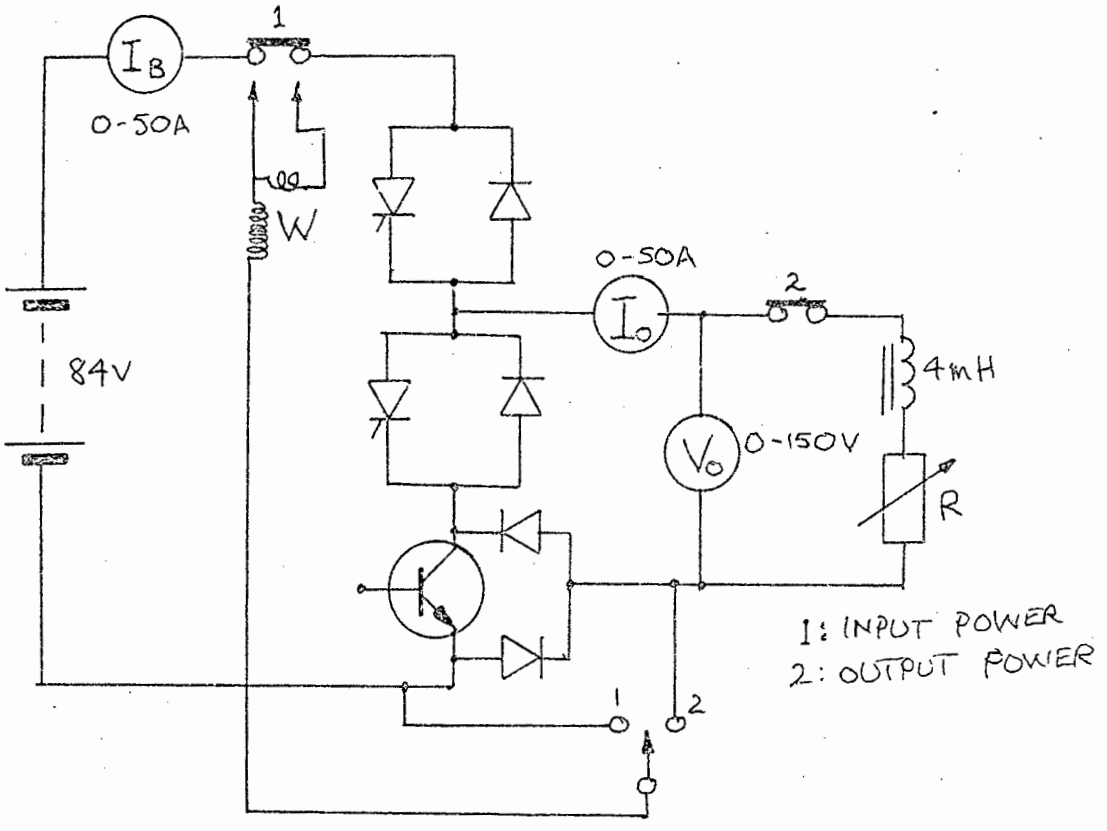

FIGURE 10.27: MEASUREMENT OF POWER LOSS AND OUTPUT VOLTAGE FOR THE TRANSISTOR/THYRISTOR CHOPPER.

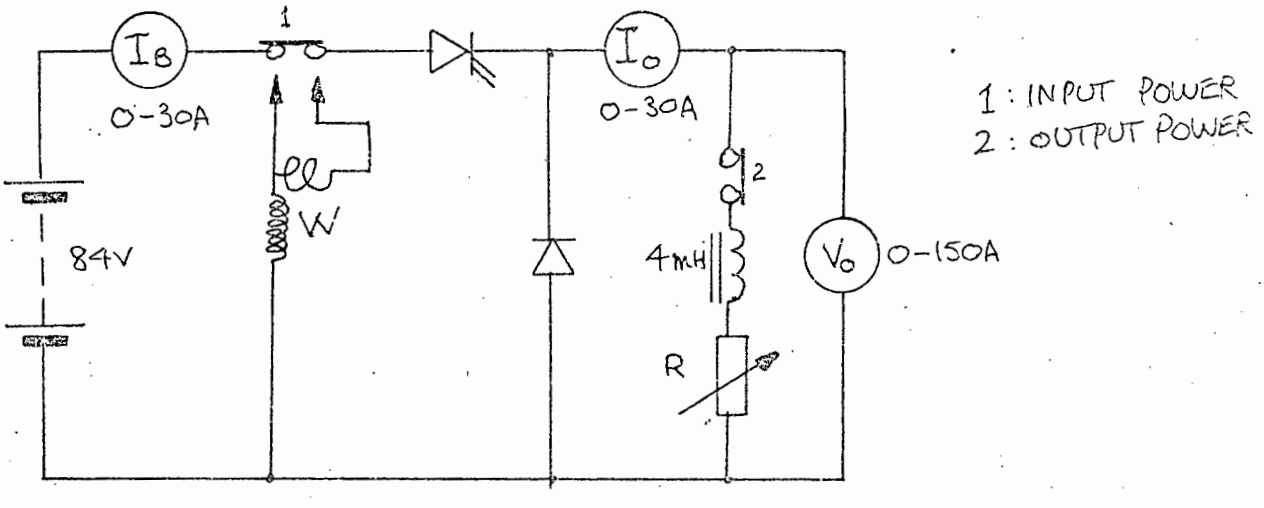

FIGURE 10.28: MEASUREMENT OF POWER LOSS AND OUTPUT VOLTAGE FOR THE THYRISTOR CHOPPER.

speed (where the motor was connected directly to the battery, with the chopper open) to 55% above base speed. The efficiencies were computed from the power curves, and the form factor and RMS current were computed from the curves for p.u. mark and average current.

(ii) Power measurements during braking
(Results shown in figure 5.7)

The input and output powers of the motor, the power regenerated to the battery and the p.u. mark were measured as functions of the speed with the connection shown in figure 10.26. The efficiency was computed from the power curves, and the form factor and RMS current were computed from the curves p.u. space and average current.

10.13 PERFORMANCE OF CHOPPERS

(i) Power loss of transistor and thyristor choppers

(Results shown in figures 7.17(a) and (b)

Power losses were measured using the connection diagram of figure 10.27 for the transistor chopper and that of figure 10.28 for the thyristor chopper. In each case, the power loss in the chopper was calculated as the difference between the input and output powers, measured on the wattmeter.

(ii) Output voltage of the transistor and thyristor choppers

(Results shown in figures 7.18 - 7.20)

The output voltage, as a function of the p.u.mark, chopper frequency and load current, was measured using a d.c. voltmeter, positioned as shown in figures 10.27 and 10.28.

REFERENCES

1. J. BYRE AND J.LACY: Compatible controller-motor system for battery-electric vehicle, Proc. IEE, 1970, Vol 117, No.2, p.p. 369 - 376.
2. K. HEUMAN: Pulse control of dc and ac motors by silicon controller rectifiers, International conference on non-linear Magnetics (Intermag), 1963.
3. J. HEMGSBERGER, U. PUTZ AND L. VETTERS: Thyristor converter for electric traction, AEG Progress, 1/2, 1965, p.p. 58 - 65 .
4. J. BEASLEY AND G. WHITE: Controlling a dc traction motor with thyristors, AEI Engineering, Mar/Apr. 1966, p.p. 92 - 95.
5. H. SIE AND R. MOSER: The behaviour of a laminated commuator traction motor when supplied via a thyristor bridge or dc chopper circuit, Bulletin Oerlikon, Jan.1970, p.p. 41 - 50.
6. H LOCKER: The dc chopper used on trolleybuses with full electronic control, Brown Boveri Review, Vol 57 No.10 Oct. 1970, p.p. 419 - 428.
7. K. BEZOLD, R. UHTHOFF AND K. WALTER: Geapuls controller for electric trucks and vehicles, AEG Progress, 1/2 1965, p.p. 70 - 73.
8. R. WAGNER: A dc chopper regulator for controlling the speed of electric vehicles, Siemens Review, 1964, Vol 31, p.p. 195 - 200.
9. M. HAGENMAIER: Thyristor - controlled battery locomotives for underground mine operation, Siemens Review, 1969, Vol 36 No.7 p.p. 276 - 278.
10. B. BIRD AND R. HARLEN: Variable characteristic dc machines, Proc. IEE, 1966. Vol 113, No 11, p.p. 1813 - 1819.
11. M. SAY AND H. FRAMPTON: Compound characteristic in regenerative braking with dc traction. Journal IEE, 1923, Vol 61 p.p. 863.
12. L. RILEY AND G. WOODS: Dynamic braking with traction motors, Trans. American IEE, 1945, Vol 64 pg 517.
13. C. ROBINSON: Redesign of dc motors for applications with thyristor power supplies, IEEE Transactions on Indus. and Gen. Appl., 1968, Vol 4, No 5, pp 508 - 514.
14. J. HINDMARSH: Variable-characteristics dc Machines, (correspondence) Proc IEE, 1967, Vol 114 No 5, pg 654.
15. B. HENDER: Recent developments on battery electric vehicles, Proc IEE, 1965, vol 112 No 12, pg 2297.
16. Discussion of recent developments in battery electric vehicles, Prof IEE, 1966, Vol 113 No 11, pg 1809.
17. A HILLS: Battery Electric Vehicles, Newnes, 1943.
18. N. LINDGREEN: Electric cars - hope springs eternal, IEEE Spectrum, April 1967, pp 48 - 60.
19. First commercial electric car, Electrical Export Review, Jan/Mar 1970, pp 12 - 13.
20. M. BARAK: Developments in Electrochemical energy conversion devices, Proc IEE, 1965, vol 112, No 7, pp 1439 - 1448.
21. M. BARAK: Batteries and fuel cells, IEE Reviews, Vol 117, Aug 1970, pp 1561 - 1584.
22. B. POULSTON AND J. KIRKLEY: Possibilities for the fuel cell in the passenger car. Proc Instn. Mech. Engrs., 1964, Vol 178, Part 2A pg 111.

23. M. CLAASSEN: A dc chopper motor speed control, B.Sc. Thesis No.42, 1969, University of Cape Town.
24. J. van RENSBURG: dc motor speed control, B.Sc. thesis 1970, University of Cape Town.
25. General Electric SCR manual, 4th edition, Chapters 3,5, 11.
26. PAYNE AND REEVES: Switch-off circuits for SCRS operating on dc Mullard Tech. Comm., No.65, June 1963, pp 158 - 161.
27. P. KNAPP: Solid state regulating units for motoring and braking dc traction vehicles, Brown Boveri Review, 1970 Vol 57 No.6/7, pp 252 - 270.
28. K. DATHER AND W. FAUST: Electronic dc chopper for trolley-bus, Brown Boveri Review, 1966, Vol 53, No.10, pp 715 -721.
29. F. MAZDA: Design of high frequency thyristor chopper circuits, Electronic Engineering, February 1970, pp 34 - 39.
30. MULLARD Power Engineering using thyristors, 1970, Vol 1, Chap. 5.
31. Westinghouse SCR designers handbook, 2nd edition, 1970, Chap. 8.
32. WEBER: Solid state dc motor control for traction driver vehicles, Motorola Appl. note AN - 189.
33. J. MILLMAN AND TAUB: Pulse, Digital and Switching waveforms. 1965, Mc Graw-Hill.
34. RCA Transistor manual, 1967 pp 19 - 20.
35. RCA Silicon power circuits manual, 1969, pp 65 - 148.
36. J. MILLMAN AND C. HALKIAS: Electronic devices and circuits, 1967, Mc Graw-Hill, pp 597 - 606.
37. RCA Specifications for 2N3773, date bulletin 6/66.
38. RCA Specifications for 2N5575 - 2N5580 file No.359.
39. R.LOCHER: On switching inductive loads with transistors, IEEE Trans. on Indus. Electronics and Control Instr., June 1970, pp 256 - 262.
40. Phillips data handbook, semiconductors and integrated circuits, September 1969, part 1.
41. General Electric transistor manual, 1964, Chapters 13, 19.
42. Circuits with semiconductor components (Siemens), 1969, Vol 1 and 2.
43. G. SCHMENGER: Monitoring of air pollution, Electronics and Instrumentation, 1971, Vol 2 No.5, pp 5 - 7.
44. RCA Specification sheets for SCR'S: 2N3870 - 2N3873; 2N3896 - 2N3899, File No.94, bulletin 6/66.
✓45. B.BERMAN: Design Considerations pertaining to a Battery Powered Regenerative System, IEEE Transactions of Industry Applications, March/April 1972, Vol.1A - 8 No.2, pp.. 184 - 189.
46. B. BERMAN: Battery Powered Regenerative SCR Drive, IEEE Transactions on Industry Applications, March/April 1972, Vol.1A - 8, No.2, pp 190 - 194.
✓47. B. BERMAN: All Solid-State Method of Implementing a Traction Drive Control, IEEE Transactions on Industry Applications, March/April 1972, Vol.1A - 8, No.2 pp 195 - 202.
48. Electric Vehicles get boost from Sodium Battery, IEE News, 16th November, 1972, pg 6.
✓ 49. G.J. MURPHY: Considerations in the Design of Drive Systems for on-the-road Electric Vehicles, Proc.IEEE, December,1972, Vol.60 No.12, pp 1519 - 1533.

50. R.W. JOHNSTON: Modulating Inverter System for Variable-Speed Induction Motor Drive (GM Electrovair II), IEEE Transactions on Power Apparatus and Systems, February 1969, Vol. PA5 - 88, No.2, pp 81 - 85.
51. The Electric Car: A design Challenge, Electro-Technology, May 1968 Vol.8 No.5, pp 57 - 68.
52. G.R. FRYSINGER: The Big Roadblock: Efficient Power, Electro-Technology, May 1968 Vol.8 No.5, pp 69 - 72.
53. M. BARAK: Recent Developments in Batteries and Voltaic Cells, Electronics and Power, August/September 1972, pp 290 - 296.
54. P. CAMPBELL: Current Problems for Electric Cars, Students Quarterly Journal, September 1972, Vol.42, No.169, pp 80 - 82.
55. J.T. SALIHI: Two for the Road, IEEE Spectrum, July 1972, pp 43 - 47.
56. J.T. SALIHI: The Electric Car - Fact and Fancy, IEEE Spectrum, June 1972, pp 44 - 48.
57. P.L. MORETON: Fuel Gauge for the Electric Car, Proc.IEE, Vol.119, No.6, June 1972, pp 649 - 654.
58. Siemens Semiconductor Manual, 1973, pp 527 - 529.
59. F.K. URBAN and J.G. FRANK: The Hall Effect comes into its own, Electronic Products Magazine, September 18, 1972, pp 59 - 62.
60. C.J. GRANDMAISON: Magnetic Fields turn on IC'S Electronic Products Magazine, September 18, 1972, pp 63 - 65.
61. K. BAHR: The Magnetoresistor: A very simple solid-state transducer, EDN/EEE, January 15, 1972, pp 36 - 39.
62. F.F. MAZDA: Thyristor Control, 1973, Butterworths, Chapter 5.